NILU: OR 20/94

NILU : OR 20/94
REFERENCE : E-93086
DATE : MARCH 1994
ISBN : 82-425-0562-4

Third Nordic Symposium on Atmospheric Chemistry

Proceedings of NORSAC '93

Edited by Claus Jørgen Nielsen

NILU

NORSK INSTITUTT FOR LUFTFORSKNING
NORWEGIAN INSTITUTE FOR AIR RESEARCH
Postboks 64 - N-2001 Lillestrøm - Norway

Proceedings of NORSAC '93

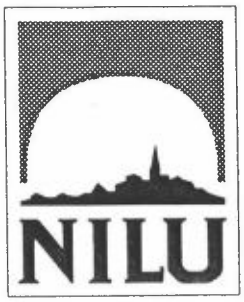

Third Nordic Symposium on Atmospheric Chemistry

Geilo, Norway Decmber 3-5, 1993

Editor
Claus Jørgen Nielsen

Preface

The Third Nordic Symposium on Atmospheric Chemistry was held from December 3rd to the 5th, 1993 at the Highland Hotel, Geilo Norway. 61 scientists and research students from the Nordic and Baltic countries attended the symposium where they heard 31 talks, 19 short poster presentations and had the chance to see the posters which were on display.

The Symposium was organized in 8 sessions starting Friday afternoon and ending Sunday at lunch time. During this short time span of 44 hours, 12 hours were taken up by oral presentations and 4 hours by poster presentations, 8 hours by breakfast/lunch/dinner and 6 hours by outdoor activities. A little arithmetic leaves 14 hours over two days for the "healing" of body and mind. Perhaps the program was a little too strenuous.

This volume is organized in three sections: Laboratory investigations, Field investigations, and Theoretical investigations. Within each section, the contributions are arranged in alphabetical order according to the first authors family name. At the end a list of the participants is given, including their phone, fax, and E-mail addresses as well as an index of authors.

Claus Nielsen
UiO/NILU
February 1994

Acknowledgement. The Third Nordic Symposium on Atmospheric Chemistry has received financial support from Nordisk Forskerutdanningsakademi, NorFA. In addition to the general support to the Symposium, NorFA also provided the financial means whereby it was possible to invite a number of Baltic researchers and research students. Financial support to student travel and additional Baltic participation was received from the Danish Research Council and the Swedish Environmental Protection Agency.

Apologies. We were extremely unlucky with the weather on the day of arrival and the Oslo airport was closed for a long time. Our Baltic colleagues were stranded in Copenhagen or Stockholm for several hours. The participants from Helsinki circled around Oslo before they were returned to Stockholm. The Stockholm participants were directed to Sandefjord and the Copenhagen participants to Kristiansand from where they were transported by bus to Oslo. The organizers were close to panic, but thanks to the positive attitude of all participants, everything eventually turned out fine.

Content

Laboratory Studies

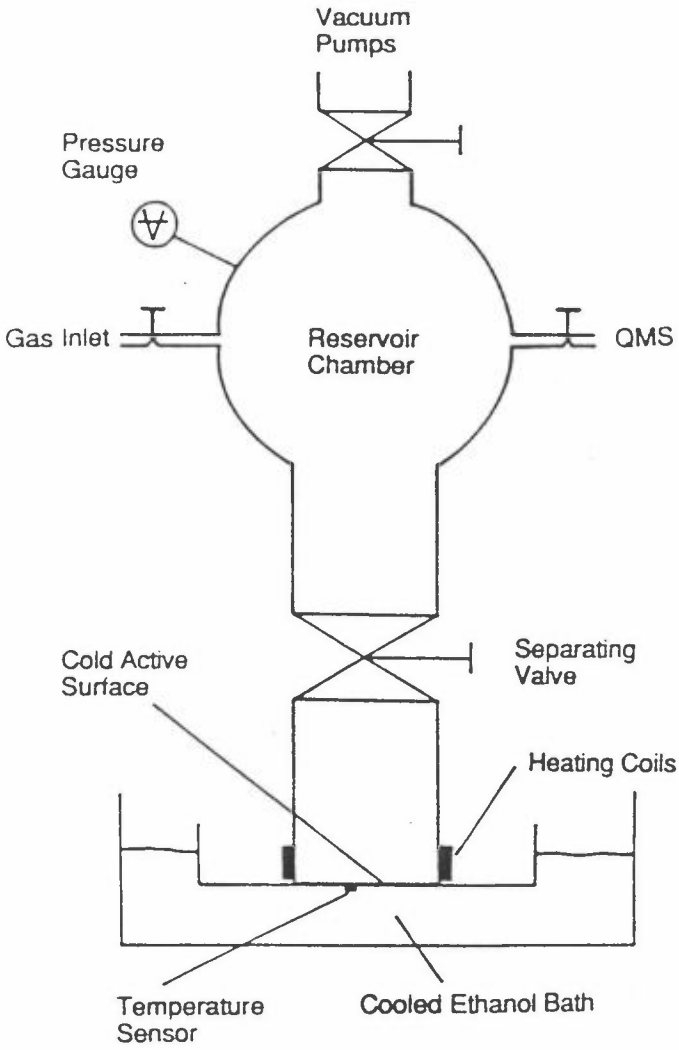

DETERMINATION OF OZONE ISOTOPOMER ABUNDANCES BY MICROWAVE- AND FTIR-SPECTROSCOPY.

LENE CHRISTENSEN, NIELS WESSEL LARSEN,
FLEMMING NICOLAISEN, THORVALD PEDERSEN,
AND GEORG OLE SØRENSEN.

Laboratory of Chemical Physics, Department of Chemistry,
University of Copenhagen, The H. C. Ørsted Institute,
Universitetsparken 5, DK-2100 Copenhagen Ø, Denmark.

SUMMARY

Deviation from the statistical ratios (2:1) between the isotopomers in mono- and di-^{18}O substituted ozone (henceforth 50-ozone and 52-ozone) has been observed in laboratory experiments aimed at studying the mechanism of ozone formation [1,2]. Similar deviations seem to occur in the stratosphere [3,4].

We have been using two methods to assess the isotopomer ratios r_{50} and r_{52}.

1. Microwave-spectroscopy, using a supposedly scrambled mixture of isotopomers. This method is experimentally relatively simple, but there is doubt about the extent to which the calibration mixture is actually scrambled.

2. FTIR-spectroscopy, using the far-infrared, rotational bands of ozone. Although conceptually straightforward this method is fairly involved experimentally. The aim is to measure the far infrared line intensities in one or perhaps two standard mixtures, and then calibrate the microwave spectrometer using the same mixtures.

INTRODUCTION

The work being presented here started out as a basic investigation of the mechanism of formation of ozone. The question being asked was whether the mechanism was **i** a straightforward *end-on addition* of an oxygen atom to an oxygen molecule, or whether one of two alternative mechanisms might apply: **ii** *insertion* of the atom into the O=O-bond and **iii** *formation via a regular triangular complex* [1,2]. The strategy applied in order to answer the question(s) was to use isotopic oxygen species and then look for the isotopic distribution in the final ozone species.

Perhaps not very surprising, a precise answer to the questions, depended critically on the the precision of the determination of the relative abundances (r_{50} and r_{52}) of the asymmetric versus the symmetric ozone species of total mass 50 u and 52 u. Microwave spectroscopy (MW) and High-resolution Fourier Transform Infrared Spectroscopy (FTIR) have been used in the required determinations. Both methods aim at using the rotational part of the spectrum, since the line intensities of rotational transitions are determined predominantly by the permanent dipole moment,

Table 1: 11 microwave lines of the parent ozone species. α_{max} denotes peak-heigth, α_{int} is the theoretical line strength. "Area" is obtained as line-width times peak-heigth: $\Delta\nu \times \alpha_{max}$.

$J_{K_{-1},K_{+1}} \rightarrow J'_{K'_{-1},K'_{+1}}$	ν/MHz	$\Delta\nu$/kHz	α_{max}	Area/α_{int}
$37_{2,36} \rightarrow 36_{3,33}$	27458.217	241	98045	79063
$40_{6,34} \rightarrow 41_{5,37}$	27862.526	235	231161	91142
$25_{3,23} \rightarrow 24_{4,20}$	28960.515	226	1658824	77448
$16_{2,14} \rightarrow 15_{3,13}$	30051.761	238	2597641	72756
$15_{1,15} \rightarrow 14_{2,12}$	30181.227	243	1443074	75118
$19_{1,19} \rightarrow 18_{2,16}$	30524.032	247	830218	75060
$47_{7,41} \rightarrow 48_{6,42}$	32102.647	227	78795	88286
$53_{7,47} \rightarrow 52_{8,44}$	35642.733	222	24505	71614
$22_{3,19} \rightarrow 23_{2,22}$	36021.922	245	2639915	87550
$17_{3,15} \rightarrow 18_{2,16}$	37832.417	235	4311980	73911
$32_{3,29} \rightarrow 33_{2,32}$	39438.106	256	492094	79562
Mean value				79228
r.m.s. dev.				6775
Rel. unc.				2.70%
99% conf.				8.68%

which is well known [8].

At the present stage of the investigation the ozone formation problem has become marginal, while the main focus for some time has been on the accurate determination of the relative abundances of all the six ozone species containing ^{16}O and ^{18}O (^{18}O will be called Q in the following). There is a need for such a method also in applied atmospheric spectroscopy prompted by, among other things, balloon observations of stratospheric enrichments of heavy isotopomers of ozone by mass spectrometry [3] and by FTIR-spectrometry [4]. The latter observations indicated non-statistical ratios between symmetric and asymmetric species of 50-ozone.

MW-METHOD

Microwave spectroscopy has the spectral resolution it takes to clearly distinguish between all the six isotopomers, it is not very suitable for quantitative determinations however as is revealed by the results shown in Table 1, where the agreement between observed and theoretical line-strength for microwave transitions of ozone is shown. The uncertainties are so large that a calibration is needed. To form a calibration

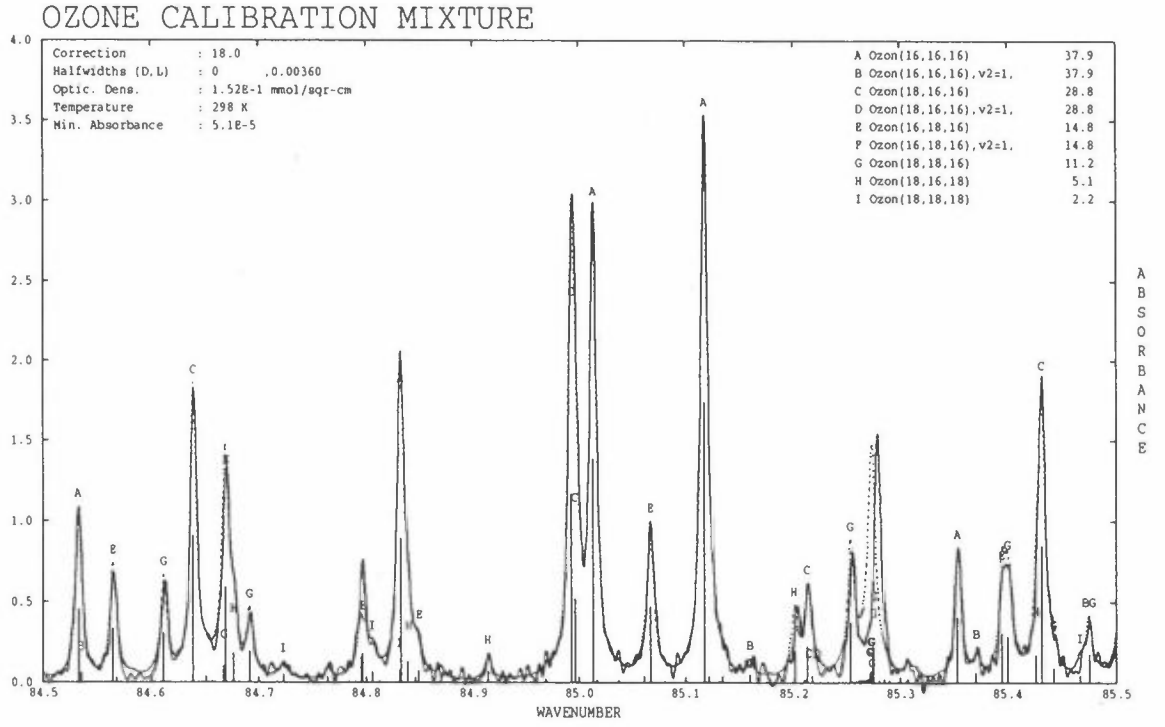

Figure 1: Rotational spectrum of an ozone isotopomer mixture in the range $84.5 - 85.5$ cm^{-1}. Observed species and evaluated abundances, see Table 3, are shown in the legend. A calculated bar spectrum and a simulated spectrum (dashed line) are also shown

mixture is however a very tricky problem [1,2], since we have no way of ascertaining that a thermodynamic equilibrium mixture (i.e. "scrambled") has been obtained (supposedly after long time of illumination with UV light or of exposure to electric discharge). Indeed Maursberger et. al. claim that such mixtures can hardly be obtained at all [5,6]. So, for the time being we aim at refining the FTIR method, which is presumably better for quantitative purposes, and then eventually use it as a primary standard to be used to calibrate the microwave method against (the latter being more easily applied for routine purposes).

FTIR-METHOD

The BRUKER HR120 FTIR which we have at our disposal allows for an ultimate resolution of 0.00186 cm^{-1}. Sofar we have not attempted to reach this resolution however because ozone breakdown in the cell puts an upper limit of about 4 hours on the scanning time. The spectra have therefore been obtained at 0.005 cm^{-1} resolution (3 hours with 33% breakdown of the sample). This resolution leaves numerous overlapping lines however. Figure 1 shows a small part of the spectrum. Shown on

Table 2: 14 selected, relatively undisturbed lines of the parent ozone species. α_{max} denotes peak-heigth, α_{int} are theoretical line strength. α^1_{int} is obtained from the permanent dipole moment, α^2_{int} from the corrected dipole operator, see text. "Area" is proportional to line-width times peak-heigth: $\Delta\nu \times \alpha_{max}$, but is obtained by our fitting program.

$J_{K_{-1},K_{+1}} \rightarrow J'_{K'_{-1},K'_{+1}}$	$\bar{\nu}/\mathrm{cm}^{-1}$	$\alpha_{\max}$	$\Delta\nu/\mathrm{cm}^{-1}$	Area/α^1_{int}	Area/α^2_{int}
$7_{7,1} \rightarrow 8_{8,0}$	53.3730	0.45370	0.0069	59.84	59.71
$23_{6,18} \rightarrow 24_{7,17}$	60.6276	0.31092	0.0077	64.90	64.25
$24_{6,18} \rightarrow 25_{7,19}$	61.4587	0.30808	0.0068	59.44	58.82
$14_{8,6} \rightarrow 15_{9,7}$	65.3640	0.45992	0.0070	59.24	58.71
$30_{6,24} \rightarrow 31_{7,25}$	66.4116	0.20552	0.0069	61.15	60.37
$16_{8,8} \rightarrow 17_{9,9}$	67.0430	0.42248	0.0080	64.18	63.49
$12_{9,3} \rightarrow 13_{10,4}$	69.7537	0.44204	0.0074	57.54	57.03
$14_{9,5} \rightarrow 15_{10,6}$	71.4342	0.43558	0.0073	58.51	57.88
$11_{10,2} \rightarrow 12_{11,1}$	74.9383	0.44852	0.0073	59.13	58.59
$20_{9,11} \rightarrow 21_{10,12}$	76.4699	0.36724	0.0070	58.13	57.20
$22_{9,13} \rightarrow 23_{10,14}$	78.1462	0.33607	0.0073	61.16	60.08
$16_{10,6} \rightarrow 17_{11,7}$	79.1394	0.37802	0.0076	59.31	58.45
$12_{11,1} \rightarrow 13_{12,2}$	81.7553	0.42290	0.0071	60.39	59.68
$18_{11,7} \rightarrow 19_{12,8}$	86.7964	0.31116	0.0077	59.58	58.48
Mean value				60.18	59.48
r.m.s. dev.				2.11	2.10
Rel. unc.				0.97%	0.98%
99% conf.				3.0%	3.0%

the figure is also a bar spectrum calculated from rotational and centrifugal distortion constants [7] and the measured permanent dipole moment [8] and a simulated spectrum. (A refinement, using higher order terms in the dipole moment operator [9], has also been applied, but since the improvement is only marginal we shall not describe the details.)

Table 2 shows the absorption lines used for ozone-48 (OOO). In Table 3 we show abundances obtained by FTIR and in Table 4 the calculated isotopomer ratios for 50- and 52-ozone.

DISCUSSION

While r_{50} is obviously much better determined by FTIR than by MW, then r_{52} is *not*. The reason for this is that the mixture chosen is deliberately relatively poor in

Table 3: Abundances of isotopomers determined from the FIR spectra of the ozone mixture. The abundance of QQQ was obtained by statistical arguments.

	OOO	OOQ	OQO	QQO	QOQ	QQQ
No. of lines	14	16	11	13	8	0
Fraction	37.9%	28.8%	14.8%	11.2%	5.1%	2.2%
Uncertainty	0.4	0.4	0.3	0.5	0.4	-
99% conf.	1.1	1.2	0.9	1.4	1.4	-

Table 4: Isotopomer ratios determined from FTIR- and MW-spectra.

FTIR	r_{50}	r_{52}
Value	1.95	2.19
Rel. unc.	2.5%	9%
99% conf.	8%	30%

MW	r_{50}	r_{52}
Value	1.75	2.53
Rel. unc.	12%	5%
99% conf.	89%	20%

the heavy isotopes. We intend to use a mixture richer in the heavy isotopes later. The reason for this procedure is that the FTIR spectrum is so dense that we need to suppress some of the lines.

The result does not prove that r_{50} and r_{52} differ from the statistical value of 2.00, although there is an indication that r_{52} could be slightly larger.

REFERENCES

[1] Wessel Larsen, N., Pedersen, T., and Sehested, J. Int. J. Chem. Kin. *23*, 331–343 (1991)

[2] Wessel Larsen, N., Pedersen, T., and Sehested, J. in J. Kaye (Ed.) ACS Symposium Series 502: Isotope Effects in Gas Phase Chemistry; 1992

[3] Mauersberger, K., Geophys. Res. Lett. *8* 935–937 (1981)

[4] Abbas, M.M., Guo, J., Carli, B., Mencaraglia, F., Carlotti, M. and Nolt, I.G. J. Geophys. Res. *92* 231–239 (1987)

[5] Morton, J., Schueler, B. and Mauersberger, K., (1989) Chem. Phys. Lett. *154* 143–145 (1989)

[6] Morton, J., Barnes, J., Schueler B. and Maursberger, K. J. Geophys. res. *95* 901–907 (1990)

[7] Depannemaecker, J.-C., Bellet, J. : Journal of Molecular Spectroscopy. *66*, 106-120 (1977)

[8] Lichtenstein, Gallagher, Clough: Journal of Molecular Spectroscopy. *40*, 10-26 (1971)

[9] Camy-Peyret C., Flaud J.-M.: Vibration-rotation dipole moment operator for asymmetric rotors Molecular Spectroscopy: Modern Research Edited by Narahari Rao K. Volume III, 244-250 (1985)

A matrix isolation study of the C1OO and ClClO radicals.

ANDERS ENGDAHL
CHEMICAL CENTER, THERMOCHEMISTRY
UNIVERSITY OF LUND

AND

KLAS JONSSON
LINKÖPING INSTITUE OF TECHNOLOGY

The UV and IR absorption spectra of the ClOO and ClClO radicals in argon matrices have been studied. An estimate of the intensities of their infrared bands is given. ClOO has a low wavenumber fundamental at 192.4 cm^{-1}. The maximum UV absorption cross section for ClClO, 1.3×10^{-17} cm^2 / molecule, is found at 280 nm. The wavelength dependency of the photochemistry of ClOO to OClO in argon matrices has been studied.

A DETAILED MECHANISM STUDY OF GAS PHASE NITRATE RADICAL INITIATED OXIDATION OF 2-BUTENES

M. HALLQUIST, I. WÄNGBERG and E. LJUNGSTRÖM
Department of Inorganic Chemistry, GU/CTH, S-412 96 Göteborg, Sweden

SUMMARY

Nitrate radical-initiated oxidation of 2-butenes was investigated using long optical path FTIR-spectroscopy. At atmospheric conditions (295 K, 1020 mbar and 21 % O_2) major products were 3-nitroxy-2-butanone, 3-nitroxy-2-butanol and acetaldehyde. The oxygen dependence of the product formation was investigated by varying the O_2 concentration. The yield of 3-nitroxy-2-butanone increased, and the formation of 3-nitroxy-2-butanol and acetaldehyde decreased, with the oxygen concentration.

1. INTRODUCTION

The reaction steps following the NO_3 radical addition to butene and other alkenes has been the subject of several previous studies [1]. These investigations have revealed mechanisms containing consecutive reactions by which alkenes are being oxidised to aldehydes and various nitrated compounds. Some features in these mechanisms seem to be common for all alkenes investigated. Among the principal reaction steps is O_2-addition to alkyl radicals to form alkyl peroxy radicals. Hydrogen abstraction from alkoxy radicals by O_2 may also occur, yielding carbonyl compounds and HO_2 radicals. Alkoxy radicals may on the other hand also react with NO_2 to form alkylnitrates or decompose, yielding carbonyl compounds and NO_2. As each route will form different products, the actual path may be investigated by varying parameters such as the O_2 or the NO_2 concentration. Here we present a re-investigation of the oxidation mechanism following NO_3 addition to *trans*-2-butene in which the oxygen concentration was varied in a systematic way. The aim of the present study was to further investigate this type of oxidation processes. Detailed knowledge of the reactions and the intermediates involved in NO_3 alkene chemistry is essential for assessment of the importance of night time NO_3 tropospheric chemistry.

2. EXPERIMENTAL

The experiments were carried out at 295 K and at 1020 mbar in a 0.153 m^3 static reactor. Reactants and products were measured by long optical path FTIR-spectroscopy using 1.0 cm^{-1}

resolution and an optical path length of 40 m. A more detailed description of the experimental set-up is found in reference [2]. NO_3 radicals were generated by the thermal dissociation of N_2O_5. N_2O_5 was produced either by mixing NO_2 and ozone in the reactor or synthesised from P_2O_5 and HNO_3 and then brought into the cell. Dry nitrogen was used as matrix gas. The oxygen concentration was varied from 0.01 to 100% by adding sufficient amounts of dry O_2. Known amounts of *trans*-2-butene were then introduced into the reactor and the reactions were followed by FTIR. Products were identified and quantified by using reference spectra from authentic compounds.

3. RESULT AND DISCUSSION

Identified products

3-nitroxy-2-butanone, 3-nitroxy-2-butanol, Acetaldehyde, 3-nitro-2-butylnitrate and $HOONO_2$ were identified as products from nitrate radical initiated oxidation of *trans*-2-butene.

Table 1. Product distribution dependence on O_2 concentration

Start concentrations (ppm)				Yields relatively to the *trans*-2-butene reacted (%)			
O_2 (%)	N_2O_5	NO_2	*Trans*-2-butene	Acetaldehyde	3-nitroxy-2-butanone	3-nitroxy-2-butanol	Mass-balance(%)
0.01	7.8	0.6	35.8	58.0	32.7	31.7	93.4
2.4	7.5	5.0	36.0	51.2	37.1	25.9	88.6
21	8.0	2.8	36.0	44.6	40.3	22.3	84.9
60	7.7	3.6	37.2	34.7	39.8	19.3	76.5
100	8.3	2.6	36.1	30.2	40.5	20.5	79.3

Mechanisms

The principal end products formed in experiments made at atmospheric pressure and with O_2 concentrations above 0.01% were 3-nitroxy-2-butanone, 3-nitroxy-2-butanol and acetaldehyde. They are all likely to be formed by self reactions of 3-nitroxy-2-butyl peroxy radicals [3,4] according to reactions (4a) and (4b) followed by reactions (5) and (6). According to Table 1, the yield of 3-nitroxy-2-butanone increased with increasing O_2 concentration. At the same time a decrease in the yields of 3-nitroxy-2-butanol and acetaldehyde was seen. The extra 3-nitroxy-2-butanone yield can be explained by reaction (6) which also gives HO_2 radicals. The presence of HO_2 radicals was indicated by the appearance of $HOONO_2$ (reaction 7), the yield of which showed a positive dependence on the O_2 concentration. Hydrogen peroxy radicals are known to

react with alkyl peroxy radicals [5]. A reaction between HO_2 and 3-nitroxy-2-butyl peroxy radicals, reaction (2), may compete with reaction (4a) and (4b). If reaction (2) produces a stable end product such as 3-nitroxy-2-butyl hydrogenperoxide, a decrease in the formation of 3-nitroxy-2-butanol and acetaldehyde is expected. Thus, such a reaction could explain the observed decrease in acetaldehyde and 3-nitroxy-2-butanol formation with increasing O_2 concentration. Attempts to verify reaction (2) by observing hydrogen peroxy bands in the infrared spectra failed. The spectra did, however show alkylnitrate bands belonging to alkylnitrates other than those identified. By comparison with reference spectra from 2,3-butandintrate it was concluded that these bands could only partly, if at all, be due to 2,3-butandintrate.

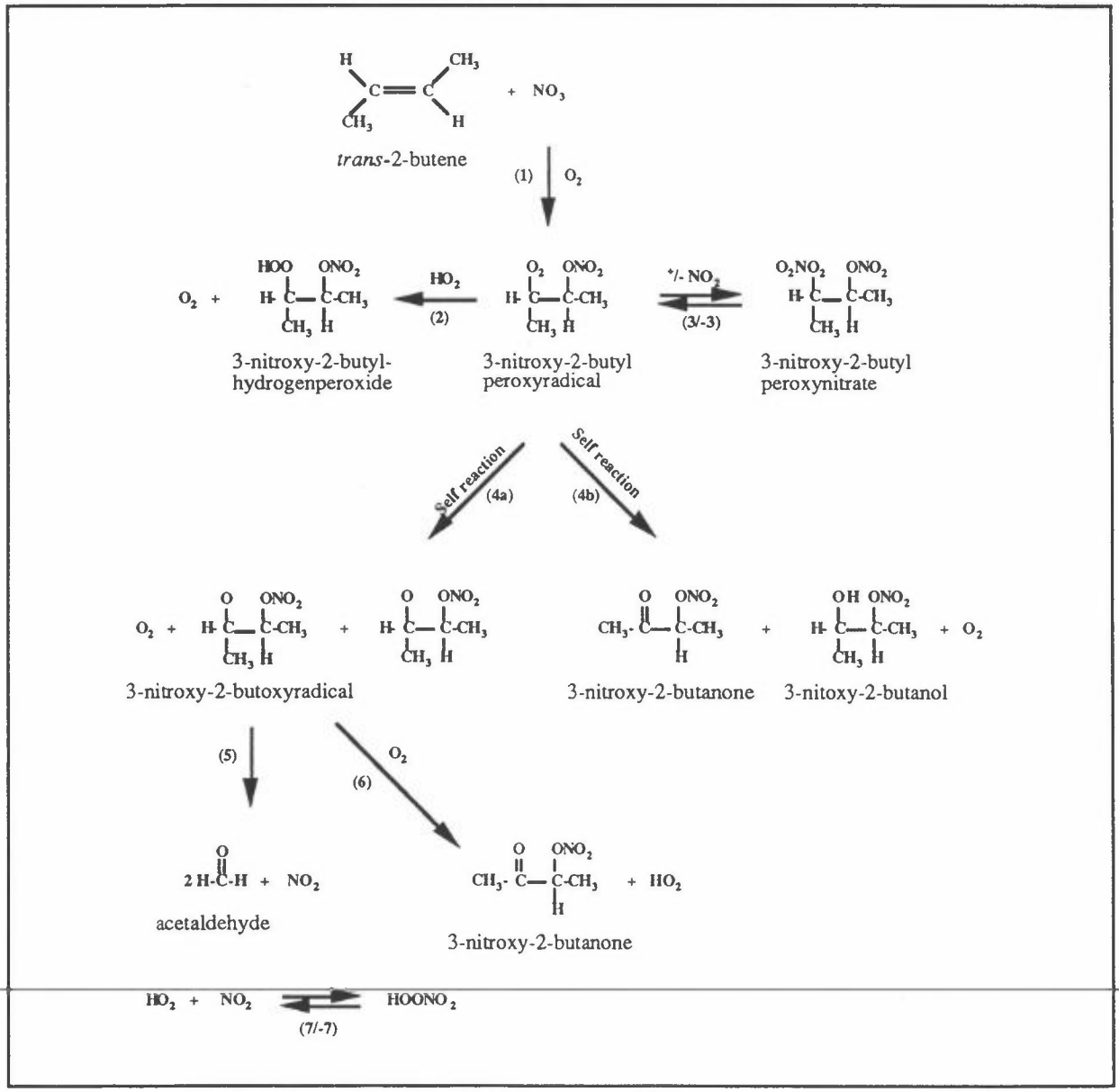

Figure 1. Reaction scheme.

4. CONCLUSIONS

The product distribution for NO_3 initiated oxidation of 2-butene is sensitive to the O_2 concentration. Under tropospheric conditions NO_3 initiated oxidation of 2-butene is expected to predominately yield 3-nitroxy-2-butanone and acetaldehyde, while formation of 2-nitroxy-3-butanol is likely to be less importance. Further work is, however needed to fully understand the atmospheric mechanism following NO_3 addition to 2-butene.

ACKNOWLEDGEMENT

The financial support of the National Swedish Environmental Protection Agency is gratefully acknowledged.

REFERENCES

[1] R.P. Wayne, I. Barnes, P. Biggs, J.P. Burrows, C.E. Canosa-Mas, J. Hjorth, G. LeBras, G.K. Moortgat, D. Perner, G. Poulet, G. Restelli and H. Sidebottom, The Nitrate Radical: Physics, Chemistry and the Atmosphere, Atmos. Environ. 1991, 25A, 1-203.

[2] Wängberg I., Ljungström E., Olsson B. E. R. and Davidsson J., The Temperature Dependence of the Reaction $NO_3 + NO_2 \rightarrow NO + NO_2 + O_2$ in the Range from 296 to 332 K, J. Phys. Chem., 1992, 19, 7640-7645.

[3] Barnes I., Bastian V., Becker K. H. and Tong Z., Kinetics and Products of the Reactions of NO_3 with Monoalkenes, Dialkenes and Monoterpenes, J. Phys. Chem., 1990, 94, 2413-2419.

[4] Hjorth J., Lohse C., Nielsen C. J., Skov H. and Restelli G., Products and Mechanisms of the Gas-Phase Reactions Between NO_3 and a series of Alkenes, J. Phys. Chem., 1990, 94, 7494-7500.

[5] Lightfoot, P. D., Cox R. A., Crowley J. N., Destriau. M., Hayman G. D., Jenkin M. E., Moortgat G. K. and Sabel F., Organic Peroxy Radicals: Kinetics, Spectroscopy and Tropospheric Chemistry, Environ. 26(A), 1992, 1805-1964.

Optical analysis of SO_2 and NO_2 in the products of fuel combustion

M.Ignatavicius, E.Kazakevicius and H.Orshewski
Vilnius University, Naugarduko 24, Vilnius, Lithuania

We report the results of measurements of absorption spectra of SO_2, NO, NO_2 in UV and visible regions. We have used the differential absorption technique based on the difference ofmolecular absorption cross sections in the maximum and minimum of absorption and thus enabling the measurement of air pollutant concentrations. We have employed 2m path length cell and Xenon flash-lamp as the light source for the investigation of gases in our laboratory. The same measurements were carried out in the enterprise "Thermal plant of Alytus ". The absorption cross sections of NO_2 and SO_2 have rather strong temperature dependences. It was possible to determine presence of SO_2 and NO_2 because of a general electronic absorption. As a result of these investigations, a unit for the measurement of sulphur and nitrogen dioxides was designed. The calibration of our unit was performed using "Testoterm" equipment as a reference.

There are more than seventy thermal plants with approximately two hundreds of different boilers for heat, technological steam and electricity production in Lithuania. Main kinds of fuel are natural gas and heavy oil. The technological equipment of these boilers were designed when fuel price was very low in comparison with prices in the world market, besides there was no atention paid to the problems of environment protection. All these circumstances determined the situation when there are no special equipment at the thermal plants for the optimization of boilers perfomance according to the air pollution level by exhausted gases and boilers performance effectiveness. The first step towards the solution of these problems is to design the equipment for the measurement of concentrations of exhausted gases. We consider that utilization of optical spectral analyzers would be one of the best technical solutions, because they haven't expensive and short-lived elements in the construction, the time-period of measurement is almost instant and measurement procedure allows to design absolutely automatic systems with data monitoring from the power-station control room.

There are quite a lot of Western companies producing such optical analyzers, for instance : OPSIS, CODEL, Lear Siegler measurement controls corporation, etc. Equipment made by these companies is quite universal and modern, but the prices of these analyzers are very high : $ 30000 - 120000.

We made efforts to create less universal, but cheaper optical spectral analyzer for the exhausted gases control. The measurement method of analyzer is based on the law of Bouguer - Beer, i.e. if light beam with intensity I_0 is directed to the absorbing medium, the intensity of transmitted light is :

$$I = I_0 \exp(-N \sigma(\nu) x),$$

where N is concentration of absorbing particles, $\sigma(\nu)$ - absorption coefficient, x - medium length.

If we have two light beams with wavelengths ν_1 corresponding to the maximum of medium absorption and ν_2 corresponding to the minimum of absorption, the intensities of transmitted beams are :

$$I_1 = I_{01} \exp(-N \sigma(\nu_1) x) ;$$

$$I_2 = I_{02} \exp(-N \sigma(\nu_2) x) .$$

Then the concentration of absorbing particles is :

$$N = \frac{\ln \frac{I_1 + I_{02}}{I_2 + I_{01}}}{\left[\sigma(\nu_1) - \sigma(\nu_2)\right]} = K \ln \frac{I_1}{I_2}$$

As can be seen from the equation, the concentration of molecules can be evaluated after the measurement of transmitted light intensities in the maximum and the minimum of absorption and after the determination of constant K. This concentration can be measured directly in the absolute units [cm^{-3}] or optical analyser can be calibrated by using other, for example chemical, methods . Second approach is more convinient and even more precise, because it is quite complicated to carry out absolute optical measurements with great precision.

The main part of air pollutants exhausted by thermal plants is carbon, sulphur and nitrogen oxides. In the begining of our investigations the sulphur and nitrogen dioxides were chosen as an object of measurement, they have electronic-vibrational bands in the region of visible and near UV light where spectral measurement devices are cheaper than in the infrared region. Two- meter length and 0,13 m^3 volume vacuum cell was made in order to imitate boiler smoke-tube. In the procedure of measurement this cell has been filled with proper concentration of gases.

Using this experimental setup the spectral characteristics of SO_2, NO_2 and other gases as well as dependence of spectra on concentration of proper gas have been investigated.

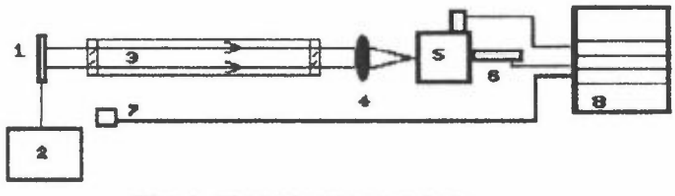

Fig 1. Experimental setup.
1-pulse lamp, 2-lamp power supply,3- gas cavity,4-lens, 5-monochromator,6- photomultiplier, 7-photodiod,8-computer

In the real smoke-tube, where the temperature reaches 150 - 200 C , the absorption spectra suffers some changes - the vibrational bands of molecules become wider. Such a thermal deformation of absorption spectra allowed to simplicize the construction of gas analyzer. Selection of broadened bands can be performed by interference filters instead of more expensive monochromators. Accuracy of such measurement is less, because the part of electronic spectrum has to be used as a reference signal instead of vibrational structure. According to the results of our measurements the region with minimal SO_2 , NO_2 and NO absorption is around 620 nm.

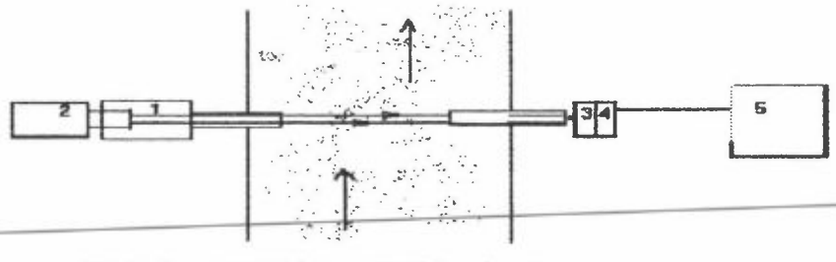

Fig 2. Experimental optical analyser.
1- pulse lamp, 2- power supply, 3- interference filters, 4-photodiods, 5-microcomputer

On the basis of these investigations the concentration measurement unit for SO_2 and NO_2 gases was created. This unit was tested in the smoke-tube of boiler of Alytus thermal plant.

Analyzer performance can be shortly described in such a way: beam of pulsed lamp (continuous spectrum) crosses smoke-tube, interference filters select relevant parts of spectrum and photo-diodes detect the selected light. Analog signal is changed to the digital one and value of this signal is placed into the memory. After collection of several hundreds single measurements, the mean value of concentration is shown in the unit display. If analizer is conected with computer, it is possible to control unit from computer directly.

Due to the calibration problem, the concentrations of gases were measured in arbitrary units. In order to evaluate absolute values of concentrations, a set of experiments were performed using our unit together with electrochemical analyzer Termo 33. Using both analyzers the concentrations of SO_2 and NO_2 gases were measured in different modes of boiler performance (α parameter).

Correlations of two measurements are shown in the fig. 3 and fig.4. As can be seen from fig.3 the results of measurements of NO using both analyzers are in good agreement. On the other hand SO concentration measurement results differ quite a lot.

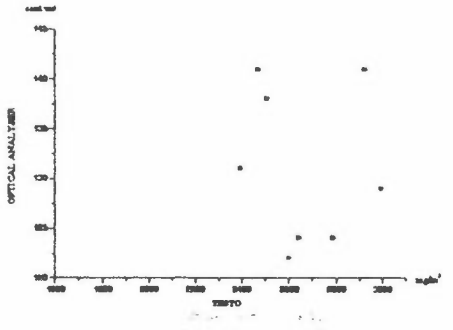

Fig.3 SO_2 measurement calibration

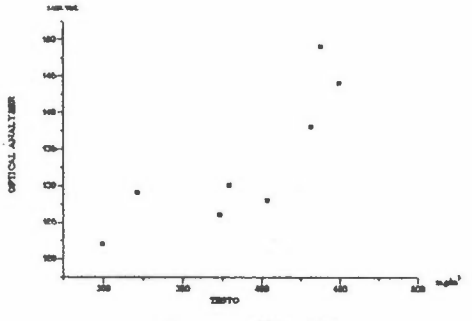

Fig.4 NO_2 measurement calibration

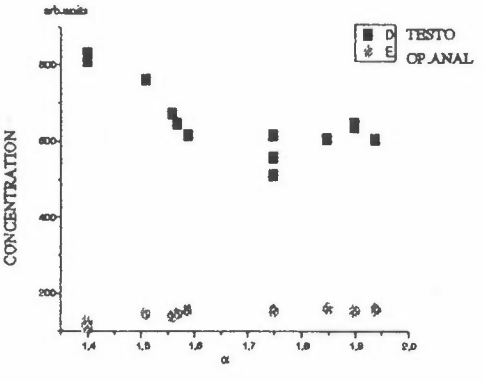

Fig.5. Measurment of SO_2 as function of α (abundance of oxygen).

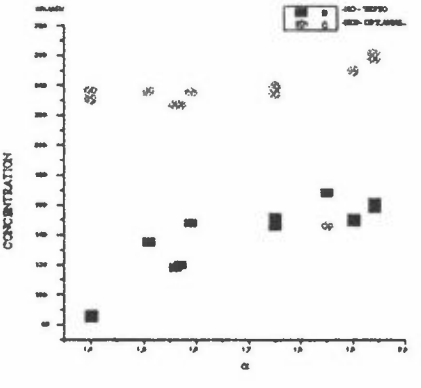

Fig.6.Measurment of NO and NO2 as function of α (abundance of oxygen).

Next set of measurements was carried out using other analyzer Termo 33 (fig, 5, 6). This unit was able to measure NO concentration instead of NO , so that it was possible to compare dependences of NO and NO_2 concentrations on boiler performance mode. It is self evident that these measurements can not be considered as a calibration procedure. It is also must be pointed out that measurement procedures using optical and electrochemical analyzers are different. Optical unit measures the number of absorbing molecules in the smoke-tube, i.e. mean value of concentrations accross the tube. Termo unit takes proper amount of gas from special place in the tube, so that the result of measurement is correct only for concrete place and concrete time. Due to airstream turbulence in the tube, the results of such measurements can be different.

In order to improve analyzer`s sensitivity, reliability and mobility, the optical and mechanical structure of our unit was changed. Special imitator of smoke-tube is being produced for the calibration procedure. It will be possible to change widely gas concentration and measure this concentration using chemical methods.

Recently some scientific attempts were made to create cheap optical analyzer for CO_2- CO gases. Utilization of NO - NO_2 - SO_2 - CO_2 - CO express analyzer would allow not only to control the boiler`s exhaust but also to control the burning procedure itself and to find the most effective way for boiler`s performance.

REACTION OF THE NITRATE RADICAL WITH SOME ALIPHATIC ETHERS

Sarka Langer and Evert Ljungström
Department of InorganicChemistry
University of Göteborg
S-412 96 Göteborg, Sweden

SUMMARY

Rate coefficients for reaction between the nitrate radical and dimethyl ether, diethyl ether, di-*n*-propyl ether and methyl-*t*-butyl ether (MTBE) have been determined at 295 K using both absolute and relative techniques. The rate coefficients determined by the fast flow-discharge technique were 0.26±0.11, 2.80±0.23, 6.49±0.65 and 0.64±0.06 (in units of 10^{-15} cm^3 $molecule^{-1}$ s^{-1}) for dimethyl ether, diethyl ether, di-*n*-propyl ether and MTBE, respectively. The rate coefficients for the reaction between nitrate radicals and the organic radicals, formed in the primary abstraction step, which is a possible secondary process, were estimated experimentally to fall in a range between 100 and 500x10^{-15} cm^3 $molecule^{-1}$ s^{-1}.

INTRODUCTION

Today there is little doubt about the key role of the nitrate radical in night-time tropospheric chemistry. Unsaturated hydrocarbons react readily with the nitrate radical *via* double bond addition and this reaction is often an important night time sink for such compounds. Saturated organic substances and their derivatives have received less attention because of their relative inertness. In this case, the nitrate radical attack proceeds *via* hydrogen atom abstraction. This is a slow process which contribute little to the night-time destruction of such hydrocarbons. However, nitrate radical reaction with saturated hydrocarbons, including compounds containing various functional groups, is a night time source of nitric acid. It is therefore important to know reaction rates and their temperature dependencies in order to assess the contribution to acid deposition.

The increasing use of ethers, especially methyl-*t*-butyl ether (MTBE), as automotive fuel additives causes increasing emissions of these compounds to the atmosphere. Nowadays, MTBE is the 8th most produced organic compound in the world. 25% of all

gasoline in Sweden contains MTBE at an average concentration of 4%, which means annual use of 60,000 metric tons of this compound.

Atmospheric destruction of the ethers proceeds during day-time *via* reaction with the hydroxyl radical. During night-time, the nitrate radical is a possible oxidising agent but almost nothing is known about the reaction rates at present. In this contribution, results are reported for reaction of the NO_3 radical with dimethyl ether, diethyl ether, di-*n*-propyl ether and methyl-*t*-butyl ether (MTBE) at 295 K.

EXPERIMENTAL

Fast flow-discharge - ether-NO_3 experiments

Conventional fast flow - discharge technique was used. NO_3 radicals were generated by reaction of nitric acid with fluorine atoms in helium and were detected optically at 662 nm. All experiments were performed under pseudo-first order conditions. The experimental pressures employed were between 2.5 and 6 mbar, the flow velocities were between 400 and 1400 cm s^{-1} and the experimental temperature was 295 K. The initial NO_3 concentration was around 1.5×10^{13} molecules cm^{-3} and the ether concentrations covered the interval from 0.2×10^{15} to 18.5×10^{15} molecules cm^{-3}.

Relative rate experiments

A 153 l reaction chamber equipped with a 2 m base-path White optical system was used for the relative rate experiments. The concentration of the ethers and of suitable reference compounds were followed by FTIR spectroscopy using an optical path length of 40 m. NO_3 radicals were generated by thermal decomposition of N_2O_5 which, in turn, was prepared *in situ* by reacting ozone with an excess of nitrogen dioxide. The experiments were made in synthetic air at 1000 mbar at 295K. The concentration of the reactants were in the following ranges: [Ether] and [Reference] between 2.5×10^{14} and 5×10^{14} molecule cm^{-3}, [N_2O_5] between 4×10^{14} and 6×10^{14} molecule cm^{-3}

Fast flow-discharge - radical-radical reaction experiments

A second discharge cavity was used to generate chlorine atoms which were reacted with the ethers to give the primary ether radical Ether ·, simulating the primary radicals from ether-nitrate radical reactions. The yield of atomic chlorine and thus of ether radicals was determined in separate experiments by reacting the chlorine atoms with an excess of chlorine nitrate according to:

$$Cl\cdot + ClNO_3 \rightarrow Cl_2 + NO_3.$$

The NO_3 produced was quantified by measuring its absolute concentrations using a σ of $(1.42\pm0.06)\times10^{-17}$ cm^2 $molecule^{-1}$ (base *e*) from an "in house" calibration. Other experimental conditions were identical to those employed in the FFD experiments with one discharge facility. Rate coefficients $k_{sec.}$ for the reaction

Ether · + NO_3 ---> Products

were estimated from the known, initial ether radical and nitrate radical concentrations, assuming a 1:1 stoichiometry and measuring the remaining nitrate radical concentration after a known reaction time.

RESULTS

Table 1 gives the measured rate coefficients.

Table 1. Summary of the determined rate coefficients. All k in units of 10^{-15} cm^3 $molecule^{-1}$ s^{-1}.

	FFD experiments		Relative Rate experiments		Estimated Ether·+NO_3
Compound	k_{ether}	reference	$k_{ref.}$	k_{ether}	$k_{sec.}$
dimethyl ether	0.26±0.11	n-hexane	0.147	0.26±0.02	500
diethyl ether	2.80±0.23	acetaldehyde	2.74	2.58±0.85	200
di-*n*-propyl ether	6.49±0.65	1-chloro-2-butene	21	6.62±0.66	100
MTBE	0.64±0.06	acetaldehyde	2.74	0.68±0.34	200

CONCLUSIONS

The rate coefficients determined in fast flow-discharge experiments are in a good agreement with the results from relative rate experiments. This shows that the fast-flow data are free from influence from secondary reactions. The reaction of ethers, both with OH and NO_3 radicals proceeds faster than reaction with the corresponding alkanes (1,2). This is caused by the -O- ether structure that weakens adjacent C-H bonds. However, even when this effect is taken into consideration, the reaction of ethers with the NO_3 radical appears to be anomalously fast.

Atmospheric lifetimes for MTBE with respect to the reaction with the hydroxyl and nitrate radical, respectively, may be calculated using the rate constants:

k_{OH} = (3.24±0.08)x10^{-12} (3) and k_{NO3} = (6.4±0.6)x10^{-16} (this work) (in units cm^3 $molecule^{-1}$ s^{-1}). Assuming atmospheric concentration of [OH] = 1x10^6 cm^{-3} and [NO_3] = 1x10^9 cm^{-3}, the lifetimes are 3.5 and 18 days, respectively.

REFERENCES

(1) R.P. Wayne, I. Barnes, P. Biggs, J.P. Burrows, C.E. Canosa-Mas, J. Hjorth, G. Le Bras, G.K. Moortgat, D. Perner, G. Poulet, G. Restelli and H. Sidebottom, *Atmos. Environ.* , 1991, **25A**, 1.

(2) R. Atkinson, *Int.J.Chem.Kin.*, 1987, **19**, 799.

(3) T.J. Wallington, J.M. Andino, L.M. Skewes, W.O. Siegl and S.M. Japar, *Int.J.Chem.Kin.*, 1990, **22**, 1111.

MOLECULAR COMPLEXES OF NITRIC ACID WITH VARIOUS BASES STUDIED BY MATRIX ISOLATION INFRARED SPECTROSCOPY

Emilie Lasson[a], Austin J. Barnes,[b] and Claus J. Nielsen[a]
a Department of Chemistry, University of Oslo,P.O. Box 1033 Blindern, N-0315 Oslo
b Department of Chemistry and Applied Chemistry,University of Salford, Salford M5 4WT

Abstract

The interaction of nitric acid with a number of bases has been investigated by infrared spectroscopy in low-temperature matrices (principally argon). The spectra show that nitrogen interacts strongly and specifically with nitric acid in argon matrices. Carbon monoxide behaves in a similar manner to nitrogen, forming complexes of the type $O{\equiv}C\cdots H\text{-}ONO_2$. Preliminary studies of nitric oxide with nitric acid shows similar behaviour to carbon monoxide. With water and dimethyl ether, hydrogen-bonded complexes of the type $R_2O...H\text{-}ONO_2$ were formed, and with ammonia a similar complex $H_3N\cdots H\text{-}ONO_2$ was apparent. The strength of interaction, as evidenced by the shifts in the O-H vibrational modes of the nitric acid, increased from nitrogen, through nitric oxide,carbon monoxide, water and dimethyl ether, to ammonia.

Introduction

Nitric acid is an important atmospheric species, acting as a stratospheric reservoir for NO_X; its relative stability allows it to be transported down to the troposphere where eventually it is rained out of the atmosphere. It is a fundamental constituent of polar stratospheric clouds, and it can also be incorporated into aerosols by reaction with ammonia to form ammonium nitrate.

The aim of the present work is to investigate the hydrogen bonding interaction of nitric acid with a number of bases, in particular species where the complexes may play a role in atmospheric chemistry. These range from the comparatively weakly interacting nitrogen to the potentially strongly interacting ammonia.

Experimental

Nitric acid was prepared by vacuum distillation from a 50:50 mixture of concentrated sulphuric acid and potassium nitrate and collected at -40 °C. For the weaker bases, a mixture of base, nitric acid and matrix gas (argon) was prepared using standard manometric techniques. For the stronger bases, separate mixtures of base - matrix gas (argon or nitrogen) and nitric acid - matrix gas were prepared. In a typical experiment, the mixture(s) were sprayed simultaneously onto a cesium iodide window maintained at 15K by an Air Products HS-4 Heliplex refrigeration system so as to give an overall ratio of ca. 1:1:200. Infrared spectra were recorded, with the matrix maintained at ca. 5K, at 1 cm^{-1} resolution using a Bruker IFS-88 Fourier transform infrared spectrometer.

Results

The spectra obtained in the present work for nitric acid isolated in argon and nitrogen matrices agree well with those previously reported.[1,2,3] The fundamental frequencies for the OH vibrations in argon are found at at 3522 cm^{-1} (OH stretch), 1304 cm^{-1} (NOH in plane bend) and 451 cm^{-1} (NOH torsion).

Nitrogen - nitric acid complexes

Spectra of nitrogen : nitric acid : argon matrices at concentrations around 1:1:200, deposited at 15K, showed a number of prominent new absorptions. The most intense new band in the OH stretching region was at 3488 cm^{-1}, a medium intensity band appeared at 3484 cm^{-1} and there were other weak absorptions on both the high and low wavenumber sides of these bands. Deposition of a 1:1:200 mixture at 5K led to very little complex being formed, while deposition of a similar mixture at 20K had a dramatic effect on the spectrum: there was practically no trace of monomer nitric acid, the 3488 cm^{-1} band was very intense, but the 3484 cm^{-1} band had disappeared.

Similar behaviour was evident in the NOH torsion region of the spectrum. In this region the strongest band was at 526 cm^{-1} with a somewhat weaker band at 534 cm^{-1}, which disappeared in the spectrum of a mixture deposited at 20K. A number of weaker absorptions were apparent on either side of the main band.

New bands attributed to the NOH in-plane bending mode appeared in the region of ca. 1350-1340 cm^{-1} and showed similar characteristics. The most intense band was at 1346 cm^{-1}, with a weaker band at 1350 cm^{-1} which disappeared in the spectrum of the matrix deposited at 20K.

Carbon monoxide - nitric acid complexes

Spectra of carbon monoxide : nitric acid : argon matrices showed rather similar behaviour to that observed for nitrogen : nitric acid : argon matrices. In the OH stretching region (Figure 1), the most intense new band was located at 3399 cm^{-1} while two bands, at 3390 and 3369 cm^{-1}, became much less intense in the spectrum of a matrix deposited at 20K. A number of weaker bands appeared on the low wavenumber side of the principal band. In the NOH torsion region, the strongest band was at 589 cm^{-1}, with a somewhat weaker band at 600 cm^{-1} which became much less intense in the spectrum of the matrix deposited at 20K. A number of weaker absorptions appeared on both the high and low wavenumber side of the main band. The bands observed in other regions of the nitric acid spectrum were very similar to those observed for nitrogen - nitric acid complexes.

In the C≡O stretching region, a number of bands appeared on the high wavenumber side of the isolated C≡O stretching mode at 2139 cm^{-1} (and also the aggregate band at 2143 cm^{-1}).

The most intense new band was at 2164 cm^{-1}, with a band at 2167 cm^{-1} becoming much less intense in the spectrum of the matrix deposited at 20K.

Nitric oxide - nitric acid complex

A 1:1:200 mixture og nitric oxide : nitric acid : argon also revealed several new absorptions. In the OH stretching region the main peak appeared at 3404 cm^{-1} with a weaker peak on the high frequency side at 3414 cm^{-1} and a fairly strong peak at 3377 cm^{-1} also with a weaker feature on the high frequency side at at 3385 cm^{-1}. Other new bands associated with the OH vibrations were found at 1360 cm^{-1} (NOH in plane bend) and at 588 cm^{-1} (NOH torsion). The unperturbed N-O stretching fundamental was found at 1872 cm^{-1} under our experimantal conditions, and in the complex it was shifted up in frequency to 1889 cm^{-1}.

Nitrogen dioxide - nitric acid complex

Although the nitric acid, prepared as described in the Experimental section, was apparently pure, varying amounts of nitrogen dioxide were observed in spectra (presumably due to surface reaction on the walls of the deposition line) giving rise to a band at 1611 cm^{-1}. Comparison of spectra containing substantial quantities of NO_2 with those containing very little suggested that bands at 3441, 1606 and 561 cm^{-1} should be assigned to the perturbed O-H stretch, the antisymmetric stretch of the NO_2 molecule and the NOH torsion, respectively, of the $NO_2 \cdots HNO_3$ complex.

Water - nitric acid complex

An approximately 1:1:200 water : nitric acid : argon matrix, obtained by simultaneous deposition, exhibited new bands in the regions of both water and nitric acid absorptions. The O-H stretching region of nitric acid showed new, relatively broad, bands at 3130, 3024, 2981 and 2784 cm^{-1}; a very broad absorption extending from ca. 3400 to 2200 cm^{-1} grew in intensity when the matrix was annealed. The NOH in-plane bend appeared at 1412 cm^{-1} and the NOH torsion at 900 cm^{-1}. The OH asymetric stretch of water was shifted from 3733 to 3718 cm^{-1}, and the bending mode from 1590 to 1582 cm^{-1}.

Dimethyl ether-nitric acid complex

When a 1:1:200 mixture of dimethyl ether : nitric acid and argon was deposited at 15K a broad new band, likely to be the OH strech of the complex was centered at 2570 cm^{-1}. Other new features appeared at 1423 and at 1081 cm^{-1}.

Ammonia - nitric acid complex

The spectrum of an approximately 1:1:200 ammonia : nitric acid : argon matrix, obtained by simultaneous deposition, reveals several new features. There are prominent new absorptions at 1616 cm^{-1}, 1460 cm^{-1} (with a weak component at 1453 cm^{-1}) and 1286 cm^{-1}, and weaker features at 1117 cm^{-1} and 786 cm^{-1}. The absorptions can all reasonably be assigned to various perturbed vibrations of the nitric acid or ammonia moieties. The perturbed O-H stretching vibration was not easy to observe, but was eventually identified as a broad structured apsorbtion around 1870 cm^{-1} .

Discussion

The strength of complexation between nitric acid and various bases is reflected in the shift of the OH stretching frequency, Table 1 and Figure 1. Nitrogen is the weakest bound complex, but even so the magnitude of the shifts indicates a pseudo hydrogen bonded complex. Because of the many bands there are probably several 1:1 complexes.[4] As expected interaction between CO and nitric acid is stronger, but otherwise similar to that of nitrogen. The C≡O streching mode is shifted to higher wavenumber indicating that the interaction is of the type $O{\equiv}C\cdots H\text{-}ONO_2$ as found for other CO complexes, for example with the hydrogen halides.[5,6,7] The NO interaction is similar in strength to that of CO, and also here there are several distinct absorptions in the OH stretching region due to this interaction For NO a complexation with the dimer must be considered, since it readily forms during 15K deposition.[8] The complexes between N_2, CO, NO and nitric acid are all weak, that is the hydrogen only interacts slightly with the base, but keeps it main bonding character to the acid.

For the water complex three of the four bands in the OH region can be explained as combination bands and the perturbed OH stretch lies at approximatly 3000 cm^{-1}. This shift, compared to the small one for the stretching frequencies in the water molecule, clearly indicates that nitric acid bonds to the water which acts as the base. The dimethyl ether complexed to nitric acid behaved as expected, bonding stronger than water and weaker than ammonia which is by far the strongest base in this series. These three molecules form stronger hydrogen bonded complexes with nitric acid where the hydrogen is shared between the acid and the base.

Nitric acid bonds with varying strength to all the molecules discussed here, even the weakly interacting nitrogen molecule. Nitric acid and ammonia form a relatively strong complex, but under our experimental conditions where there is no stabilisation from a surrounding solvent they do not react to form ammonium nitrate.

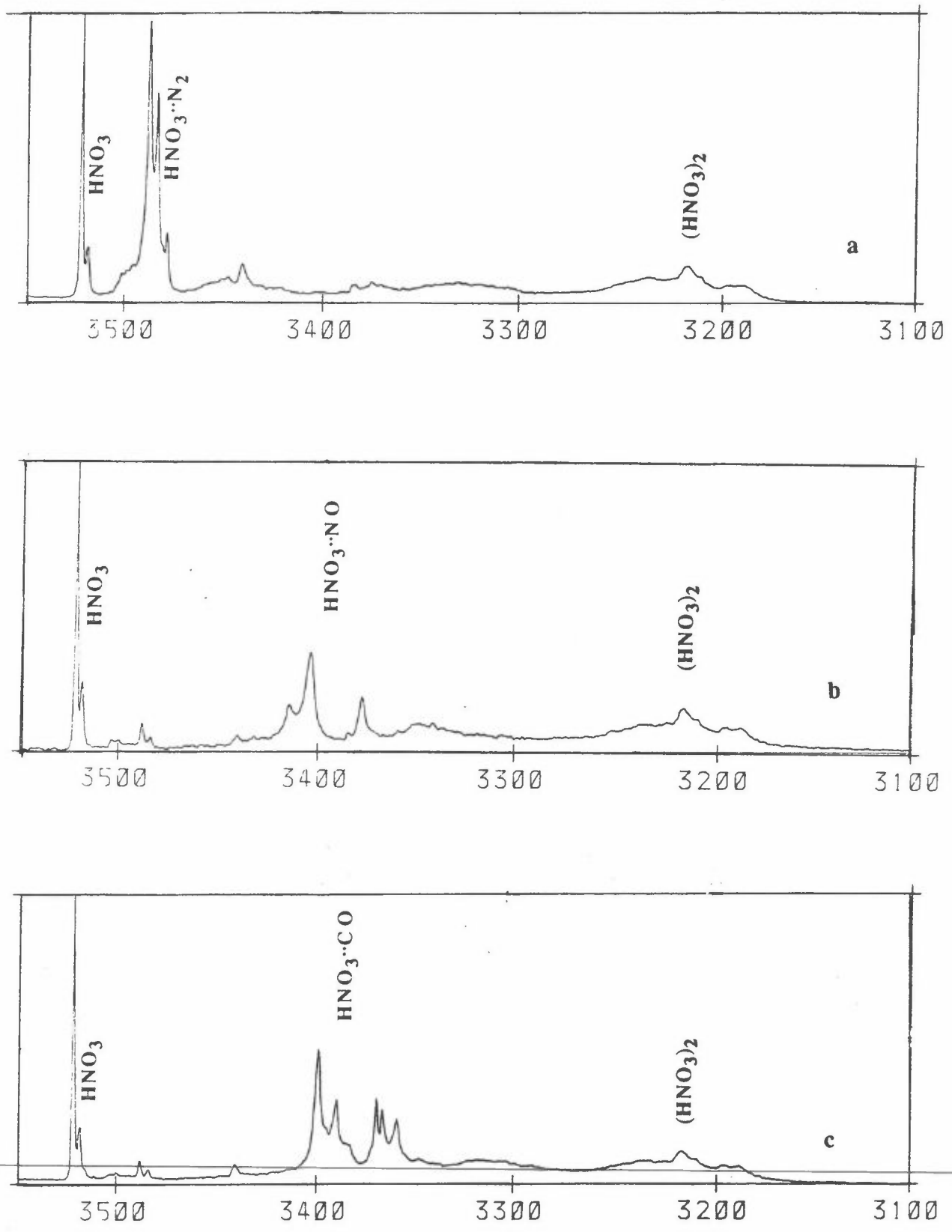

Figure 1. The OH streching area for the complexes of nitric acid with a) nitrogen, b) nitric oxide and c) carbon monoxide.

Table 1. Shifts (cm^{-1}) in the OH vibrational modes of nitric acid complexed with various bases.

Base	OH strech	NOH in-plane bend	NOH torsion
Nitrogen	-34	+42	+75
Nitrogen dioxide	-81		+110
Nitric oxide	-118	+56	+137
Carbon monoxide	-123	+75	+138
Nitric acid	-306	+76	+242
Water	-500	+108	
Dimethyl ether	-950	+119	
Ammonia	-1650	+156	

References

1 W.A. Guillory and M.L. Bernstein, J. Chem. Phys., 62 (1975) 1058.

2 B.-M. Cheng, J.-W. Lee and Y.-P. Lee, J. Phys. Chem., 95 (1991) 2814.

3 W.-J. Chen, W.-J. Lo, B.-M. Cheng and Y.-P. Lee, J. Chem. Phys., 97 (1992) 7167.

4 A.J. Barnes, E. Lasson and C.J. Nielsen, to be published.

5 A.C. Legon, P.D. Soper, M.R. Keenan, T.K. Minton, T.J. Balle and W.H. Flygare, J. Chem. Phys., 73 (1980) 583.

6 A.J. Barnes, H.E. Hallam and G.F. Scrimshaw, Trans. Faraday Soc., 65 (1969) 3172.

7 L. Andrews, R.T. Arlinghaus and G.L. Johnson, J. Chem. Phys., 78 (1983) 6347.

8 H.E. Hallam, Vibrational Spectroscopy of Trapped Species, John Wiley and Sons (1973)

Investigation of the Thermal Reactions of NO_2 with CH_3SH and CH_3OH

ANDERS LUND, K. FAGERSTRÖM AND G. MAHMOUD
IFM, LINKÖPING UNIVERSITY

E. RATAJCZAK
DEPT. OF PHYSICAL CHEMISTRY
MEDICAL ACADEMY, WROCLAW

P. PAGSBERG AND A. SILLESEN
RISØ NATIONAL LABORATORY

The kinetics of the thermal reactions of NO_2 with CH_3SH and CH_3OH have been studied in static systems with different surface/volume ratios by UV spectroscopy and IR diode laser spectroscopy at six temperatures between 297 and 365 K, and in the pressure range of 20-500 mbar. The NO_2 decay profiles, in the large excess of CH_3SH and CH_3OH, were fitted to a double exponential with a standard non-linear procedure. The values of the rate constants derived should be considered as upper limits to the homogenous gas-phase reactions.

The first mechanistic study of the reaction between NO_2 and CH_3SH was performed by Balla and Heicklen [1] using mass spectrometry. In the present studies we employed IR and GC/MS methods for analysis of the products. The nature of the reaction depends on the reaction conditions.

[1] R.J. Balla and J. Heicklen, J. Phys. Chem., 88, 6314 (1984)

Wide Range Particle size Spectrometry and Atmospheric Pollution analysis

AADU MIRME
DEPT. OF ENVIRONMENTAL PHYSICS
TARTU UNIVERSITY

Particulate pollution is a minor but important part of the air pollution. The effect of particulate pollution differs from that of gaseous pollution because of the different composition and deposition. In order to study the aerosol sources and model the polluting effect, information on both, particle size distribution and distribution of polluting substances in particles is needed.

Wide range Electric Aerosol Spectrometer (EAS) measures aerosol distribution in nearly full range of particle sizes. The features of EAS allow it to be used for analysis of particles composition.

Distribution of a substance can be evaluated if measurements of EAS are combined with those of an instrument measuring total concentration of the substance in the aerosol and the variances of the results are analyzed. Classification of particles according to their sizes and deposition on electrodes inside EAS can be used for collecting size selected samples of particles for chemical composition analysis. The distribution of elementary Black Carbon (BC) measured by Aethalometer, was estimated to be proportional to particle surface with some dependence on local polluting activities. The matter of particles was detected in fractions with particle diameters 70 nm and larger in aerosol samples collected by EAS from laboratory air.

ATMOSPHERIC CHEMISTRY OF HFCs

Ole John Nielsen, Jens Sehested and Thomas Ellermann
Chemical Reactivity Section,
Environmental Science and Technology Department
Risø National Laboratory, DK-4000 Roskilde, Denmark

and

Timothy J. Wallington
Research Staff, SRL-E3083, Ford Motor Company
Dearborn, P. O. Box 2053, Michigan 48121-2053, USA

SUMMARY

As part of a collaborative study between Risø and Ford on the atmospheric fate of hydrofluorocarbons (HFCs), we have conducted experimental studies of a series of HFCs: CH_3F, CH_2F_2, CHF_3, CF_3CFH_2, CF_2HCF_2H, and CF_3CF_2H. A pulse radiolysis technique was used to measure the UV absorption spectrum, self reaction kinetics, and the rate of reaction with NO of the peroxy radicals. The products following the self reaction of the peroxy radicals were determined using a FTIR spectrometer coupled to an atmospheric reactor. Selected results especially on the halogenated alkyl peroxy radicals from both experimental systems are reported in this presentation.

1. INTRODUCTION

By international agreement, industrial production of CFCs will be phased out. HFCs are one class of potential CFC substitutes. Prior to large scale industrial use, it is important to establish the environmental impact of the release of HFCs into the atmosphere. Following release, HFCs will react with OH radicals in the lower atmosphere to produce fluorinated alkyl radicals which will, in turn, react with O_2 to give peroxy radicals. There is relatively little information available concerning the atmospheric fate of the fluorinated alkyl peroxy radicals. Also the atmospheric oxidation of HFCs, like HFC-134a (CF_3CFH_2) and HFC-125 (CF_3CF_2H) containing a CF_3-group, are known to produce CF_3O_2 radicals [1,2]. Because HFC-134a is a potential substitute for CFCs in cooling systems, a substantial production of this compound is likely to occur before the year 2000. Consequently, investigation of the fates of HFC-134a, CF_3O_2 and CF_3O in the atmosphere have been the subject to a substantial international research effort.

2. EXPERIMENTAL

Two different experimental systems were used as part of the present work. A pulse radiolysis transient UV kinetic spectrometer was used to study e.g., the UV absorption spectrum and self reaction kinetics of RO_2 radicals, while a Fourier transform infrared (FTIR) spectrometer was used to investigate the products follow-

ing the self reaction of RO_2 radicals. The experimental systems have been described in detail in previous publications [3,4] and will only be discussed briefly here.

Peroxy radicals were generated by the radiolysis of $SF_6/O_2/HFC$ gas mixtures in a one liter stainless steel reactor with a 30 ns pulse of 2 MeV electrons from a Febetron 705B field emission accelerator. SF_6 was always in great excess and was used to generate fluorine atoms:

$$SF_6 + 2\text{-MeV } e^- \rightarrow F + \text{product} \quad (1)$$

$$F + HFC \rightarrow R + HF \quad (2)$$

$$R + O_2 + M \rightarrow RO_2 + M \quad (3)$$

Two sets of experiments were performed using the pulse radiolysis system. First, the ultraviolet absorption spectrum of RO_2 radicals was measured by observing the maximum in the transient UV absorption at short times (10-40μs). Second, using a longer time scale (0.5-2 ms), the subsequent decay of the absorption was monitored to determine the kinetics of reaction (4):

$$RO_2 + RO_2 \rightarrow \text{products} \quad (4)$$

To monitor the transient UV absorption, the output of a pulsed 150 Watt xenon arc lamp was multi-passed through the reaction cell using internal White cell optics (40 cm path-length). Reagent concentrations used were; SF_6, 948 mbar; O_2, 2 mbar; and HFC 50 mbar. All experiments were performed at 298±2K.

The FTIR system was interfaced to a 140 liter pyrex reactor. Radicals were generated by the UV irradiation of mixtures of HFC and Cl_2 in air at 700 torr total pressure at 298K using 22 blacklamps (GE-BLB-40). The loss of reactants and the formation of products were monitored by FTIR spectroscopy, using an analyzing path-length of 28 meters and a resolution of 0.25cm^{-1}. Infrared spectra were derived from 128 co-added spectra. Reference spectra were acquired by expanding known volumes of a reference material into the reactor.

3. RESULTS AND DISCUSSION

The UV spectra of CH_2FO_2, CHF_2O_2, CF_3O_2, $CF_3CF_2O_2$, $CF_2HCF_2O_2$, and CF_3CFHO_2 radicals were measured using the pulse radiolysis technique. After the pulse radiolysis of $HFC/O_2/SF_6$ mixtures a rapid increase in absorption in the ultraviolet was observed, followed by a slower decay. No absorption was observed in the absence of SF_6. We ascribe the UV absorption following radiolysis of $HFC/O_2/SF_6$ mixtures to the formation of fluorinated peroxy radicals and their subsequent loss by self reaction.

To illustrate some typical data we present here detailed results for CH_2FO_2 [5]. Results for CHF_2O_2 [6], CF_3O_2 [7], $CF_3CF_2O_2$ [2], $CF_2HCF_2O_2$ [8], and CF_3CFHO_2 [9] radicals are available elsewhere.

Measurement of absolute absorption spectra requires calibration of the initial F atom concentration. Additionally, experimental conditions have to be chosen such that there is stoichiometric conversion of F atoms to the appropriate radical. The yield of F atoms was established by two techniques. First, by monitoring the transient absorption at 216.4 nm due to methyl radicals produced by radiolysis of SF_6/CH_4 mixtures and using a value of 4.12×10^{-17} $cm^2molecule^{-1}$ for $\sigma(CH_3)$ at 216.4 nm [10]. Second, by monitoring the transient absorption at 250 nm due to CH_3O_2 radicals following radiolysis of $SF_6/CH_4/O_2$ mixtures and using $\sigma(CH_3O_2)=3.92\times10^{-18}$ $cm^2molecule^{-1}$ at 250 nm [11]. Values of $[F]_o$ derived from both methods differed by less than 10%.

To work under conditions where the F atoms are converted stoichiometrically into CH_2FO_2 radicals, it is necessary to consider potential interfering secondary chemistry. Potential complications include: (ii) competition for the available F atoms by reaction with molecular oxygen;

$$F + O_2 + M \rightarrow FO_2 + M \quad (5)$$

(ii) reaction of CH_2F radicals with CH_2FO_2 radicals:

$$CH_2F + CH_2FO_2 \rightarrow CH_2FO + CH_2FO \quad (6)$$

and (iii) reaction of F atoms with CH_2F and/or CH_2FO_2 radicals:

$$F + CH_2F \rightarrow \text{products} \quad (7)$$

$$F + CH_2FO_2 \rightarrow CH_2FO + FO \quad (8)$$

The rate constant for reaction (5) has been measured previously in our laboratory [12], $k_5 = 1.4$ and 2.0×10^{-13} $cm^3molecule^{-1}s^{-1}$ at 600 and 1000 mbar of SF_6 diluent, respectively. There are no literature data concerning the kinetics of reactions (6-8). Hence, we cannot calculate their importance. Instead, to check for the presence of complications in our experiments caused by unwanted radical-radical reactions, two series of experiments were performed. First, the transient absorption at 240 nm was observed in experiments using $[CH_3F] = 10$ mbar, $[O_2] = 40$ mbar, and $[SF_6] = 550$ mbar with the radiolysis dose varied by over an order of magnitude. Figure 1 shows the observed maximum of the transient absorption of CH_2FO_2 at 240 nm as a function of the dose. Second, the maximum in the transient absorption was measured in experiments using full dose, $[CH_3F] = 10$ mbar, $[O_2] = 40$ mbar with the SF_6 concentration varied between 50 and 950 mbar. Figure 2 shows the maximum absorption at 240 nm plotted as a function of SF_6 concentration. From Figure 1 and 2 it can be seen that, with the exception of the data obtained using full dose and SF_6 concentrations greater than 600 mbar, the initial absorption was linear with both the radiolysis dose and the SF_6 concentration. Under our experimental conditions, the formation of CH_2FO_2 increased linearly with the initial yield of F atoms and hence reactions (6-8) are of negligible importance. For experiments employing the full radiolysis dose and SF_6 concentrations greater than 600 mbar initial absorptions were 10-20% lower than expected based upon extrapolation of the data obtained at lower SF_6 concentrations. This behaviour is ascribed to secondary chemistry at high F atom concentrations resulting in incomplete conversion of F into CH_2FO_2. Consequentially, the majority of our experiments were performed using $[SF_6] < 600$ mbar.

To test for complications caused by reaction (5), experiments were performed with the CH_3F concentration varied over the range 0.8-20 mbar with all other parameters fixed (full dose, $[SF_6] = 550$ mbar, $[O_2] = 40$ mbar). Within our experimental reproducibility (± 5%) no effect on the maximum transient absorption at 220 nm was discernable indicating that the formation of FO_2 radicals is not significant under our experimental conditions. Using a value for $\sigma(FO_2)$ at 220 nm of 1.34×10^{-17} $cm^2molecule^{-1}$ [13], we calculate that less than 2% of the fluorine atoms react to form FO_2 under experimental conditions of $[CH_3F] = 10$ mbar and $[O_2] = 40$ mbar. This observation, combined with a previous measurement of $k_5 = 1.4\times10^{-13}$ $cm^3molecule^{-1}s^{-1}$ at 600 mbar of SF_6 diluent[18], leads to a lower limit for the rate constant of the reaction of the reaction of F with CH_3F of $k(F+CH_3F) \geq 3\times10^{-11}$ $cm^3molecule^{-1}s^{-1}$.

The solid lines in Figures 1 and 2 are linear least squares fits to the data obtained using SF_6 concentrations less than 600 mbar and have slopes of 0.324 ± 0.012 and $(5.67 \pm 0.26)\times10^{-4}$ respectively (errors represent 2σ). From these slopes absorbances ($\log_{10}$) of 0.324 and 0.567 are calculated for experiments using full radiolysis dose and

either 550 or 1000 mbar of SF_6 respectively. Combining these initial absorbances with the calibrated yield of F atoms of 2.7×10^{15} cm^{-3} at 1000 mbar of SF_6 at full irradiation dose gives $\sigma_{CH2FO2}(240\ nm)=(4.19\pm0.16)$ and $(4.03\pm0.18)\times10^{-18}$ $cm^2molecule^{-1}$, respectively. Within the quoted errors these determinations are in agreement. We choose to quote the average of these values with error limits which encompass the uncertainties associated with each determination, hence $\sigma_{CH2FO2}(240\ nm)=(4.11\pm0.26)\times10^{-18}$ $cm^2molecule^{-1}$. Errors quoted thus far represent the statistical uncertainty associated with our measurements, we estimate that, in addition, there is 10% uncertainty in the absolute calibration of the F atom yield. Combining the statistical and possible systematic errors, we arrive at $\sigma_{CH2FO2}(240)=(4.11\pm0.67)\times10^{-18}$ cm^{-2} $molecule^{-1}$.

To map out the absorption spectrum of CH_2FO_2 radicals, experiments were performed to measure the initial absorption between 220 and 300 nm following the pulsed irradiation of $SF_6/CH_3F/O_2$ mixtures with SF_6=550 mbar. Initial absorptions were then scaled to that at 240 nm and converted into absolute absorption cross sections. Results are shown in Figure 3.

The pulse radiolysis technique was also used to measure the UV spectra of CHF_2O_2, CF_3O_2, $CF_3CF_2O_2$, $CF_2HCF_2O_2$, and CF_3CFHO_2 radicals. In general, there is reasonable agreement between the various studies.

The fate of RO_2 radicals in the atmosphere is determined by reaction with NO, NO_2, HO_2, or other RO_2 radicals:

$$RO_2 + NO \rightarrow \text{products} \quad (9)$$

$$RO_2 + NO_2 + M \rightarrow RO_2NO_2 + M \quad (10)$$

$$RO_2 + HO_2 \rightarrow \text{products} \quad (11)$$

$$RO_2 + R'O_2 \rightarrow \text{products} \quad (12)$$

The relative importance of reactions 9-12 depends on NO, NO_2, HO_2 and RO_2 concentrations as well as the values of the respective rate constants k_9-k_{12}. In remote areas NO_x concentrations as low as 1 ppt have been measured [14], decreasing the importance of reactions 9 and 10. However, in urban areas with higher NO_x, concentration reaction 9 and 10 will be the major sink for RO_2 radicals.

4. CONCLUSIONS

The main primary stable products from the HFC degradation in the atmosphere are: $C(O)F_2$, HC(O)F, $CF_3C(O)F$, $CF_3C(O)H$ and CF_3OH. Formation of these products can be rationalised from the chemical fate of alkoxy radicals, RO, formed in the reactions 9-12 for the HFCs. Some of these five molecules are likely to be photolysed to a significant extent in the troposphere. For others the physical removal is important to prevent them for accumulation in the atmosphere. Trifluoroaceticacid (TFA) can be formed by hydrolysis of $CF_3C(O)F$. $CF_3C(O)F$ is formed in a yield of about 40% (± a factor of 2) from the atmpsheric oxidation of HFC-134a. TFA is photolysed in the stratosphere but not in the troposphere. Slow gas phase removal by reaction with OH radicals is likely to occur with a lifetime of greater than 20 days. Removal in precipitation is likely to be the main loss process for TFA out of the atmosphere.

REFERENCES

1. J. Sehested and T.J. Wallington, Environ. Sci. Tech., 27, 146 (1993).

2. J. Sehested, T. Ellermann, O.J. Nielsen, T.J. Wallington, and M.D. Hurley, Int. J. Chem. Kinet., paper in press (1993).

3. O.J. Nielsen, Risø-R-480 (1984).

4. T.J. Wallington and S.M. Japar, J. Atmos. Chem., **9**, 399 (1989).

5. T.J. Wallington, J.C. Ball, O.J. Nielsen, and E. Bartkiewicz, J. Phys. Chem., **96**, 1241 (1992).

6. O.J. Nielsen, T. Ellermann, E. Bartkiewicz, T.J. Wallington, and M.D. Hurley, Chem. Phys. Lett., **192**, 82 (1992).

7. O.J. Nielsen, T. Ellermann, J. Sehested, E. Bartkiewicz, T.J. Wallington, and M.D. Hurley, Int. J. Chem. Kinet., **24**, 1009 (1992).

8. O.J. Nielsen, T. Ellermann, J. Shested, and T.J. Wallington, J. Phys. Chem., **96**, 10875 (1992).

9. T.J. Wallington and O.J. Nielsen, Chem. Phys. Lett., **187**, 33 (1991).

10. T. MacPherson, M.J. Pilling, and M.J.C. Smith, J. Phys. Chem., **89**, 2268 (1985).

11. T.J. Wallington, P. Dagaut, and M.J. Kurylo, Chem. Rev., **92**, 667 (1992).

12. T. Ellermann, J. Sehested, O.J. Nielsen, P. Pagsberg, and T.J. Wallington, Chem. Phys. Lett., accepted (1993).

13. P. Pagsberg, E. Ratajczak, and A. Sillesen, Chem. Phys. Lett., **141**, 88 (1987).

14. B.A. Ridley, M.A. Carroll, and G.L. Gregory, J. Geophys. Res., **92**, 2025 (1987).

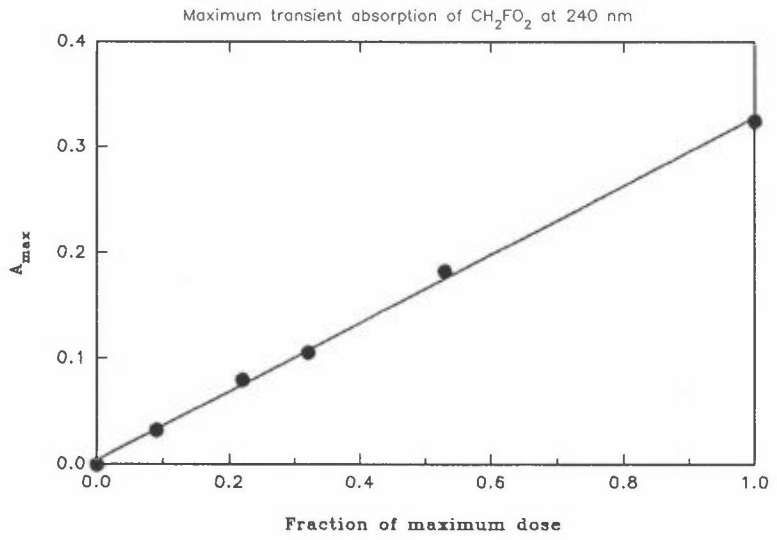
Maximum transient absorption of CH_2FO_2 at 240 nm
A_{max}
0.0
0.1
0.2
0.3
0.4
0.0
0.2
0.4
0.6
0.8
1.0
Fraction of maximum dose

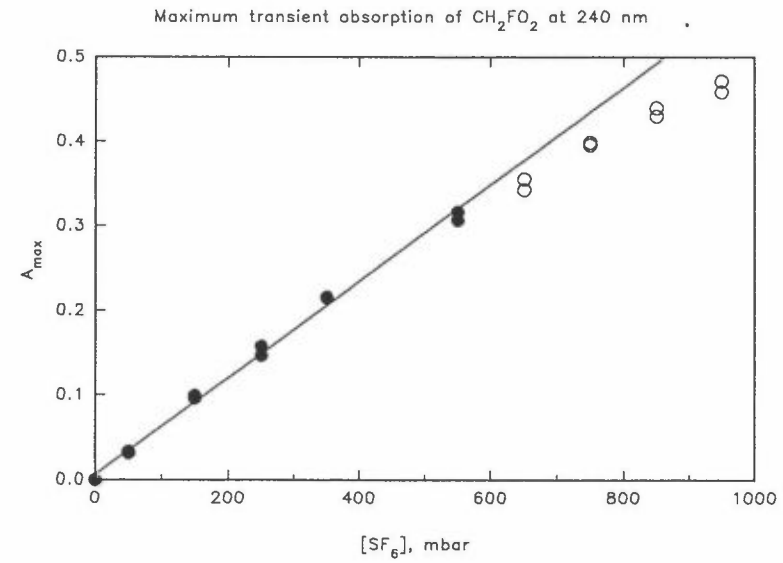
Maximum transient absorption of CH_2FO_2 at 240 nm
A_{max}
0.0
0.1
0.2
0.3
0.4
0.5
0
200
400
600
800
1000
$[SF_6]$, mbar

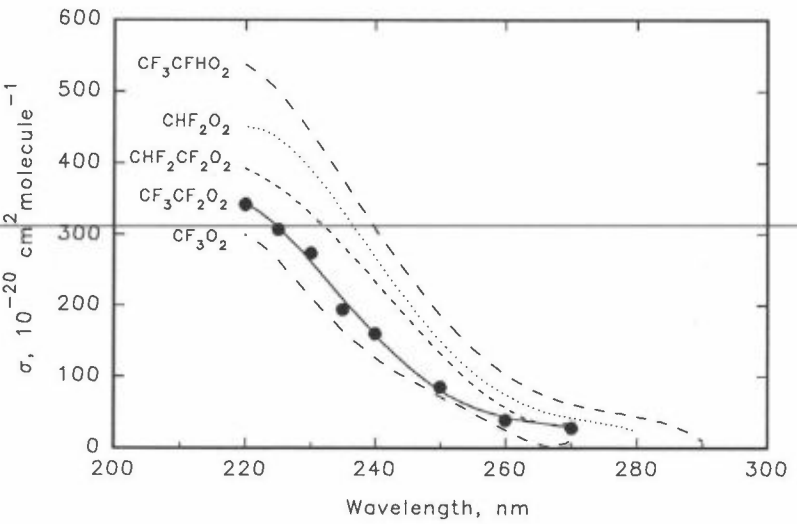
σ, 10^{-20} cm^2 $molecule^{-1}$
CF_3CFHO_2
CHF_2O_2
$CHF_2CF_2O_2$
$CF_3CF_2O_2$
CF_3O_2
0
100
200
300
400
500
600
200
220
240
260
280
300
Wavelength, nm

The IR beam line at the Lund University storage ring.

BENGT NELANDER,
CHEMICAL CENTER, THERMOCHEMISTRY
UNIVERSITY OF LUND

Synchrotron radiation from the Lund University storage ring has been used for high resolution infrared absorption spectroscopy with a Bruker HR 120 Fourier transform spectrometer. In the far infrared region the line widths of isolated water rotation lines, measured with the maximum resolution of the spectrometer are 0.0011 cm^{-1}, close to the width expected from the combination of the unapodized width of the spectrometer, 0.00087 cm^{-1}, and the Doppler width. The effective diameter of the source is 1.5 mm. The storage ring therefore makes it possible to carry out experiments which require a source which is more brilliant than a conventional black body radiator.

The main problem with the storage ring as a source for far infrared spectroscopy has been intensity variations resulting from oscillations of the radiating electron beam. These oscillations are due to varations in the energy of the orbiting electrons. A change in the electron optics of the ring, which significantly decreased the sensitivity of the position of the source point to the electron energy decreased the noise level in spectra taken with the ring as a source to values close to those observed with the globar of the spectrometer.

A gas cell, with White optics, is under construction. The cell is designed to operate at temperatures between 77K and 350K. The maximum optical path length is expected to be more than 250 m.

STUDIES OF THE GAS PHASE OXIDATION OF DMS.

Ole John Nielsen and Thomas Ellermann
Chemical Reactivity Section,
Environmental Science and Technology Department
Risø National Laboratory, DK-4000 Roskilde, Denmark

and

Timothy J. Wallington
Research Staff, SRL-E3083, Ford Motor Company
Dearborn, P. O. Box 2053, Michigan 48121-2053, USA

SUMMARY

A pulse radiolysis technique has been used to measure the UV spectra of CH_3SCH_2 and $CH_3SCH_2O_2$ radicals over the range 225-350 nm. At 285 nm, $\sigma_{CH3SCH2} = (9.97 \pm 2.21) \times 10^{-18}$; at 250 nm, $\sigma_{CH3SCH2O2} = (4.26 \pm 0.68) \times 10^{-18}$ $cm^2 molecule^{-1}$. Observed self reaction rate constants, defined as $-d[CH_3SCH_2]/dt = 2k_7[CH_3SCH_2]^2$, and $-d[CH_3SCH_2O_2]/dt = 2k_{8obs}[CH_3SCH_2O_2]^2$, were $k_7 = (3.2 \pm 0.7) \times 10^{-11}$ and $k_{8obs} = (7.9 \pm 1.4) \times 10^{-12}$ $cm^3 molecule^{-1} s^{-1}$. Errors are statistical (2 standard deviations) plus our estimate of potential systematic uncertainty (15%). A rate constant of $k_2 = (5.7 \pm 0.4) \times 10^{-12}$ $cm^3 molecule^{-1} s^{-1}$ was derived for the addition reaction $CH_3SCH_2 + O_2 \rightarrow CH_3SCH_2O_2$. A rate constant of $k_3 = (2.5 \pm 0.9) \times 10^{-11}$ $cm^3 molecule^{-1} s^{-1}$ is reported for the channel of the reaction of $CH_3SCH_2O_2$ radicals with NO that produces NO_2. Errors for k_2 and k_3 are 2 standard deviations. Results are discussed with respect to the atmospheric chemistry of dimethyl sulfide.

1. INTRODUCTION

Dimethyl sulfide (DMS) is a by-product of the biodegradation of organo-sulfur compounds in marine environments [1,2,3] and was first detected in the upper levels of the oceans by Lovelock et al. [4]. Each year 75-85 Mega-tonnes of dimethyl sulfide (DMS) escapes into the atmosphere from the oceans. DMS represents approximately 25% of the total flux of sulfur into the atmosphere [1,3,5] and so plays an important role in the global sulfur cycle. Atmospheric oxidation of DMS leads to methanesulfonic and sulfuric acids which serve as cloud condensation nuclei [6] and contribute to the natural acidity of precipitation. It has been proposed that emission of DMS may provide a means of biological climate regulation [6]. Recognition of the importance of DMS has lead to a significant research effort to understand the atmospheric chemistry of this species.

The current state of knowledge on the atmospheric chemistry of DMS has been reviewed recently by Tyndall and Ravishankara [5] and Plane [7]. The principal atmospheric fate of DMS is reaction with OH radicals. Hynes et al. [8] have shown that reaction (1) proceeds via two channels. Under ambient conditions (295K, 760 Torr of air) approximately 70% of reaction (1) proceeds via channel (1a)

to give CH_3SCH_2 radicals with the remaining 30% giving the adduct via channel (1b) [8].

$$OH + CH_3SCH_3 \rightarrow CH_3SCH_2 + H_2O \quad (1a)$$
$$OH + CH_3SCH_3 + M \rightarrow CH_3S(OH)CH_3 + M \quad (1b)$$

The CH_3SCH_2 radical formed in reaction (1a) is thought to rapidly add molecular oxygen to give $CH_3SCH_2O_2$.

$$CH_3SCH_2 + O_2 + M \rightarrow CH_3SCH_2O_2 + M \quad (2)$$

The peroxy radical, $CH_3SCH_2O_2$, will react with trace species in the atmosphere such as NO, NO_2, HO_2, or other peroxy radicals (RO_2), to give a variety of products. By analogy with other peroxy radicals, reaction with NO is likely to be an important fate of $CH_3SCH_2O_2$ radicals.

$$CH_3SCH_2O_2 + NO \rightarrow CH_3SCH_2O + NO_2 \quad (3)$$

There has been an extensive experimental research effort to investigate the kinetics and products of the OH initiated atmospheric photooxidation of DMS. However, to the best of our knowledge, the key gas-phase radical intermediates CH_3SCH_2 and $CH_3SCH_2O_2$ have yet to be observed directly.

As part of a collaboration between our laboratories to study the atmospheric chemistry of peroxy radicals [9,10,11,12] and the environmental fate of volatile organic compounds, we have performed an experimental study of CH_3SCH_2 and $CH_3SCH_2O_2$ radicals. A pulse radiolysis technique was used to measure the UV absorption spectrum and self reaction kinetics of CH_3SCH_2 and $CH_3SCH_2O_2$ radicals. In addition, we have studied the kinetics of reactions (2) and (3).

2. EXPERIMENTAL

The pulse radiolysis transient UV absorption spectrometer used in the present experiments has been described previously [13]. CH_3SCH_2 radicals were generated by the radiolysis of SF_6/CH_3SCH_3 gas mixtures in a one liter stainless steel reactor with a 30 ns pulse of 2 MeV electrons from a Febetron 705B field emission accelerator. SF_6 was always in great excess and was used to generate fluorine atoms:

$$SF_6 + e^- \rightarrow SF_6^* + e^- \quad (4)$$
$$SF_6^* \rightarrow F + \text{products} \quad (5)$$
$$F + CH_3SCH_3 \rightarrow CH_3SCH_2 + HF \quad (6a)$$
$$CH_3SCH_2 + O_2 + M \rightarrow CH_3SCH_2O_2 + M \quad (2)$$

Four sets of experiments were performed. First, the ultraviolet absorption spectra of CH_3SCH_2 and $CH_3SCH_2O_2$ radicals were determined by observing the maximum in the transient UV absorption at short times (10-40 μs) following the pulse radiolysis of SF_6/CH_3SCH_3 and $SF_6/CH_3SCH_3/O_2$ mixtures, respectively. Second, using a longer time scale (100-400 μs), the subsequent decay of the absorption was monitored to determine the kinetics of reactions (7) and (8):

$$CH_3SCH_2 + CH_3SCH_2 \rightarrow \text{products} \quad (7)$$
$$CH_3SCH_2O_2 + CH_3SCH_2O_2 \rightarrow \text{products} \quad (8)$$

Third, the rate of conversion of CH_3SCH_2 into $CH_3SCH_2O_2$ radicals was monitored as a function of the concentration of O_2 present to derive a value for the rate constant of reaction (2). Fourth, the rate of NO_2 formation following the pulse radiolysis of $SF_6/DMS/O_2/NO$ mixtures was used to measure k_3.

To monitor the transient UV absorption, the output of a pulsed 150 Watt xenon arc lamp was multi-passed through the reaction cell using internal White cell optics (40, 80, or 120 cm path-length). Reagent concentrations used were; SF_6, 95-1026 mbar; O_2, 0-30 mbar; DMS, 0.5-5.0 mbar; and NO, 0-1.8 mbar. All experiments were performed at 298K. Ultra high purity O_2 was supplied by L'Air Liquide, SF_6 (99.9%) was supplied by Gerling and Holz, DMS (>99%) was obtained from the Aldrich Chemical Company, and NO (>99.8%) was supplied by Messer Griesheim. The DMS sample was degassed before use by repeated freeze-pump-thaw cycling. All other reagents were used as received.

3. RESULTS

Measurement of the absolute absorption spectrum of CH_3SCH_2 radicals requires calibration of the initial F atom concentration and having a 100% conversion of F atoms to CH_3SCH_2 radicals. The yield of F atoms was established by monitoring the transient absorption due to methyl peroxy radicals produced by radiolysis of $SF_6/CH_4/O_2$ mixtures as described previously. The yield of F atoms at 1000 mbar of SF_6 was measured to be 3.3×10^{15} cm^{-3} at full irradiation dose, estimated to be accurate within $\pm 15\%$. Using this values we find $\sigma_{285nm}(CH_3SCH_2) = (9.8 \pm 1.7) \times 10^{-18}$ $cm^2 molecule^{-1}$.

Figure 1 shows a typical transient absorption trace obtained for the self reaction of CH_3SCH_2 radicals, together with a nonlinear least squares second-order fit. The decay of the transient absorption following radiolysis of DMS/SF_6 mixtures was monitored at wavelengths between 270 and 320 nm. At all wavelengths the decay was well represented by a second-order least squares fit. Using a normal linear least squares analysis of the second order data gines $1/2k_7 = (1.55 \pm 0.13) \times 10^{10}$ $cm^{-3} molecule^{-1} s^{-1}$. Including our estimate of a potential 15% uncertainty in the absolute radical yield calibration gives $k_7 = (3.2 \pm 0.6) \times 10^{-11}$ $cm^3 molecule^{-1} s^{-1}$.

The UV spectrum of $CH_3SCH_2O_2$ radicals was studied by the pulsed radiolysis of $DMS/O_2/SF_6$ mixtures. Following radiolysis a rapid increase in absorption in the ultra-violet at 225-250 nm was observed followed by a slower decay. The observed absorption is ascribed to the formation of $CH_3SCH_2O_2$ radicals and their loss via self reaction. Using the calibrated yield of F atoms we find $\sigma_{250nm}(CH_3SCH_2O_2) = (4.3 \pm 0.7) \times 10^{-18}$ $cm^2 molecule^{-1}$. Spectra are shown in figure 2.

k_2 was measured monitoring the first-order loss of CH_3SCH_2 at 290 nm following the pulse radiolysis of 990-1000 mbar of SF_6, 5 mbar of DMS and 0.6-11.7 mbar of O_2, $k_2 = (5.7 \pm 0.4) \times 10^{-12}$ $cm^3 molecule^{-1} s^{-1}$.

The decays of the transient absorption at wavelengths of 225-270 nm from 1-400 μs after the pulsed radiolysis of mixtures of 30 mbar of O_2, 5 mbar of SF_6, 965 mbar of SF_6 were fitted using a second order expression, and k_{8obs} was found, $(7.9 \pm 1.4) \times 10^{-12}$ $cm^3 molecule^{-1} s^{-1}$.

The kinetics of reaction (3) were studied by monitoring the formation of NO_2 at 400 nm following the radiolysis of mixtures of 0.47-1.87 mbar of NO, 5 mbar of DMS, 10 mbar of O_2 and 984 mbar of SF_6. Linear least squares analysis gives $k_3 = (1.9 \pm 0.6) \times 10^{-11}$ $cm^3 molecule^{-1} s^{-1}$.

4. DISCUSSION

Following release into the atmosphere, DMS reacts with OH radicals, and to a lesser extent, NO_3 radicals and Cl atoms. A substantial fraction, if not the majority, of DMS is converted into CH_3SCH_2 radicals. In the present work it has been shown that CH_3SCH_2 radicals react rapidly with O_2. From the value of k_2 measured in this work we calculate an atmospheric lifetime of 34 nanoseconds for CH_3SCH_2 radicals with respect to conversion into $CH_3SCH_2O_2$ radicals. $CH_3SCH_2O_2$ radicals have been shown here to react rapidly with NO. Using $k_3 = 2.5 \times 10^{-11}$ $cm^3 molecule^{-1} s^{-1}$ together with an estimate for the background tropospheric NO level of 1.9×10^8 cm^{-3} the lifetime of $CH_3SCH_2O_2$ radicals is calculated to be 3.5 minutes. Other competing loss processes include reaction with HO_2, other peroxy radicals (RO_2), and NO_2. The relative importance of these processes depends on their relative concentrations and reactivities. Tropospheric concentrations of NO, NO_2, and RO_2 (represented by CH_3O_2) have been estimated by Atkinson to be comparable at 2.5×10^8 cm^{-3}. The concentration of HO_2 is somewhat higher at approximately 10^9 cm^{-3}. The reactivities of $CH_3SCH_2O_2$ radicals towards NO_2, HO_2 and RO_2 are unknown. It seems reasonable to assume that the reactivities towards NO_2 and HO_2 are comparable to those displayed by other peroxy radicals. Also, we can assume that the reactivity towards RO_2 radicals is the same as that measured for the self reaction. Using $k_{17} = 1.0 \times 10^{-11}$, $k_{18} = 5.0 \times 10^{-12}$, and $k_{19} = 8.0 \times 10^{-12}$ $cm^3 molecule^{-1} s^{-1}$ the atmospheric lifetimes of $CH_3SCH_2O_2$ radicals with respect to reaction with NO_2, HO_2 and RO_2 are estimated to be 7, 3, and 8 minutes respectively:

$$CH_3SCH_2O_2 + NO_2 + M \rightarrow CH_3SCH_2O_2NO_2 + M \quad (17)$$

$$CH_3SCH_2O_2 + HO_2 \rightarrow CH_3SCH_2OOH + O_2 \quad (18)$$

$$CH_3SCH_2O_2 + RO_2 \rightarrow \text{products} \quad (19)$$

Clearly, reactions (3), (17), (18) and (19) could all play significant roles in the atmospheric degradation of DMS. Kinetic data for reactions (17-19) are needed for a more complete understanding of the atmospheric photooxidation mechanism of DMS.

REFERENCES

1. Andreae, M. O.; Raendonch, H., Science, **1983**, 221, 744.

2. Andreae, M. O., "The Emission of Sulfur to the Remote Atmosphere: Background Paper", in "The Biogeochemical Cycling of Sulfur and Nitrogen in the Remote Atmosphere", J. N. Galloway et al., Eds. D. Reidel Publishing Co., pp5-25, 1985.

3. Taylor, B. F.; Kiene, R. P., in "Biogenic Sulfur in the Environment", Saltzman,

E. S., Cooper, W. J., editors, A.C.S., Washington D.C., **1989**, Symposium Series 393, pp202.

4. Lovelock, J. E.; Maggs, R. J.; Rasmussen, R. A., Nature, **1972**, 237, 452.

5. Tyndall, G. S.; Ravishankara, A. R., Int. J. Chem. Kinet., 23, 483 (1991).

6. Charlson, R. J.; Lovelock, J. E.; Andreae, M. O.; Warren, S. G., Nature, **1987**, 326, 655.

7. Plane, J. M. C., in "Biogenic Sulfur in the Environment", Saltzman, E. S., Cooper, W. J., editors, A.C.S., Washington D.C., **1989**, Symposium Series 393, pp404.

8. Hynes, A. J.; Wine, P. H.; Semmes, D. H., J. Phys. Chem., **1986**, 90, 4148.

9. Wallington, T. J.; Nielsen, O. J., Chem. Phys. Lett., **1991**, 187, 33.

10. Wallington, T. J.; Ball, J. C.; Nielsen, O. J.; Bartkiewicz, E., J. Phys. Chem., **1992**, 96, 1241.

11. Nielsen, O. J.; Ellermann, T.; Bartkiewicz, E, Wallington, T. J.; Hurley, M. D., Chem. Phys. Lett., **1992**, 192, 82.

12. Nielsen, O.J.; Ellermann, T.; Sehested, J.; Bartkiewicz, E.; Wallington, T.J.; Hurley, M.D., Int. J. Chem. Kinet., **1992**, 24, 1009.

13. Nielsen, O.J. Risø-R-480 (1984).

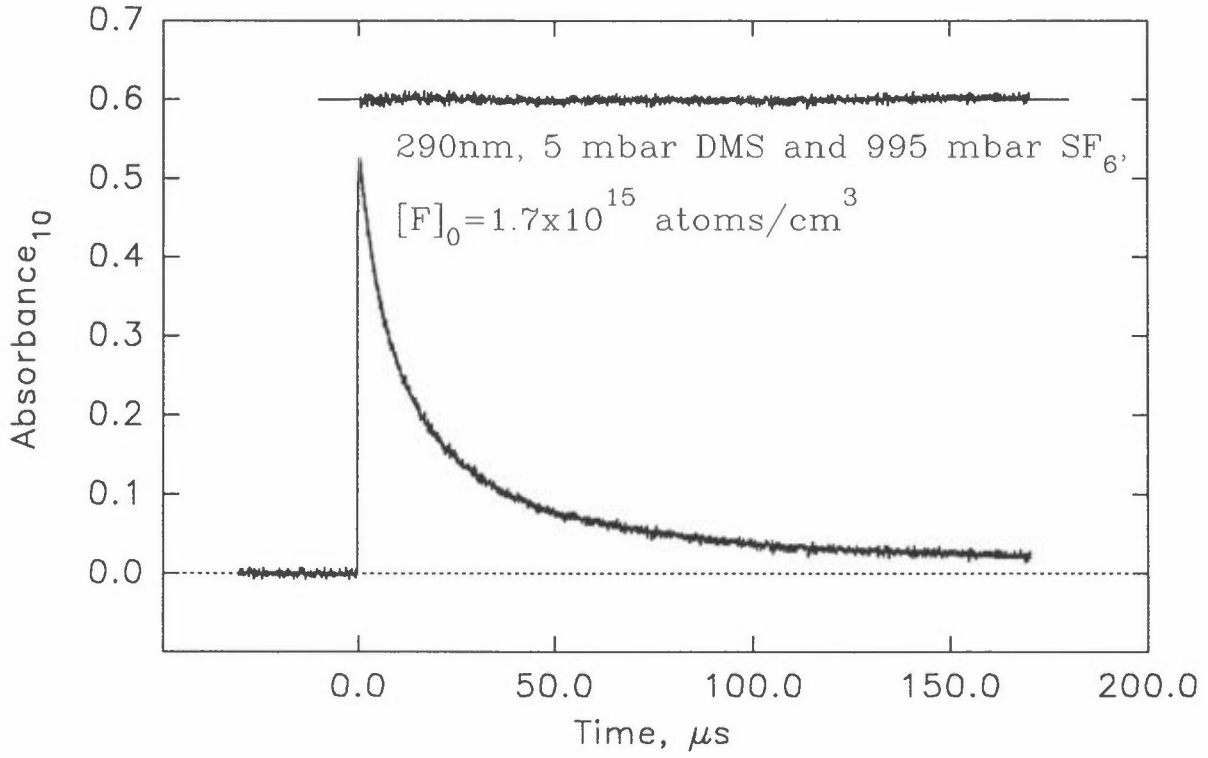

Dashed line is recommended CH_3O_2 spectrum

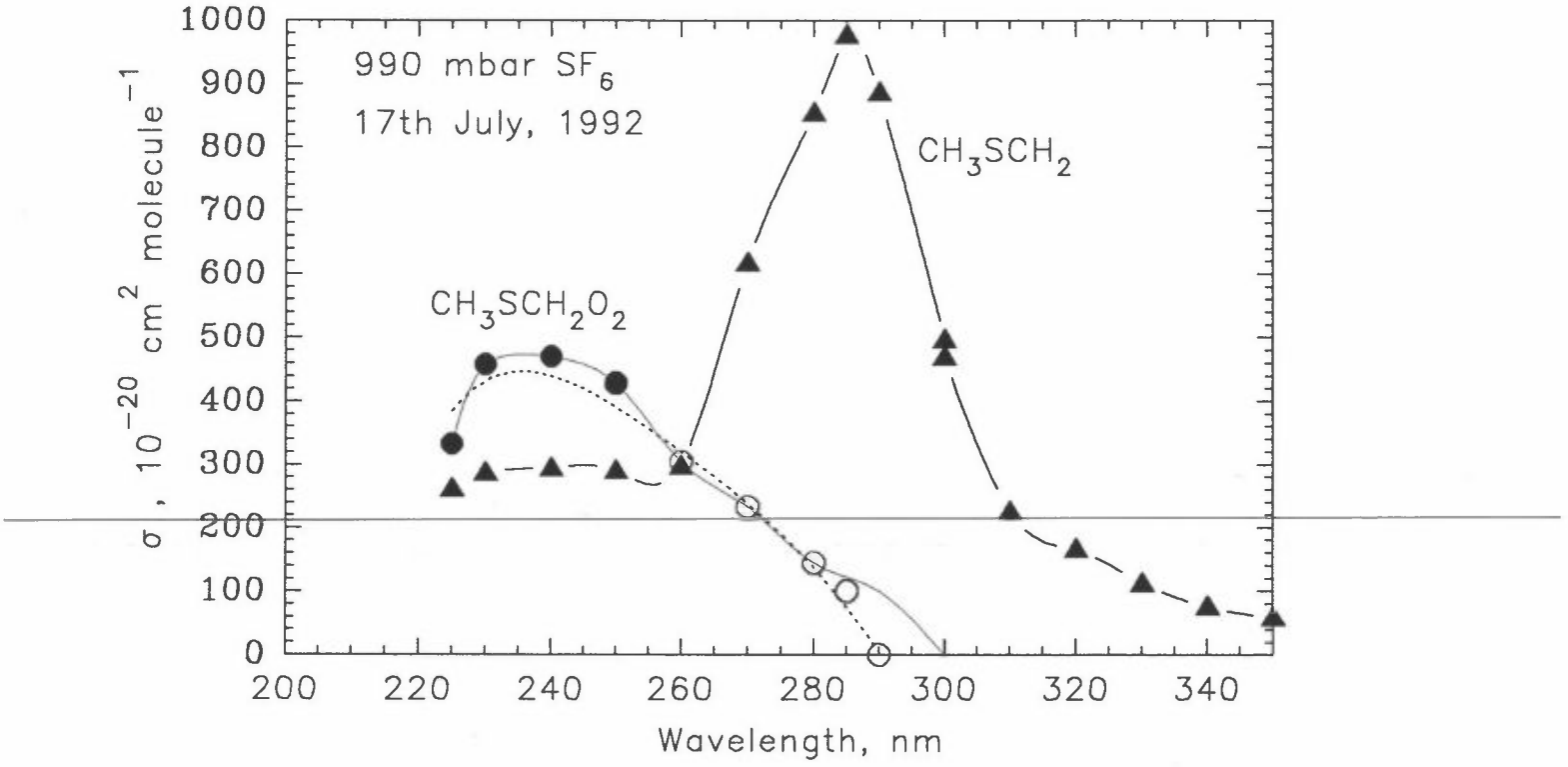

REACTIONS OF NO WITH A SERIES OF PEROXY RADICALS

Ole John Nielsen and Jens Sehested
Chemical Reactivity Section,
Environmental Science and Technology Department
Risø National Laboratory, DK-4000 Roskilde, Denmark

and

Timothy J. Wallington
Research Staff, SRL-E3083, Ford Motor Company
Dearborn, P. O. Box 2053, Michigan 48121-2053, USA

SUMMARY

The rate constants for the reaction of NO with a series of peroxy radicals were measured at 298 K and a total pressure of 1 atm. The rate constants were obtained using the absolute technique of pulse radiolysis combined with time resolved UV-VIS spectroscopy. The results are discussed in terms of reactivity trends and the atmospheric chemistry of peroxy radicals.

1. INTRODUCTION

Peroxy radicals, RO_2, are important intermediates in the atmospheric degradation of organic compounds emitted to the atmosphere. The alkyl radical, R, can be produced from emitted organic compounds in several ways, e.g., by reactions with OH, or NO_3, radicals, or by photolysis. Alkyl radicals will react rapidly with atmospheric O_2 to form peroxy radicals, RO_2:

$$R + O_2 + M \rightarrow RO_2 + M \qquad (1)$$

where M is a third body, N_2 and O_2, in the atmosphere. The fate of RO_2 radicals in the atmosphere is determined by reaction with NO, NO_2, HO_2, or other RO_2 radicals:

$$RO_2 + NO \rightarrow \text{products} \qquad (2)$$
$$RO_2 + NO_2 + M \rightarrow RO_2NO_2 + M \qquad (3)$$
$$RO_2 + HO_2 \rightarrow \text{products} \qquad (4)$$
$$RO_2 + R'O_2 \rightarrow \text{products} \qquad (5)$$

The relative importance of reactions (2-5) depends on the NO, NO_2, HO_2 and RO_2 concentrations and the values of the respective rate constants. In remote areas NO_x concentrations as low as 1 ppt have been measured, decreasing the importance of reactions (2) and (3). However, in urban areas with higher NO_x concentrations reaction (2) and (3) will be the major sink for RO_2 radicals.

The reaction of RO_2 radicals with NO proceeds through two channels:

$$RO_2 + NO \rightarrow RO + NO_2 \qquad (2a)$$

$RO_2 + NO + M \rightarrow RONO_2 + M$ (2b)

In this work we have used the pulse radiolysis technique to investigate reaction 2 for a number of alkyl peroxy and halogenated alkyl peroxy radicals: CH_3O_2, $C_2H_5O_2$, $(CH_3)_3CCH_2O_2$, $(CH_3)_3CC(CH_3)_2CH_2O_2$, CH_2FO_2, CH_2ClO_2, CH_2BrO_2, CHF_2O_2, CF_2ClO_2, $CHF_2CF_2O_2$, $CF_3CF_2O_2$, $CFCl_2CH_2O_2$, and $CF_2ClCH_2O_2$.

2. EXPERIMENTAL

The experimental set-up used, pulse radiolysis combined with kinetic spectroscopy in the visible wavelength region, has been described in detail previously [1]. The experiments were carried out in a 1 liter stainless steel gas cell equipped with an internal White type mirror system adjusted to give an optical path-length of 120 cm. A pulsed xenon lamp delivers the analytical light, which is guided through the reaction cell to a detection system consisting of a 1 m McPherson grating UV-VIS monochromator and a Hamamatsu photomultiplier. A Biomation digitizer recorded the transmittance as function of time, and a PDP11 minicomputer handled the data.

The radical reactions were initiated by irradiation of the gas mixtures in the cell with a 30 ns pulse of 2 MeV electrons from a Febetron 705B field emission accelerator. SF_6 was used as diluent gas and the experiments were carried out at a total pressure of 1 bar. The first chemical step is formation of fluorine atoms which produce the alkyl radical, R, by hydrogen abstraction from the compounds in question, RH,

$SF_6 + 2MeV\ e^- \rightarrow F + products$ (6)
$F + RH \rightarrow HF + R$ (7)

The alkyl radical, R, reacts with O_2 to form RO_2, which subsequently reacts with NO:

$R + O_2 + M \rightarrow RO_2 + M$ (1)
$RO_2 + NO \rightarrow products$ (2a)

Typical reagent concentrations used were: 890-1000 mbar SF_6; 10-40 mbar O_2; 0-2.5 mbar NO; and different pressures of the precursor compounds.

3. RESULTS

The observed formation of NO_2 was always first order. No significant difference between experiments performed at 400 nm and 450 nm was detected. Hence the data from 400 nm and 450 nm have been plotted together.

Before a value for k_2 can be extracted from the observed kinetics of the NO_2 formation the impact of potential secondary reactions needs to be considered. Peroxy radicals, RO_2, are known to react with NO_2 to form peroxy nitrates. Hence, following the formation of NO_2 from reaction (2), there is a competition between reactions (2) and (3) for the available RO_2 radicals:

$RO_2 + NO \rightarrow products$ (2)
$RO_2 + NO_2 + M \rightarrow RO_2NO_2 + M$ (3)

Similarly, alkoxy radicals produced in reaction (2) also react with both NO and NO_2:

$$RO + NO + M \rightarrow RONO + M \quad (8)$$
$$RO + NO_2 + M \rightarrow RONO_2 \quad (9)$$

Reactions (3) and (9) remove NO_2 from the system with an efficiency which increases at long reaction times. The removal decreases the time taken for the NO_2 concentration to reach a maximum. Hence, reaction (3) and (9) lead to an increase in the apparent pseudo first order rate constant for NO_2 formation. This effect is most pronounced under low $[NO]_0$ concentrations leading to positive intercepts in plots of k^{1st} versus [NO]. Positive intercepts were observed for all the alkyl peroxy radicals studied here. Interestingly, similar plots for the halogenated peroxy radicals have intercepts which are zero, within the experimental uncertainty. To assess the impact of reactions (3), (8) and (9) and, hence, to compute corrections for such, detailed modelling of the experimental data was performed using the Acuchem chemical kinetic modelling program [2] with a mechanism consisting of reaction (2), (3), (8), and (9). This modelling and the results have been discussed in detail elsewhere [3].

In view of the corrections applied to the data for CH_3O_2, $C_2H_5O_2$, $(CH_3)_3CCH_2O_2$, and $(CH_3)_3CC(CH_3)_2CH_2O_2$ radicals, we choose to add an additional 10% and 20% uncertainty range to the measured rate constants of the reactions of CH_3O_2 and $C_2H_5O_2$ radicals, and $(CH_3)_3CCH_2O_2$ and $(CH_3)_3CC(CH_3)_2CH_2O_2$ radicals with NO, respectively. Values cited in Table 1 reflect these additional uncertainties. The absolute accuracy of the rate constants depends on the precision of reactant concentrations and possible unidentified systematic errors. The overall accuracy of the measured rate constants is estimated to be of the order ±25%. In Table 1 we compare our results to those available in the literature.

4. DISCUSSION

The rate constant for the reaction of CH_3O_2 with NO has been subject of 7 previous investigations. All values reported, except one, fall within experimental uncertainty around an average value of 7.5×10^{-12} $cm^3 molecule^{-1} s^{-1}$. The reason for the low value by Adachi and Basco [4], has been discussed in detail by Sander and Watson [5]. Our value of $(8.8 \pm 1.4) \times 10^{-12}$ $cm^3 molecule^{-1} s^{-1}$ is in agreement with the average value.

The rate constant for the reaction of $C_2H_5O_2$ with NO has only been measured by two other groups and they disagree by a factor of 3. Again Adachi and Basco [6] report a lower value using the same technique as in their investigation of the CH_3O_2+NO reaction. Our value of $(8.5 \pm 1.2) \times 10^{-12}$ $cm^3 molecule^{-1} s^{-1}$ supports the higher value of Plumb et al. [7].

With our technique we are not able to investigate the reactions of i-$C_3H_7O_2$ and t-$C_4H_9O_2$ with NO, because F-atoms used in our system to generate the alkyl radicals will produce a mixture of different isomers of these radicals. However, for molecules with equivalent H-atoms, we can study the reactions of the peroxy radicals with NO. In this work we studied the reaction of neopentyl peroxy and $(CH_3)_3CC(CH_3)_2CH_2O_2$ radicals, and we derive rate constants of $(4.7 \pm 0.4) \times 10^{-12}$ $cm^3 molecule^{-1} s^{-1}$ and $(1.8 \pm 0.2) \times 10^{-12}$ $cm^3 molecule^{-1} s^{-1}$ for the reaction of these radicals with NO.

For the reaction of halogenated ethyl peroxy radicals with NO, only results from our group are available. The rate constants for the 5 reactions presented in Table 1 are indistinguishable within the experimental error. For the reactions of $CF_3CF_2O_2$ and $CHF_2CF_2O_2$ radicals with NO, the alkoxy radicals formed decompose to give another alkyl radical which can then react with NO to give more NO_2. For these two peroxy radicals the yield of NO_2 was greater than unity. The presence of additional processes forming NO_2 subsequent to reaction (2) increases the time taken for the NO_2 to reach a maximum. Hence, only lower limits can be establi-shed for the reaction of $CF_3CF_2O_2$ and $CHF_2CF_2O_2$ radicals with NO. In all cases the halogenated C_2 peroxy radicals are more reactive towards NO than ethyl peroxy radicals.

Of the rate constants for reactions of halogenated methyl peroxy radicals with NO determined by our group, only those involving CF_3O_2 and CF_2ClO_2 have been investigated previously. Within the experimental uncertainties, the results from the present work are in agreement with those previously reported. As in the C_2 case, the halogenated C_1 peroxy radicals are more reactive than CH_3O_2.

Comparison of all the available data demonstrates two different trends. Firstly, the rate constants decrease with increasing alkyl chain length and branching going from C_1 to C_8. Secondly, halogen substituents, especially chlorine, increase the RO_2+NO rate constant. It is possible to rationalize the first trend in terms of steric effects associated with the increasing alkyl chain length and branching. The same trend is observed in the peroxy radical self reaction kinetics. The second trend is more difficult to explain, but may reflect a decrease in the RO-O bond strength caused by the electron withdrawing halogen atom. Ab initio theoretical studies are needed to shed further light on the reactivity trends.

Finally we need to consider the implication of the results from the present work to our understanding of atmospheric chemistry of halogenated organic compounds. In all cases the peroxy radicals derived from haloalkanes were observed to react rapidly with NO with rate constants in the range of $(9.7\text{-}18.7)\times10^{-12}$ $cm^3molecule^{-1}s^{-1}$. A resonable estimate for the global avarage tropospheric NO concentration is 2.5×10^8 cm^{-3}. Hence the lifetimes of halogenated peroxy radicals with respect to reaction with NO will be 4-7 minutes. In the atmosphere reaction (2) competes with reactions (3), (4) and (5) for available RO_2 radicals:

$$RO_2 + NO_2 + M \rightarrow RO_2NO_2 + M \qquad (3)$$
$$RO_2 + HO_2 \rightarrow \text{products} \qquad (4)$$
$$RO_2 + R'O_2 \rightarrow \text{products} \qquad (5)$$

Kinetic data for reactions (4) and (5) are not available for the halogenated RO_2 radicals studied here. Kinetic data are available for the reaction of CF_2ClO_2, $CFCl_2O_2$, CCl_3O_2 and CF_3O_2 with NO_2. At one atmosphere total pressure these reactions are at or close to the high pressure limit with rate constants of 6.0×10^{-12} $cm^3molecule^{-1}s^{-1}$ [?]. Resonable estimates of the global avarage tropospheric NO_2, HO_2, and RO_2 (represented by CH_3O_2) are 2.5×10^8, 10^9, and 1.3×10^8 cm^{-3}. Based upon the data base for other peroxy radicals we estimate that the halogenated peroxy radicals studies have $k_3=6\times10^{-12}$, $k_4=6\times10^{-12}$, and $k_5=4\times10^{-12}$ $cm^3molecule^{-1}s^{-1}$. The atmospheric lifetimes of the halogenated RO_2 radicals with respect to reactions (3), (4) and (5) are likely to be of the order of 11, 3, and 32 minutes, respectively. Kinetic data for reactions (3), (4) and (5) are needed for a more complete understanding of the atmospheric chemistry for halogenated organic compounds.

Table 1. Summary of rate constants for RO_2+NO -> products reactions

Species	Technique[a)]	$10^{12}k_2$[bc)]	Reference
CH_3O_2	FP-UV	3.0±0.2	[4]
	FP-UV	7.1±1.4	[5]
	DF-MS	6.5±2.0	[8]
	FP-UV	7.7±0.9	[9]
	DF-MS	8.6±2.0	[10]
	LP-LIF	7.8±1.2	[11]
	LP-LA	7.0±1.5	[12]
	PR-UV	8.8±1.4	This work
$C_2H_5O_2$	FP-UV	2.7±0.2	[6]
	DF-MS	8.9±3.0	[7]
	PR-UV	8.5±1.2	This work
i-$C_3H_7O_2$	FP-UV	3.5±0.2	[13]
	DF-MS	5.0±1.2	[14]
t-$C_4H_9O_2$	DF-MS	4.0±1.1	[14]
$(CH_3)_3CCH_2O_2$	PR-UV	4.7±0.4	This work
$(CH_3)_3C(CH_3)_2CH_2O_2$	PR-UV	1.8±0.2	This work
CF_3CHFO_2	PR-UV	12.8±3.6	[15]
$CHF_2CF_2O_2$	PR-UV	>9.7±1.3	This work
$CF_3CF_2O_2$	PR-UV	>10.7±1.5	This work
$CFCl_2CH_2O_2$	PR-UV	12.8±1.1	This work
$CF_2ClCH_2O_2$	PR-UV	11.8±1.0	This work
CH_2FO_2	PR-UV	12.5±1.3	This work
CH_2ClO_2	PR-UV	18.7±2.0	This work
CH_2BrO_2	PR-UV	10.7±1.1	This work
CHF_2O_2	PR-UV	12.6±1.6	This work
CF_3O_2	DF-MS	17.8±3.6	[16]
	LP-MS	14.5±2.0	[17]
	PR-UV	16.9±2.6	[18]
CF_2ClO_2	LP-MS	16±3	[17]
	PR-UV	13.1±1.2	This work
$CFCl_2O_2$	LP-MS	16.0±2.0	[19]
	LP-MS	14.5±2.0	[17]
CCl_3O_2	DF-MS	18.6±2.8	[20]
	LP-MS	17.0±2.0	[17]

[a)] FP-UV, Flash Photolysis - UV Absorption; DF-MS, Discharge Flow - Mass Spectrometry; LP-LIF, Laser Photolysis - Laser Induced Fluorescence; LP-LA, Laser Photolysis - Laser Absorption; PR-UV, Pulse Radiolysis - UV Absorption; LP-MS, Laser Photolysis - Mass Spectrometry

[b)] in units of $cm^3molecule^{-1}s^{-1}$

[c)] errors quoted for results from this work are $\pm 2\sigma$ and represent precision only.

REFERENCES

1. O. J. Nielsen, Risø-R-480 (1984).

2. W. Braun, J.T. Herron, and D.K. Kahaner, Int. J. Chem. Kinet., 20 (1988) 51.

3. J. Sehested, O.J. Nielsen, and T.J. Wallington, Chem. Phys. Lett. **213** (1993) 457.

4. H. Adachi and N. Basco, Chem. Phys. Lett., 63, (1979) 490.

5. S.P. Sander and R.T. Watson, J. Phys. Chem. 85, (1980) 2960.

6. H. Adachi and N. Basco, Chem. Phys. Lett. 67 (1979) 324.

7. I.C. Plumb, K.R. Ryan, J.R. Steven, and M.F.R. Mulcahy, Int. J. Chem. Kinet. 14 (1982) 183.

8. R.A. Cox and G.S. Tyndall, J. Chem. Soc. Faraday Trans. 2 76, (1980) 153.

9. R. Simonaitis and J. Heicklen, J. Phys. Chem. 95, (1981) 2946.

10. I.C. Plumb, K.R. Ryan, J.R. Steven, and M.F.R. Mulcahy, J. Phys. Chem. 85, (1981) 3136.

11. A.R. Ravishankara, F.L. Eisele, N.M. Kreutter and P.H. Wine, J. Chem. Phys. 74 (1981) 2267.

12. R. Zellner, B. Fritz, and K. Lorentz, J. Atmos. Chem. 4, (1986) 241.

13. H. Adachi and N. Basco, Int. J. Chem. Kinet. 14, (1982) 1243.

14. J. Peeters, J. Vertommen, and I. Langhans, Ber. Bunsenges. Phys. Chem., 96 (1992) 431.

15. T.J. Wallington and O.J. Nielsen, Chem. Phys. Lett., 187 (1991) 33.

16. I.C. Ryan and K.R. Ryan, Chem. Phys. Lett. 92 (1982) 236.

17. A.M. Dognon, F. Caralp, and R. Lesclaux, J. Chim. Phys. 82 (1985) 349.

18. J. Sehested and O.J. Nielsen, Chem. Phys. Lett., 206 (1993) 369.

19. R. Lesclaux and F. Caralp, Int. J. Chem. Kinet. 16 (1984) 1117.

20. K.R. Ryan and I.C. Plumb, Int. J. Chem. Kinet. 16 (1984) 591.

Matrix isolation studies of the reaction between atomic oxygen and 1,1,1-trichloroethane

M.V. Pettersen[1], L. Schriver-Mazzuoli[2], A. Schriver[2] and E. Lasson[1]

[1]Department of chemistry, University of Oslo, P.O Box 1033 Blindern, N-0315 Oslo, Norway

[2]Laboratoire de Physique Moleculaire et Applications, CNRS UPR 136, Université Pierre et Marie Curie, Tour 13, Bte 76, 4, Place Jussieu, 75252 Paris Cedex 05, France

Matrix isolation coupled with FTIR spectroscopy has been employed to investigate the mechanism of the 1,1,1-trichloroethane photooxydation by ozone at 11 K by UV light. Spectra obtained after irradiation were very complex and very sensitive to initial conditions (light source, concentration, irradiation time). At least three pathways were observed leading respectively to acetylchloride, 1,1-dichloroethene and to a yet undefined compound X, characterized mainly by absorptions at 820 and 568 cm^{-1}, as the primary products. These primary products are easily photodissociated and numerous secondary products such as Cl_2CO, CH_2CO,CCl_2CO, ClCO, CHCCl, OClO, Cl_2O and ClO were identified.

INTRODUCTION

Halogenated compounds in the stratosphere can contribute to the destruction of ozone. 1,1,1-trichloroethane, CH_3CCl_3, is one of the most employed industrial solvents, and is mainly used for the cleaning of metals and in dry-cleaning. CH_3CCl_3 has an ODP of 0.1, and an atmospheric lifetime of 6 years [1]. Reaction with the OH-radical, direct photolysis or the reaction with $O(^1D)$ can lead to the formation of secondary products which can contribute to the pollution of the lower atmosphere. This work presents results from FTIR studies of the reaction between CH_3CCl_3 and $O(^1D)$ in an argon matrix at 15K. Oxygen atoms in triplet or singlet state were generated in situ by a dissociation process following the UV photolysis of ozone molecules.

EXPERIMENTAL

Mixtures of 1,1,1-trichloroethane/argon and ozone/argon were co-deposited onto a CsI window at 15K. A closed cycle helium cryostat; Air Product Displex Model 202A was used to attain this temperature. $O(^1D)$ was generated in situ using the following UV-sources: a medium pressure mercury-lamp (Philips 93136 Hg), a xenon-lamp with 350 and 280 nm cut-off filters, and the 532 and 266 nm lines from a Nd-YAG laser (QUANTEL YG718C). The IR spectra were recorded with a resolution of 0.5 cm^{-1} using BRUKER IFS 113V and IFS 88 spectrometers.

Ozone was prepared by silent electrical discharge through oxygen in a closed system cooled with liquid nitrogen using N45 purity O_2 from Air Liquid.

Additional experiments have been carried out with CD_3CCl_3 as well as with scrambled $^{16-18}O_3$. However, these results will not be discussed here.

RESULTS

1. Preliminary experiments

The photostability of CH_3CCl_3 was investigated in the 240-800 nm range. A medium pressure mercury-lamp and the 266 nm Nd-YAG laser line was used. When the mercury-lamp (unfiltered) was employed on a matrix of 1/1000 CH_3CCl_3 in argon, weak features appeared at

2822, 2834.3, 872.4, 842-839 and 785.6 cm^{-1} after prolonged photolysis. No new bands appeared after photolysis with the 266 nm line from the laser.

The weak absorptions at 872.4 and 785.6 cm^{-1} were attributed to the formation of CH_2CCl_2 by comparison to reference spectra. The band at 2822 cm^{-1} probably characterizes HCl complexed with CH_2CCl_2. The photodissociation of CH_3CCl_3 was negligible and was not considered important in the overall description of the matrix reactions.

2. Vibrational spectra after photolysis of CH_3CCl_3/ozone/Ar mixtures

2-1. $CH_3CCl_3/^{16}O_3/Ar$

The experiments were performed using a medium pressure mercury-lamp, a xenon-lamp and a 266 nm laser line. Different results were obtained according to *i)* the nature of the radiation source, *ii)* the lifetime of the lamp, *iii)* the radiation time and *iv)* the relative CH_3CCl_3/O_3 concentration. Figure 1 illustrates this special behaviour and Table 1 summarizes observed products. Bands labelled from A to F were distinguished in addition to familiar product bands. They are described for four typical experiments noted 1 to 4.

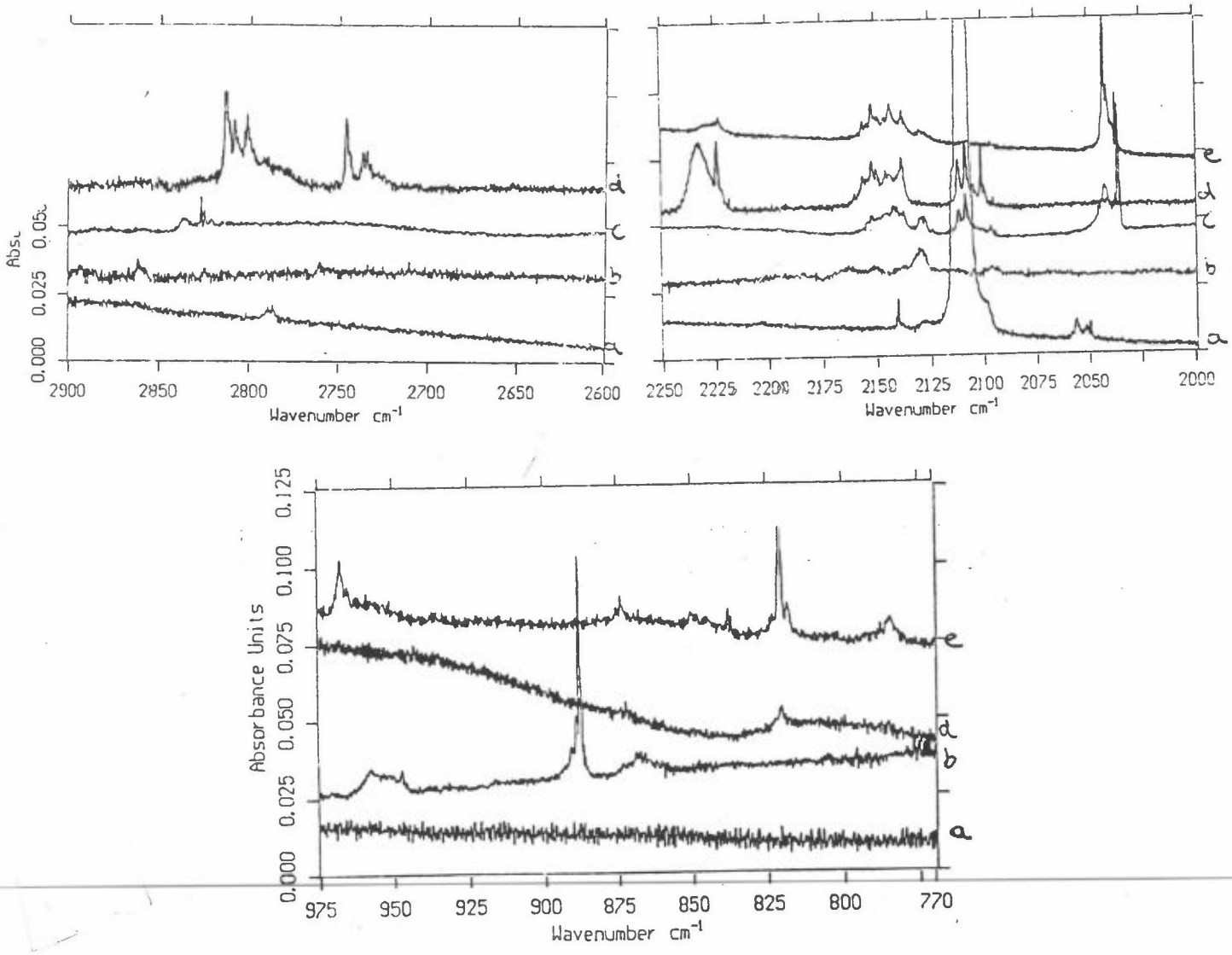

Fig.2. Matrix isolation FTIR spectra of CH_3CCl_3 and its reaction products with atomic oxygen in the 2900-2600, 2250-2000 and 975-770 cm^{-1} regions. (a) After deposition at 17K of $CH_3CCl_3/O_3/Ar$=1/5/1000; (b) after irradiation with the medium pressure Hg lamp for 3 h, exp.1; (c) after additional 9 h irradiation, exp.2; (d) after irradiation with a Xe-lamp for 10 h, exp.3; (e) after irradiation with the 266 nm laser line for 20 min., exp.4.

Experiment 1: *medium pressure mercury lamp, $CH_3CCl_3/O_3/Ar$ = 2/1/1000.*

The total irradiation time was 4 1/2 hours, and 20 per cent of the ozone then remained. Known product bands were observed: complexed H_2O at 3724.5, and complexed and free CO at 2151 and 2138 cm^{-1}. These bands appeared after 1 1/2 hours irradiation time and grew upon extended photolysis. Traces of CH_2CCl_2 (875-785 cm^{-1}) appeared in the beginning of the photolysis, but remained unchanged after 3 hours of irradiation and annealing of the photolyzed matrix. The same behaviour was observed for two other sets of bands labelled A and B characterized by absorptions at 1811, 1100.3, 598 cm^{-1} and at 1354.6, 1212, 1138, 1002, 820 and 568 cm^{-1}. Numerous bands appeared after prolonged photolysis; they were found in the OH region at 3313 cm^{-1}, in the HCl region at 2837.4, 2830, 2821.8, 2813.7, 2745.5 and 2736.6 cm^{-1} and at lower wavenumber at 2234, 2224, 2100, 1287 and 1270 cm^{-1}.

Experiment 2: *medium pressure mercury lamp, $CH_3CCl_3/O_3/Ar$ = 1/1/1000.*

This matrix was irradiated for 12 hours consuming all the ozone and giving both primary and secondary products. The products A, B and CH_2CCl_2 all appeared. After annealing the bands assigned to A disappeared. Two new bands at 818 and 824.9 were seen close to the band at 820 cm^{-1} from product B. Other bands that appeared were grouped on the basis of their behaviour upon further photolysis and annealing: four quite intense bands at 2042, 2035.9, 2034.8 and 1103.5 cm^{-1} labelled C and two strong bands at 3620 and 1243 cm^{-1} labelled D. Absorptions probably belonging to HCl-complexes were observed at 2827.4 and 2825.4 cm^{-1}. In the C=O region, bands appeared at 2152, 2143.1 (labelled F) and 2141.8 cm^{-1}. Free CO at 2138.4 cm^{-1} was present in the matrix already before photolysis. Finally, new absorptions at 1877.1 and 849.7cm^{-1} were noted, and so was a feature at 1820 cm^{-1} which appeared after photolysis.

Experiment 3: *Xenon lamp, $CH_3CCl_3/O_3/Ar$ = 1/5/1000.*

The total irradiation time was 10 hours, reducing the ozone by 90%. Weak features corresponding to A, B and CH_2CCl_2 were observed at the beginning , and they all diminished upon extended irradiation. The absorptions of C also appeared early in the photolysing process and seemed to diminish as the irradiation continued. Absorptions at 3312.2 and 3313.3 cm^{-1} in the OH region and at 2101 and 1270.3 cm^{-1} appeared after prolonged photolysis as in experiment 1. In the HCl region, bands were noted at 2814.4, 2809.1, 2802.1, 2746.2, 2737 and 2734.2 cm^{-1}. A new, broad feature at around 2234 cm^{-1} and a sharp band at 2224 cm^{-1} arose after respectively 90 and 40 minutes of irradiation.

Experiment 4: *266 nm laser line, $CH_3CCl_3/O_3/Ar$ = 2/3/1000.*

The irradiation time in this experiment was 20 minutes with the 266 nm line. The ozone had totally disappeared after 10 minutes. All of the products A, B, C, D and E were observed in the beginning, in addition to traces of CH_2CCl_2. After 5 minutes of irradiation, a new band arose at 818 cm^{-1} as in exp. 2. A set of new bands labelled F, appeared after 5 minutes of photolysis and was characterized by absorptions at 1812.3, 1811.6, 837.6 and 836.7 cm^{-1}. These bands diminished upon extended photolysis. Traces of complexed HCl were observed at 2827.1, 2750.2 and 2748.4 cm^{-1}. In the C=O region, four bands appeared; at 2156.1, 2152, 2143.6 (product E from experiment 2) and at 2142.1 cm^{-1}. The absorptions at 2224 cm^{-1} previously reported in experiment 3, appeared after 5 minutes of irradiation. Weak bands at 850.3 cm^{-1} and 1820 cm^{-1}, both observed in experiment 2, appeared.

DISCUSSION

1. Identification of the product bands

Assignment of the product bands is complicated for two main reasons: i) due to the small yield of some products, not all bands of the compounds are observed, ii) when the photoprocess involves atom detachment, the atoms can escape their argon cage, and some molecules can be complexed to products outside the cage. Tentative identification of some product absorptions are given below based on literature data and the recording of the reference spectra.

Two product groups will be considered. One where bands appeared at the beginning of the irradiation which can be classified as primary products, the other where bands grew in after prolonged photolysis and ozone depletion which could arise from photolysis of primary products.

1-1 Primary products

Primary product bands were labelled A and B as well as CH_2CCl_2. CH_2CCl_2 is identified as a primary product of the ozone-CH_3CCl_3 reactions. It appears after laser irradiation in a domain where CH_3CCl_3 is not dissociated (see section 2-1), and the band intensity after 50 min of photolysis with the Hg lamp is stronger than that observed after 3 hours and 45 minutes of irradiation of CH_3CCl_3 alone.

Bands labelled A (1811.9, 1100.3, 598.4 cm^{-1}) can be assigned to the CH_3COCl molecule on the basis of the gas spectrum [2] and by comparison with the spectrum recorded in argon. Recent studies of the UV dissociation of acetylchloride [3] showed that it photodissociates into ketene (CH_2=C=O) characterized by bands at 3062, 2142, 1381, 591 and 525 cm^{-1} [4]. After prolonged photolysis, the strongest band appeared at 2143 cm^{-1} in two spectra and were labelled F. Bands labelled B are difficult to assign. Measured frequencies could suggest the formation of 1,1-dichloro-oxirane by comparison with ethylene oxide spectra [5]. At this experimental stage this product is referred to as X. The proportions between the yields of CH_3COCl and X and CH_2CCl_2 were very different in each experiment, indicating that these products do not have the same origin.

1-2 Secondary and ternary products

Numerous bands appeared after prolonged photolysis in the ν_{HCl} region at lower frequencies than the HCl monomer absorption suggesting formation of complexes between HCl and other species produced in the matrix. From literature data [6,7] the set of bands about 2815 cm^{-1} can be assigned to the $(HCl)_xCO$ species while bands about 2740 cm^{-1} might correspond to the HCl submolecule in interaction with unsaturated organic species. Recent spectroscopic studies of OClO and ClOO isolated in an argon matrix [8,9] allow us to assign bands labelled C to OClO. From literature data, it is also possible to assign reasonably the bands at 2156, 2103, 1877, 967 and 850 cm^{-1} respectively to CCl_2CO [10], CHCCl [11], ClCO [12], Cl_2O [13] and ClO [14]. At last, bands labelled F are in good agreement with the spectra of Cl_2CO observed previously in argon matrix [15]. Table 1 summarizes these tentative assignments.

Table 1. Observed wavenumbers for the $CH_3CCl_3/O(^1D)$ reaction system and a tentative spectral assignment .

Product	Waveno. cm^{-1}	Assignment	Obs. in exp.	Mode
A	1811.9 1100.3 598.4	CH_3COCl	1, 2, 3, 4	ν_{CO} ν_{CH} ν_{CCl}
	1616.2 872.4 784.5-783.6	CH_2CCl_2	1, 2, 3, 4	ν_{CC} ν_{CCl} ν_{CCl}
B	1354.6 1212 1138 1002 820 568	X	1, 2, 3, 4	
C	2042 2035.9-2034.8 1103.5	OClO	2, 3, 4	$2\nu_{ClO}$ $2\nu_{ClO}$ ν_{ClO}
D	3620 1243		2, 4	
E	2143.6	CH_2CO	2, 4	ν_{CO}
F	1812.3-1811.6 837.6-836.7	Cl_2CO	4	ν_{CO} ν_{CCl}
	3313.3-3312.2	complexed OH	1, 3	ν_{OH}
	2827.4-2825.4 2802.1 2750.2	complexed HCl	1, 2, 3, 4	ν_{HCl} ν_{HCl} ν_{HCl}
	2815.1 2813.4 2152.0	CO -- HCl	2, 3, 4	ν_{HCl} ν_{HCl} ν_{CO}
	2156	CCl_2CO		ν_{CO}
	2100	CHCCl		ν_{CC}
	1877.1	ClCO	2	ν_{CO}
	967.5	Cl_2O	2, 4	ν_{ClO}
	850.3	ClO	2, 4	ν_{ClO}
	1270	H_2O_2	1, 3	ν_{OH}
	2138.4	CO	1, 2, 3, 4	ν_{CO}

2. Photolytic process

The experimental data described above give evidence to that there are at least three distinct chemical pathways for the reaction between CH_3CCl_3 and the $O(^1D)$ atom.

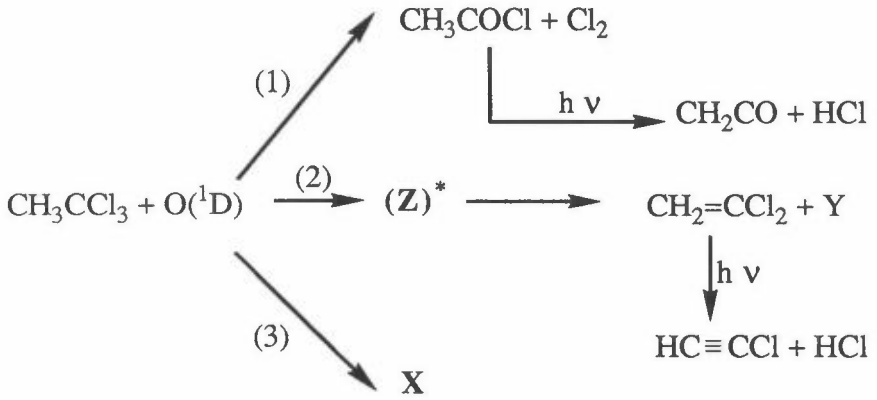

Only route 1 is well established: the abstraction of Cl_2 with formation of a carbonyl compound is in agreement with similar product and mechanism observed in the reaction between $O(^1D)$ and CCl_4 [16] or $CHCl_3$ [17]. Formation of CH_2CCl_2 in route 2 arises from a vibrationally excited unstable intermediate species containing an oxygen atom. If we take in account that insertion of an $O(^1D)$ atom in a CH-bond has been observed in matrix in the reaction CH_4 + $O(^1D)$ [18], CH_3OH + $O(^1D)$ [18] and CH_3CN + $O(^1D)$ [19], the vibrational excited species could be CH_2OHCCl_3. However in absence of the ClOH identification in our spectra, which perhaps dissociates, this assumption remains speculative. Route 3 which appears more important than the two other ones, is not yet determined and requires the X-species identification with isotopic species. Kinetic studies are also needed to confirm the formation of primary, secondary and ternary products. This work which is very complex is in progress.

REFERENCES

[1] B.J. Alloway and D.C. Ayres, *Chemical Principles of Environmental Pollution,*
[2] J. Overend, R.A. Nyquist, J.D. Evans, W.J. Potts *Spectrochim. Acta*, 1961, 17, 1207
[3] N.Kogure, T. Ono, E. Suzuki, F. Watari *J. Mol. Struct.* in press
[4] C.B. Moore, G.C. Pimentel *J. Chem. Phys*, 1963, 38, 2816
[5] N.W. Cant, W.J. Armstead *Spectrochim. Acta*, 1974, 31A, 839
[6] J.P. Perchard, J. Cipriani, B. Silvi, D. Maillard *J. Mol. Struct.* 1983, 100, 317
[7] L. Andrews, R.T. Arlinghaus, G.L. Johnson *J. Chem. Phys.* 1983, 78, 6347
[8] A. Arkell, I. Schwager *J. Am. Chem. Soc.* , 1967, 89, 5999
[9] K. Johnsson, A. Engerdahl, B. Nelander *J Phys. Chem.* , 1993, 97, 9603
[10] M. Torres, J. Ribo, A. Clement, O.P. Strausz *Nov. J. Chim.* , 1981, 5, 351
[11] T. Shimanouchi *Nat. Stand. Ref. Data Ser.* , 1972, 39, 73
[12] M.E. Jacox, D.E. Milligan *J. Chem. Phys.* 1965, 43, 866
[13] K. Johnson, A. Engerdahl, P. Ouis, B. Nelander *J. Phys. Chem.* , 1992, 96, 5778
[14] R.O. Carter, L. Andrews J. *Phys. Chem,*. 1981, 85, 2351
[15] H. Schnöckel *J. Mol. Struct.*, 1975, 29, 123
[16] C. Lugez, A. Schriver, E. Lasson, C.J. Nielsen and L. Schriver-Mazzuoli *J. Phys. Chem.*, 1993, 97, 11617
[17] L. Schriver-Mazzuoli, B. Gauthier-Roy, D. Carrere, A. Schriver and L. Aboaf-Marguin *J. Chem. Phys.*, 1992, 163, 357
[18] C. Lugez, A. Schriver, R. Levant and L. Schriver-Mazzuoli *J. Chem. Phys,* in press
[19] Z. Mielke, M. Hawkins and L. Andrews *J. Phys. Chem.*, 1989, 93, 558

Laboratory studies of trace gas uptake on stratospheric aerosol mimics

Ole W. Saastad, Cathrine E. Lund, Thomas Ellermann & Claus J. Nielsen
Department of Chemistry, University of Oslo

Abstract

A static reaction chamber attached to a mass spectrometer was employed to study the physi- and chemisorption of trace gases onto cold surfaces with varying concentrations of sulphuric acid, nitric acid and perchloric acid.

Results from studies of the uptake of HCl, HBr, NO and NO_2 are presented and discussed in relation to the depletion of stratospheric ozone.

Introduction

The total column of ozone over Antarctica in the Antarctic spring have shown a dramatic decrease since about 1979. Since the publication of these low values of ozone in 1985 [Farman85], a lot of new chemistry have been discovered. The spring of 1993 set a new record in low total ozone column. In october the total column was less then 90 DU.

Reactions of stable molecules on surfaces of sulphate aerosols and on solid ice particles play a critical role in the depletion of stratospheric ozone. Field measurements combined with model calculations have shown that gas phase chemistry cannot explain the observed ozone depletion. Further the large abundance of active chlorine in the stratosphere is associated with the presence of particles suspended in the stratosphere. On the surface of these particles heterogeneous processing of chlorine and bromine reservoir species are going on. These heterogeneous processes have been demonstrated to occur in laboratory studies [DeMore90].

The following heterogeneous reactions have been shown to play a crucial role in the photo chemical mechanism leading to the Antarctic ozone hole [Solomon88]:

$$ClONO_2 + H_2O \rightarrow HOCl + HNO_3 \quad (1)$$

$$N_2O_5 + H_2O \rightarrow 2\,HNO_3 \quad (2)$$

$$ClONO_2 + HCl \rightarrow ClNO_2 + HNO_3 \quad (3)$$

$$N_2O_5 + HCl \rightarrow ClNO_2 + HNO_3 \quad (4)$$

$$HOCl + HCl \rightarrow Cl_2 + H_2O \quad (5)$$

$$BrONO_2 + H_2O \rightarrow HOBr + HNO_3 \quad (6)$$

In the laboratory these reactions proceed rapidly over water and nitric acid surfaces. In the stratosphere the occurrence of sulphate aerosol particles can act as surfaces for reactions 1 to 6. The composition of stratospheric sulphate aerosols depends on the partial pressure of water and the temperature. For typical stratospheric conditions the composition is estimated between 60 and 80 wt.% H_2SO_4 [Steele81].

One of the limiting factors for reactions 3, 4, 5 is the availability of the second reactant HCl in the sulphate aerosol particle [Williams93]. It is therefore important to know the uptake of HCl and HBr on such surfaces.

Experimental

The experimental setup consists of a static reaction chamber (0.82 dm^3) with two compartments separated by a valve: a main reservoir containing the chemical species to be studied, and a smaller compartment with a cold, temperature regulated surface (8.5 cm^2) where different ices and liquids can be deposited (see Figure 1). The water and acid mixtures were

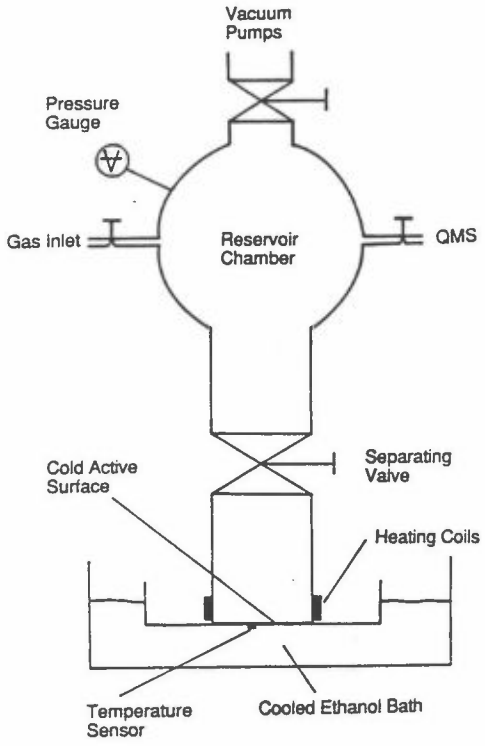

Figure 1: Schematic drawing of the reaction chamber

deposited as 1-2 mm liquid layers and subsequently cooled to the desired temperature. The cold, active surface temperature can be regulated from room temperature down to 173 K. The total vapor pressure is measured by a Baratron model 127A (full scale 10 Pa), and the gas concentration in the gas phase are monitored by a Balzers QMG 125 quadrupole mass spectrometer with a gas-tight axial ion source. The output from the mass spectrometer is recorded by an attached PC for further analysis. With the present experimental configuration the upper limit for uptake coefficients that can be determined is about 0.05 .

Results

The change in partial pressure p(t), of the examined species is giver by:

$$p(t) = \frac{N_0 \cdot R \cdot T}{V} \exp(-(\frac{k_{QMS}}{V} + k_{ads}) \cdot t) \tag{7}$$

where N_0 is the initial number of molecules present, and V_0 is the volume of the compartment containing the gas (V increases by 23% at t=0 when the valve is opened). k_{QMS}/V is the parameter describing the loss rate by effusion to the QMS.

After the valve is opened, k_{ads} is related to the zero coverage uptake coefficient, γ_0, by :

$$k_{ads} = \gamma_0 \cdot (1 - \theta) \cdot A \cdot \bar{c}/4V \tag{8}$$

where θ is the fractional surface coverage; A, the geometric surface area; and $\bar{c}$, the mean velocity of the vapor phase molecules. θ, in turn, was calculated from the geometrical surface area and an estimated site size of 0.1nm^2 assuming a coverage of less than one monolayer, following the Langmuir isotherm.

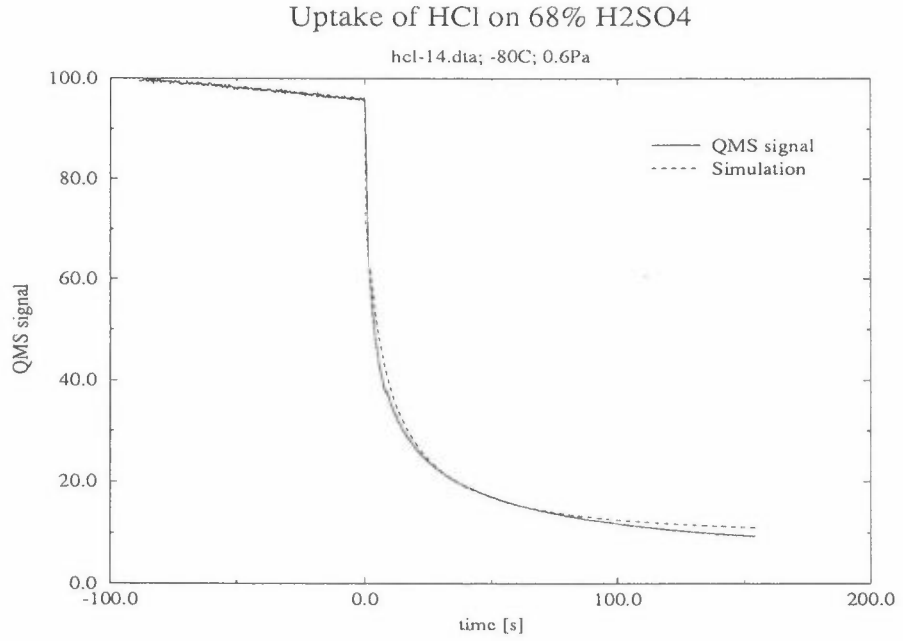

Figure 2: Typical profile of QMS output

The zero coverage uptake coefficient, γ_0, and number of sites are adjusted in the simulation so that the simulation will fit the experimental curve. Normally we obtain a good agreement shown in Figure 2. This simple model does not take into account the diffusion of adsorbed *HCl* into the bulk of the solution. A further treatment of the *HCl* and *HBr* data will follow in a forthcoming paper.

We have measured the uptake of NO and NO_2 on sulphuric acid surfaces [Saastad93]. Burley and Johnston suggested a mechanism involving nitrosyl sulphate acid, NSA, that could affect the balance of NO_y, Cl_y and ozone in the lower stratosphere [Burley92]. Based on information from the atmospheric and chemical literature they suggested a new channel

H_2SO_4 −80°C	
Acid wt.%	Uptake coef. γ_0
50	$3\ 10^{-2}$
60	$1.4\ 10^{-2}$
62.5	$8.5\ 10^{-3}$
65	$6\ 10^{-3}$
66.5	$9\ 10^{-4}$
68	$2\ 10^{-4}$
70	$2\ 10^{-4}$
75	$1\ 10^{-5}$
80	$5\ 10^{-6}$

Table 1: HCl uptake on H_2SO_4

for chlorine reactivation involving NSA. Model calculations showed that if γ(NO) for the NSA formation were greater than $2 \cdot 10^{-3}$, then the rate of the NSA reaction would equal or exceed the rate of conversion of HCl to Cl by hydroxyl radicals and this would perturb the balance of NO_y, Cl_y and ozone in the lower stratosphere.

Our results showed an insignificant uptake of NO and NO_2 on sulphuric acid surfaces at the relevant temperature of the stratosphere. We established an upper limit for the uptake of NO and NO_2 onto sulphuric acid surfaces of 10^{-6}, which rule out the suggested pathway.

We have also measured uptake of HCl and HBr on sulphuric, nitric and perchloric acid. Data for HBr resemble those of HCl but they have not yet been fully interpreted. Therefore only HCl data will be shown in full detail.

A typical plot of raw data is shown in Figure 2. The plot shows the measured time profile of the mass spectrometer signal and superimposed is an evaluation of equation 7 on the same profile. The agreement between measured time profiles and simulations is good. By varying the acid concentration different values for the reaction coefficient was obtained. We have varied the acid concentrations from zero (pure water) to concentrated acids. Due to the limitations in the experimental setup we were not able to distinguish between the uptake coefficients on pure water and 30–40% acid.

HNO_3 −80°C	
Acid wt.%	Uptake coef. γ_0
50	$5\ 10^{-3}$
54	$2\ 10^{-4}$
65	$1\ 10^{-5}$

Table 2: HCl uptake on HNO_3

Table 1 shows the uptake of HCl on varying sulphuric acid. It is clearly seen that the uptake coefficient decreases rapidly with increasing acid strength. The same picture is evident for nitric and perchloric acid, Table 2 and Table 3 respectively.

$HClO_4$ −80°C	
Acid wt.%	Uptake coef. γ_0
35	$6\ 10^{-3}$
50	$4\ 10^{-3}$
62.5	$1\ 10^{-5}$
65	$5\ 10^{-6}$

Table 3: HCl uptake on $HClO_4$

We used perchloric acid to test for differences in acid strength. Perchloric acid is a factor 1000 times stronger than sulphuric acid. The change in uptake takes place at about the same mole fraction of acid. This lead us to the conclusion that it is the availability of water that governs the uptake of HCl and HBr on these surfaces and solutions. At low acid mole fractions a large amount of water molecules are free and can interact with HCl, but as the acid mole fraction increases less and less water are available to interact with the adsorbing acid.

References

[Burley92] Burley, J.D., and H.S. Johnston
Geophys.Res.Lett. 19, 1363-1366, (1992)

[DeMore90] DeMoore, W. B. et al.
Chemical Kinetice and Photochemical data for use in the Stratospheric Modeling, Evaluation no. 8 NASA JPL Pub. 92-20.

[Farman85] Farman J.C., B.G. Gardiner and J.D. Shaklin
Nature, 315, 207, (1985)

[Saastad93] Saastad, O.W., T. Ellermann, and C.J.Nielsen
Geophys.Res.Lett. 20, 1191-1193, (1993)

[Solomon88] Solomon, S., Rev.Geophys. 26, 1129-1144, (1988)

[Steele81] Steele, H.M., and P. Hamill, J.Aerosol. Sci. 12, 517-28 (1981)

[Williams93] Leah R. Williams and David Golden, Geophys.Res.Lett. 20, 2227-2230, (1993)

ATMOSPHERIC CHEMISTRY OF CF_3O_x RADICALS.

Jens Sehested and Ole John Nielsen
Chemical Reactivity Section,
Environmental Science and Technology Department
Risø National Laboratory, DK-4000 Roskilde, Denmark

SUMMARY

Using a pulse radiolysis UV absorption technique and subsequent simulations of experimental NO_2 and FNO absorption transients, rate constants for reaction between CF_3O and CF_3O_2 radicals with NO were determined:

$$CF_3O_2 + NO \rightarrow CF_3O + NO_2 \quad (1)$$
$$CF_3O + NO \rightarrow CF_2O + FNO \quad (2)$$

k_1 was derived to $(1.68 \pm 0.26) \times 10^{-11}$ cm^3 molecule^{-1} s^{-1}, and $k_2 = (5.2 \pm 2.7) \times 10^{-11}$ cm^{3}molecule^{-1}s^{-1}. Results are discussed in the context of the atmospheric chemistry of halocarbons.

1. INTRODUCTION

Recognition of the adverse environmental effect of chlorofluorocarbons (CFC) release into the atmosphere has led to an international agreement to phase out CFCs by the end of 1995. Efforts have been made to find environmental acceptable alternatives. Among these alternatives are hydrofluorocarbons (HFCs). Prior to large scale industrial use the environmental impact of HFCs must be investigated. HFCs, when released to the atmosphere, will react with OH to form alkyl radicals which will, in turn, react with O_2 to form peroxy radicals [1]. In the case of CF_3H (HFC-23):

$$CF_3H + OH \rightarrow CF_3 + H_2O \quad (3)$$
$$CF_3 + O_2 + M \rightarrow CF_3O_2 + M \quad (4)$$

An important reaction of CF_3O_2 in the atmosphere is reaction with NO. The reaction of CF_3O_2 with NO is known to give predominantly if not solely, NO_2 and CF_3O [2,3]:

$$CF_3O_2 + NO \rightarrow CF_3O + NO_2 \quad (1)$$

The alkoxy radical CF_3O is of considerable interest because it is formed as a product from the atmospheric degradation of at least three different HFCs: CF_3H (HFC-23) [4], CF_3CF_2H (HFC-125) [5], and CF_3CFH_2 (HFC-134a) [6]. The atmospheric oxidation of other HFCs containing CF_3-groups will probably also produce CF_3O radicals.

The atmospheric fate of CF_3O radicals is uncertain [1]. It have been shown recently, that CF_3O radicals react with hydrogen containing species [6,7,8,9] by hydrogen abstraction:

$$CF_3O + RH \rightarrow CF_3OH + R \quad (5)$$

The fate of CF_3OH in the atmosphere is either decomposition to CF_2O and HF or reaction with water droplets to HF and CO_2.

CF_3O radicals have also been shown to react fast in reaction (2) with NO to form CF_2O and FNO [7,9,10]. Bevilaqua et al. [7] and Zellner et al. [9] report the rate constant k_2 to be $(2\pm1)x10^{-11}$ and $(2.5\pm0.4)x10^{-11}$ $cm^3molecule^{-1}s^{-1}$, respectively.

The main objective of this study is to determine k_2. Since the CF_3O radical cannot be detected by UV-absortion in our system, we had to derive k_2 indirectly. This is done by fitting FNO UV-absorption transients using the chemical mechanism shown in Table 1. The rate of formation of FNO in our kinetic system is rather insensitive to other rate constants than k_1 and k_2. We have therefore determined k_1 by simulations of NO_2 absorption transients. Values for both k_1 and k_2 are reported in this work.

2. EXPERIMENTAL

The experimental technique used for this work has been described in detail previously [11] and will only be briefly described here.

Radicals were produced in a one liter stainless steel reaction cell upon a 30 ns irradiation by 2 MeV electrons from a Febetron 705B field emission accelerator. The irradiation dose was varied by inserting stainless steel attenuators between the cell and the Febetron. A chromel/alumel thermocouple measured the temperature inside the reaction cell close to the center. All experiments were performed at 295 ± 2 K.

The gas mixture was analyzed using UV-VIS light from a pulsed xenon lamp. This light beam was reflected 11 times in the gas cell by internal White type optics giving a total optical pathlength of 120 cm. The analyzing light was passed into a McPherson 1 m grating monochromator operated at spectral resolution of 0.8 nm and was detected by a Hamamatsu photomultiplyer coupled to Biomation digitizer. Data handling and storage were done on a PDP11 computer.

The gas mixtures always contained SF_6 in great excess. F atoms are produced upon irradiation of SF_6 with high energy electrons [11]:

$$SF_6 + 2\ MeV\ e^- \rightarrow F + products \quad (6)$$

The yield of F atoms were determined by irradiation of gas mixtures of 5 mbar CH_4, 35 mbar O_2, and 960 mbar SF_6. CH_3O_2 radicals formed in this system was detected at 240 nm. The absorbance at 240 nm was measured as a function of the dose. The absorbance was proportional to the dose up to 53% of maximum dose. A linear regression analysis of the absorption data up to this dose gave a slope of 0.237 ± 0.010. Using the reported absorption cross section for CH_3O_2 at 240 nm, $4.42x10^{-18}$ $cm^2molecule^{-1}$ [2], an initial fluorine atom concentration at full dose of $(3.23\pm0.35)x10^{15}$ molecules cm^{-3} was found for irradiation of 1000 mbar SF_6. The reported uncertainty in the fluorine atom yield contains uncertainties in the recorded absorption at 240 nm and 10% uncertainty in σ_{CH3O2}. The initial F atom yield used in

the simulations was calculated from the dose and the fluorine atom yield at full dose reported above.

CF_3O radicals were generated by pulse radiolysis of mixtures of $CF_3H/O_2/NO/SF_6$. The subsequent reactions are shown in Table 1 and are discussed below.

Reagents and concentrations used were: SF_6, 889-894.5 mbar, supplied by Gerling and Holz at a stated purity of 99.9%; NO(>99.8%), 0.3-1.0 mbar, received from Messer Griesheim; Ultra high purity O_2, 5-10 mbar, obtained from L'Air Liquide; CF_3H(>99.3%), 100 mbar, delivered by Fluorochem Ltd. All reagents were used as received.

3. RESULTS

CF_3O_2 + NO.

To determine the rate constant for the reaction between CF_3O_2 and NO, we have performed 7 different experiments in which dose, [NO], and $[O_2]$ have been varied. The experimental conditions and results are shown in Table 2. The results are obtained as the best fit of the simulated transient using the chemical reaction mechanism in Table 1 with k_2 set at 5.0×10^{-11} $cm^3molecule^{-1}s^{-1}$ to the experimental NO_2 transients. Figure 1 shows a measured absorption transient obtained at 400 nm following pulse radiolysis of 0.5 mbar NO, 10 mbar O_2, 100 mbar CF_3H, and 889.5 mbar SF_6. This figure also contains three simulations of the absorption transient using the chemical mechanism in Table 1, with $k_1 = 1.6$, 1.7, and 1.85×10^{-11} $cm^3molecules^{-1}s^{-1}$, respectively. As shown in the figure both the simulated transients using $k_1 = 1.6\times10^{-11}$ $cm^3molecules^{-1}s^{-1}$ and $k_1 = 1.85\times10^{-11}$ $cm^3molecules^{-1}s^{-1}$ fall outside the noise level in the data. In this way we have obtained an uncertainty in k_1. We choose to report $k_1 = (1.70\pm0.15)\times10^{-11}$ $cm^3molecule^{-1}s^{-1}$. The other obtained values for k_1 shown in Table 2 were obtained in a similar way. Using the average of the k_1 values in Table 2 and conventional propagation of error we obtain $k_1 = (1.68\pm0.18)\times10^{-11}$ $cm^3molecule^{-1}s^{-1}$. We choose to add an extra 5% uncertainty because the result is derived from a complexed kinetic mechanism. The reported value is therefore $k_1 = (1.68\pm0.26)\times10^{-11}$ $cm^3molecule^{-1}s^{-1}$. This value is in excellent agreement with the values from two previous investigations, $(1.78\pm0.36)\times10^{-11}$ $cm^3molecule^{-1}s^{-1}$ and $(1.45\pm0.2)\times10^{-11}$ $cm^3molecule^{-1}s^{-1}$

CF_3O + NO.

The rate constant for the reaction of CF_3O with NO was derived by simulation of experimental absorption transients, in this case FNO transients recorded at 310.5 nm. 7 experimental transients were fitted using the chemical reaction mechanism in Table 1. An example of an absorption transient is shown in Figure 2. The transient displayed in Figure 2 is recorded at the same conditions as the transient in Figure 1: $[SF_6] = 889.5$ mbar, $[NO] = 0.5$ mbar, $[O_2] = 10$ mbar, $[CF_3H] = 100$ mbar and full dose. Included in Figure 2 are three simulations using $k_2 = 3$, 5, and 7×10^{-11} $cm^3molecule^{-1}s^{-1}$. In all three simulations $k_1 = 1.7\times10^{-11}$ $cm^3molecule^{-1}s^{-1}$ was used. It is seen from figure 2 that the simulated transient is not consistent with the experimentally obtained transient for $k_2 = 3\times10^{-11}$ or 7×10^{-11} $cm^3molecule^{-1}s^{-1}$. Therefore we chose to report $k_2 = (5\pm2)\times10^{-11}$ $cm^3molecule^{-1}s^{-1}$. k_2 values are determined from the 6 other FNO

transients in a similar way. The results are given in Table 2. Using the average and conventional propagation of error calculations we get $(5.2\pm2.4)\times10^{-11}$ $cm^3molecule^{-1}s^{-1}$. By adding an extra 5% uncertainty because the result is derived from a complexed mechanism we arrive at $(5.2\pm2.7)\times10^{-11}$ $cm^3molecule^{-1}s^{-1}$.

The absorbance transient in Figure 2 was also simulated using $k_1 = 1.6$ and 1.85×10^{-11} $cm^3molecule^{-1}s^{-1}$. When $k_1 = 1.6\times10^{-11}$ $cm^3molecule^{-1}s^{-1}$ was used a k_2 of $5\text{-}7\times10^{-11}$ $cm^3molecule^{-1}s^{-1}$ fitted the absorbance transient in Figure 2 well. However, an important difference from using $k_1 = 1.7\times10^{-11}$ $cm^3molecule^{-1}s^{-1}$ was that the model became very insensitive to increase in k_2. When $k_1 = 1.85\times10^{-11}$ $cm^3molecule^{-1}s^{-1}$ was used, $k_2 = (4\pm1)\times10^{-11}$ $cm^3molecule^{-1}s^{-1}$ gave the optimal fit of the model calculated transient to the experimental transient. It is important to note that using $k_2 = 3\times10^{-11}$ $cm^3molecule^{-1}s^{-1}$ gave too slow formation of FNO.

4. DISCUSSION

The obtained rate constant for reaction between CF_3O and NO, $k_1 = (5.2\pm2.7)\times10^{-11}$ $cm^3molecule^{-1}s^{-1}$ is 2-3 times larger than the values reported by Bevilaqua et al. [7], $k_2 = (2\pm1)\times10^{-11}$ $cm^3molecule^{-1}s^{-1}$ and by Zellner [9] $k_2 = (2.5\pm0.4)\times10^{-11}$ $cm^3molecule^{-1}s^{-1}$. Eventhough the one of the previously reported values for k_2 is within our reported error limits and the the uncertainty of the other value overlabs our uncertainty it should be noted that none of our experimental transients could be fitted with $k_2 = 3\times10^{-11}$ $cm^3molecule^{-1}s^{-1}$. The reason for this discrepancy is unknown at present time. We recommend further investigations of the reaction between CF_3O and NO.

The rate constants known for CF_3O_x reactions of stratospheric interest are listed in Table III. Most of the rate constants have been determined at room temperature only. Changing the temperature from 295 K to 220 K will slow down the bimolecular reactions listed in Table III. However, for an order-of-magnitude calculation the room temperature rate constants will be sufficient. The key reactions in the possible cyclic stratospheric ozone destruction can be divided into three groups: the chain initiating step, formation of CF_3O_x from HFCs containing CF_3 groups; the chain propagating steps, CF_3O_x reactions with ozone; and the terminating steps, CF_3O reaction with NO and CH_4. In addition holding processes and "zero" ozone destruction cycles are also important. An example of a holding process is the reaction of CF_3O_2 with NO_2 producing a reservoir species, $CF_3O_2NO_2$. This reaction decrease the amount of CF_3O_x radicals available for ozone destruction. A prominent "zero" ozone destruction cycle consists of the reaction of CF_3O with ozone followed by reaction of CF_3O_2 with NO and NO_2 photolysis. The O atoms from the NO_2 photolysis react with O_2 to give ozone. Hence, no net ozone destruction results from this cycle.

In Figure 3 the estimated lifetimes of CF_3O_x with respect to the trace species in the stratosphere are displayed as a function of altitude. For the reactions of CF_3O_x with ozone, upper limits of $k_1 < 0.5\times10^{-14}$ $cm^3molecule^{-1}s^{-1}$ and k_2 from the following papers [?,?], $k_2 < 5\times10^{-14}$ $cm^3molecule^{-1}s^{-1}$, have been used in the calculations. It can be seen from Figure 3 that the reaction of CF_3O_x radicals with ozone is still the main reaction channel for these radicals in the stratosphere. As seen from figure 3 the CF_3O radical can deplete a maximum of 10 O_3 molecules before it is scavenged by NO, thus making CF_3O unimportant with respect to O_3 depletion.

After the completion of this manuscript we have been informed that the value for k_2 obtained previously by Bevilaqua et al. [7] have been superseded by a recent more direct determination giving $k_2 = 6x10^{-11}$ $cm^3molecule^{-1}s^{-1}$ [12]. Also at a recent workshop on the atmospheric degradation of HCFCs and HFCs R. Zellner [13] presented an new and updated value for k_2 of around $5x10^{-11}$ $cm^3molecule^{-1}s^{-1}$. It seems the different determinations of k_2 now all tends agree within the experimental uncertainty

REFERENCES

1. Alternative Fluorocarbon Environmeltal Acceptability Study, W.M.O. Global Ozone Research and Monitoring Project, Report #20; Scientific assesment of stratospheric ozone, Vol 2, 1989.

2. T.J. Wallington, P. Dagaut, and M.J. Kurylo, Chem. Rev. 92 (1992) 667.

3. P.D. Lightfoot, R.A. Cox, J.N. Crowly, M. Destriau, G.D. Hayman, M.E. Jenkin, G.K. Moortgat, and F. Zabel, Atmos. Environ. 26A (1992) 1805.

4. O.J. Nielsen, T. Ellerman, J. Sehested, E. Bartkiewicz, T.J. Wallington, and M.D. Hurley, Int. J. Chem. Kinet. 24 (1992) 1009.

5. J. Sehested, T. Ellermann, O.J. Nielsen, T.J. Wallington, and M.D. Hurley, submitted for publication in Int. J. Chem. Kinet.

6. J. Sehested and T.J. Wallington, Environ. Sci. Tech. 27 (1993) 146.

7. T.J. Bevilaqua, D.R.Hanson, and C.J. Howard, accepted for publication in J. Phys. Chem.

8. J. Chen, T. Zhu, H. Niki, and G.J. Mains, Geophys. Res. Lett. 19 (1992) 2215.

9. R. Zellner, private communication 1993.

10. J. Chen, T. Zhu, and H. Niki, J. Phys. Chem. 96 (1992) 6115.

11. O.J. Nielsen, Risø National Laboratory Report Risø-R-480, 1984.

12. A.R. Ravishankara, A.A. Turnipseed, N.R. Jensen, S. Barone, M. Mills, C.J. Howard, and S. Solomon, Science (1993) in press.

13. R. Zellner, presentation at the NASA/NOAA/AFEAS Workshop on Atmospheric Degradation of HCFCs and HFCs, Boulder (USA), 17th-19th November (1993).

Fig. 1: NO_2 absorbance transient at 400 nm

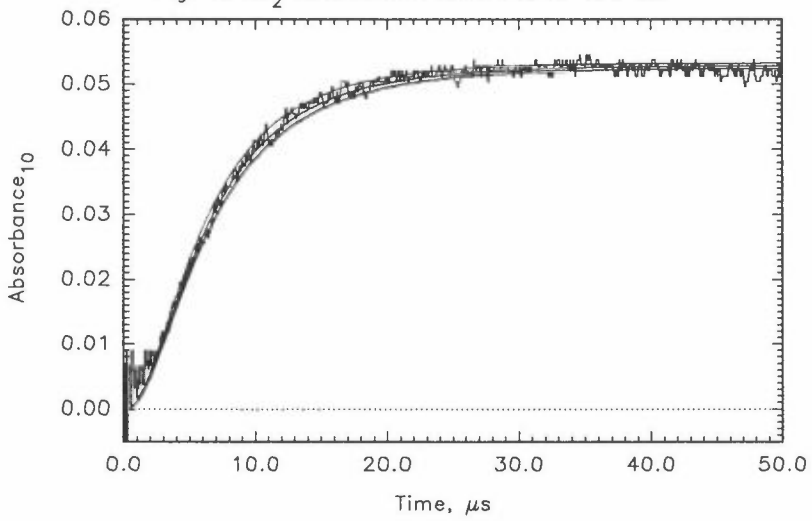

Fig. 2: FNO absorbance transient at 310.5 nm

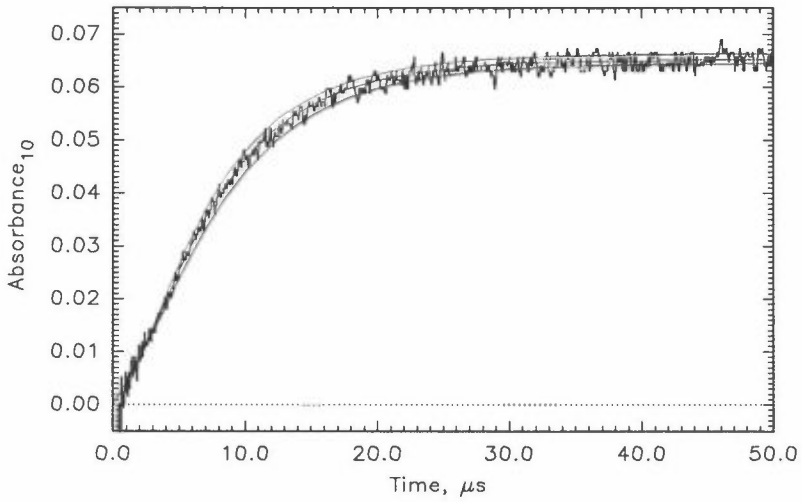

Fig. 3: CF_3O lifetime (t=1/(k*[X]) with respect to X

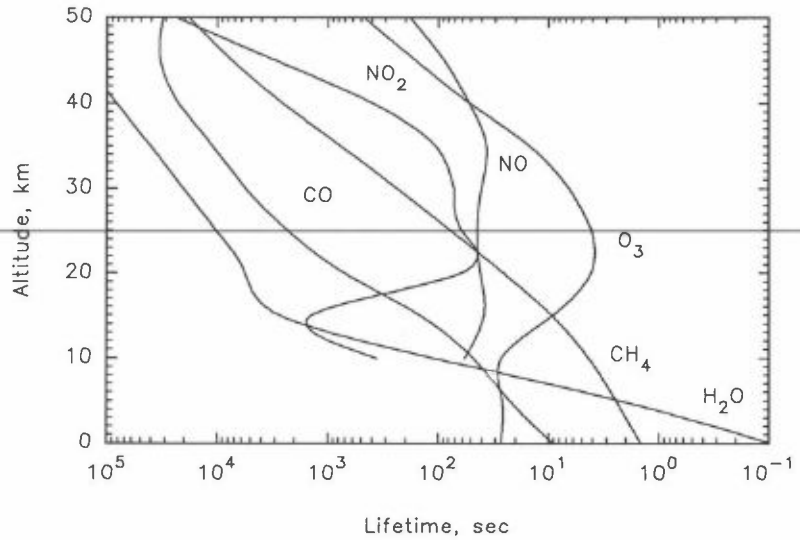

An FTIR study of the vapour phase reaction between the nitrate radical and 2-butyne.

J.G. SELAND, I.M.W. NOREMSAUNE and C.J. NIELSEN

Department of Chemistry, University of Oslo
P.O. Box 1033 Blindern, N-0315 Oslo 3, Norway

SUMMARY

The vapour phase reaction at 298K and 1013 hPa between the nitrate radical and 2-butyne has been studied by long path FTIR spectroscopy. The following products have been identified by their IR spectra: butadione, carbon monoxide, formaldehyde, ketene, and PAN. In addition, the IR spectra indicate the formation of acetyl nitrate. The product distribution has been rationalized in terms of a reaction mechanism different from that previously proposed for alkynes.

INTRODUCTION

Data on reactions between the nitrate radical and alkynes are scarce. One of the alkynes for which data exists, 2-butyne, has been chosen as a model compound for our study of the NO_3 initiated degradation, although it is not an important atmospheric pollutant. The rate constant for the NO_3 reaction with 2-butyne has been reported as $(6.7\pm1.5)10^{-14}$ cm^3 $molecule^{-1}$ s^{-1} [1], i.e. the reaction is relatively fast. The importance of this nitrate radical reaction is also reflected in the atmospheric lifetime of 2-butyne: ca. 9 hours with respect to OH (0.04 ppt) but less than 2 hours with respect to NO_3 (0.1 ppb).

Only guesses as to how the reaction proceeds is found in the literature [2], and the primary goal of this work is to illucidate the reaction mechanism and thereby to help predict the product distribution resulting from the night time degradation of alkynes in general. The reaction mechanism for the OH initiated oxidation of 2-butyne has previously been published by Hatakeyama et al. [3], but to our knowledge the present communication is the first mechanistic study of the NO_3/alkyne reaction.

EXPERIMENTAL

A Bruker IFS 88 interferometer was employed to obtain infrared spectra of reaction mixtures contained in a 2.2 m long, 40 cmØ, stainless steel chamber containing White type multireflection optics. The reactions were carried out in purified air at 298 K and 1013 hPa total pressure. The optical pathlength was 120 m and the spectral resolution was 0.5 cm^{-1}. 2-butyne and some of the reference compounds were commercial products, which were purified prior to use, while the nitrate radical was produced in situ by thermal decomposition of N_2O_5. Reactions were also carried out with ^{15}N labled N_2O_5. Typical starting concentrations of the reactants were: 2-butyne (20 ppm), N_2O_5 (10 ppm), NO_2 (10 ppm). Eventually the NO_3 reactions were terminated by adding excess NO to the system.

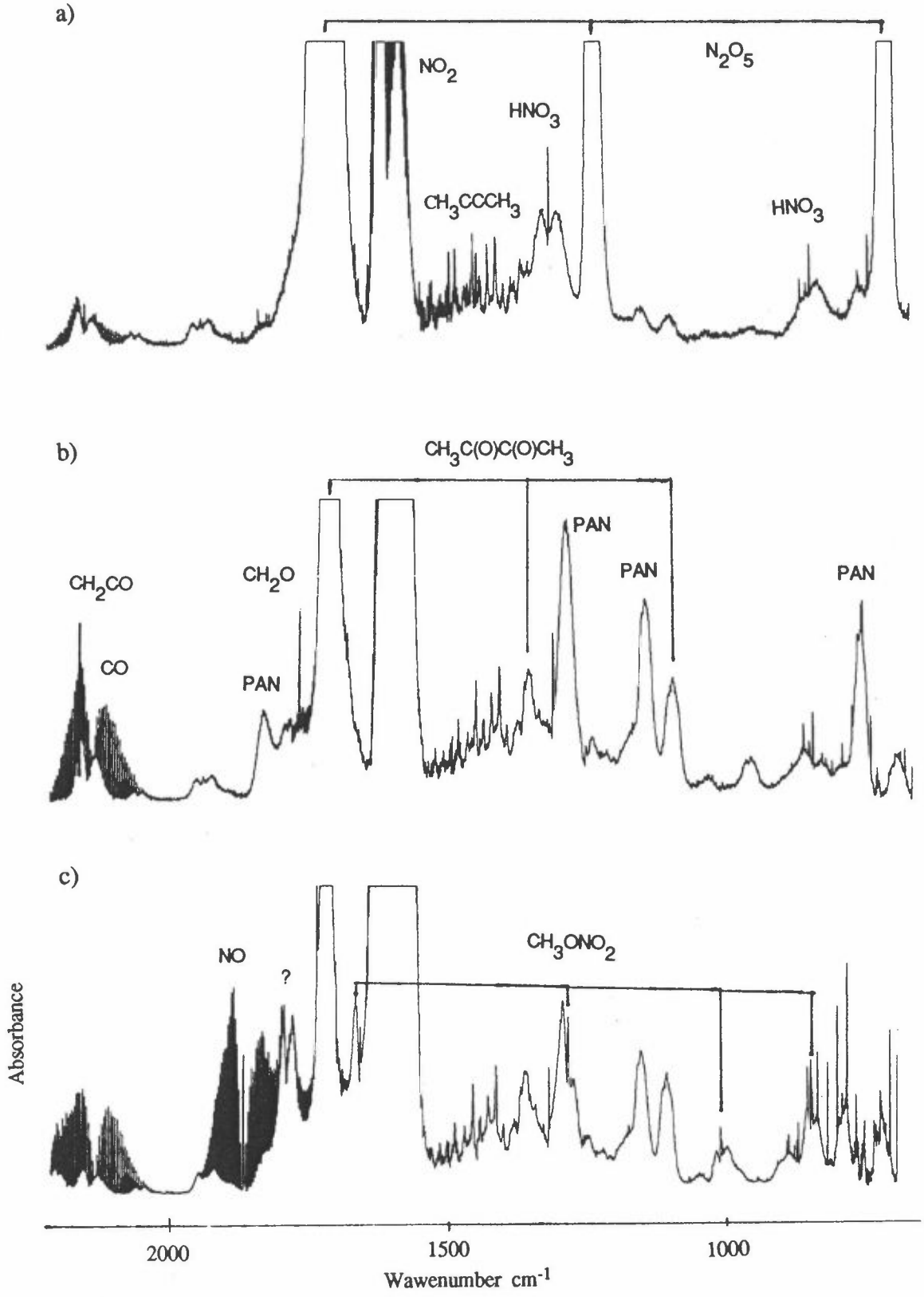

Fig.1. IR spectra of the reaction mixture but-2-yne and N_2O_5. a) Immediately after mixing. b) Two hours later. c) After addition of excess NO. H_2O is subtracted from the spectra.

RESULTS

IR spectra of the reaction mixture obtained immediately after mixing, two hours later, and after adding excess NO are shown in Fig. 1. Absorption bands distinct from those of the reactants and NO_2 and HNO_3 are quickly building up and can be observed already in the first recorded spectrum of the reaction mixture.

From spectra of pure reference compounds, the following products can unambiguously be identified: 2,3-butadione, ketene, PAN, carbon monoxide, and formaldehyde. Unfortunately, we are not able to identify CO_2 as a product. 2,3-butadione accounts for roughly one third of the reacted 2-butyne and is thus an important oxidation product. The nitrooxy absorption bands around 1720, 1310 and 790 cm^{-1} appear prominent, and may be explained by PAN alone. However, minor traces of other nitrooxy compounds cannot be excluded. It is highly significant that the typical nitrate absorption bands around 1670, 1290 and 835 cm^{-1}, which normally also appear as quite strong in in the IR spectra, are not observed at all. It should also be noted that pernitric acid was not observed.

When an excess of NO is added to the reaction mixture, there is no dramatic change in the spectra. Even after three hours with excess NO present, there is only a roughly 50 % decrease in the nitrooxy bands anticorrelated with the build-up of new absorption bands centred at 1800, 1675, 1291, 1019, and 853 cm^{-1}. The latter four bands are due to methylnitrate while the B-type band at 1800 cm^{-1}, marked with a question mark in Fig. 1c, at the moment remains unidentified. The bands due to 2,3-butadione and carbon monoxide show no significant increase after adding excess NO, in contrast to the formaldehyde bands that grow by almost 40%.

Ketene appears to be quite stable in our reaction system and only decomposes slowly. However, ketene reacts reasonably fast with NO_3 forming formaldehyde and CO [4].

DISCUSSION

There was no indication of hydrogen abstraction by NO_3, and the observed product distribution has been interpreted solely in terms of a mechanism initiated by NO_3 adding to the carbon-carbon tripple bond

$$H_3C\text{-}C{\equiv}C\text{-}CH_3 + NO_3 \rightarrow H_3C\text{-}C(ONO_2){=}\dot{C}\text{-}CH_3$$

It has been postulated that the NO_3-alkyne adduct may undergo a Wolff rearrangement [2]. In the present case, such a rearrangement would lead to dimethylketene which is definitely not observed. Instead, it seems more probable that the next step is a reaction with O_2

$$H_3C\text{-}C(ONO_2){=}\dot{C}\text{-}CH_3 + O_2 \rightarrow H_3C\text{-}C(ONO_2){=}C(\dot{O}_2)\text{-}CH_3$$

Following the scheme from analogue alkene reactions [5], the peroxy radical enters an equilibrium with NO_2 forming a nitrooxy nitrate compound. However, there are several indications

that this equilibrium is completely shifted towards the reactants. First, there is little or no sign of nitrate absorption bands before excess NO is added to the system, and these nitrate bands are normally quite strong. Second, after excess NO is added, there is a significant decrease in the nitrooxy absorption bands, but there is little, if any, increase in the bands due to 2,3-butadione. This is in contrast to what one expects if the nitrate-peroxy radical is just slightly stable. Our interpretation is also in agreement with Hatakeyama et al. [3] who studied the analogue reaction between 2-butyne and OH and concluded that the hydoxy-peroxy radical had a very short lifetime. Accordingly, we have left out this equilibrium reaction from the mechanism and only take the (fast) peroxy to oxy radical conversion into consideration

$$H_3C\text{-}C(ONO_2)=C(\dot{O}_2)\text{-}CH_3 + \begin{matrix} RO_2 \\ NO \\ NO_3 \end{matrix} \rightarrow H_3C\text{-}C(ONO_2)=C(\dot{O})\text{-}CH_3$$

Two reaction channels are normally considered for alkoxy radicals: dissociation and isomerization. We discard the dissociation channel, as the hypothetical radicals formed do not lead to the observed products, and are left with isomerization as the main path

$$H_3C\text{-}C(ONO_2)=C(\dot{O})\text{-}CH_3 \rightarrow H_3C\text{-}\dot{C}(ONO_2)\text{-}C(O)\text{-}CH_3$$

The alkyl radical may then either split off NO_2 and thereby form the observed 2,3-butadione, or react further with oxygen

$$H_3C\text{-}\dot{C}(ONO_2)\text{-}C(O)\text{-}CH_3 \rightarrow H_3C\text{-}C(O)\text{-}C(O)\text{-}CH_3$$

$$H_3C\text{-}\dot{C}(ONO_2)\text{-}C(O)\text{-}CH_3 + O_2 \rightarrow H_3C\text{-}C(\dot{O}_2)(ONO_2)\text{-}C(O)\text{-}CH_3$$

Again, the peroxy radical may be involved in an equilibrium with NO_2 but as before the observations do not support this and the next step is presumably the peroxy to oxy radical conversion

$$H_3C\text{-}C(\dot{O}_2)(ONO_2)\text{-}C(O)\text{-}CH_3 + \begin{matrix} RO_2 \\ NO \\ NO_3 \end{matrix} \rightarrow H_3C\text{-}C(\dot{O})(ONO_2)\text{-}C(O)\text{-}CH_3$$

followed by a cleavage of the central carbon-carbon bond and leading to the PAN precursor, the acetyl radical, and to electronically excited acetyl nitrate

$$H_3C\text{-}C(\dot{O})(ONO_2)\text{-}C(O)\text{-}CH_3 \rightarrow H_3C\text{-}\dot{C}{=}O + \left[(ONO_2)\text{-}C(O)\text{-}CH_3\right]^{\ddagger}$$

In their study of the analogue OH reaction, Hatakeyama et al. [3] observed both PAN and 2,3-butadione production in the presence of NO_x. However, they did not observe the formation of ketene, only acetic acid, corresponding to acetyl nitrate in the NO_3 initiated reaction. We tentatively suggest that electronically excited acetyl nitrate decomposes into ketene and nitric acid through a rearrangement of a 6-membered ring

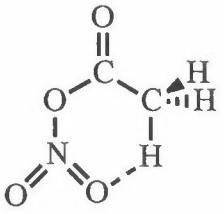

$\longrightarrow$ $CH_2CO + HNO_3$

According to the proposed mechanism ketene and nitric acid should be formed in equal amounts. However, the spectra show a decrease in nitric acid vapour from reaction start to end. Most likely, the nitric acid is deposited on the stainless steel walls of the reaction chamber.

Ketene reacts further with NO_3 to give formaldehyde, CO, and probably CO_2 as well, thus accounting for the production of these compounds prior to adding excess NO. The significant increase in formaldehyde and the formation of methylnitrate after adding excess NO is connected with the break-down of PAN via the peroxy-acetyl, oxo-acetyl, methyl, peroxymethyl radicals. The large NO_2 concentration that is a consequence of excess NO, ensures that the methyl radicals forming acetyl nitrate. Indeed, the formation of absorption bands at 1800, 1675 and 853 cm^{-1} may very well be explained by acetyl nitrate. Formaldehyde also seems to be a secondary product since its concentration increases by about 40% after addition of NO.

REFERENCES

[1] CANOSA-MAS, C.E., SMITH, S.J., TOBY, S., AND WAYNE, R.P. (1988). J. Chem. Soc. Faraday Trans. 2, Vol. 84, 247-262.

[2] WAYNE, R.P., BARNES, I., BIGGS, P., BURROWS, J.P., CANOSA-MAS, C.E., HJORTH, J., LE BRAS, G., MOORTGAT, G.K., PERNER, D., POULET, G., RESTELLI., G., AND SIDEBOTTOM, H. (1991). Atmospheric Environment, Vol. 25A, 114-116.

[3] S. HATAKEYAMA, N. WASHIDA AND H. AKIMOTO, J. Phys. Chem. 1986, Vol. 90, 173-178.

[4] SELAND, J.G., NOREMSAUNE, I.M.W.O., AND C.J. NIELSEN, to be published.

[5] HJORTH, J., LOHSE, C., NIELSEN, C.J., SKOV, H., AND RESTELLI, G. (1990). J. Phys. Chem., Vol. 94, 7494-7500.

Adsorption and phototransformation of PAHs on model atmospheric particles

HEIKKI TANNER, AARNE BOGDANOV and LIA PAALME
Institute of Chemical Physics and Biophysics,
Estonian Ac. Sci., Tallinn EE0100,Rävala pst.10,Estonia

SUMMARY

We have previously reported that different oxidants can activate Polycyclic Aromatic Hydrocarbons (PAHs) supported on the surface of model particulate matter. We have since conducted similar trials with UV-exposed aerosols. The trials focused on aerosol matrices of SiO_2, Al_2O_3 and fly ash and their relative effects on the adsorption and degradation kinetics of three PAHs: Pyrene (Pyr), Chrysene (Chr) and Benzo(a)pyrene (BaP). The degree of PAH adsorption and degradation varied significantly with the particulate matrix used. Shale-oil fly ash proved to adsorb the largest quantity of PAHs and in the least selective manner. In contrast, Al_2O_3 adsorbed the lowest quantity of PAHs and displayed the largest selectivity.

The photo-oxidation rate of the PAHs studied was the largest on SiO_2, followed closely by Al_2O_3; half-lives in the range of 4-6 min. The half-lives for oil-shale fly ash measured in days. Variation in transformation rates between the various PAHs on any given matrix was found to be less significant than the variation seen on different matrices. Pyr was constantly the most reactive compound, followed by BaP and finally Chr, regardless of the matrix used.

The ability of carcinogenic PAHs to adsorb to and form relatively stable particles with fly ash may have serious public health implications for Estonia and other countries of the Baltic region.

INTRODUCTION

Polycyclic Aromatic Hydrocarbons (PAHs) are a class of complex organic molecules which are made up of carbon and hydrogen atoms and comprise of 5- and 6-membered ring structures in which the interlinked rings have at least two carbon atoms in common. As a consequence, there are literally hundreds of PAH compounds. PAHs are most frequently encountered as the byproducts of the incomplete combustion of organic materials and are emitted from fossil fuel fired power plants, internal combustion and diesel automobile engines, industrial processes, forest fires, cooking,

refuse incinerators and cigarettes, cigars, pipes.
Many of the PAH which were found in ambient air have been shown to be carcinogenic. The results of the analysis indicated that the oil-shale fired plants in northeastern Estonia were the sources of pollution of this region with mineral components and carcinogenic PAHs. The total intensity of PAH here was 8 mg/ha per year. These plants are the biggest air pollution courses and this region is a most heavily polluted area in Estonia.
Because of their high molecular weight, concomitant low vapor pressures, and affinity for particle surfaces, the PAH have been considered to be associated exclusively with particulate matter.
In northeastern Estonia, most of the PAH in atmosphere are adsorbed on the surface of fly ash particles, emitted from oil-shale fired plants because of out-date burning technology.
Various parameters may modify chemical and photochemical transformation of PAHs in the atmosphere, including light intensity, concentration of gaseous pollutants (O_3,NO_x,SO_x) and chemico-physical characteristics of particulates or substrates into which the PAHs are adsorbed; depending of these variables, the half-life of benzo(a)pyrene in the atmosphere according to literature varies from 10 minutes to 72 days [1].
Chemical reactivity of PAH compounds adsorbed on the surface of different atmospheric aerosol particles are studied by several autors.
The trials with UV-exposed aerosols were conducted in our laboratory. The trials focused on aerosol matrices of SiO_2, Al_2O_3 and fly ash and their relative effects on the adsorption and degradation kinetics of three PAHs: Pyrene (Pyr), Chrysene (Chr) and Benzo(a)pyrene (BaP).

EXPERIMENTAL

Photodegradation experiments were carried out with 0.2 g of adsorbent in rotating quartz test tube exposed to UV-radiation from high pressure mercury lamp.

Coating of adsorbent with PAH was performed during 30 minutes in acetone. Then adsorbent was dryed in vacuum exicator. Exposed adsorbent was washed with acetone. After that acetone was removed and PAH was transferred into 5 or 10 ml of hexane. PAH were analyzed by Specord M-40 UV-VIS spectrophotometer at 240 - 450 nm.

RESULTS

A technique was developed which gives error from no-homogeneous coating about ± 10 %. Adsorption isoterm for Pyrene on Silicagel (Fig.1) and photodegradation cruves for Pyr (Fig.4,5) and Chr (Fig.2,3) on model adsorbents were obtained. Silicagel was used as model aerosol because SiO_2 is main mineral component in atmospheric aerosols. Half-life of 108 min. for 60 μg/g Pyr on SiO_2 and several days for Pyr, Chr and BaP on fly ash were established.

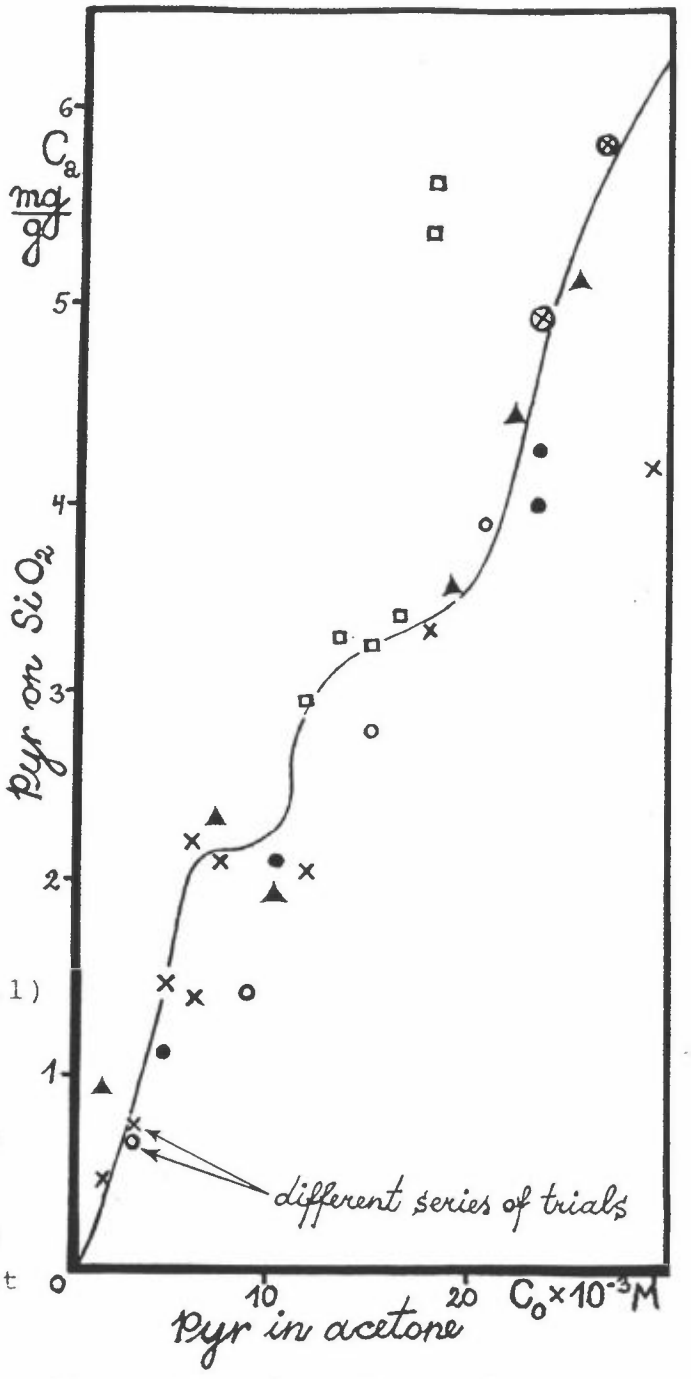

Figure 1. Adsorption of Pyrene on Silicagel (0.5 g, 40/100 μ) from its solution in acetone (10 mL).

DISCUSSION

From the viewpoint of environmental self-purification in the atmosphere under natural sunlight real fly ash particles seems to be low selective matrix for different PAH. In model experiments particulate adsorbent is more important and photo-oxidation process more rapid.

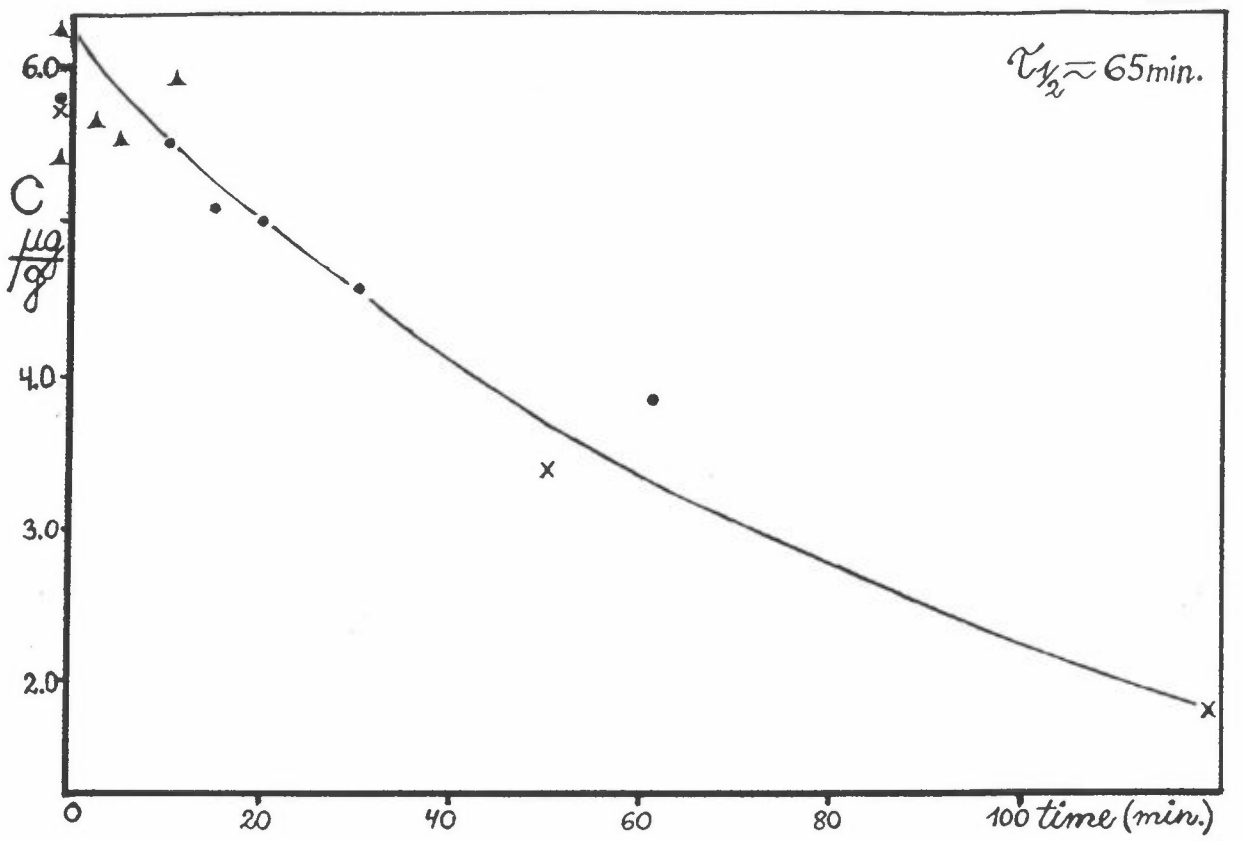

Figure 2. Photodegradation of UV-exposed Chr adsorbed on SiO_2.

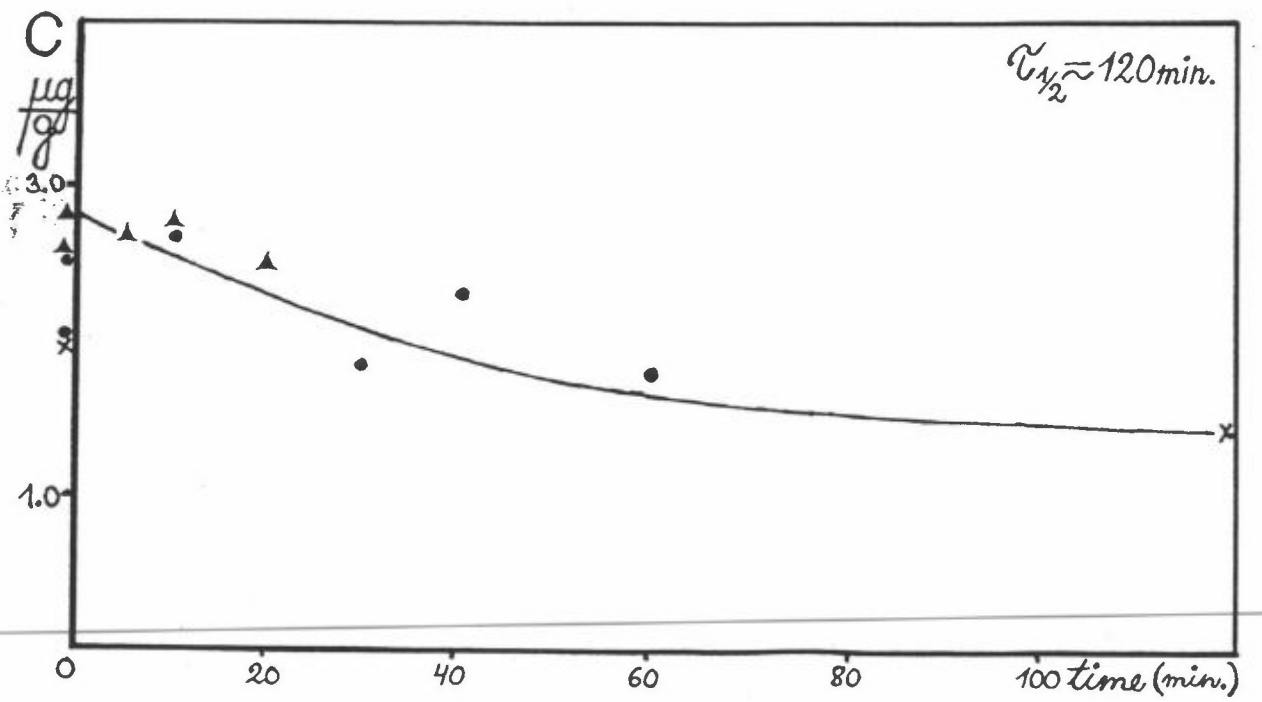

Figure 3. Photodegradation of UV-exposed Chr adsorbed on Al_2O_3.

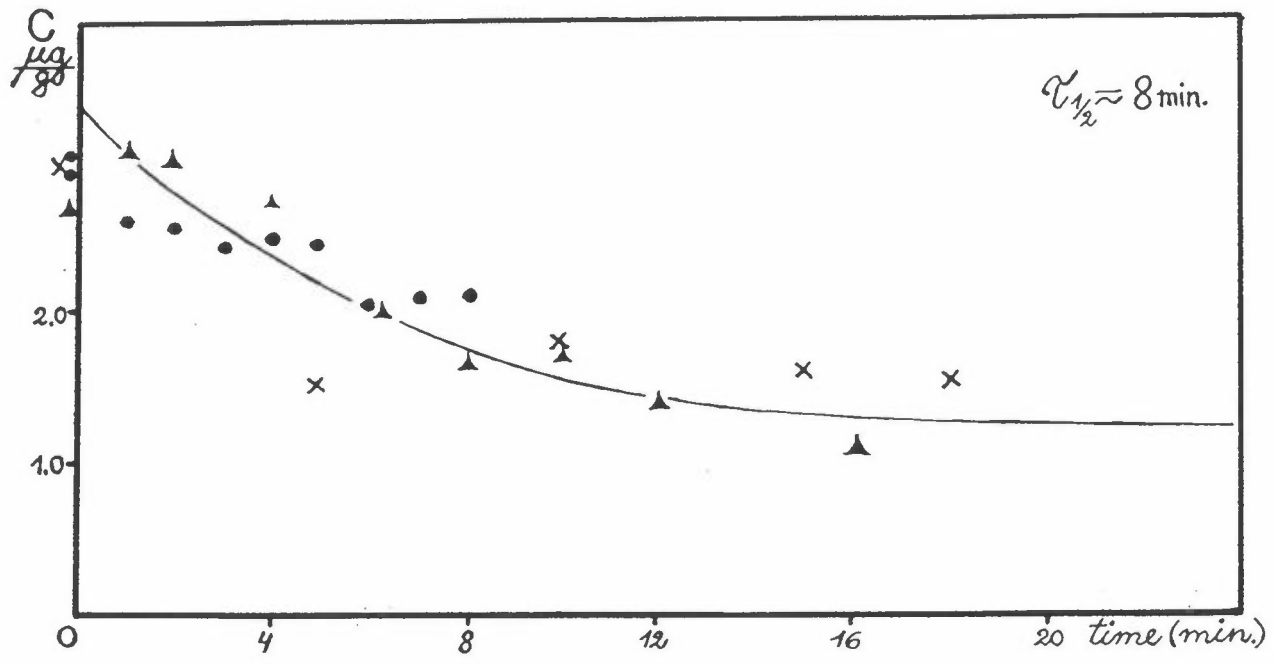

Figure 4. Photodegradation of UV-exposed Pyr adsorbed on SiO_2.

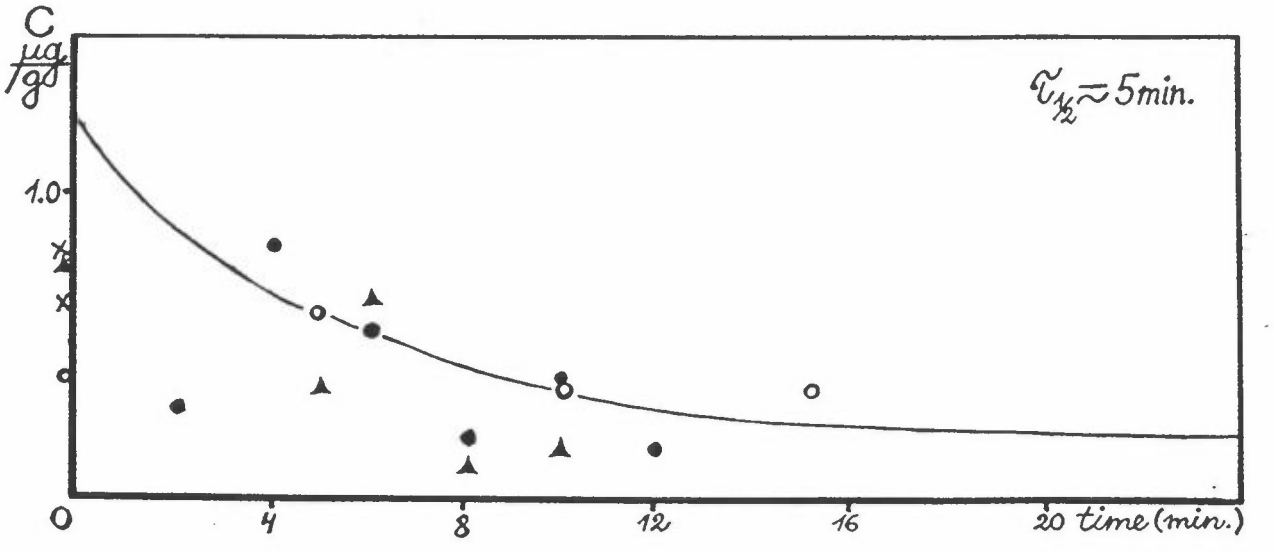

Figure 5. Photodegradation of UV-exposed Pyr adsorbed on Al_2O_3.

REFERENCES

[1] Valerio et al. "Chemical and photo-chemical degradation of polycyclic aromatic hydrocarbons in the atmosphere". Sci. Total Environ., 1984, Vol. 40, 169-188.

Laboratory studies of heterogeneous reactions of $ClONO_2(g)$ AND $HNO_3(g)$ on NaCl(s) and NaBr(s)

RAIMO S. TIMONEN AND MING-TAUN LEU
EARTH AND SPACE SCIENCES DIVISION, JET PROPULSION LABORATORY, CALIFORNIA INSTITUTE OF TECHNOLOGY, PASADENA

A laboratory study of the following heterogeneous reactions of potential importance for volcanic and marine aerosols was performed.

(1) $ClONO_{2(g)} + NaCl_{(s)} \rightarrow Cl_{2(g)} + NaNO_{3(s)}$
(2) $ClONO_{2(g)} + NaBr_{(s)} \rightarrow BrCl_{(g)} + NaNO_{3(s)}$
(3) $HNO_{3(g)} + NaCl_{(s)} \rightarrow HCl_{(g)} + NaNO_{3(s)}$
(4) $HNO_{3(g)} + NaBr_{(s)} \rightarrow HBr_{(g)} + NaNO_{3(s)}$

Reactions (1) - (4) are of interest because of the conversion of NaCl and NaBr into photochemically active halogen species (Cl_2, BrCl, HCl, and HBr). The photolysis of these molecules forms Cl and Br atoms which can remove ozone by the well known catalytic reactions in the stratosphere.

A modified fast flow reactor with six fixed gas inlets coupled to a quadrupole mass spectrometer1 was used for investigating the reaction probabilities of the reactions (1) - (4). The surface areas of the solid samples were measured using the BET adsorption isoterm method. The areas were also measured from scanning electron micrographs and these results are consistent of the areas from the BET measurements.

In this paper the results, their implications to atmospheric chemistry, and the problems of the measurements will be discussed.

1. Leu M.-T., J.E. Blamont, A.D. Anbar, L.F. Keyser, and S.P. Sander, J. Geophys. Res., 97, 1992, 2621.

THE FIRST STUDIES IN THE FIELD OF SPECTROSCOPY AND PHOTOCHEMISTRY OF ATMOSPHERE IN LATVIA

ARNOLDS ŪBELIS
Department of Spectroscopy, University of Latvia
19 Raina bulv., Riga LV-1586, Latvia

In 1991 the Science Council of Latvia accepted our application in order to obtain the grant for the theme: "Spectroscopy and Photochemistry of Polluted Atmosphere".This was the starting point for the research in this field.

The theme was announced as a new direction of research at the University of Latvia, and also in Latvia. The announcement was founded on the previous experience in the field of atomic physics and photochemistry. The research group was studying the characteristics of Se, Te, Pb, Sn atoms and compounds of these elements and their activity in the collision processes. The announcement was motivated by desire to turn to the direction of studies which would be connected with environmental protection and particularly with physics and photochemistry of atmosphere.

Three major aims were defined for this theme:

* first of all, the research in spectroscopy and photochemistry of atmosphere gases and atmosphere polluting gases, pollution aerosols and heavy metals disparaged in atmosphere;

* second, the study of the projects of pollution analyzers based on the methods of UV and VUV spectroscopy ;

* third, to work with students delivering lectures and involving them in to practical investigations;

Unfortunately, the constraint finance situation did not allowed us to fulfill the program envisaged. In spite of this we can mention some previous results useful for our future studies. A review of appropriate periodical publications, monographs and patents was prepared. UV and VUV spectroscopy methods were selected as the main tools and experimental set-ups and specially constructed reaction vessels and specific sources of light for the UV and VUV region of spectrum were prepared and could be used more widely. Some

experiments on SO_2 and formaldehyde were undertaken. Methods of analysis of the aerosols based on their atomization in the frequency discharge were proposed. The most successful was the realization of the third task of work, to connect the research with tutorial work. The workers of the group delivered specialized courses of lectures to the students who are preparing for the baccalaureate and the master's degrees and supervised the students scientific work. In this connection we can mention on the following titles of undergraduate and diploma theses:

O.Priednieks. The Advantages of the UV Spectroscopy Methods in the Measurement of Atmosphere Pollution. 1991, Undergr.Thesis.

O.Kudryashov. The Problem of the Ozone Layer. 1991, Undergr. Thesis.

V.Bishans. Spectroscopy of the Sulfur Dioxide Molecule and Its Role in Elementary Processes in Polluted Atmosphere. 1992, Diploma Thesis.

R.Buchmis. Spectroscopy of the Formaldehyde Molecule and Formaldehyde in Atmosphere. 1991. Diploma Thesis.

M.Orlov. The Detection of the Environment Pollution by Oil Products Using Laser Fluorescence. 1992, Diploma Thesis.

K.Orlovsky. The Investigation of Biological Products and Air Pollution Using Laser Induced Fluorescence Methods. 1993, Diploma Thesis.

We are looking forward to find out possibilities how to use our experience in the fields of UV and VUV spectroscopy,photo-chemistry, light sources technology and the technique of flash photolysis for the purpose of atmospheric chemistry research. Nowadays it is hard to realize this task at the University of Latvia without international cooperation and we expect some suggestions on it from the Nordic countries.

Fast-Flow Discharge Measurements of the NO_3 Radical Addition Rate of Some Cyclic Alkenes

Ingvar Wängberg, Evert Ljungström and Sarka Langer
Department of Inorganic Chemistry
University of Göteborg and Chalmers University of Technology
S-412 96 Göteborg, Sweden

In a fast-flow discharge investigation of the NO_3 radical addition rate to cyclopentene, cyclohexene and 1-methyl-cyclohexene[1], a new approach for evaluating experimental data was developed to account for flow tube pressure drop. The method is useful for evaluating rate constants from experiments made under second order kinetic conditions that require high gas flow rates. The method will be presented, and the need of accounting for pressure drop will be outlined.

Introduction

Figure 1 represents a fast flow set-up consisting of a flow tube, a sliding injector and a detector. With the present experimental set-up NO_3 radicals were detected by a multi path *vis*-spectroscopic detection system. By sliding the injector different contact lengths and thus different contact times are obtained. A detailed description of experimental setup used in this investigation is found in [1] and [2].

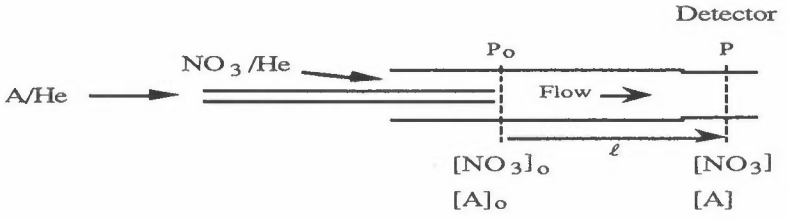

Figure 1. A flow tube. P_0, $[NO_3]_0$ and $[A]_0$ are the pressure and concentration of reactants at the mixing location while P, $[NO_3]$ and [A] are pressure and reactant concentrations at the detector. ℓ is the contact length.

A gas flow in a tube always sets up a pressure gradient. According to Figure 1, P_0 is therefore expected to surpass P. As a consequence, the concentration of all gas constituents will decrease downstream the flow tube.

In experiments with the actual experimental setup, the pressure drop was decreasing linearly downstream the tube in agreement with calculations assuming viscous flow. Pressure gradients measured were between 12 and 15 Pa m^{-1}. Under the present conditions, i.e., contact lengths of up to 1.3 m and P_0 pressure of range 120 to 250 Pa, the pressure drop along the tube will be about 6 - 16%. This means that the reactants will not only be consumed through reaction; they will also be significantly diluted along with the pressure drop. When working under pseudo first order kinetic conditions this normally constitutes no problem. In order to obtain sufficient time resolution, however, experiments sometimes must be made under second order kinetic

conditions. In this paper we report how problems concerning evaluation of rate coefficients from flow tube measurements in conjunction with pressure gradients and second order kinetic conditions may be overcome.

Results and discussion

In order to investigate the effects of pressure gradients, both chemical and physical depletion of the reactants in the flow tube were numerically calculated. The computer code was designed so that flow tube experiments, made under different conditions, could be simulated. Figure 1 shows a comparison between the NO_3 removal from one experiment and that from the corresponding simulation.

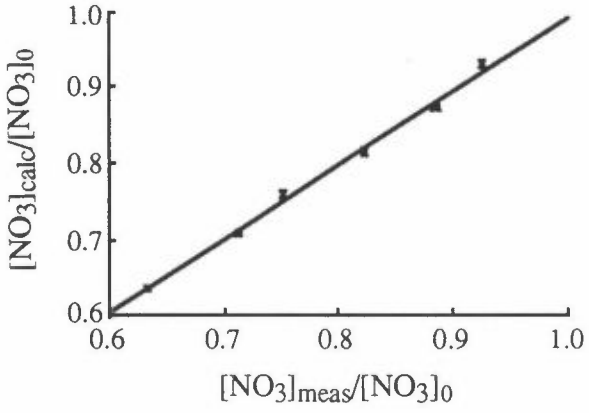

Figure 2. The $[NO_3]_{calc}/[NO_3]_0$ ratio against the $[NO_3]_{meas}/[NO_3]_0$ ratio from an experiment with cyclohexene at 294 K. $[NO_3]_{meas}$ was measured at different contact times in the flow tube. $[NO_3]_{calc}$ originates from a numerical simulation of that experiment.

According to the calculation about 10% of the depletion of reactants were due to pressure drop. As seen there is an excellent fit between measured and calculated data. The above relation was tested for a variety of experimental conditions each giving excellent fits. Thus it was concluded that the numerical model could describe both the chemical and physical behaviour in the flow tube. The result also implies the urgency of accounting for pressure gradients when evaluating rate coefficients from the experiments described. A set of simulations were made with linear gas flow rate altering between 3 to 30 m s^{-1} while the pressure P_0 at the upstream end of the flow tube was kept constant. This variation of gas flow rate, in turn, caused the pressure gradient to vary from 2 to 19 Pa m^{-1}. Data from these simulations were used to evaluate rate coefficients by applying different evaluation methods. The standard procedure of rate coefficients evaluation, not accounting for pressure gradients, is as follows:

$$NO_3 + A \longrightarrow \text{products} \qquad (1)$$

$$\frac{d[NO_3]}{dt} = -k_1[NO_3]([X]+[NO_3]) \qquad (a)$$

$$[X] = [A]_0 - [NO_3]_0 \qquad (b)$$

$$\frac{1}{[X]} \ln \frac{([X]+[NO_3])[NO_3]_0}{([X]+[NO_3]_0)[NO_3]} = k_1 \cdot t \qquad (c)$$

Given a 1:1 stoichiometry, the differential equation (a), with [X]+[NO_3] substituted for [A], is valid for reaction (1). On integration, equation (c) is obtained. When the left hand side of equation (c) is plotted against the contact time the rate coefficient is obtained as the slope of the plot.

Ratios between the rate coefficient used in the simulations and the rate coefficients retrieved by applying different evaluation methods of rate coefficients are presented in Figure 3.

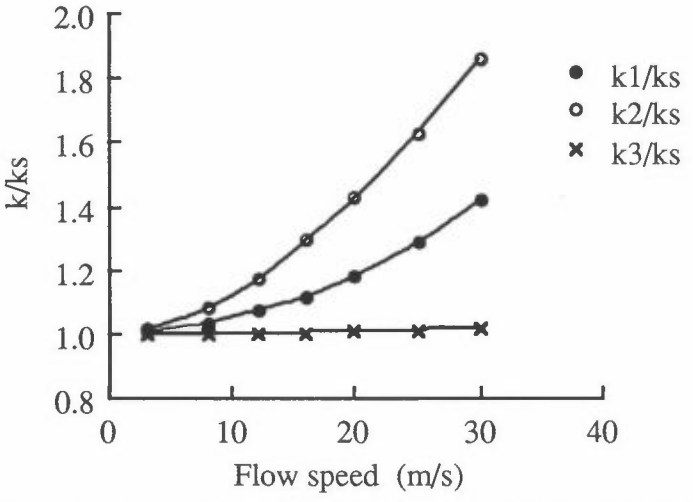

Figure 3 Rate coefficient ratios obtained from simulations of the NO_3 depletion in the flow tube. The rate coefficients are presented as k/k_S ratios where k are rate coefficient obtained by different evaluation methods, and k_S is the rate coefficient used in the simulations. P_0 = 124 Pa, flow tube cross area = $7.1 \cdot 10^{-4}$ m^2, k_S = $6.5 \cdot 10^{13}$ cm^{-3} $molecules^{-1}$ s^{-1}.

The k_1/k_S ratio in Figure 3 corresponds to the rate coefficient ratio obtained using equation (c). As seen this ratio differs significantly from unity at high gas flow rates. Thus rate coefficients obtained by equation (c) tend to be overestimated at high flow rates. The k_2/k_S ratio corresponds to rate coefficients obtained by equation (c) where $[NO_3]_0$ was made up for the pressure drop, and an average [X] were used. However, as seen, this did not improve the results.

A method suitable for rate coefficients evaluation allowing for pressure gradients is clearly required. A new mathematical expression that accounts for pressure gradients was therefore

derived. The differential equation (a) was replaced by equation (d) to which an additional term C is added.[1]

$$\frac{d[NO_3]}{dt} = -k_3[NO_3]([X]+[NO_3]) - C[NO_3] \qquad (d)$$

$$C = \frac{n_t RTG}{AP^2} \ (s^{-1}) \qquad (e)$$

C is the first order rate constant by which NO_3 radicals are depleted due to flow tube pressure drop. C consists of the total molar gas flow rate n_t [mol s^{-1}], the gas constant R [J $K^{-1}mol^{-1}$], absolute temperature T [K], flow tube cross area A [m^2], flow tube pressure P [Pa] and the pressure gradient G [Pa m^{-1}]. To obtain a form, useful for determining k_3, P and [X] were approximated by the average P and [X].

$$\frac{1}{[X+C/k_3]} \ln \frac{([X]+[NO_3]+C/k_3)[NO_3]_0}{([X]+[NO_3]_0+C/k_3)[NO_3]} = k_3 \cdot t \qquad (f)$$

On integration, expression (f) is obtained, differing from (c) by containing the C term; in addition, k_3 is included in both sides of the equation. The k_3 rate coefficient was extracted by least-squares fitting of the left hand side values of (f), calculated for each measurement of an experiment versus the corrected contact times t[1]. As k_3 is included also in the left hand side of (f), an iterative procedure was applied using an estimated starting value of k_3. The fit gives a new k_3 used for calculating new left hand side values of equation (f) and so on. The k_3-value converged within a few such cycles. In Figure 3, k_3/k_S represents the results from using equation (f). As seen the k_3/k_S ratio is close to unity in the entire investigated gas flow rate interval.

Conclusion

Under certain conditions, flow tube pressure drop must be taken account of in order not to overestimate the real reaction rate. Deviation from the real rate coefficient occurs in situations where the depletion of reactants due to a pressure gradient is comparable to that due to the chemical reaction. This situation occurs when the C/k ratio approaches the magnitude of ([X]+[NO_3]). However, by using the suggested method it is still possible to extract accurate rate coefficients.

References

[1] Evert Ljungström, Ingvar Wängberg and Sarka Langer, J. Chem. Soc. Faraday Trans., 1993, 89, 2977.

[2] Sarka Langer, Evert Ljungström and Ingvar Wängberg, J. Chem. Soc. Faraday Trans., 1993, 89, 425.

Field Studies

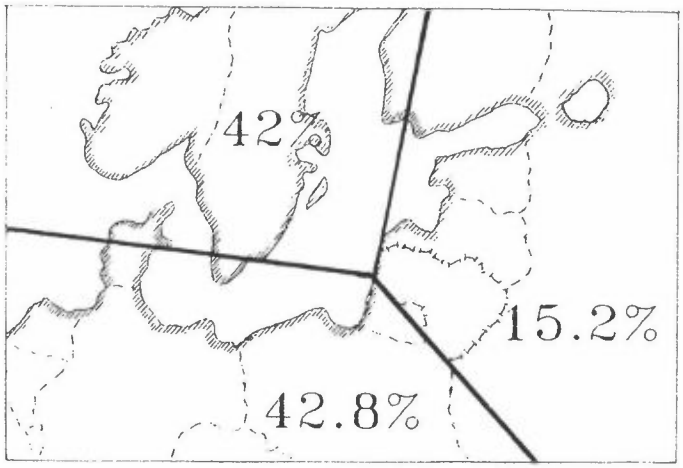

Fig.1. Variation of air mass trajectories into sectors (1980-1990).

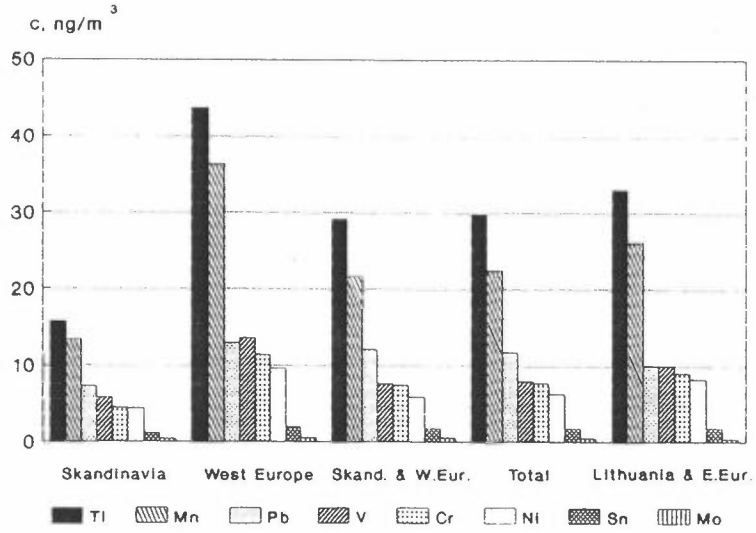

Fig.2. Distribution of the averaged heavy metal concentrations into sectors (1980-1990).

NOx, PAN, Alkyl Nitrates, NOy and O_3 Measurements During Spring in Interior Alaska

Harald J. Beine[1], Daniel A. Jaffe[1], Elliot Atlas[2]

[1] Geophysical Institute, University of Alaska, 903 Koyukuk Dr., Fairbanks, AK 99775-7320, U.S.A.

[2] NCAR, P.O. Box 3000, Boulder, CO 80303, U.S.A.

Summary

Measurements of the atmospheric concentrations of NO, NO_2, NOy, O_3, peroxyacetylnitrate (PAN), alkyl nitrates and hydrocarbons were made in a boreal forest ecosystem in the interior Alaska in April and May 1993. Median mixing ratios for background periods of NOx, NOy and O_3 were 150 [ppt], 506 [ppt] and 25 [ppb] respectively. The PAN contribution to NOy was about 30%. PAN is correlated with ozone, but not with NOx, suggesting that both, PAN and ozone were produced at a distant sources and were transported to the site.

Introduction

Reactive nitrogen oxides play a significant role in tropospheric chemistry. In the Arctic reservoir NOy species, such as peroxyacetylnitrate (PAN) are transported from far away sources. During spring these species are thermally and photochemically decomposed, yielding NOx (Honrath and Jaffe, 1992). NOx is a key species in that it affects ozone production as well as the lifetime of the hydroxyl radical. The ultimate sink for NOx is HNO_3, which affects acid deposition. The principal objectives of this work are to understand the composition of the NOy reservoir, and to explain the origin of tropospheric ozone in the Arctic and Subarctic during the winter - spring transition. NOy accumulates during winter in the Arctic. From previous measurements a decay of this NOy reservoir is expected during the winter - spring transition.

Experimental

Measurements were made at Poker Flat Research Range, Alaska (64°11'N, 147°43'W, 501 m mean sea level) from March 25, to May 14, 1993 (Julian days 84 to 134) in a boreal forest ecosystem. NO, NO_2 and total reactive nitrogen oxides (NOy = $NO+NO_2+HNO_3+PAN+RONO_2+N_2O_5+...$) were determined using high-sensitivity ozone chemilumiescence detectors. NO_2 was detected as NO following photo-dissociation by a 1000 W Xe-arc lamp. NOy was also detected as NO, following reduction by CO in a 300°C catalytic gold converter. A Dasibi UV-analyzer was used to measure ozone concentrations. A GC-ECD

was used for the PAN measurements, alkyl-nitrates were collected on sorbent beds and analyzed by GC-ECD and GC-MS (E. Atlas, NCAR). CO and NMHC samples were collected in stainless steel cans for analysis by GC-FID, however the data are not available yet.

RESULTS

Daily averages for the concentrations of NOx, PAN, alkyl-nitrates, NOy and ozone are shown in figures 1 to 3. Statistics are given in table 1.

Table 1: Statistics of the daily averages for measured values.

Species	Mean	Median	Min.	Max.
NOx [ppt]	183.7	150.5	17.4	899.4
PAN [ppt]	142.9	141.2	49.5	284.9
Alkyl nitrates [ppt]	33.7	33.7	13.8	65.9
NOy [ppt]	511.4	506.3	283.1	756.9
Ozone [ppb]	24.4	25.5	6.5	35.8

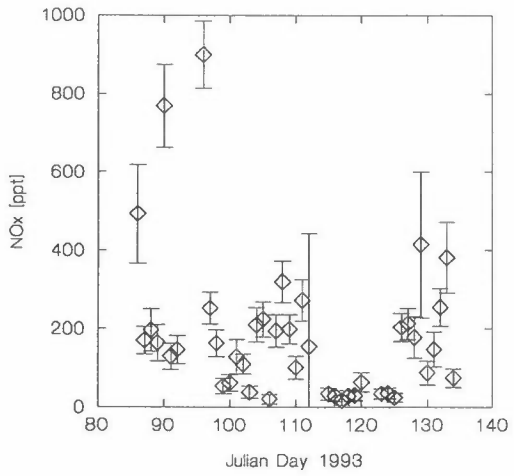

Figure 1: Daily averages of NOx [ppt]. Error bars indicate 95% confidence interval.

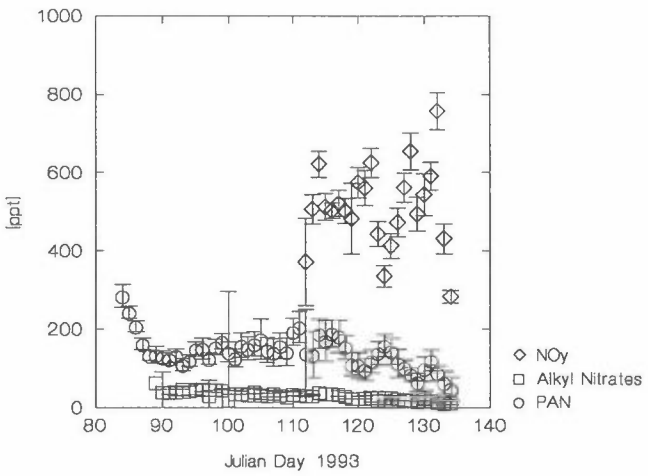

Figure 2: Daily averages of NOy species [ppt].

NO and NOy show about the same concentration range in Poker Flat as during previous measurements in Barrow, Alaska (Honrath and Jaffe, 1992). NOy seems quite high for a site in the Subarctic in spring, especially since the airmasses were mostly transported from the south. PAN and alkyl-nitrate concentrations decreased during the measurement period as expected.

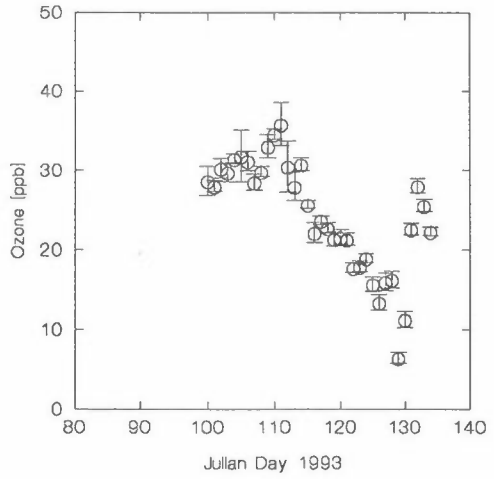

Figure 3: Daily averages of O_3 [ppb]

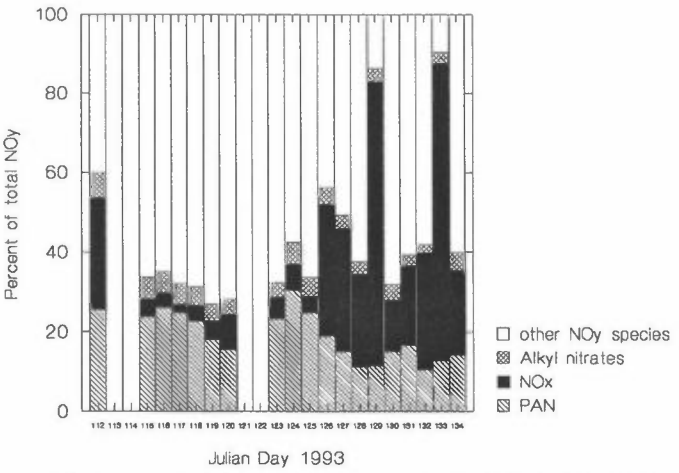

Figure 4: Contribution of measured species to NOy [%].

DISCUSSION

The contribution of NOx, PAN and Σ alkyl nitrates to total NOy can be seen in fig.4. PAN contributed about 15 to 30% to NOy.

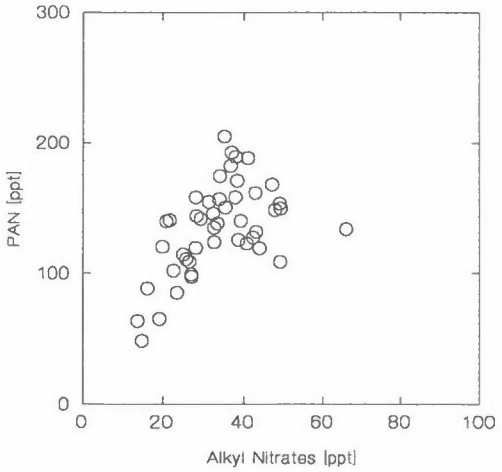

Figure 5: Correlation of PAN vs. alkyl nitrates.

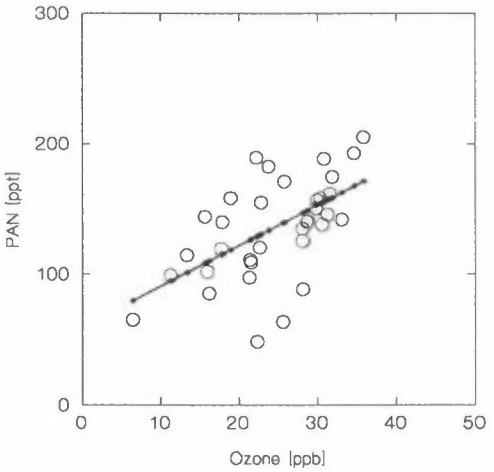

Figure 6: Correlation of PAN vs. ozone. The line shows a linear regression with a slope of 3.123 [ppt PAN/ppb O_3] being statistically significant at the 99.9% level.

This is less than observed at an Arctic site in spring (Bottenheim, 1993), but corresponds closer to the PAN fraction to NOy during summer (Singh et al., 1992), indicating that thermal decomposition of PAN has taken place in Poker Flat during spring. Alkyl nitrates amount to less than 5% of total NOy. This seems in agreement with observations from rural sites (Ridley et al., 1990), but again much lower than previously detected in the Arctic (Bottenheim, 1993). A correlation between PAN and alkyl-nitrates (fig.5) suggests that sources and sinks are partly similar for these compounds, which is somewhat surprising, since alkyl nitrates are not thermally de-

composed. The fraction of NOx showed the highest variability, with values of 5 to 70 % of the total NOy. This high variability is due to local sources. Careful screening is required for further analysis. The partitioning leaves a large fraction (up to 70%) of NOy unaccounted for. Part of that could consist of HNO_3. This missing NOy seems mainly responsible for the high NOy values. The ozone concentrations show a clear correlation with both, PAN (fig.6) and alkyl-nitrates, but not with NOx. This suggests, that ozone production has occurred at a distant location and then this ozone, together with NOy was transported to the site.

CONCLUSIONS

Measurements of NOy, NOx, PAN, and alkyl nitrates leave up to 70% of NOy unaccounted for. Correlation of ozone with PAN and alkyl nitrates suggests a distant anthropogenic source for ozone in subarctic tropospheric airmasses in spring. Except for high measured NOy concentrations our results are in reasonable agreement with other studies in the Arctic. Analysis of the measured data will continue, including measured data of CO, NMHC and J_{NO2} to understand the origin of ozone in the subarctic Troposphere.

REFERENCES

Jan W. Bottenheim, Leonard A. Barrie, Elliot Atlas, 'The partitioning of nitrogen oxides in the lower Arctic Troposphere during spring 1988', J. Atm. Chem. (17), 15-27, 1993

Richard E. Honrath, Daniel A. Jaffe, 'The seasonal cycle of nitrogen oxides in the Arctic Troposphere at Barrow, Alaska', J. Geophys. Res., (97), 20,615-20,630, 1992.

B. A. Ridley, J. D. Shetter, J. G. Walega, S. Madronich, C. M. Elsworth, F. E. Grahek, F. C. Fehsenfeld, R. B. Norton, D. D. Parrish, G. Hübler, M. Buhr, E. J. Williams, E. J. Allwine, H. H. Westberg, 'The behavior of some organic nitrates at Boulder and Niwot Ridge, Colorado', J. Geophys. Res. (95), 13,949-13,961, 1990.

H. B. Singh, D. Herlth, D. O. Hara, K. Zahnle, J. D. Bradshaw, S. T. Sandholm, R. Talbot, P. J. Crutzen, M. Kanakidou, 'Relationship of peroxyacetyl nitrate to active and total odd nitrogen at northern high latitudes: Influence of reservoir species on NOx and O_3', J. Geophys. Res., (97), 16,523-16,530, 1992.

ATMOSPHERIC DEPOSITION MONITORING IN LITHUANIA

D.Budvytyte and D.Sopauskiene
Institute of Physics, A.Gostauto 12, 2600 Vilnius, Lithuania

During the last decades the assessment of the atmospheric pollution load on ecosystems have been carried out in most European countries [1-5]. Atmospheric precipitation have been considered to contribute a considerable part of pollutants from the atmosphere to ecosystems. The continuous atmospheric precipitation chemistry monitoring was established in Lithuania in 1981. The main objectives of the monitoring programme were to determine the regional background air pollution and to assess pollutants load from the atmosphere to the ecosystems. Bulk collectors for precipitation were arranged at three rural sites relatively far from local antropogenic pollution sources. These sites represent different parts of Lithuania,Preila - coastal site in W of Lithuania, Zuvintas - inland site in SW of Lithuania, and Moletai - inland forest area in E of Lithuania (Fig.1), and therefore, they can be treated as being representative for Lithuanian regional conditions. Monthly precipitation samples were collected and analyzed for all major ions using classical analytical chemistry methods [6].

Fig. 1. Location of sampling sities.

The comparison of bulk and wet-only collectors was included in our investigation program. The obtained results have shown that bulk and wet-only collectors give comparable results for SO_4^{2-}, NO_3^-, NH_4^+, H^+ indicating a low dry deposition flux to the samplers funnel [7]. Average contribution of dry deposition to bulk collector was about 14% for SO_4^{2-}, 9% for NO_3^-, 4% for NH_4^+ and 11% for H^+. Noticeable dry deposition was observed for seasalt components and it was about 20%.

Table 1. Precipitation volume weighted means (μeq/l) of the major ions for Preila, Moletai and Zuvintas, 1981-1990.

Site	Ions						
	SO_4^{2-}	NO_3^-	Cl^-	NH_4^+	Na^+	Ca^{2+}	H^+
Preila	116.4	47.0	74.5	68.1	64.8	34	54.6
Moletai	126.4	38.6	26.1	82.8	16.6	39	23.6
Zuvintas	164.8	46.0	34.4	82.8	22.2	61	29.7

Data in Table 1 show that the concentration field for major components, except sea salt, is rather uniform all over Lithuania. These data are considered as quite reliable for regional background concentration of pollutants in precipitation. High concentrations of Na^+ and Cl^- in Preila are accounted for the sea spray. The agricultural and biological activities especially during the warm period influence the Ca^{2+} and NH_4^+ concentrations in air as wel in precipitation in Zuvintas. The SO_4^{2-} concentrations, presented here, are without any correction for the contribution of seasalt. The correlation analysis confirms the existence of ammonium sulfate and ammonium nitrate, and these compounds dominate almost in all precipitation samples. About 75% of precipitation samples with pH less than 5.0 have been found at every site. Therefore, this accounts for mean pH value 4.26 in Preila, 4.53 in Zuvintas and 4,63 in Moletai.

Seasonal averaged concentrations of all components as well as precipitation amount show the existence of a seasonal cycle rather similar at three sites.Most of the non-seasalt components show a maximum in concentrations during spring. The higest concentrations of SO_4^{2-} and NH_4^+ during the spring months could be atributed to the small amount of precipitation and long-range transport of these pollutants from Western Europe and the Ukraina [8]. Concentrations of seasalt component are maximum during autumn and winter extremely at Preila - sea-shore, mainly due to the windy period and increased sea spray. As concern to H^+ concentrations, the lowest pH values are detected during winter , when the emissions of Ca^{2+} and NH_3 are reduced and, conversely, the emissions of SO_2 as well as NO_x are highest.The local changes in the supply with alkaline species (like as Ca^{2+} and NH_4^+) are mostly reflected on seasonal variation of H^+ concentrations.

The results of precipitation quality investigations were used to assess wet deposition of chemical components. The annual averaged wet deposition values for nearly all of major components are presented in Table 2 for the period since 1981 to 1990.

These wet deposition values for components are considered as the background ones for Lithuania. Low sulfur wet deposition values (60 - 100 mg S m^{-2} $month^{-1}$) were calculated during for the period of winter-early spring and the highest those (about 200 mg S m^{-2} $month^{-1}$) were calculated during summer-early autumn.

Table 2. Annual deposition (g m^{-2} yr^{-1}) of chemical components from bulk precipitation samples for the period 1981-1990. Variation limits in bracets.

Component	Preila	Moletai	Zuvintas
SO_4^{2-}- S	1.3	1.3	1.25
	[0.7-2]	[1-2]	[1-2]
NO_3^--N	0.48	0.34	0.32
	[0.23-0.90]	[0.23-0.45]	[0.23-0.41]
Cl^-	1.96	0.57	0.62
	[1.13-4.12]	[0.25-0.74]	[0.31-1.20]
H^+	0.04	0.015	0.015
	[0.02-0.09]	[0.008-0.024]	[0.006-0.025]
Na^+	1.11	0.25	0.26
	[0.62-2.36]	[0.15-0.34]	[0.15-0.43]
NH_4^+-N	0.69	0.75	0.58
	[0.21-1.24]	[0.47-1.24]	[0.39-0.58]
Ca^{2+}	0.51	0.48	0.62
	[0.31-0.66]	[0.20-0.69]	[0.33-0.82]
Precipit.	743	656	505
(mm)	[451-947]	[560-996]	[350-725]

The interannual variation of wet deposition of H^+ shows the upward time trend, which can be related to the slight upward time trend of NO_3^- and more evident downward trend of Ca^{2+}. The observed downward time-trend in SO_4^{2-} depositions in Lithuania seems to be caused by the reduction of the SO_2 emission in Europe in the recent 10 years [9].

In order to determinate a contribution of the main local sources of emission into the regional air pollution, the network of precipitation sampling sites was expanded in 1992 up to 19 sites. All bulk samplers were set in the upwind side of available local emission sources. Concentration data of components from network sites were averaged for the subregions (Fig.1.) such as North-Western, South-Western, South, Central and North-Eastern. There are different sorts of industrial enterprises in all subregions. Every year approximately 1 million tons of pollutants are emitted into the atmosphere from all of those pollution sources. Oil refinery and cement factories and other chemical plants are in N-W subregion. In S-W subregion there are in operation the furniture and paper industry plants. Ignalina Nuclear power plant is located in the N-E subregion. The main thermoelectric power plant of Lithuania and fertilizers producing several factories are situated in C subregion. A number of small industrial enterprises are in S subregion.

Area-weighted annual deposition of components, which are important regarding the acid deposition, are shown in Table 3.

Table 3. Area-weighted annual deposition (g m^{-2} yr^{-1}) of chemical components in Lithuania 1992

Subregion	Precip mm	Component					
		SO_4^{2-}-S	NO_3^--N	Cl^-	NH_4^+-N	Ca^{2+}	H^+
N-W	604	1.7	0.43	1.2	1.0	0.5	0.023
S-W	663	2.0	0.54	1.5	1.2	0.5	0.021
C	600	2.0	0.50	1.1	1.2	1.0	0.001
S	607	1.5	0.50	1.1	1.1	0.7	0.011
N-E	564	1.1	0.41	0.8	1.1	0.4	0.020
Means	607	1.6	0.46	1.17	1.1	0.6	0.017

Data indicate that precipitation amount has much smaller spatial variability than depositions. The maximum load of pollutants have been found in West and Central Lithuania, which gradually decreases towards East. Very evident West to East gradient are observed for seasalt components. The highest Ca^{2+} concentrations in precipitation and deposition observed in Central Lithuania are due to the larger density of towns and more intensive industrial activity, and, therefore, most of precipitation samples have pH above 5.

The spatial trends in deposition fluxes of nearly all the major non sea-salt components are quite similar and in this respect these primary results lead us to think that the main characteristics of precipitation chemistry on a regional scale depend on non-local sources.

REFERENCES

[1] Meszaros, E. „The importance of deposition measurements in the study of an application of BAPMoN data", Idojaras, 1983, vol 87, No 6, 309-318.

[2] Laurila, T. „Wet deposition trends of major inorganic ions in Finland based on daily bulk deposition samples", Water, Air and Soil Pollution, 1990, 52, 295-324.

[3] Taugbol, G. „Acid precipitation monitoring and research. Review of current Norwegian activities", The Science of the Total Environment, 1990, vol 96, No 1/2, 23-43.

[4] Goulding, K.W.T. et al. „Atmospheric deposition at Rot-hamsted, Gaxmundham, and Woburn Experimental stations, England, 1969-1984". Water, Air and Soil pollution, 1986, 29, 1, 17-49.

[5] Horvath, L. and Meszaros, L. „The composition and acidity of precipitation in Hungary", Atmospheric Environment, 1984, vol 18, No 9, 1843-1847.

[6] Sopauskiene D., Budvytyte D. and Juozefaite, V. „The character and variation in the chemical composition of atmospheric precipitation in Lithuania". J.Ecol. Chem., 1993, N 2-3, 161-167.

[7] Sopauskiene, D., Davidaviciene, L. „The changes in chemical composition of precipitation in the bulk collectors", Atmospheric physics, Aerosol and gaseous admixtures in the environment, 1986, No 11, 159-165, Vilnius, Institute of Physics.

[8] Sopauskiene, D., Budvytyte, D. and Juozefaite, V. „Chemical characteristics of atmospheric aerosol in rural site of Lithuania". Annual Report, 1992, 44-48, Institute of Physics, Vilnius.

HEAVY METALS IN THE INTERACTION ATMOSPHERE - EARTH'S SURFACE

D. Ceburnis

Institute of Physics, Gostauto 12, Vilnius 2600, Lithuania

Summary

A quantitative comparison of precipitation data, moss analyses data and direct air measurements (carried out in Lithuania during 1990-1993) was made to evaluate the influence of the non atmospheric origin sources (dust from the soil surface, higher vegetation, etc.) to the content of trace metals in the moss. It was estimated that about 40% of Cr content in the moss and more than 60% of Fe comes from sources other than atmospheric deposition. An average metal retention efficiency factor up to 60% in the moss was evaluated but the variation of this factor between different elements is very significant. Deposition velocity rates for different elements range from 0.30 to 1.48 cm/s.

Very close and complex interactions between atmosphere and other environmental systems is well known. Mechanisms of these interactions are very interesting and important, but also there are many uncertainties in this field. There are a lot of different methods for the investigation of the atmospheric heavy metals, but direct investigations not always can truly represent the origin of the heavy metal sources.

The moss technique as a means of surveying atmospheric heavy metal deposition was developed in Sweden (Ruhling & Tyler 1968). While moss studies are useful for assessing temporal and relative spatial differences in trace metal input, they don't provide information on the absolute magnitude of atmospheric deposition of the heavy metals, which can be estimated by precipitation analyses (Ross, 1990). Quantitative comparison of these methods allows to identify non atmospheric origin sources which may contribute to the content of metals in the moss and also to estimate the retention efficiency of the moss. It has been reported (Steinnes et al.,1991) that other non atmospheric sources can be the following origin: root uptake in vascular plants from soil and subsequent transfer to the moss by leaching from living and dead material; mineral particles, mainly windblown and dead material. Mentioned contribution of sources was noticed for Zn and Cr (Steinnes, 1991, Ross, 1990).

Samples of *Hylocomium splendens* were taken from 144 localities in Lithuania in 1990. Precipitation samples were collected in 32 sites during 1991-1992 and 9 sites during 1993. Samples for air quality measurements were collected in background monitoring station in Preila. Eight elements - Pb, Cd, Cu, Ni, Cr, V, Fe, Zn - were analyzed by the same method in all analyses. For data comparison from the different experiments territory of Lithuania was divided into 5 regions and averaged data from these regions are presented in this study as 5 independent sampling stations.

In Fig.1 concentrations of metals in moss are plotted as a function of atmospheric deposition. The general linear relationship is expressed by the regression equation:

$$\lg(M)=0.73+1.08\lg(D) \qquad (1)$$

M - concentration in the moss mg/kg(dry weight)
D - atmospheric deposition mg/m^2*yr

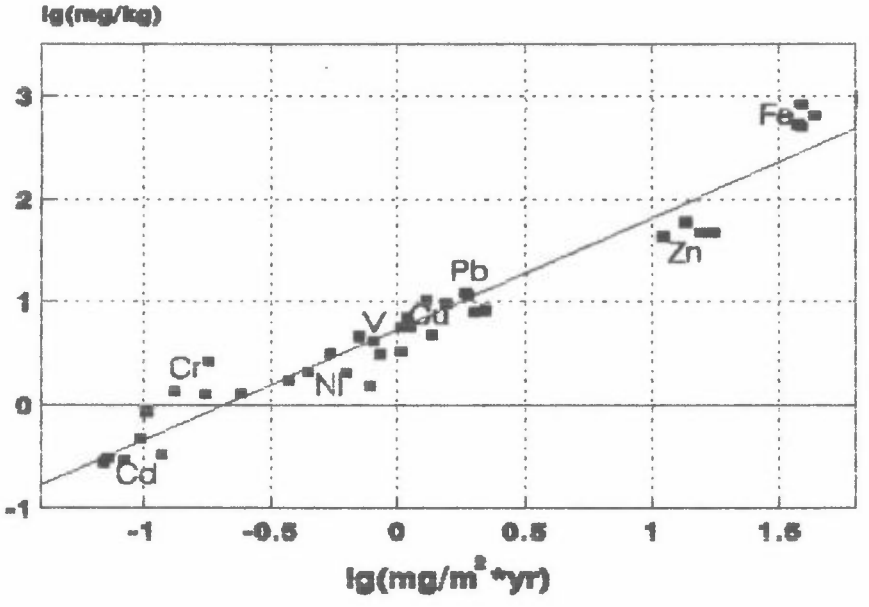

Fig.1. Concentrations of metals in moss as a function of atmospheric deposition.

Comparing concentrations in the mosses and atmospheric deposition values with the average growth of Hylocomium splendens 116 g/m^2*yr (Ruhling et al. 1992) an average metal retention up to 60% in the moss was evaluated. The variation of the retention efficiency between different elements is very significant. In order to use semiquantitative equation (1) to

convert moss concentrations to deposition rates it is necessary to establish relative efficiency factors of the moss for the different elements. Assuming the retention efficiency factor for lead of 100% (Ruhling et al. 1992) the following efficiency factors were estimated from moss concentrations and deposition data in Lithuania. They are presented in Table 1.

According to the reference data in the Table 1 there are remarkable differences for some elements.

Table 1

Relative efficiency factors

Metal	Present study data	Reference data (Ruhling et al.1992)
Ni	72%	
Cd	66%	65%
Cu	81%	
Fe	269%	
Cr	147%	84%
Zn	58%	41%
V	76%	54%

According to the data of this study up to 40% of chromium amount is non atmospheric origin. At the same time moss technique is well suited to characterize the chromium deposition pattern from local or distant sources. It was estimated that only 40% of iron is the atmospheric origin, and more than 60% comes from the sources like higher vegetation, soil dust and etc. as it was mentioned above. It becomes clear that concentrations of iron depend very strongly on the sources other than atmospheric deposition.

Direct air quality measurements were performed in background monitoring station in Preila for 15 years, but only the filters, collected in 1992, were analyzed by the same method as precipitation and mosses. By this reason results are primarily accepted. According to the air quality data deposition velocity for several elements was calculated. Deposition data from all sampling stations were averaged for calculations. Results are presented in Table 2.

All the investigations are performed in different areas, in urban as well as in background areas, so it is not surprizing that remarkable differences are founded.

Table 2

Deposition velocity for different elements

Metal	Deposition velocity, cm/s	
	Present study data	Reference
Pb	0.38	0.30[1]/0.74[2]
Cr	0.56	1.57[2]
Ni	0.76	0.69[2]
Mn	0.78	1.09[2]
V	0.83	0.72[2]
Zn	1.09	0.50[1]/1.13[2]
Cd	1.48	0.15[1]/0.56[2]

[1] Tripathi et al., 1993, [2] Shantroch, 1989

The main advantage of this study is the fact that sources of the different origin than atmospheric deposition may contribute to the content of some heavy metals in the living matter and also primarily calculations have been done. To make more reliable conclusions and to establish more exact values it is necessary to perform the next detail investigation at the similar conditions.

References:

[1] Ruhling,A. et al. "Atmospheric heavy metal deposition in Northern Europe". NORD, 1992:12.

[2] Ross,H. "On the use of mosses (*Hylocomium splendens* and *Pleurosium schreberi*) for estimating atmospheric trace metal deposition". Water, Air and Soil Pollution, 1990,50,63-76.

[3] Ruhling,A & Tyler,G."An ecological approach to the lead problem". Botaniska Notiser, 1968, 122, 248-343.

[4] Steinnes,E., Rambaek,J.P., Hanssen,J.E."Large scale multi-element survey of atmospheric deposition using naturally growing moss as biomonitor". Chemosphere, 1991 (submitted).

[5] Ross, H."Trace metals in precipitation in Sweden". Water, Air and Soil Pollut., 1987, 36,349-363.

[6] Shantroch, Ya."Heavy metals in atmospheric aerosol and suspended particulate matter at a region in Czechoslovakia".Atmospheric Physics, 1989, 13, 158-163. (in Russian).

[7] Tripathi, R.M. et al."Atmospheric deposition of Pb, Cd, Cu and Zn in Bombay, India". Atm. Environ., 1993, V27B, No.2, 269-273.

APPLICATION OF TRACERS IN ATMOSPHERIC DISPERSION EXPERIMENTS

THOMAS ELLERMANN, ERLING LUND THOMSEN, AND ERIK LYCK

National Environmental Research Institute,
Department of Emission and Air Pollution,
Fredriksborgvej 399, DK-4000 Roskilde, Denmark.

SUMMARY

Inert tracers, SF_6 and perfluorocarbons, are used in studies of the transport and dispersion of air pollutants. The tracer is released to the atmosphere and the ground level concentrations are measured at a network of sampling units placed downwind from the release point. The aim is to examine the relationship between emission and the resulting concentration distribution for various meteorological conditions and to provide data for assessing the quality of theoretical dispersion models. SF_6 and perfluorocarbons are used as tracers due to their physical and chemical properties, - inert, nontoxic, low detection limit etc. SF_6 can be used in experiments on a range from 1 - 150 km. The perfluorocarbons (perfluoromethylcyclopentane, perfluoromethylcyclohexane, perfluorodimethylcyclohexane) can be used in experiments ranging up to thousands of km. This presentation outlines the SF_6 and perfluorocarbon tracer techniques as used at the National Environmental Research Institute.

INTRODUCTION

Tracer technique based on SF_6 has for long time been used at the National Environmental Research Institute in full scale atmospheric experiments to study the transport and dispersion of air pollutants from various emission sources[1]. The aim is primarily to measure the dispersion of air pollutants under controlled conditions. Secondly, the experiments provide valuable data which can be used to assess of the quality and possibly improve the theoretical dispersion models. These models describe dispersion over homogeneous terrain rather well. However, complex terrain, which is closer to reality, is still exceedingly difficult to include properly in the models. The direct measurements of the influence of large buildings, valleys, coast lines etc. on the dispersion of air pollutants are therefore still important. The study of these local effects are usually carried out with SF_6 as tracer. SF_6 is inert in the lower atmosphere, nontoxic and easy to detect by gas chromatography with electron capture detection. However, industrial applications of SF_6 in which some SF_6 is lost to the atmosphere limits SF_6 tracer experiments in some areas due to local sources. Further, the commercial use of SF_6 has led to a background concentration of 2-3 x 10^{-12} by volume. The use of SF_6 as tracer is therefore limited to experiments on a range of up to about 100-150 km.

Experiments on a range of thousands of kilometres are on the other hand of interest in order to provide data for evaluation of the models for long range transport of pollutants. For this reason we are currently implementing the technique for the use of perfluorocarbon (PFC) compounds as tracers, especially perfluoromethylcyclopentane

(PMCP, C_6F_{12}), perfluoromethylcyclohexane (PMCH, C_7F_{14}), and perfluorodimethyl-cyclohexane (PDCH, C_8F_{16}). As fully fluorinated compounds they have in many respects similar physical and chemical properties as SF_6. However, both the background concentration and the detection limit are two to three orders of magnitude lower than for SF_6. With these compounds it is possible to carry out full scale experiments to simulate the long range transport of pollutants across Europe, which for example is relevant in connection with major industrial accidents, like the Chernobyl accident. This presentation outlines the SF_6 and PFC tracer techniques as used at the National Environmental Research Institute.

EXPERIMENTAL

Full scale tracer experiments are designed according to the specific aim of the experiment and the local conditions; - release height, range of experiment, meteorology etc. In general the tracer is released either alone from a pipe at a chosen height to simulate a plume (without buoyancy) or together with the effluent from a smoke stack to mark the plume with the tracer. The tracer is released constantly prior and throughout the entire sampling period. The presampling release ensures that the tracer has spread fully downwind in the sampling area before sampling begins. The air sampling units are typically positioned in 2 or 3 arcs downwind and orthogonal to the wind direction. The distance in the arcs between the units is 2-3 degrees as seen from the release point. This set-up enables a measurement of the crosswind time averaged distribution of the tracer concentration at ground level and at several distances from the release point (see Figure 2). In addition to the sampling units a mobile SF_6 analyzer is available which instantly measures the tracer concentration with a frequency of about 2 min. During the field experiments basic meteorological parameters (mean wind direction, wind speed etc.) are measured.

SF_6 release

The tracer is released to the atmosphere by emission directly from the SF_6 cylinders. The heat flux from the surroundings is used to evaporate the liquid SF_6 in the cylinder. A sufficient constant flow is obtained by use of a flow regulator and measured with a flowmeter. The final emission rate is calculated from the cylinder weight before and after the release and the duration of the release. A nylon pipe is used to add the tracer to the effluent in a smoke stack or to guide it to the release point, eg. at a meteorological mast. The release is kept constant to within a few percent throughout the sampling period. The release rate depends on the specific conditions of the experiment. The rate is typically between 0.5 to 6 g/s for experiments in the range from 1 to about 50 km.

Sampling units

The air samples are collected at ground level (0.5 m above ground). The home build sampling units samples at a constant rate typically 200 ml/min. The outlet from the unit is connected to three saran plastic bags, which in sequence are filled for a preset sampling period of 20, 30, or 60 min. Magnetic valves controls the flow in the units and the power is supplied by a rechargeable battery. At present 60 sampling units are available and from two vans they can be positioned in the sampling area in less than two hours. The sampling units are initiated simultaneously either by an electronic timer or by use of radio signals.

SF_6 analysis and calibration

The tracer concentrations are measured using gas chromatographs with electron capture detection designed and build at our laboratory. A continuous analyzer for airborne use was developed[2]. For groundlevel experiments two analyzers were build primarily for analyses of sampling bags. One of the gas chromatographs can be installed in a van for time resolved mobile measurements of SF_6 during the release. Molecular Sieve 5A columns and N_2 (99.9999% pure) carrier gas are employed.

The gas chromatographs are calibrated relative to a Matheson Primary Standard containing 1 ppm ±1% SF_6 in N_2. One-step dilutions are prepared in Tedlar bags. The accuracy of the standard dilutions are estimated to about ±10%. The accuracy of the measured concentrations is estimated to about ±15% and the precision is ±5%. The reproducibility of the GC is about ±5%

PFC analysis

The concentrations of the perfluorocarbons are analyzed by a commercial dual trap perfluorocarbon tracer gas analyzer. The air sample is initially loaded at room temperature onto a 6.75" trap packed with 75 mg Ambersorb XE-348. The majority of oxygen is then removed by purging with the carrier gas and finally the trap is heated to 300 C^0 in about 5 s to desorb the PFC's and inject them onto the precolumn and column. The GC contains a catalytic converter and uses a mixture of 5% H_2 in N_2 as carrier gas (both 99.999%). The remaining oxygen is reduced to water by hydrogen in the catalytic converter. Airborne halocarbons other than the fully fluorinated substances are also reduced in the catalytic converter. The gas chromatograph is preliminary calibrated relative to a gas mixture of approximately 10 ppbv PMCP, 10 ppbv PMCH, and 10 ppbv PDCH purchased from Airco Special Gases, Riverton USA.

SOME RECENT WORK

A typical SF_6-chromatogram obtained during a field campaign is shown in Figure 1. The first peak with a retention time of about 0.5 min corresponds to 19 pptv SF_6. The large peak following SF_6 is due to atmospheric oxygen. The sloping base line corresponds to the tail of the oxygen peak from the previous sample analyzed.

A series of dispersion experiments were carried out during july, 1992 at Borris Moor, which is a flat and homogeneous area. The aim of the experiments was primarily to study the short time variations of the dispersion over non complex terrain (the results of this campaign will be presented elsewhere during spring, 1994). For this presentation we have chosen to illustrate the field experiments by a single data set from this campaign showing the 30 minutes mean distribution of the SF_6 concentration (Figure 2). The tracer was released from a meteorological mast at a height of 21 m and with a release rate of 0.59 g/s. Downwind from the release position 50 sample units were placed in three arcs in distances of 300 m, 430 m, and 615 m. The meteorological situation was moderately unstable (high wind speed: 8.9 m/s, moderate solar radiation) and the tracer plume was very variable in time and space. Anyhow the crosswind tracer concentration distribution became rather well defined gaussian and the maximum SF_6 concentration was found in the second of the three arcs (Figure 2). Such measurements are very valuable to test and to improve models.

At present we are implementing the technique for PFC tracer experiments. The first steps have been to calibrate the PFC analyzer approximately and to measure the back-

ground concentration of PFC's at Risø near our institute. Knowledge about the background concentration is important for the planning of the release rate etc.. Figure 3 curve A shows the chromatogram obtained from a dilution of a PFC mixture with approximately known concentrations; the peaks corresponds to 780 ml of 0.5 pptv of PMCP (r.t.= 1.40 min); PMCH (r.t.= 2.34 min), and PDCH. The PFC mixture contains different isomers of PDCH. The double peak (r.t.= 4.81 and 5.32 min) surrounded by two smaller peaks (r.t.= 4.0 and 5.7 min) represents this mixture of PDCH isomers.

Figure 3 curve B shows a chromatogram obtained by analysis of 1040 ml of air sampled the 24th. november 1993 at Risø, Roskilde, Denmark. The sample unit was placed upwind from the laboratories to avoid any influence from our PFC laboratory. The chromatogram shows several peaks of which only the PMCP, PMCH, and PDCH peaks can be identified. The concentration of the three PFC's were determined by use of the calibration curves inserted in figure 3: [PMCH]= 0.0049 pptv, [PMCH]= 0.0035 pptv, and [PDCH]= 0.027 pptv. The concentration of the different isomers in atmospheric air differs from the mixture of the PDCH isomers in the PFC mixture. The total concentration of PDCH was therefore determined by addition of the peak heights from all four PDCH peaks and correlating this with the sum of peak heights from the PFC mixture. This is based on the assumption that the response factor of the different isomers are equal. The reproducibility of the PFC analyzer is better than ±5%. The day to day reproducibility of preparing the dilutions and measuring the PFC concentrations is estimated to ±10%. The values obtained in this work for the background concentration of the PFC are comparable with atmospheric background values given in the literature: [PMCP]= 0.002 pptv[3], [PMCH]= (0.002-0.0034) pptv[3-5], and [PDCH]= (0.026-0.036) pptv[3,5,6].

The first field campaign employing the PFC technique is planned to take place during summer, 1994. Further more, we are going to participate in the European Tracer Experiment which will take place during late 1994 and which is coordinated by Katrin Nodop at the Joint Research Centre-ISPRA, Italy. An intercalibration of the PFC analyzer has been planned to take place during spring, 1994.

ACKNOWLEDGEMENT

Per Jens Løfstrøm, Birte Vaabengaard, Hans Ahleson, and Morten Hildan are acknowledged for their valuable help during this work. Part of the work is carried out under the Danish Environmental Research Programme in cooperation with the Meteorological Department, Risø National Laboratory, Roskilde.

REFERENCES

[1] Lyck, E.:"A tracer technique for full-scale atmospheric dispersion experiments". Preprint from the Ninth Symposium on Turbulence and Diffusion. April 30 - May 3, 1990, Risø, Roskilde, Denmark. Publ. by American Meteorological Society, Boston, Massachusetts, USA.

[2] Lund Thomsen, E., and J.E. Lovelock:"A continuous and immediate method for the detection of SF_6 and other tracer gases by electron capture in atmospheric diffusion experiments". Atmos. Environ., 1976, vol. 10, 917-920.

[3] Lovelock, J.E., and G. Ferber: "Exotic tracers for atmospheric studies". Atmos. Environ., 1982, vol. 16, 1467-1471.

[4] D'Ottavio, T.W., R.W. Goodrich, and R.N. Dietz: " Perfluorocarbon Measurement Using an Automated Dual-Trap Analyzer". Environ. Sci. Technol., 1986, vol. 20, 100-104.

[5] Hefter, J.L., G.J. Ferber, and P.W. Krey "Atmospheric tracer experiments for regional dispersion studies". Proc. - Semin. Radioact. Releases Their Dispersion Atmos. Hypothetical React. Accid., CEC:Luxembourg, Luxembourg, 1980, vol. 2, 953-69. CODEN:44WSA8.

[6] de Bortoli, M., and E. Pecchio: "Sensitive Determination of Perfluorocarbon Tracers in Air by Intermediate Trapping and GC-ECD Analysis". J. HRC & CC, 1993, vol. 8, 422-425.

Figure 1:
Typical SF_6 chromatogram obtained by analysis of an air sample collected during a SF_6 release. The SF_6 peak corresponds to a concentration of 115 ng/m^{-3} = 18.8 pptv.

Figure 2:
Example of 30 minutes mean SF_6 concentration distribution measured during a SF_6 release carried out at Borris Moor, 22/6, 1992. Release height: 21 m; release rate: 0.59 g/s. The geographical position of each sample unit (symb.: x) is given relative to the release position (0,0). The x and y axis represent the distances from release position in the north and east directions. The dashed line indicates the mean wind direction. The bars represent the measured SF_6 concentration in the 2. bag at each sample unit. The SF_6 measurements have been corrected for the background SF_6 level. Note the scale of the SF_6 concentration at the top of the figure.

Figure 3:
(A) Chromatogram obtained by analysis of 780 ml of a gas mixture of 0.5 pptv of PMCP, PMCH, and PDCH. The arrow indicates the time when the PFC's are desorbed from the trap and injected into the precolumn. (B) Chromatogram obtained by analysis of 1040 ml of an air sample collected at Risø, Roskilde, Denmark, 24/11, 1993. Note that the sensitivity is 25 times higher for B than for A. Insert: Calibration curves for PMCP, PMCH and PDCH.

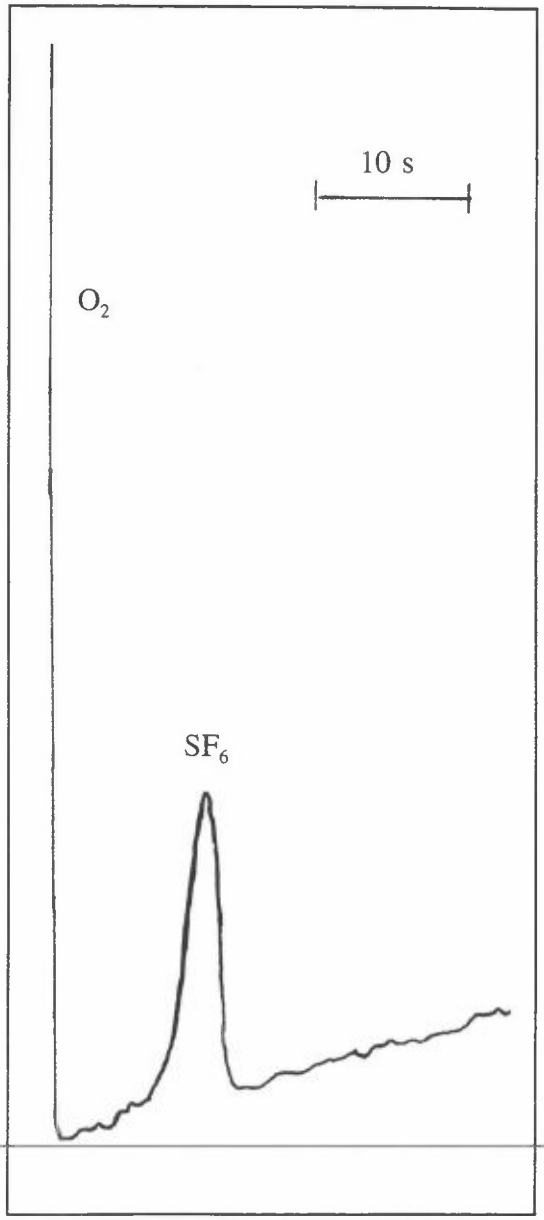

Figure 1

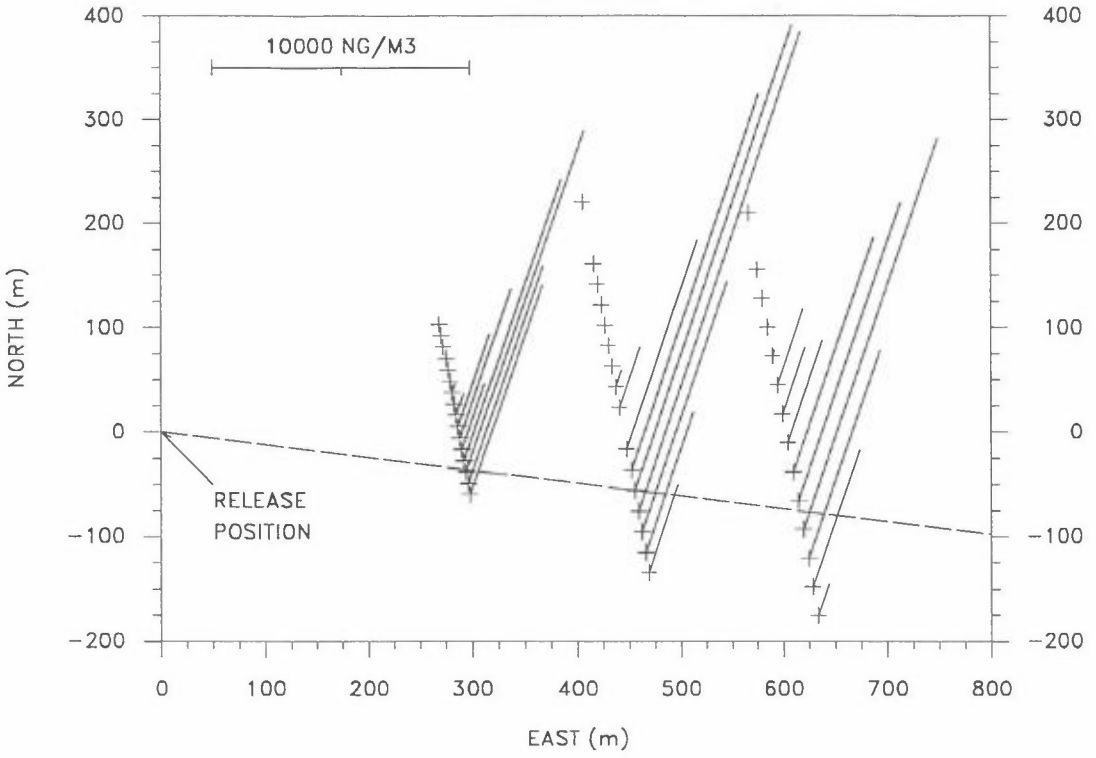

Figure 2

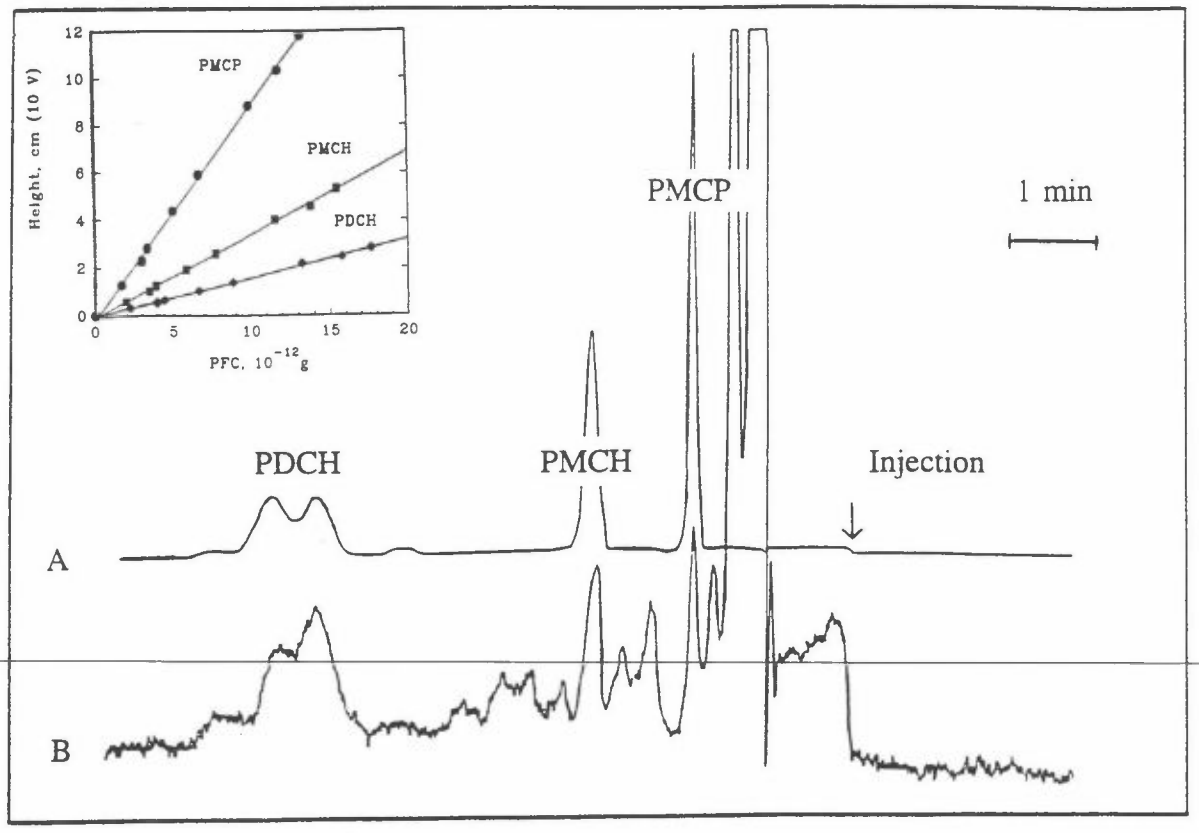

Figure 3

TIME TRENDS IN SURFACE OZONE

RASA GIRGZDIENE

Institute of Physics, A.Gostauto 12, 2600 Vilnius, Lithuania

SUMMARY

Ozone is one of the dangerous atmospheric pollutants. A linear trend of 1 to 3% surface ozone per year is observed over rural regions in Europe. Continuous surface ozone measurements have been carried out at the background coastal station Preila and the western suburb of Vilnius in Lithuania. The increase of ozone concentration at Preila station was 2.6% per year and at the Vilnius station it was 3% per year. Data show a considerable increase of the ozone level at both stations during the warm period (Preila 4.6% per year and Vilnius 4.3% per year). Different tendencies were registered in the cold seasons (October - March) of the analyzed period: a decrease at Preila station (-0.8% per year) an increase at the Vilnius station (1.6% per year).

INTRODUCTION

Analysis of the long-term surface ozone records from rural stations confirm the continuous increase of ozone concentrations, about 1% per year, during the last two decades in the Northern Hemisphere. Meanwhile, a linear trend of 1 to 3% per year is observed over rural Europe regions. The increase in surface and tropospheric ozone could have important environmental consequences, as this gas is phytotoxic and a "greenhouse."
Surface ozone variations reflect influence of many factors, such as: season, time of a day, specific geographical and topographical location of the station, synoptical situation, variation of meteorological parameters, concentration of other atmospheric pollutants, etc. The investigations have shown that the influence scale of the mentioned factors can differ [1]. For example, if specific geographical-topographical station situation, change of wind direction, nocturnal inversions, local circulations have great influence on the ozone concentration course only at that site; meanwhile influence scale of the synoptic situation (anticyclone and cyclone, front) is significantly larger. It can influence ozone variation in several located sufficiently remote station simultaneously. Various

atmospheric pollutants, such as NO_x, SO_2, aerosol and other, may have local as well as regional influence as they from local emission sources can be transported medium- and long-range distances away. As stations cannot be situated in identical conditions, all the mentioned factors should be evaluated by using and comparing the ozone monitoring data.

RESULTS AND DISCUSSION

Surface ozone concentrations have been continuously measured at the background coastal station Preila (55°20′ N and 21°13′ E) since 1980 and at the western suburb of Vilnius (54°38′ N and 25°10′ E) since 1982. Valuable information concerning the peculiarity of formation ozone levels can be obtained from the averaged diurnal ozone course for separate months. The data show, that averaged diurnal ozone course (Fig.1) at coastal site (Preila) is less evident in comparison with continental one (Vilnius). The difference between extreme values in diurnal course fluctuates from 6 $\mu g/m^3$ in January to 40 $\mu g/m^3$ in August at Preila station. Meanwhile at the suburban site ozone concentration variations are considerably greater and difference between extremes are 8 and 52 $\mu g/m^3$ in January and August respectively. Night

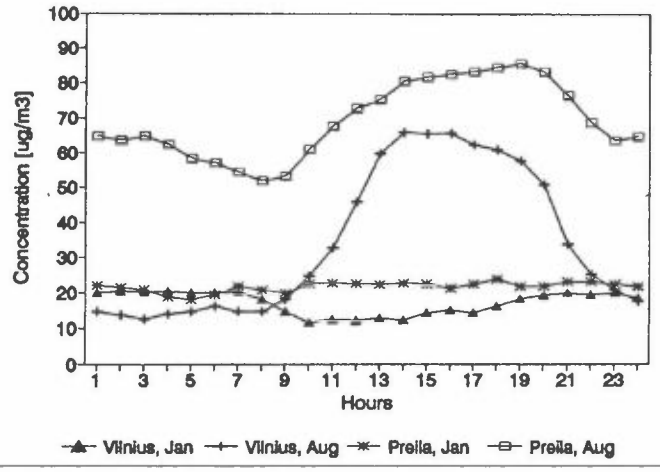

Fig.1. Average diurnal ozone courses at Preila and Vilnius stations, 1990.

destruction of ozone in the suburban area is the main cause of this phenomenon. It is most distinctly expressed in warm season of a year, i.e., from April to September.

If compare frequency distribution of hourly ozone concentrations in Vilnius and Preila (Fig.2), it should be noticed that percentage of low ozone concentrations recurrence in Vilnius is significantly higher. Nevertheless comparison of the ozone valuesin the interval between 1 p.m. and 8 p.m., when vertical mixing process is well expressed and night inversion is already

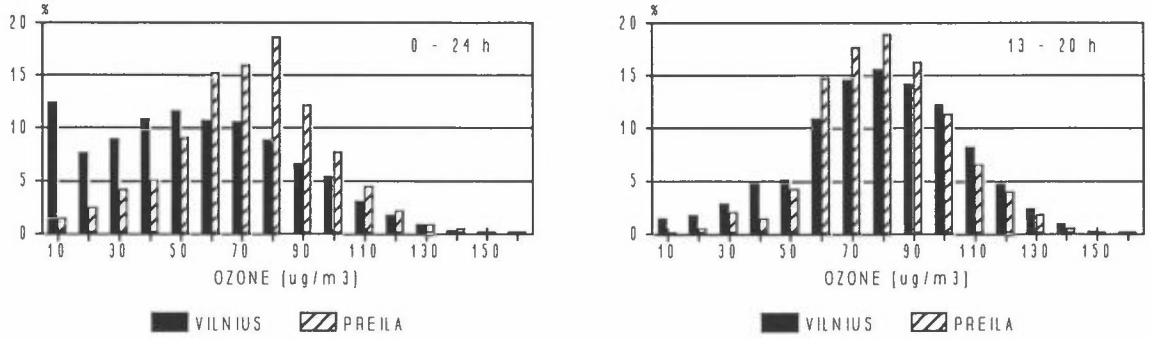

Fig.2. Frequency distribution of hourly ozone concentrations, APR-SEP 1991.

destroyed, shows that distributions of hourly ozone values are highly alike at both sites. Also a number of hourly ozone concentrations exceeding 120 $\mu g/m^3$, i.e., concentrations extreme for Lithuania conditions as are noted in [2], are very similar. This suggests the same source of these concentrations in both stations. The previous our investigations [2] showed, that the high ozone levels mostly have photochemical origin and are caused by a long-range transport of ozone and its precursor from other polluted regions, mainly from west Europe. It should be noted, that the interval between extreme diurnal ozone values can vary in different years, but still average variation interval at coastal background station is always smaller than that in suburb of Vilnius. That is result from the influence of specific locations of the stations. That should be considered in the estimations of the long time ozone fluctuations and trends.

Analysis of averaged ozone courses in warm period at Vilnius station for different years shows that ozone diurnal course as well as its level has changed in the ten years period. Ozone diurnal maximum in 1982 was observed practically at the same time

as in rural station Preila, which is nearly 5 p.m. of local time. Maximum values in 1991 were registered at Vilnius station earlier. Rapid growth of ozone in the morning hours and earlier observed diurnal maximum suggests, that this station in 10 years period has approached to one with urban conditions. These phenomena are caused by the built thermal power station 2 km west from station also by increase of traffic intensity, which is the main source of the air pollution.

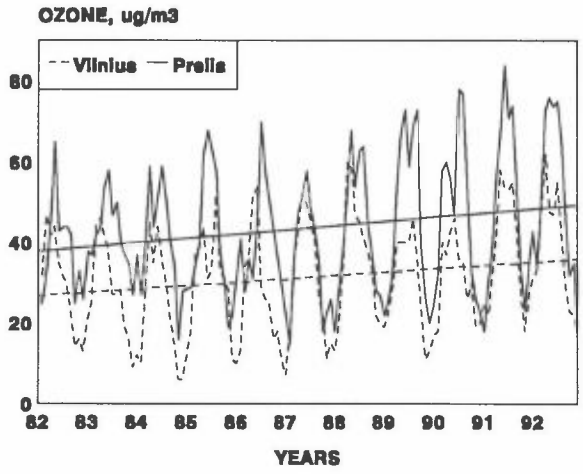

Fig.3. Trends in surface ozone

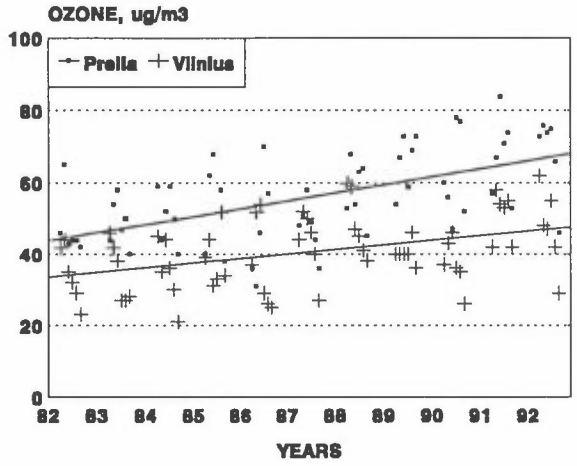

Fig.4. Trend in surface ozone in warm period (April-September)

Monthly mean ozone data are presented in Fig.3. The linear trend for each station has been calculated over the common period 1982-1992. An increase of ozone concentration at Preila station was 2.6% per year while at Vilnius station it was 3% per year. These results show good agreement with those published in [1]. Both linear trends lines are nearly parallel. The difference between annual mean ozone concentration values is determined by specific conditions of the station location. Data in Fig.4 show the increase of ozone level at both stations during the warm period (4.7% per year, Preila and 4.3% per year, Vilnius). Though different tendencies were registered in cold seasons (October-March) of analyzed period: decrease at Preila station (-0.7% per year) and increase at Vilnius station (1.6% per year).

CONCLUSIONS

Frequency distributions of hourly ozone concentrations at both stations are different, if we take all ozone values from 1 a.m. to 12 p.m. hours in to consideration, and close if we take hourly values only from 1 p.m. to 8 p.m.

The recurrence of the extreme ozone concentrations (>120 $\mu g/m^3$) in Lithuania at both stations is at the same level.

An increase of annual ozone concentrations has been observed at the coastal Preila station and at Vilnius suburban sites, 2.6% and 3% per year respectively.

Both stations results reflect common regional tendencies of ozone changes in different geographical conditions.

REFERENCES

[1] Low, P.S., Kelly, P.M. and Davies, T.D. "Variations in surface ozone trends over Europe." J.Geophys.Res., 1992, Vol.19, 1117-1120.

[2] Girgzdiene, R. "Surface Ozone Measurements in Lithuania." Atmospheric Environment, 1991, Vol.25, 1791-1794.

H_2O_2 measurements from Denmark and Northern Greenland.

K. Granby[1], O. Hertel[1], A.H. Egeløv[1], C. Lohse[1] and P. Hummelshøj[2].

[1]National Environmental Research Institute, Frederiksborgvej 399, DK-4000 Roskilde, Denmark.
[2]Risø National Laboratory, P.O. Box 49, DK-4000 Roskilde, Denmark

H_2O_2 measurements have been performed in a Danish rural area by means of a diffusion scrubber method (1 min. averages every 15 min.). The measurements for the period June 30 - July 9 1992 showed H_2O_2 concentrations from 0 to 2 ppbv. Significant correlations were found between H_2O_2 and radiation (r=0.51), temperature (r=0.49), O_3 (r=0.45) and SO_2 (r=0.10). The NO and NO_y concentrations showed negative correlation with H_2O_2. Model result of H_2O_2 and O_3, using a one-dimensional trajectory model, were at the same level as the measured concentrations but the model showed smaller fluctuations. This may be due to the presence of stable nocturnal boundary layers during the period, where H_2O_2 decreases more rapidly at the ground level as it is deposited or reacted with nitrogen oxides from local sources.

A pilot study in the Greenland Arctic (81°36 N), August 7-11 1993 showed H_2O_2 concentrations from 0.17-0.33 ppbv (12 hour averages, collection on impregnated filters). The diurnal variation was as expected insignificant at this high latitude with midnight sun.

INTRODUCTION

Hydrogen peroxide is primarily formed as a product of radical photochemistry through the recombination of HO_2 radicals. Some H_2O_2 is however formed in reactions of ozone with alkenes, isoprene and terpenes[1]. The deposition of H_2O_2 is one of the major odd-hydrogen radical removal processes operating in the clean atmosphere[2]. The production of H_2O_2 is favoured by low NO to hydrocarbon ratios and by the photolysis of O_3 in moist air.

Field studies in Los Angeles air 1985-88 showed that gaseous H_2O_2 are best correlated with solar intensity whereas O_3 is correlated with temperature[3]. Another study showed significant correlation between H_2O_2 and O_3 (R^2 =0.42)[4]. In the U.S. have observations shown a latitudinal gradient with decreasing levels with increasing latitude[5]. The present survey include ground based measurements of H_2O_2 from relatively high latitudes (81°36 N and 55°42 N) compared to other investigations.

MATERIALS AND METHODS

Semi continuous measurements of H_2O_2 were performed by a diffusion scrubber system based on principles developed by Dasgupta *et al.*[6]. The ambient air was sucked through a perfluoroalkoxy tube in which a microsporous polypropylene membrane was centred. In the membrane flows a scrubber liquid and collected H_2O_2 is carried to reaction with *p*-hydroxyphenyl acetic acid and peroxydase. Frequent calibration with H_2O_2 gas was performed by passing zero air through a microsporous polypropylene membrane submerged in a thermostatic H_2O_2 solution. Collection of H_2O_2 on filters was performed according to Ferm[7] except for omission of particle filters in front of the Ti(IV)-impregnated glass fibre filters. Measurements of O_3, SO_2, NO and NO_y were performed by conventional Monitorlabs monitors. These measurements are a part of the Danish Air Quality Monitoring Programme. The meteorological measurements include global radiation measured at 1.5 m by a Eppley pyranometer, temperature measured at 9.5 m by Pt-500 thermometers, relative humidity measured at 10 m by a Rotronic MP-100 and the wind direction with a P2021 Wind Vane and a P2058 Wind Direction Transmitter.

RESULTS FROM DENMARK

The sampling was performed in an agricultural area 35 km west of Copenhagen. The position is 55°42 N, 12°07 E, 15 m a.s.l.. The period June 30 - July 9 1992 was selected for comparison with relevant chemical and meteorological parameters as well as model results. For Danish weather conditions the temperature was high the first two days, 28-29°C while for the rest of the period the daily maximum temperature was 19-23°C. The H_2O_2 concentrations reached 2 ppbv during the first 3 days and 1.0-1.3 ppbv the rest of the period (Fig.2). The O_3 concentrations were high the first 2 days (max. 100-110 ppbv) and then they dropped to max. 40-60 ppbv. The relatively high H_2O_2 and O_3 concentrations the former two days may partly be due to long range transport of photochemical pollution from southerly directions. This was also reflected in increased SO_2 concentrations.

At July 2. the H_2O_2 concentrations were still high in spite of the decrease in O_3 concentrations and temperature. This may be explained by the fact that the relative humidity was relatively high at that afternoon (55%) compared to the other afternoons(20-35 %). The rate constant increases for the bimolecular self reaction of $HO_2\cdot$ with the presence of water vapour[8]. This is because of the formation of $HO_2\cdot H_2O$ complexes[9], which react more rapidly with other $HO_2\cdot$ radicals. For example it has been modelled[10] that twice as much H_2O_2 will be formed at 100% relative humidity as that formed at 50% relative humidity.

The H_2O_2 concentrations were strongest correlated with solar radiation (r=0.51) and temperature (r=0.49). They had a significant positive correlation with O_3 (r=0.45) less with SO_2 (r=0.10) and a significant negative correlation with NO (r=-0.02) and NO_y (r=-0.17). The negative correlation with NO is due to competition between the bimolecular self reaction of $HO_2\cdot$ and the NO oxidation by $HO_2\cdot$.

The measurements of H_2O_2 and O_3 have been compared to results from a one-dimensional trajectory model (Atmospheric Chemistry and Deposition (ACDEP) model) that includes chemical reactions, dry and wet deposition and vertical transport described by eddy diffusion. The model is divided logarithmic in 10 vertical layers. The model is advected along trajectories 96 hours backwards and shows results every 6 hours (Fig.2). More details about the model and relevant references are given in Hertel *et al.*[11].

The measurements and model results are about the same level but the model results show smaller fluctuations. This may be explaned by the presence of stable nocturnal boundary layers during the period (positive temperature differences were measured), where H_2O_2 concentrations decreases more rapidly at the ground level (sampling were performed at 3 m's height) as it is deposited. Local NO_x emissions (there is a road 600 m from the station) may also remove $HO_2\cdot$ radicals left in the stable layer close to the ground.

RESULTS FROM THE GREENLAND ARCTIC

From August 7-11 1993, ground based measurements of H_2O_2 (12 hour averages) were performed in the Arctic atmosphere 81°36 N, 16°40 W. The detection limit was < 0.05 ppbv. Loss of H_2O_2 was checked by adding H_2O_2 to filters and transporting them with the other filters. The recovery was 85 and 96% respectively. Filters were exposed in series of two to secure the sampling efficiency.

Concentrations of H_2O_2 measured at this high latitude with midnight sun varied between 0.17 and 0.33 ppbv (Fig. 3). The diurnal variation was as expected insignificant. The temperature during the period was just above the freezing point, the local wind was blowing from westerly to southerly directions and the surface was only sparsely covered with snow. Sigg et al.[9] measured H_2O_2 concentrations of 0.3-3.5 ppbv in Central Greenland (June-July 1990, 72° N, 3220 m a.s.l.). However, too many differences in the conditions when sampling (e.g. latitude, altitude, time and surface) render a comparison impossible.

Fig.1 Meteorological data, 30/6 — 9/7 — 92

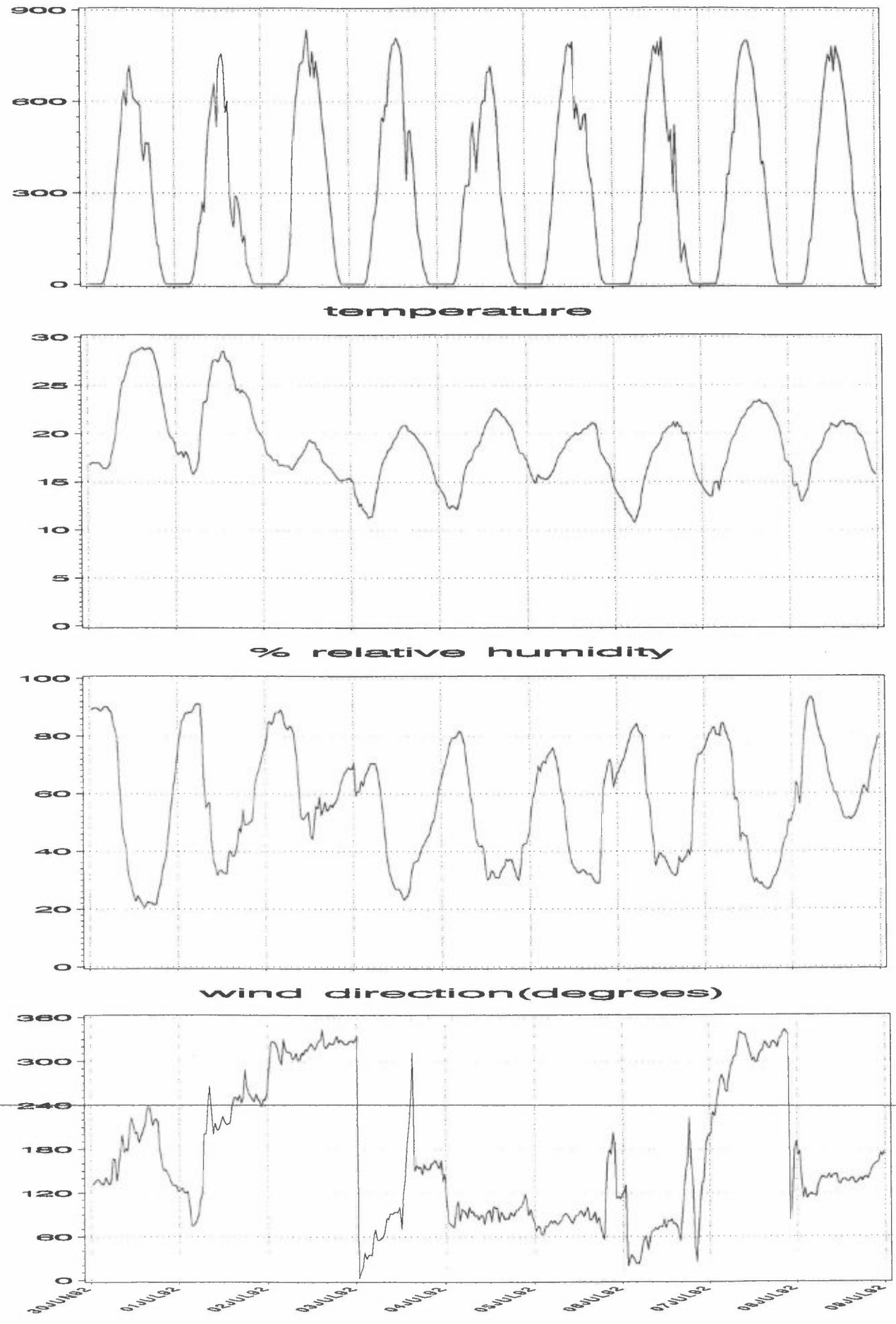

Fig.2 Hydrogen peroxide and ozone, measured versus modelled
Lille Valby, June 30th. – July 9th. 1992

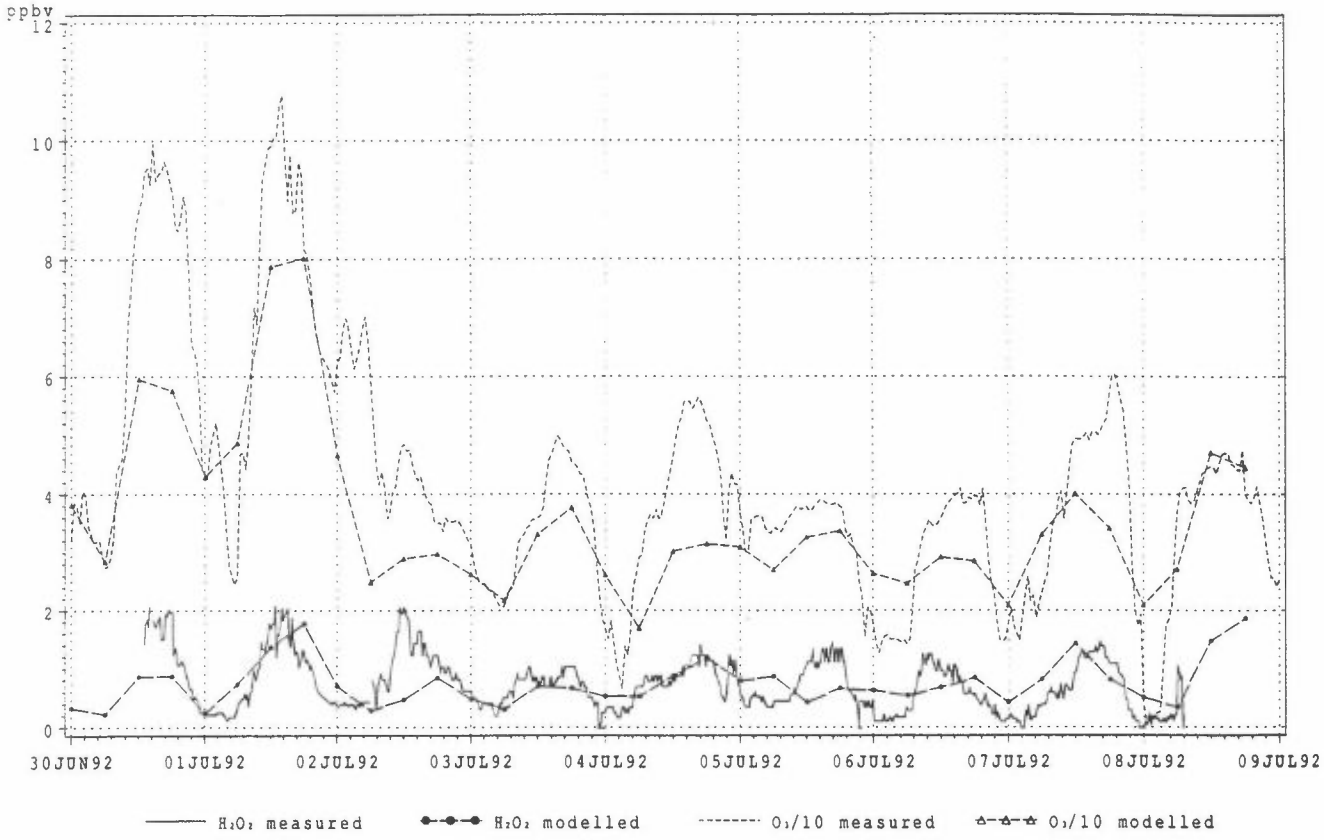

Fig.3 Hydrogen peroxide, 12 h averages
Greenland Arctic, August 1993
81 36N, 16 40W, 30 m a.s.l..

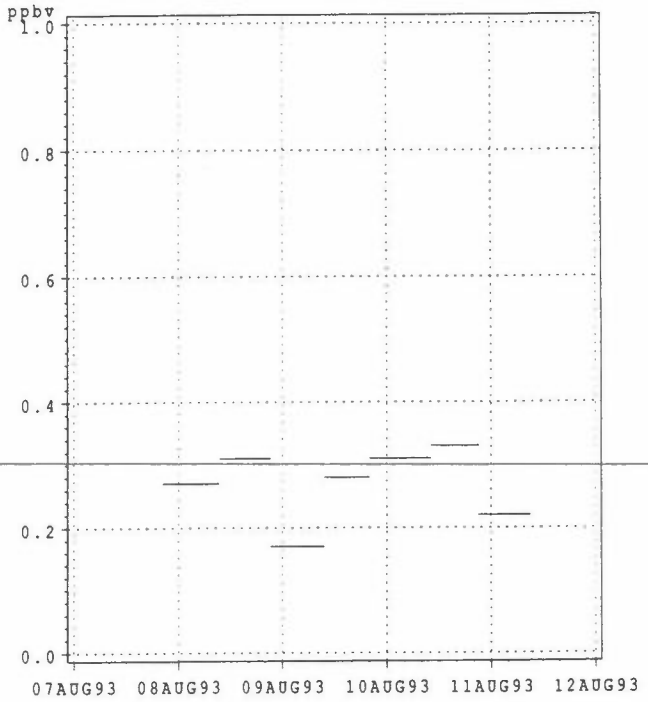

REFERENCES

1. Becker K.H., Bechara J. and Brockmann K.J., 1993. Atmos. Environ, 27A, 57-61.
2. Logan J.A., Prather M.J., Wofsy S.C. and McElroy, M.B., 1981. J. Geophys. Res., 86, 7210-7252.
3. Sakugawa H and Kaplan I.R., 1989. J. Geophys. Res., 94, 12957-12973.
4. Olszyna K.J., Meagher J.F. and Bailey E.M., 1989. Atmos. Environ., 22, 1699-1706.
5. Van Valin C.C., Luria M., Ray J.D. and Boatman J.F., 1987. J. Geophys. Res, 95, 5689-5695.
6. Dasgupta P.K., Dong S., Hwang H., Yang H.C. and Genfa Z., 1988. Atmos. Env., 22, 949-963.
7. Ferm, M. EMEP-CCC-Report 4/1988.
8. Atkinson R. and Lloyd A.C., 1984. J. Phys. Chem. Ref. Data, 13, 315-444.
9. Hamilton E.J. and Lii R.R., 1977. Int. J. Chem. Kinet., 9, 875-885.
10. Calvert J.G. and Stockwell W.R., 1983. Environ. Sci. Technol., 17, 428A-443A.
11. Hertel O., Christensen J., Berkowicz R., Asman W.A.H., Granby K., Hovmand M.F. and Hov Ø., 1993. Deposition of gases and particles in the PBL: Evaluation of the influence of a vertical resolution in atmospheric transport models. Paper to be presented at the International Technical Meeting on Air Pollution Modelling and its Application, Valencia, Spain, 29 Nov.- 3 Dec., 1993.
12. Sigg A., Staffelbach T. and Neftel A., 1992. J. Atmos. Chem. 14, 223-232.

CFC-11 TRENDS AT SPITSBERGEN

Ove Hermansen, Sverre Solberg
Norwegian Institute for Air Research (NILU), P.O. Box 64, N-2000 Lillestrøm, Norway

SUMMARY

NILU has been measuring CFCs at Birkenes in southern Norway and at Mt. Zeppelin on Spitsbergen since 1990. Samples are analyzed for CFC-12, CFC-11, CFC-113, CH_3CCl_3, CCl_4 and N_2O. Until now preliminary data analysis has been carried out only for CFC-11 at Ny Ålesund. Compared with measurements made in 1982-1983 they show an annual increase of 10.7 ppt/yr in the period 1982-1990. The calculated annual increase from 1990 to 1992 is 7.3 ppt/yr. More detailed data analysis will be carried out when the data from 1993 are ready.

SAMPLING AND ANALYSIS

Air samples are collected in electropolished stainless steel canisters and sent to NILUs laboratory for analysis. The pressurized canisters are analyzed by GC/ECD with injection loop and a cryofocusing unit (fig. 1 and 2).

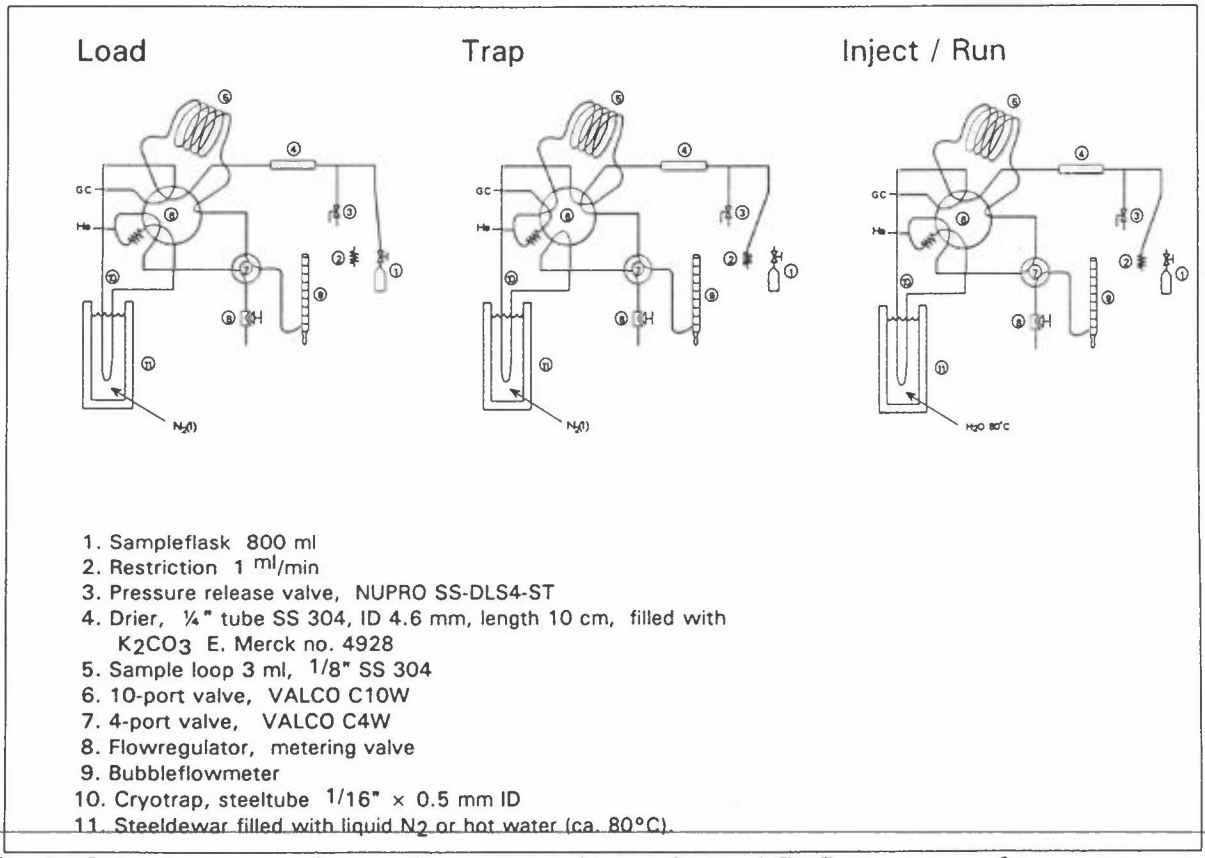

fig. 1: Injection system for gaschromatographic analysis of CFCs in air samples.

Calibration is carried out against a gas-standard from Biospheric Research Corp., Oregon USA. Preparation of the standard is described by Rasmussen and Lovelock [1].

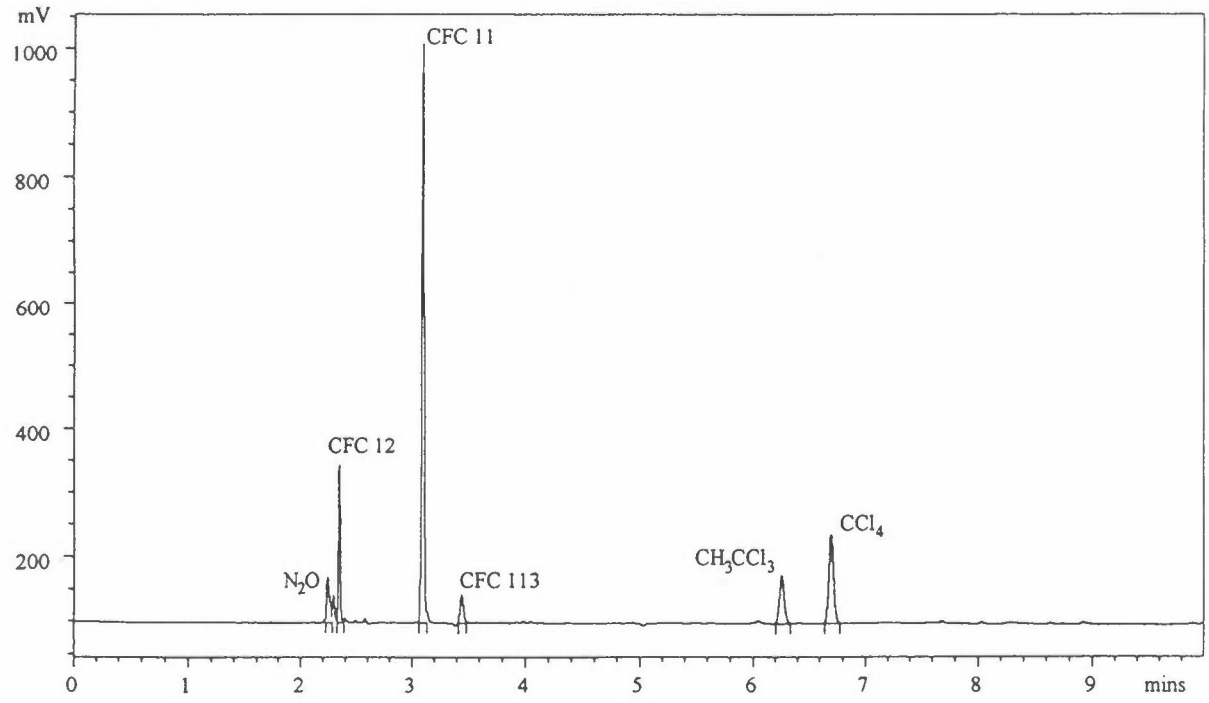

fig. 2: Chromatogram of an air sample

RESULTS

The number of samples was 46 in 1990, 101 in 1991 and 107 in 1992. The annual increase from 1990 to 1992 is calculated from quarterly means. In 1982-83, several samples were taken at Spitsbergen [2]. Together with samples from 1990 they show an annual increase of 10,7 ppt/yr, while the data from 1990 to 1992 show an annual increase of 7,3 ppt/yr (fig. 3).

DISCUSSION

The analysis of the data is only preliminary. The trends are calculated from quarterly means with no weighting. Sampling has been carried out with three samples a week, but there have been some periods without sampling. For example, the first quarter of 1991 consists of only five samples, and three of these have unusually low values. This gives a disproportionate contribution to the calculated trend. The samples from 1982 and 1983 were analyzed by a different method in another laboratory. Therefore they should be used with care in connection with the rest of the data. However, both the data from the early eighties and the data from the nineties are close to the concentrations measured at other remote sites in the northern hemisphere [3], suggesting a trend similar in magnitude to that observed elsewhere during this period. The CFC-11 trend has been relatively steady through the eighties, but there has been reported a decrease in growth rate the last few years [4]. This seems to be reflected in the data from Ny Ålesund.

When the data from 1993 are ready, a thorough analysis of all compounds quantified will be completed.

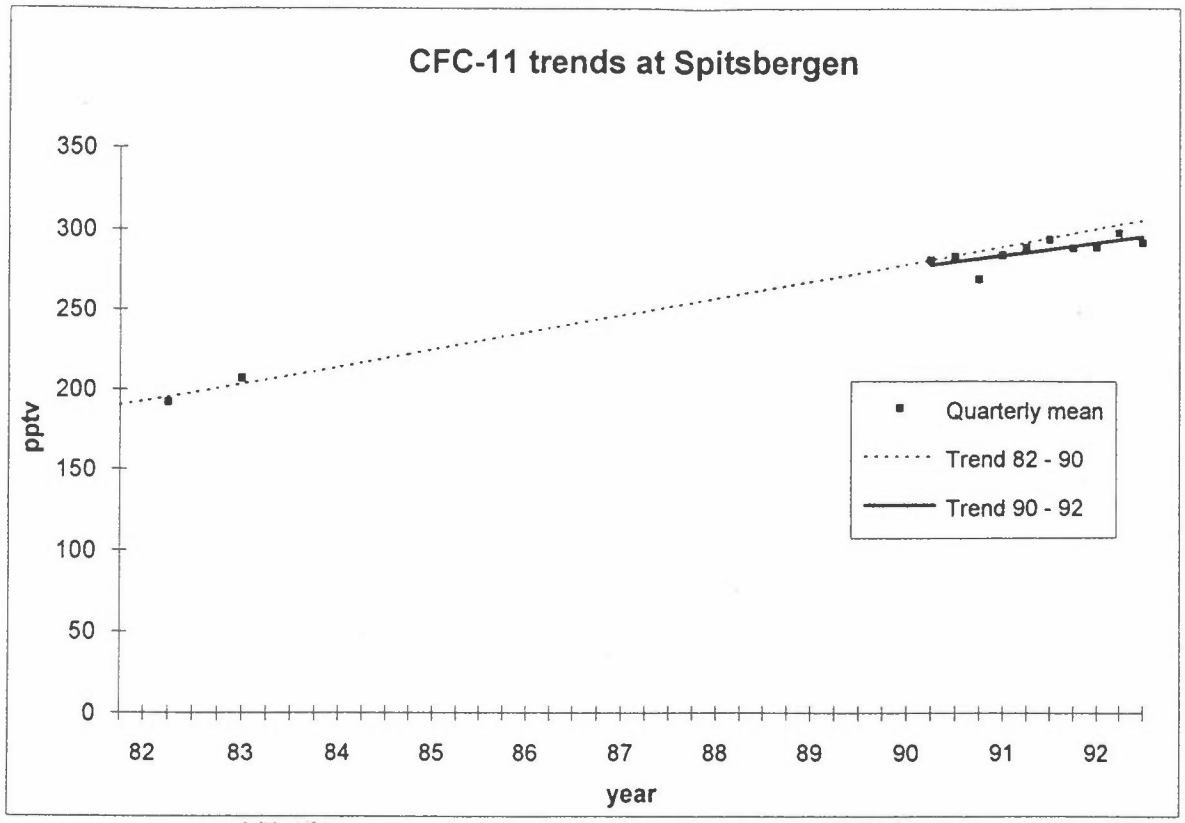

fig. 3: Quarterly means and calculated growth rates

REFERENCES

[1] R.A. Rasmussen, J.E. Lovelock
The atmospheric lifetime experiment, 2. Calibration
Journal of geophysical research, vol 88, no. C13, October 20 1983, p. 8369-8378

[2] Ø. Hov, S.A. Penkett, I.S.A. Isaksen, A. Semb
Organic gases in the Norwegian Arctic
Geophysical Research Letters, vol. 11, no. 5, May 1984, p. 425-428

[3] W.T. Sturges et al.
Summary report 1990, Nitrous Oxide and Halocarbons group
Climate Monitoring and Diagnostics Laboratory, No. 19, p. 63-71

[4] J.W. Elkins et al.
Decrease in the growth rates of atmospheric chlorofluorocarbons 11 and 12
Nature, vol 364, 26 August 1993, p. 780-783

TROPOSPHERIC NITROGEN OXIDES IN THE ARCTIC

Dan Jaffe
Geophysical Institute and Department of Chemistry
University of Alaska Fairbanks
Fairbanks, Alaska 99775 USA

INTRODUCTION

Nitrogen oxides play an important role in tropospheric photochemistry. NOx ($NO+NO_2$) is important due to its critical role in ozone production. The major end product of NOx oxidation is HNO_3, which is a primary component of "acid precipitation". Other nitrogen oxides, such as peroxyacetyl nitrate(PAN), may provide a temporary reservoir of NOx and therefore be important in transporting NOx to remote regions. Since the atmospheric lifetime of NOx is of order one day or less, most of the global atmosphere contains very low concentrations of NOx.

There is good evidence that increasing anthropogenic NOx and hydrocarbon emissions have affected O3 and nitric acid concentrations in remote regions of the Northern Hemisphere. Ozone data in both rural and remote regions indicate substantial increases over the last several decades (Crutzen 1988 and references therein). In the Arctic, the continuous record of surface O3 from Barrow, Alaska (1973-1992) shows a steady increase in concentrations of about 1.5% per year during summer (Oltmans 1993). During other seasons, no statistically significant trend is present. Nitrate in the Greenland ice core also show a substantial anthropogenic effect, with concentrations approximately doubling since 1955 (Mayewski, 1896).

In the Arctic, anthropogenic pollutants are known to be present in relatively high concentration during the winter-spring period (Barrie and Bottenheim, 1991). However as stated above, the tropospheric ozone increase is only evident during summer when other pollutants generally show a minimum. Understanding this long term increase in tropospheric ozone in the Arctic is one of the primary objectives of our work.

HYPOTHESES

Several possible hypotheses can be advanced to explain the long term trends in surface O_3 in the Arctic.

1)Anthropognic nitrogen oxides are transported into the Arctic during spring. Decomposition of reservoir NOy species (mainly PAN) supply sufficient NOx to produce O_3 during late spring.

2)Ozone is produced at lower latitudes and transported to the Arctic.

3)Local NOx sources (either industrial or natural biomass burning) provide sufficient NOx to account for the increased O_3 concentrations during summer.

EXPERIMENTAL

The NOAA GMCC station at Barrow, Alaska provides routine observations of O_3, CO_2, CH_4, meteorology, and other trace gases. Our experimental work has focused on making observations of nitrogen oxides using a high sensitivity O_3 chemiluminescence detector built by us for this work. The instrument detects NO directly and uses a catalytic technique to detect other reactive nitrogen oxides (NOy). Details are provided in several published papers (Jaffe et al., 1991, Honrath and Jaffe, 1992). Over the past 5 years, a total of 4 campaigns have been conducted in Barrow and Poker Flat, Alaska. During the winter-spring period of 1994 measurements are being made at NyAlesund.

RESULTS

The most complete record of nitrogen oxides in the Arctic was obtained during our 1990 campaign. Figure 1 shows the concentration at the surface of NOy measured at Barrow, Alaska over nearly a full year period. During the same period NO concentrations were found to be generally very low. Figure 2 shows the daily averaged (daytime) NO concentrations observed during 1990. Since NO has a well known diurnal cycle due to titration by ambient ozone, its concentration is expected to go to zero at night, and this is a good test of instrumental offsets at which are sometimes present at these very low levels. For comparison, average nighttime values are shown in Figure 3.

DISCUSSION

The annual NOy cycle is similar to other anthropogenic pollutants in the Arctic. This is due to both enhanced transport and longer atmospheric lifetime of these species with respect to deposition. The fact that NO concentrations are very low throughout the year show that most anthropogenic NOx emissions are oxidized to other forms prior to their arrival at Barrow. This is similar to the results shown by Barrie and Bottenheim (1991), who find that PAN is the major NOy component at Alert in the Canadian Arctic. The "pulse" of NO observed during the spring period may indicate that thermal decomposition of PAN is supplying additional NOx. However it is also possible that the NO is the result of photolysis of NO_2 which was already present. A rigorous test of this hypothesis will require simultaneous measurements of NO, NO_2 and PAN.

During the summer, NO levels were always very low except for two brief periods. During these periods, air flow was coming from the interior of Alaska in the vicinity of major boreal forest fires. The level of NO observed was sufficient to change the balance of ozone production/ destruction. However during the period when enhanced NO was observed, enhanced O_3 concentrations were not observed. To what extent are northern boreal forest fires important in the oxidation budget of the high latitudes remains an open question. However it should be pointed out that over the past 20 years, temperature have warmend substantially in Alaska, consistent with our current understanding of the "Greenhouse Effect". Hopefully as a result of our future observational campaigns we will be able to shed more light on the cause of the longterm tropospheric ozone increase in the Arctic.

REFERENCES

Barrie L.A. and Bottenheim J.W. (1991) Sulfur and nitrogen in the Arctic Atmosphere. in Pollution of the Arctic Atmosphere, ed by W.Sturges, Elsevier Pub. N.Y.

Crutzen P.J. (1988) Tropospheric Ozone: An Overview, in Tropospheric Ozone, edited by I.S.A. Isaksen, D.Reidel, Norwell Mass.

Honrath R.E. and Jaffe D.A. (1992) The Seasonal Cycle of Nitrogen Oxides in the Arctic Troposphere at Barrow, Alaska. J.Geophys. Res. 97, 20,615-20,630.

Jaffe D.A.et al., (1991) Measurements of Nitrogen Oxides at Barrow, Alaska During Spring: Evidence for Regional and Global Sources of Pollution. J.Geophys. Res. 96, 7395-7405.

Mayewski P.A. et al (1986) Sulfate and Nitrate Concentrations from a South Greenland Ice Core. Science 232, 975-977.

Oltamans S.J. (1993) Climatology of Arctic and Antarctic Tropospheric Ozone. in The Tropospheric Chemistry of Ozone in the Polar Regions. ed H.Niki and K.H. Becker. NATO ASI Series. Springer-Verlag Pub. N.Y.

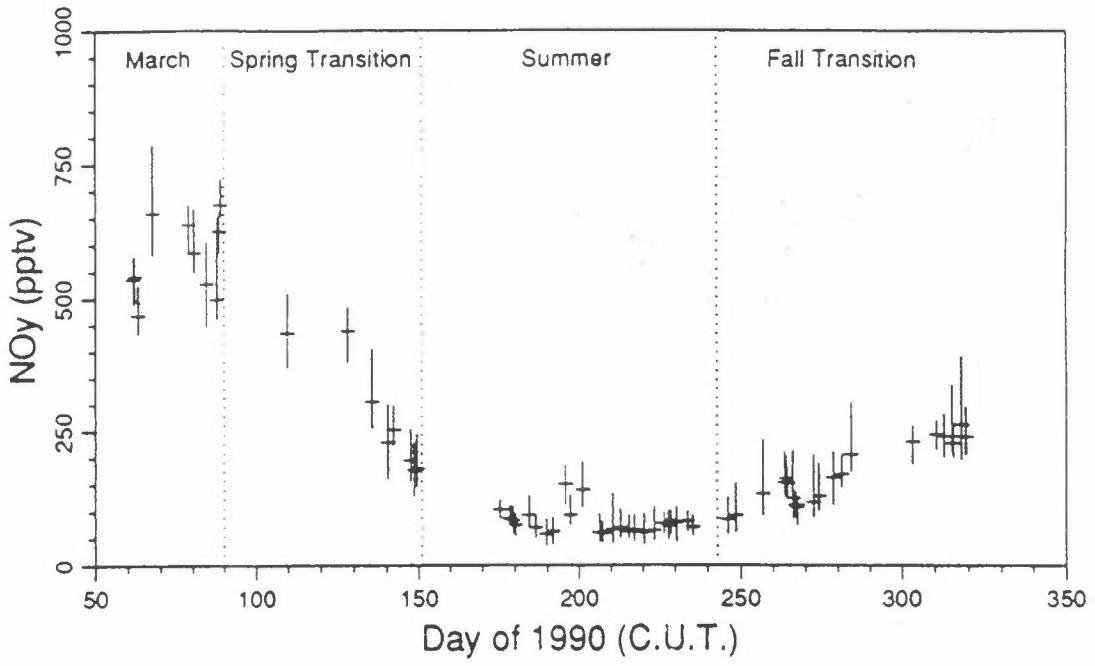

Figure 1: The 1990 seasonal cycle of NOy at Barrow. The data have been screened to eliminate the effects of local and regional (Prudhoe Bay) sources. Median concentrations during each event are shown with a cross and the vertical bar gives the range of measured 20-second averages during that period.

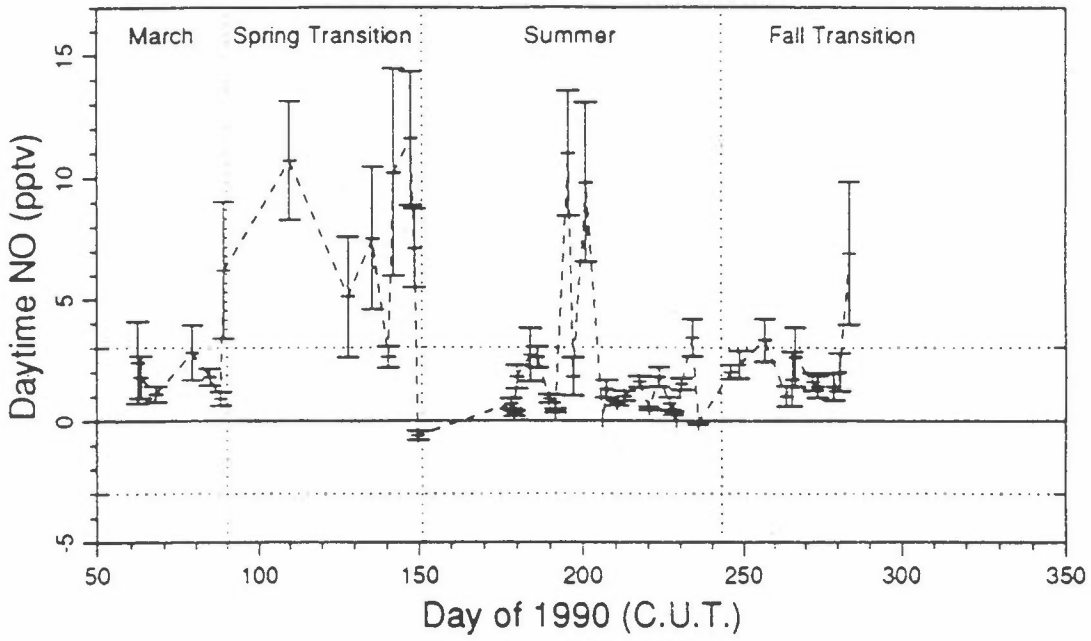

Figure 2: Daytime measurements (solar zenith angle less than 80°) of NO during 1990 background periods. The symbols indicate the average daytime NO concentrations and the error bars show two standard deviations about the mean. The observed detection limit for these measurements, 3 pptv, is shown by the horizontal dotted line.

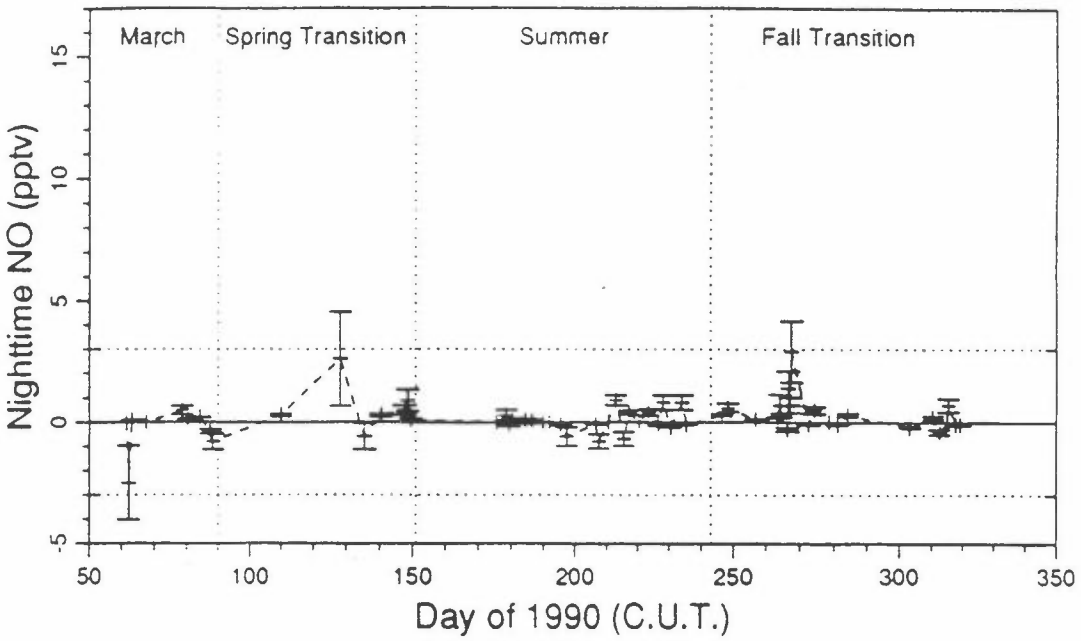

Figure 3: Nighttime measurements (solar zenith angle greater than 85°) of NO during background periods. The symbols indicate the average nighttime NO concentrations during each background period and the error bars show two standard deviations about the mean. The observed detection limit for these measurements, 3 pptv, is shown by the horizontal dotted line.

Heavy Metals in the Atmosphere in Finland

Jalkanen, L.[1], Virkkula, A.[1], Hillamo, R.[1] and Häsänen, E.[2]
[1]Finnish Meteorological Institute, Air Quality Department, Sahaajankatu 22 E, FIN-00810 Helsinki, Finland
[2]Technical Research Centre of Finland, Reactor Laboratory, P.O. Box 200, FIN-02151 Espoo, Finland

Introduction

Precipitation samples are analyzed routinely for heavy metals from seven background stations in Finland by the Finnish Meteorological Institute (FMI). Two of the stations are located on islands off the coast, the others are distributed in different parts of Finland (Fig. 1.). The collection at the Integrated Monitoring (IM) stations was started in June 1990, at the other stations earlier. In order to be able to compare the deposition at all the stations, the results discussed here are for the years 1991-1992.

Atmospheric aerosol samples, divided into two fractions, were collected on the Finnish EMEP-stations Utö, Virolahti and Ähtäri in the summer and autumn of 1991 and the winter of 1992 and in Sevettijärvi in the winter of 1993 (Fig.1.). The surroundings of these stations differ in nature. Utö is a nearly treeless island about 80 km from the southwest coast of Finland, Virolahti is located in the southeast, close to the Russian border, Ähtäri is in forested Central Finland and Sevettijärvi in Northern Lapland. The stations are susceptible to transport of air pollutants from different sources. Utö is the first location for the deposition of pollutants from Central Europe. At Virolahti, the emissions from the St. Petersburg area and Estonia are predominant during easterly to southerly winds. Sevettijärvi is close to the emission sources in Kola peninsula.

Major emission sources of heavy metals in Finland, deposition from precipitation, and concentrations in atmospheric aerosols are discussed.

Experimental

Precipitation samples (bulk) for trace elemental analysis are collected by the FMI at seven background stations, two of which belong to the EGAP (Group of Experts on Airborne Pollution of the Baltic Sea Area) and four to the IM (Integrated Monitoring) network. The special station at Värriö is used for monitoring the pollution originating in the Kola peninsula. The weekly and monthly samples are analyzed by AAS graphite furnace technique with a Perkin-Elmer 3030 instrument. Cadmium, copper, lead and zinc are analyzed at all the stations, and in addition chromium and iron at the IM and Värriö stations.

The 24 hour aerosol samples were collected on Nuclepore AP 8 μm (coarse fraction), and Millipore FS 3 μm (fine fraction) filters. The air volume was about 90 cubic meters and sample mass about 150-1000 μg per filter.

The filters were weighted on a micro balance. The elements Ag, Al, As, B, Ba, Be, Bi, Ca, Cd, Co, Cr, Cu, Fe, K, Li, Mg, Mn, Mo, Na, Ni, Pb, Sb, Se, Si, Sr, Th, Ti, Tl, U, V, and Zn were determined in the aerosol samples by inductively coupled plasma mass spectrometry, using a Perkin-Elmer ICP-MS SCIEX ELAN 5000 instrument, at the Geological Survey of Finland. Because of the small mass and unique samples, handling

and preparation of the samples is crucial. In this work, a simple method with high recoveries has been developed for the dissolution of the samples for analysis with ICP-MS.[1]

Emission sources

In Finland, over half of the emissions of Cd, Co, Cr, Cu, Ni, Pb and Zn originate from industry. For vanadium, energy production, primarily the use of oil, is the major source. Many of the metals are mainly emitted from one source. The five major ones belong to metallurgical industries. Of these, Harjavalta, located in Southwestern Finland, is the largest. Even after the changes in the process, which will reduce the emissions and be completed in 1995, the copper and nickel smelters in Harjavalta will be responsible for over half of the cadmium, copper and nickel emitted by industry in Finland.[2]

Table 1. Estimate of total annual emissions of heavy metals in Finland (t/a).[2]

Cd	Cu	Ni	Pb	V	Zn
5.54	119	86.1	447	109	586

The nearby principal foreign sources, that affect air quality in Finland, are located in Estonia and Russia. The emissions of lead and zinc from the two oil shale fueled power plants in Estonia are greater than those and the emissions of cadmium and copper about half of those caused by the energy production in Finland.[3] However, these are insignificant when compared with the total emissions in Finland, including industrial ones. The St. Petersburg area is a major source, but reliable data is not available. In the Kola peninsula, the major sources are the copper-nickel smelters at Nikel and Monchegorsk. According to crude estimates given by the russians, about 100 t of copper and 200 t nickel in the Nikel area and 2 000 t copper and 3 000 t nickel in Monchegorsk area are emitted annually.[4] The latter are about twenty and thirty times the respective total emissions of Finland (Table 1).

Results and discussion

The average values calculated from the *precipitation* results for 1991[5] and 1992[6] are listed in geographical order, south to north, in Table 2 with the two coastal stations listed first. The coastal stations, especially Haapasaari, receive the largest amount of deposition except for copper. The deposition decreases northward with clearly the lowest deposition value in the northern tip of Finland; the trends for the individual years are the same. Värriö is an exception to this northward decreasing trend. Copper and chromium deposition is the highest there of all the stations. This is due to the proximity of the nickel-copper smelters in the Kola peninsula.

The concentrations of heavy metals in *aerosols* in Finland are of the same order of magnitude as in Nordmoen, Norway[7], and Dorset, Canada[8] (Table 3).

Table 2. Average annual deposition of heavy metals in precipitation ($\mu g/m^2$).

Station	Cd	Cu	Pb	Zn	Cr	Fe
Haapasaari	71	1 360	5 200	17 500		
Hailuoto	36	1 400	2 230	12 200		
Kotinen	52	910	1 910	2 920	100	21 100
Hietajärvi	27	990	1 400	2 660	127	14 050
Pesosjärvi	16	1 190	860	1 480	48	9 850
Värriö	25	2 500	1 070	3 400	314	13 000
Vuoskojärvi	10	680	400	640	43	4 790

Table 3. The average cobalt, copper, iron, lead, vanadium and zinc concentrations (ng/m^3) of total aerosols in the summertime samples and in Nordmoen[7] and Dorset[8].

Station	Co	Cu	Fe	Pb	V	Zn
Utö	0.067	1.37	70	11.7	4.85	12.8
Virolahti	0.092	1.05	149	7.6	3.17	8.3
Ähtäri	0.068	1.17	70	7.7	1.26	7.0
Nordmoen -88	0.193	0.72	107	11.4	0.86	18.6
Dorset		6.1	55	18.8	1.3	

Table 4. Concentrations of aluminium, copper, nickel, lead, vanadium, and zinc (ng/m^3) in the fine fraction in Sevettijärvi in the winter of 1993.

Date	Al	Cu	Ni	Pb	V	Zn
14.1.	0.88	<0.07	0.04	0.55	<0.07	0.47
15.1.	7.94	4.68	2.89	1.52	2.03	1.25
5.-6.3.	2.13	0.22	0.63	0.66	1.56	0.67

The concentrations of trace elements in aerosols in *Sevettijärvi* are generally very low, as on Jan. 14, 1993 (Table 4), with southwest as the predominant wind direction. The concentrations on Jan. 15 are higher than the elevated values on March 5.-6. This is due to the air masses arriving from the Monchegorsk area (Fig. 2a), whereas on the latter date they have traveled through the Nikel area (Fig. 2b), where the emissions, although closer to Sevettijärvi, are only a tenth of those in the Monchegorsk area.

References

1. Jalkanen, L., and Häsänen, E., The analysis of aerosol samples with ICP-MS, Euroanalysis VIII Conference, Edinburgh, September 1993.
2. Aunela, L., and Larjava, K., Heavy metal emissions in Finland, Technical Research Centre of Finland, Research Notes 1181, Espoo 1990.
3. Aunela, L., Larjava, K., Mehtonen, A., Kinnunen, V., Häsänen, E., Salmikangas, T., Leskelä, J. and Loosaar, J., Emission measurements in oil shale power plants in Estonia, First Finnish Conference of Environmental Sciences, Kuopio 1993 (poster).
4. Laurila, T., Tuovinen, J.-P., and Lättilä, H., Lapin ilmansaasteet (Air Pollutants in Lapland), Finnish Meteorological Institute, 1991.
5. Leinonen, L. and Juntto, S. (edits), Air Quality Measurements 1991, Finnish Meteorological Institute, Helsinki 1992.
6. Leinonen L. (edit.), Air Quality Measurements 1992, Finnish Meteorological Institute, Helsinki 1993.
7. Maenhaut, W., Ducastel, G., Hillamo, R. E., Pakkanen, T. A. and Pacyna, J. M., Atmospheric aerosol studies in Southern Norway using size-fractionating sampling devices and nuclear analytical techniques, J. Radioanal. and Nucl. Chem. 1993, **167**, 271.
8. Hopper, J. F., and Barrie, L. A., Regional and background aerosol trace elemental composition observed in eastern Canada, Tellus 1988, **40B**, 446.

Figure 1. The stations used for the collection of the precipitation and aerosol samples.

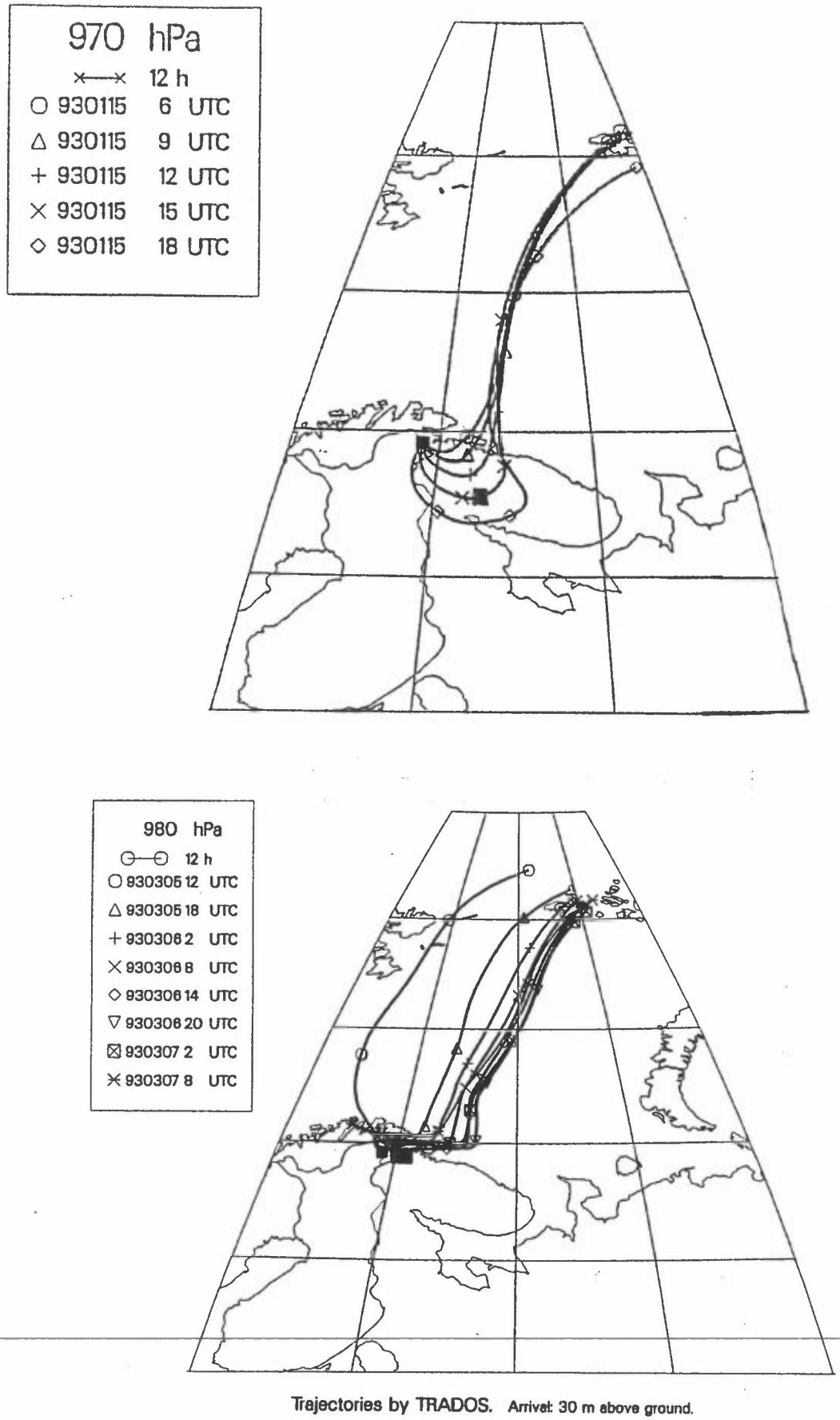

Figure 2. Trajectories in Sevettijärvi on January 15 (above) and March 5.-6. (below). Sevettijärvi, Monchegorsk (above) and Nikel (below) are marked with black squares.

NORSAC III, 3-5 December 1993, Geilo - Norway

LONG RANGE TRANSPORT OF ATMOSPHERIC HEAVY METALS

Kęstutis KVIETKUS and Jonas ŠAKALYS

Institute of Physics, Goštauto 12, Vilnius 2600, Lithuania

Summary

The regional background levels of the atmospheric heavy metals (Pb, Sn, Cr, Mn, Ni, Mo, V, Ti) during the long term observation are presented. The input of the heavy metals to the Baltic sea region and Lithuania from the main prevailing wind directions is analyzed and estimated.

Trace metal concentrations in the atmosphere have not been measured in Lithuania and neighbor countries before 1975 years (Kvietkus et al., 1981; Perkauskas et al., 1981). Later in publications (Pacyna et al., 1984; Swietlicki et al., 1987) and in many other publications (Borbely-Kiss et al., 1991; Remoudaki et al., 1991) there are a lot of interesting, useful and a new information about heavy metals in the atmosphere.

During the past ten years the heavy metals (Pb, Sn, Cr, Mn, Mo, Ni, V, Ti) concentrations at the Preila Background Monitoring station near the Baltic Sea were measured (Sakalys and Kvietkus, 1989). The purposes of this study were to investigate distribution properties of the heavy metal concentrations in the atmosphere of the south eastern Baltic sea region, to estimate seasonal variations, to determine origin and sources of the heavy metals, to evaluate input of the long range air mass transport to the pollution of the atmosphere, to evaluate amounts of the heavy metals transported from other countries to Lithuania, to evaluate the atmospheric heavy metal background levels in Baltic Sea region, to determine the main prevailing transport directions of pollutants and to estimate possible anthropogenic load.

For these purposes an atmospheric aerosol sampling equipment and analyzing methods were developed and improved: a new cascade impactor was designed in which the aerosols from the air are deposited directly on the spectric-carbon type electrodes and spectroscopic method was developed. The previous spectroscopic method for the heavy metal measurements after collection onto the aerosol filters was improved too.

At first, the heavy metal concentrations in the atmosphere at different locations in Lithuania were measured. Latter, according to the special criteria such as correlation of the concentrations, Fourier analysis, seasonal variations and air mass transport directions, origin and sources of the heavy metals were determined. According to these results the area for the background monitoring station was suggested in Preila (Fig.1). This location is very useful to control pollution of the atmosphere in Lithuania and Baltic sea region because about 85% of prevailing wind directions are from south-west and north-west directions.

The average background levels of the heavy metals concentrations measured during ten years period are presented in the Table 1. The air pollution of Lithuania is determined by the geographical location, climatic and synoptic conditions. Analysis of the air mass trajectories and heavy

Table 1. The background levels of the atmospheric heavy metal concentrations in the Lithuania, ng/m^3

Pb	Sn	Cr	Mn	Ni	Mo	V	Ti
12,1	1,78	8,95	26,9	6,50	0,67	12,7	32,0

metal concentrations is one of the methods to evaluate long range input and to determine regional background levels of these elements in the atmosphere (Fig.2). It can be seen from the Fig.2 that the main transport and the main input of heavy metals to the Lithuania and Baltic states are from West Europe countries.

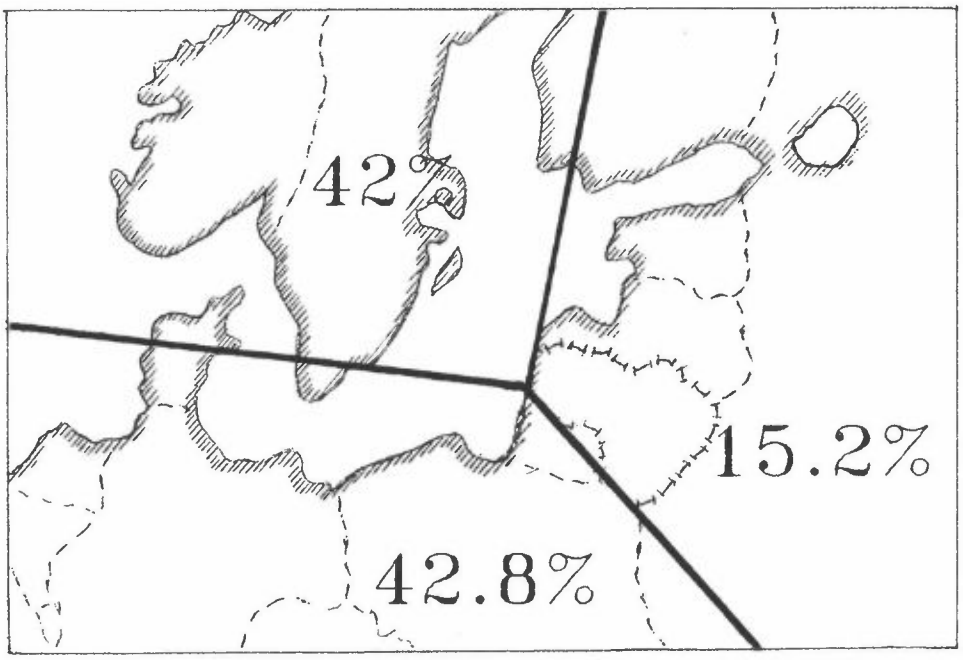

Fig.1. Variation of air mass trajectories into sectors (1980-1990).

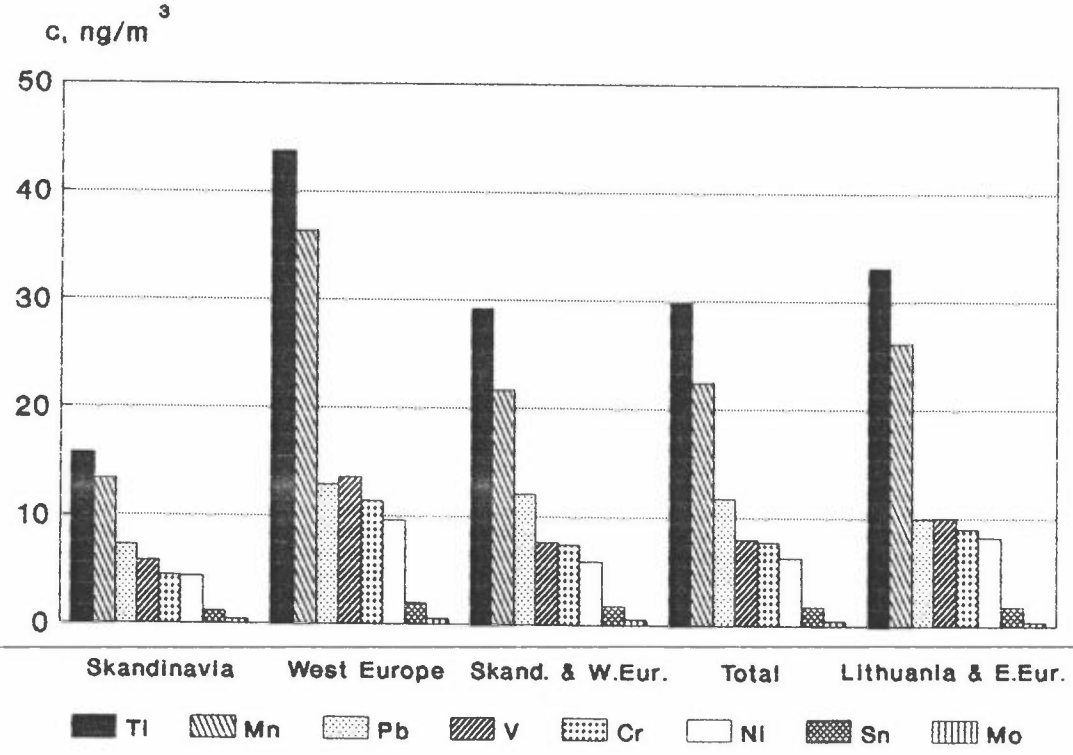

Fig.2. Distribution of the averaged heavy metal concentrations into sectors (1980-1990).

The results of the investigation presented in this study are valuable for evaluation of pollution input from the local industrial regions to the atmosphere.

References

1.Kvietkus K., Sakalys J. and Vebra E. (1981) Metal concentrations seasonal fluctuations in the Vilnius suburbs atmosphere. Atmospheric Physics 7, 91-93 (Vilnius Mokslas Publishers).

2.Perkauskas D., Sakalys J., Kvietkus K., Senuta K. and Cesonis K. (1981) Use of the Fourier fast transform method for the determination of some metals concentrations periodicity in atmosphere. Atmospheric Physics 7, 135-138 (Vilnius Mokslas Publishers).

3.Pacyna J.M., Semb A. and Hanssen J.E. (1984) Emission and long-range transport of trace elements in Europe. Tellus 36B, 163-178.

4.Swietlicki E., Hansson H.C., Svantesson B., Martinsson G. and Asking L. (1987) Source area identification of long range transported aerosols. J. Aerosol Sci. 18, 597-600.

5.Sakalys J. and Kvietkus K. (1989) Investigation regional background of heavy metal concentrations in the South Baltic atmosphere. Atmospheric Physics 13, 148-158 (Vilnius Mokslas Publishers).

6.Borbely-Kiss I., Bozo L., Koltay E., Meszaros E., Molnar A. and Szabo Gy. (1991) Elemental composition of aerosol particles under background conditions in Hungary. Atmospheric Environment 25A, 661-668.

7.Remoudaki E., Bergametti G., and Losno R. (1991) On the dynamics of the atmospheric input of copper and manganese into the Western Mediterranean Sea. Atmospheric Environment 25A, 733-744.

ATMOSPHERIC MERCURY - SOURCES, SPECIATION AND DEPOSITION

JOHN MUNTHE
Swedish Environmental Research Institute (IVL), P.O. Box 47086,
S-402 58 Göteborg, Sweden.

SUMMARY

The atmosphere is important in the environmental cycling of mercury since it serves as a medium for transport from sources to remote areas. Chemical and physical transformations occur in the atmosphere leading to deposition of mercury. The rate of deposition of mercury from the atmosphere is highly dependent on the speciation. In Sweden, annual mean concentrations of total mercury and methylmercury in precipitation as well as wet deposition fluxes are higher in the south than in the north indicating an influence of the industrialized and densely populated areas of northern and central Europe.

EMISSIONS OF MERCURY

Mercury is emitted from various industrial activities and natural sources. Natural sources include volatilization from water surfaces and soil with a high mineral content of mercury. Natural and anthropogenic emissions to the atmosphere are believed to be of the same order of magnitude [1]. However, mercury emitted from natural surfaces (soil, water) may emanate from previous anthropogenic emissions since deposition and re-emission of the mercury may occur. Global emissions to the atmosphere have been estimated to be in the range 5000 to 15 000 tons $yr.^{-1}$ [1], [2].

Releases to the atmosphere from combustion processes can be either in the form of elemental mercury (Hg^0), oxidized forms (Hg(II)) or mercury bound to particles (Hg(p)). Once emitted to the air, Hg^0 will add to the global background level in the atmosphere whereas any emitted Hg(II) or $Hg_{(p)}$-compounds will deposit more readily leading to increased deposition on a local or regional scale. Major sources of atmospheric mercury in Sweden are waste incineration and crematories whereas combustion of coal is the dominant source on the European continent.

SPECIATION AND TRANSFORMATION OF ATMOSPHERIC MERCURY

The predominant form of mercury in air is Hg^0, which is not very water-soluble . Deposition occurs after the elemental mercury has been converted to more water-soluble forms that can be subject to rain-out or wash-out. Dry deposition of mercury may also occur [3], [4]. The mechanisms responsible for the dry deposition of mercury are not known in any detail but may also include transformations into water-soluble forms on plant surfaces [5].

Transfoirmations processes may occur in both gaseous and aqueous phases, but the predominance of Hg^0 over other forms of mercury in air suggests that aqueous processes are more important. The secondary formation of particulate mercury in gas or aqueous phase, i.e. oxidation followed adsorption of mercury compounds on particles, may also be of importance, but experimental results are not available. Reduction of dissolved Hg(II)-compounds are also of interest [6], [7] since it provides a pathway for the removal of mercury from cloud- and rainwater back to the air.

Total concentrations of mercury in ambient air are usually in the range 1 to 4 ng m^{-3} [4], [8], [9], [10], [11]. Several attempts have been made to speciate the mercury content of ambient air. Particulate mercury can be analyzed after collection on glass wool plugs or filters. Reported concentrations are usually around or less than 0.1 ng m^{-3} i.e. < 5% of the total airborne Mercury [4], [12]. Several attempts have also been made to measure the concentration of methylmercury forms in air. The most recently reported concentrations of methylmercury in air are consistent with values around 0.5 to 20 pg. m^{-3} [13], [14], [15], [16]. The methylmercury concentrations measured in air may explain the methylmercury levels found in precipitation, considering the air/water distribution constant.

Mercury in rain is present in both the dissolved and the particulate phases. A major fraction is associated with particles, at least in industrialized and urban regions [4], [17], [18]. The dissolved fraction consists of both inorganic divalent mercury complexes and methylmercury forms. Typical background concentrations of total mercury are usually in the range 1 - 25 ng L^{-1}, depending on the proximity to industrial activities emitting mercury, with occasional values of up to 100 ng L^{-1} during pollution events [1], [4]. Typical concentrations of methylmercury range from <0.01 ng L^{-1} in rain over the remote Pacific Ocean [14] to up to 0.68 ng L^{-1} in coastal areas in southwest Sweden [18].

The aqueous oxidation of Hg^0 by O_3 is probably one of the major pathways for the transfer of volatile Hg^0 to water-soluble Hg(II). The reaction is relatively fast with $k = 4.7 \times 10^7$ M^{-1} s^{-1} [6], but due to the low solubility of both Hg^0 and O_3, the actual mass transfer of mercury to the aqueous phase is relatively slow under atmospheric conditions. In a volume of air of 1 m^3 containing 0.5 mL liquid water (i.e. a typical value for a cloud) the rate of conversion of $Hg^0(g)$ to aqueous Hg(II) is only 2 to 3 % per day at gaseous concentrations of 3 ng m^{-3} Hg^0 and 30 ppb O_3. Divalent mercury is reduced by dissolved SO_2 (S(IV)) [7].

DEPOSITION OF MERCURY

Measurements of concentrations of mercury in rain and snow have been performed in the several regions during the last decades. Wet deposition of total mercury in Sweden ranges from around 4 $\mu g\ m^{-2}$ in the northern parts to 13 in the south [20]. Measurements of methylmercury in precipitation has shown that a clear south-north gradient exists also for methylmercury deposition with maximum average values of 0.29 $\mu g\ m^{-2}\ yr.^{-1}$ on the west coast, and 0.07 $\mu g\ m^{-2}\ yr.^{-1}$ in the north [18]. This gradient is similar to that for deposition of total mercury [4] which is believed to originate from industrial activities in northern and central Europe.

Field measurements of mercury in open field rain and throughfall have shown that the passage through the forest canopy increases the concentration of mercury in rain-water during summer months [19]. This effect was attributed to a dry deposition of mercury compounds on the needle surfaces, followed by wash-off by the rain falling through the canopy. Furthermore, the amounts of mercury reaching the forest floor with litterfall is of the same order of magnitude, or higher, as the total deposition via throughfall. In the investigated area (SW Sweden), mercury deposition via throughfall was calculated to be about 12 $\mu g\ m^{-2}\ yr.^{-1}$ with an additional 4 to 7 $\mu g\ m^{-2}\ yr.^{-1}$ attributed to dry deposition on the needle surfaces. An estimate of the litterfall flux to the forest soil yielded 25 $\mu g\ m^{-2}\ yr.^{-1}$.

REFERENCES

1 Lindqvist, O., Johansson, K., Aastrup, M, Andersson, A., Bringmark, L., Hovsenius, G., Håkanson, L., Iverfeldt, Å., Meili, M. and Timm, B. Mercury in the Swedish environment - Recent research on causes, consequences and corrective methods. *Water, Air, and Soil Pollution* **55**, 261 p., 1991.

2 Fitzgerald, W.F. Cycling of mercury between the atmosphere and oceans. In: The role of air-sea exchange in geochemical cycling. (P. Buat-Menard, Ed.), NATO Advanced Institute Series, Reidel Publishing Co., Dordrecht, The Netherlands, 363-408, 1986.

3 Lindberg, SE., Turner, RR., Meyers, T.P., Taylor Jr., G.E. and Schroeder, W.H. Atmospheric Concentrations and Deposition of Hg to a Deciduous Forest at Walker Branch Watershed, Tennessee, USA. *Water, Air, and Soil Pollution* **56**, 577 - 594, 1991.

4 Iverfeldt, Å. Occurrence and turnover of atmospheric mercury over the Nordic countries. *Water, Air, Soil Pollut.* **56**, 251-265, 1991.

5 Lindberg, S.E., Owens, J.G. and Stratton, W. Application of throughfall methods to estimate dry deposition of mercury. In: *Mercury as a Global Pollutant - Toward Integration and Synthesis.* Watras and Huckabee (Eds.), Lewis Publishers, NY, 1993, In press.

6 Munthe, J. The aqueous oxidation of elemental mercury by ozone. *Atmos. Environ.* **26A**, 1461 - 1468, 1992.

7 Munthe, J., Xiao, Z.F. and Lindqvist, O. The aqueous reduction of divalent mercury by sulfite. *Water, Air, Soil Pollut.* **56**, 621 - 630, 1991.

8 Gill, G.A. and Fitzgerald, W.F. Mercury in surface waters of the open ocean. *Global Biogeochemical Cycles* **1**, 199 - 212, 1987.

9 Slemr, F., Schuster, G. and Seiler, W. Distribution, speciation and budget of atmospheric mercury. *J. Atm. Chem.* **3**, 407 - 434, 1985.

10 Brosset, C. The behaviour of mercury in the physical environment. *Water, Air, Soil Pollut.* **34**, 145-166, 1987.

11 Brosset, C. Total airborne mercury and its possible origin. *Water, Air, Soil Pollut.* **17**, 37-50, 1982.

12 Fitzgerald, W.F., Gill, G.A. and Kim, J.P. An equatorial pacific ocean source of atmospheric mercury. *Science* **224**, 597- 599, 1983.

13 Bloom, N.S. and Fitzgerald, W.F. Determination of Volatile Mercury Species at the Picogram Level by Low-Temperature Gas Chromatography with Cold - Vapour Atomic Fluorescence Detection. *Anal. Chim. Acta* **208**, 151 - 161, 1988.

14 Mason, R.P., Fitzgerald, W.F. and Vandal, G.M. The sources and composition of mercury in Pacific Ocean rain. *J. Atmos. Chem.* **14**, 489-500, 1992.

15 Fitzgerald, W.F., Mason, R.P. and Vandal, G.M. Atmospheric cycling and air - water exchange of mercury over mid - continental lacustrine regions. *Water, Air, and Soil Pollution* **56**, 745 - 767, 1991.

16 Brosset, C. and Lord, E. Personal communication.

17 Ferrara, R., Maserti, B., Petrosino, A. and Bargagli, R. Mercury levels in rain and air and the subsequent wash-out mechanism in a central Italian region. *Atmos. Environ.* **20**, 125-128, 1986.

18 Ahmed, R., May, K. and Stoeppler, M. Wet Deposition of Mercury and Methylmercury from the Atmosphere. *Sci. Tot. Environ.* **60**, 249 - 261, 1987.

18 Munthe, J. and Iverfeldt, Å. Wet deposition of methylmercury in Sweden. Presented at the EPA/A&WMA Symposium *Measurement of Toxic and Related Air Pollutants.*, Durham, NC, May 3-7, 1993.

19 Iverfeldt, Å. Mercury in forest canopy throughfall water and its relation to atmospheric deposition. *Water, Air, Soil Pollut.* **56**, 553-564, 1991.

20 Persson, K., Lövblad, G. and Munthe, J. IVL Report L 93/186 Swedish Environmental Research Institute (IVL), Göteborg, Sweden. (In Swedish).

Polychlorinated Biphenyls and Organochlorine Pesticides in the Baltic Sea

OTT ROOTS

MINISTRY OF THE ENVIRONMENT OF ESTONIA,EE0013 TAILINN,KOTKA STR.2
ESTONIA

SUMMARY

The work approach will be use toxic chlororganic compounds as tracers for nonpolar organic contaminants cycling in the environment.These processes can best be studied in a system-oriented programme localized to one specific region -the Gulf of Riga.The region near the city Riga is by far the most PCB contaminated in the Baltic Sea.From this study it can be concluded that PCB's seems to be a substance of interest.

Atmospheric deposition of chlorinated hydrocarbons seems to dominate the inflow to the Baltic Sea ecosystem(I).In the air above the open part of the sea PCB concentrations by authors data did not exceed in 1984 - 0,13 ng/m^3,and the summary DDT - 0,09 ng/m^3 (2).In Swedish data the concentration values of PCB's at the same time (1984-1985) ranged between 0,01-0,36 ng/m^3,with a mean of 0,09 ng/m^3.The airborne fallout of the summary DDT over Sweden significantly decreased from 1972-1973 to 1984-1985,the fallout of PCB's was similar during the two periods(3).

Since the beginning of the 1980 the use of 25-50 m.capillary columns in gas chromatography started and made the determination of main PCB components possible.Separate congeners determination is necessary for a number of reasons.First,congeners differ in their toxic properties.Secondly,their half-life in organisms can differ considerably.

Finally,the challenge in studying organochlorines biochemical behavior in marine ecosystems also requires a separate determination of these compounds(Table I) and the products of their metabolism.

At present it is very difficult to compare the results of the analyses of chlororganic compounds taken in different countries.

Only possibility is to collect the samples in different coun-

tries using some equipment and methods(Fig.I and 2) or to analyse them in one laboratory.If we analyse the air and rain samples the second variant is advisable.First to suggest this kind of co-operation was the professor of Lund University - Per Larsson.Fifteen air monitooring stations have been established along the Baltic Sea coast and at islands(Fig.3).The stations in Sweden,Estonia,Latvia,Poland and Lithuania are included.Analyses of pollutants loads at these stations is presently carried out, and preliminary results show high PCB load in Gulf of Riga area (near city Riga)(4)(Fig.3,station 2).One of the smallest PCB concentrations in air and precipitations were detected in Estonian Lahemaa station(5)(Fig.3,station I).If authors takes the PCB relative concentration in Lahemaa station air and precipitation as - I,0,then Latvian Salaspils station(Fig.3,station 2) air and precipitation PCB concentrations were 7,6 and 8,7 times and Lithuanian Ventes Ragos station(Fig.3,station 3) I,3 and 2,6 times higher.

The atmosphere is an important contributor of antropogenic matter to the marine ecosystem.The above-mentioned results point out the necessity to analyze the Baltic herring(2 or 3 - year old) feeding on the plankton in the upper layers of the Gulf of Riga(Table I).The knowledge of chlorinated compounds in the Gulf of Riga is very limited(6).Depending on structural differences between the various congeners different PCB's might bioaccumulate and metabolize at different rates.During the last year attention has been drown to the most toxic PCB isomers.Among the PCB, the congeners with no chlorine substances in the ortho-positions show high toxicity,e.g.3,3',4,4'-tetrachlorobiphenyl(PCB No.77); 3,3',4,4',5-pentachlorobiphenyl(PCB I26),and 3,3',4,4',5,5'-hexachlorobiphenyl(PCB I69).Several congeners substituted in one of the ortho-positions,although less potent,also have tetrachlorodibenzo-p-dioxin like toxicity:2,3,3',4,4'-pentachlorobiphenyl, (PCB I05);2,3',4,4',5-pentachlorobiphenyl(PCB II8);2,3,3',4,4',5-hexachlorobiphenyl(PCB I56) and 2,3,3',4,4',5'-hexachlorobiphenyl(PCB I57).

Studies on accumulation of PCB components and chlorinated pesticides in air,precipitations,in fish and s.o.may contribute to

the better understanding of contaminants migration ways in the Baltic Sea ecosystem.

REFERENCES

1 Roots,O."PCB and chlorinated pesticides in the Baltic Sea ecosystem".Tallinn Technical University,1992,1-181(in Russian,tables and figures in English).

2 Roots,O.,Aps,R."PCB and organochlorine pesticides in Baltic herring and sprat".Toxicological and Environmental Chemistry, 1993,Vol.37,3-4,195-205.

3 Larsson,P.,Okla,L."Atmospheric transport of chlorinated hydrocarbons to Sweden in 1985 compared to 1973".Atmospheric Environment,1989,Vol.23,8,1699-1711.

4 Larsson,P.,Okla,L."Transport and process for persistent pollutants to the Baltic Sea".Baltnews,1991,3,7-8.

5 Larsson,P.,Järnmark,C.,Okla,L.,Bremle,G."Atmospheric transport of persistant pollutants to the Baltic Sea-Report October 1993 (in press).

6 Roots,O.,Aps,R."PCB,s isomers and chlorinated pesticides in the Gulf of Riga herring".I.C.E.S.,Marine Environment Quality Committee C.M.,1993/E:11.

7 Bouchertall,F."Atmospheric transport of PCB to the Baltic Sea" Fifth Meeting of the EGAP,Gdynia,25-29 April 1988,EGAP 5/Inf.7.

8 Roots,O."Levels of Toxic Organochlorines in Seal blubber in the Riga Bay".Eesti Arst,1992,4,258-261(in Estonian,summary in English and Russian).

9 Haraguchi,K.,Athanasiadou,M.,Bergman A.,Hovander L.,Jensen,S. PCB and PCB Methyl Sulfones in selected groups of seals from Swedish waters".AMBIO,1992,Vol.21,546-549.

Acknowledgement:This research was partly supported by the Research Support Scheme of the Central European University.

Table I.

Concentrations of some PCB congeners in rainwater(7) and 2 year old Riga Bay herring muscle tissue.

PCB No. IUPAC	rainwater		baltic herring	
	pg/dm^3	%	ng/mg	%
52	I74,5	4,2	0,05535	3,4
49	86,4	2,I	0,02762	I,7
44	68,3	I,6	0,02272	I,4
I0I	567,6	I3,7	0,I5990	9,9
I5I	I97,2	4,7	0,05637	3,5
I49	I78,7	4,3	0,26420	I6,4
II8	330,9	8,0	0,20450	I2,7
I53	607,0	I4,6	0,26970	I6,7
I4I	22I,6	5,3	0,05468	3,4
I38	93I,7	22,4	0,22700	I4,I
I83	50,2	I,2	0,02I3I	I,3
I28	II2,3	2,7	0,II490	7,I
I80	322,8	7,8	0,07055	4,4
I70	307,6	7,4	0,06609	4,I
summary:	4I56,8	I00	I,6I489	I00

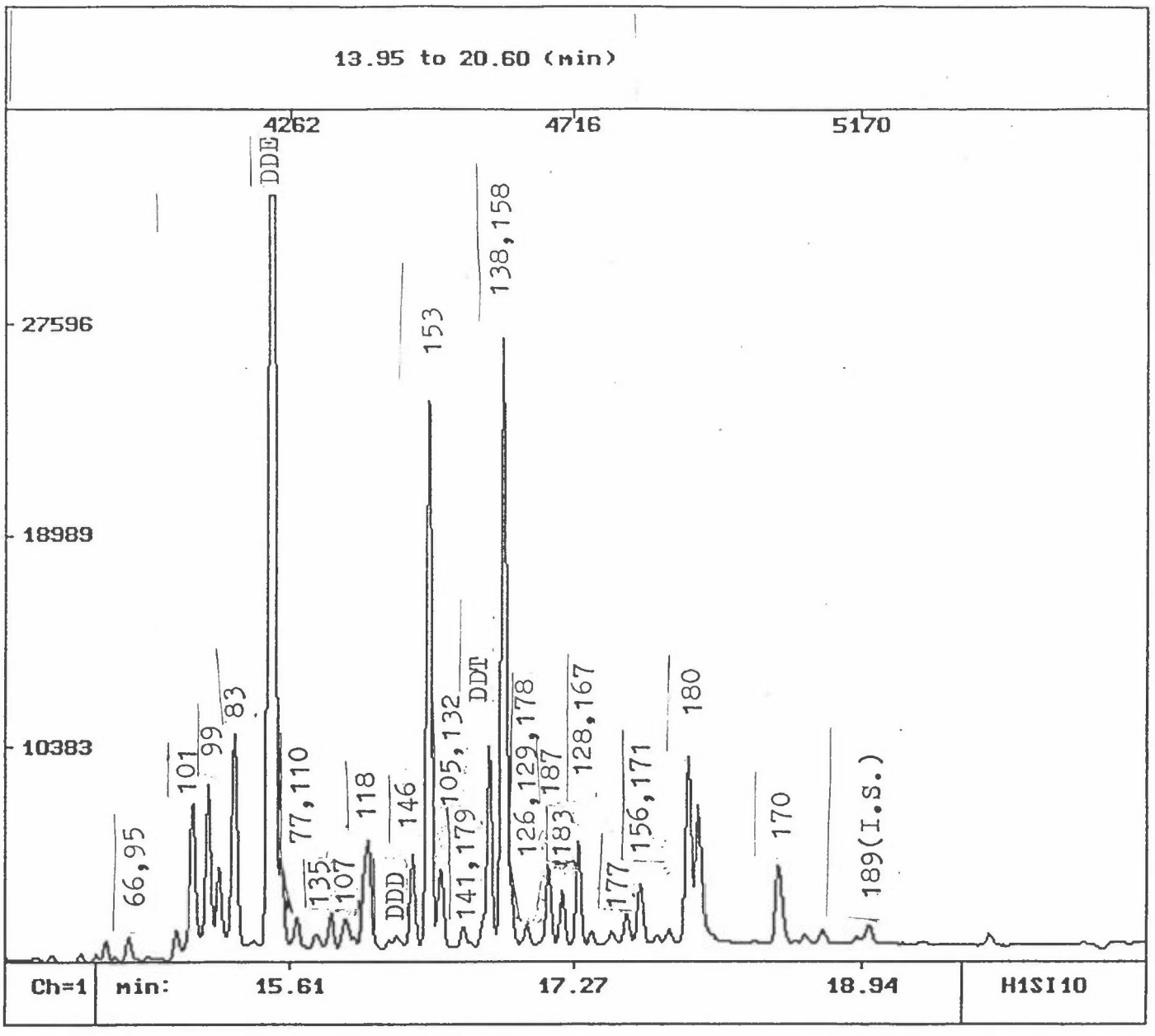

Fig.I .A chromatogram of CB's in blubber extract from a ringed seal from the Gulf of Riga.IUPAC Numbers of the major PCB congeners are shown in the chromatogram(C.Roots,1992)(8).

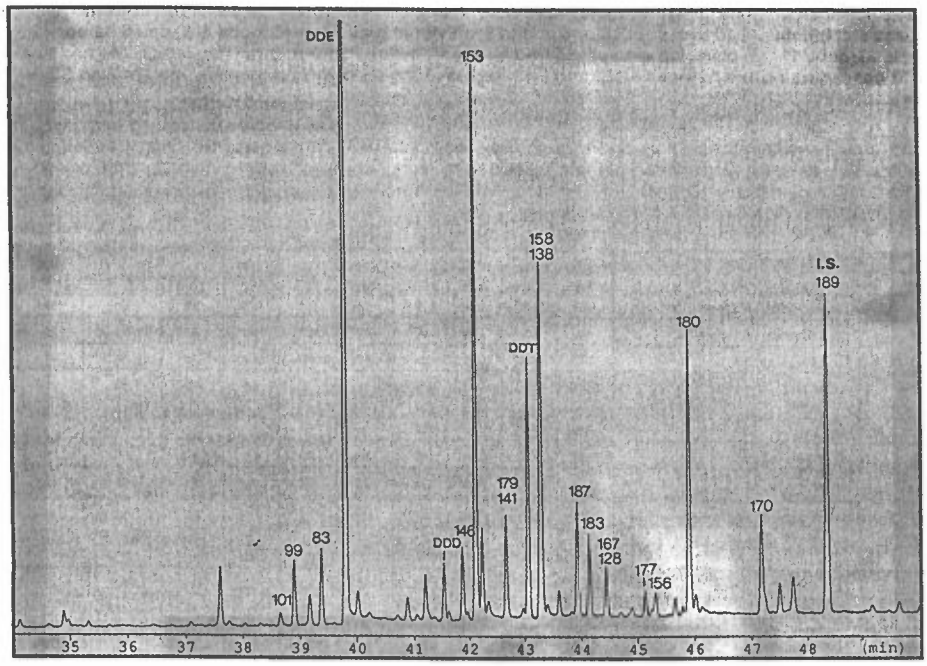

Fig. 2 .A gas chromatogram of CB's in blubber extract from a homogenate of adult,male grey seal from the Baltic. IUPAC Numbers of the major PCB congeners are shown in the chromatogram(K.Haraguchi,et al.,1992).(9).

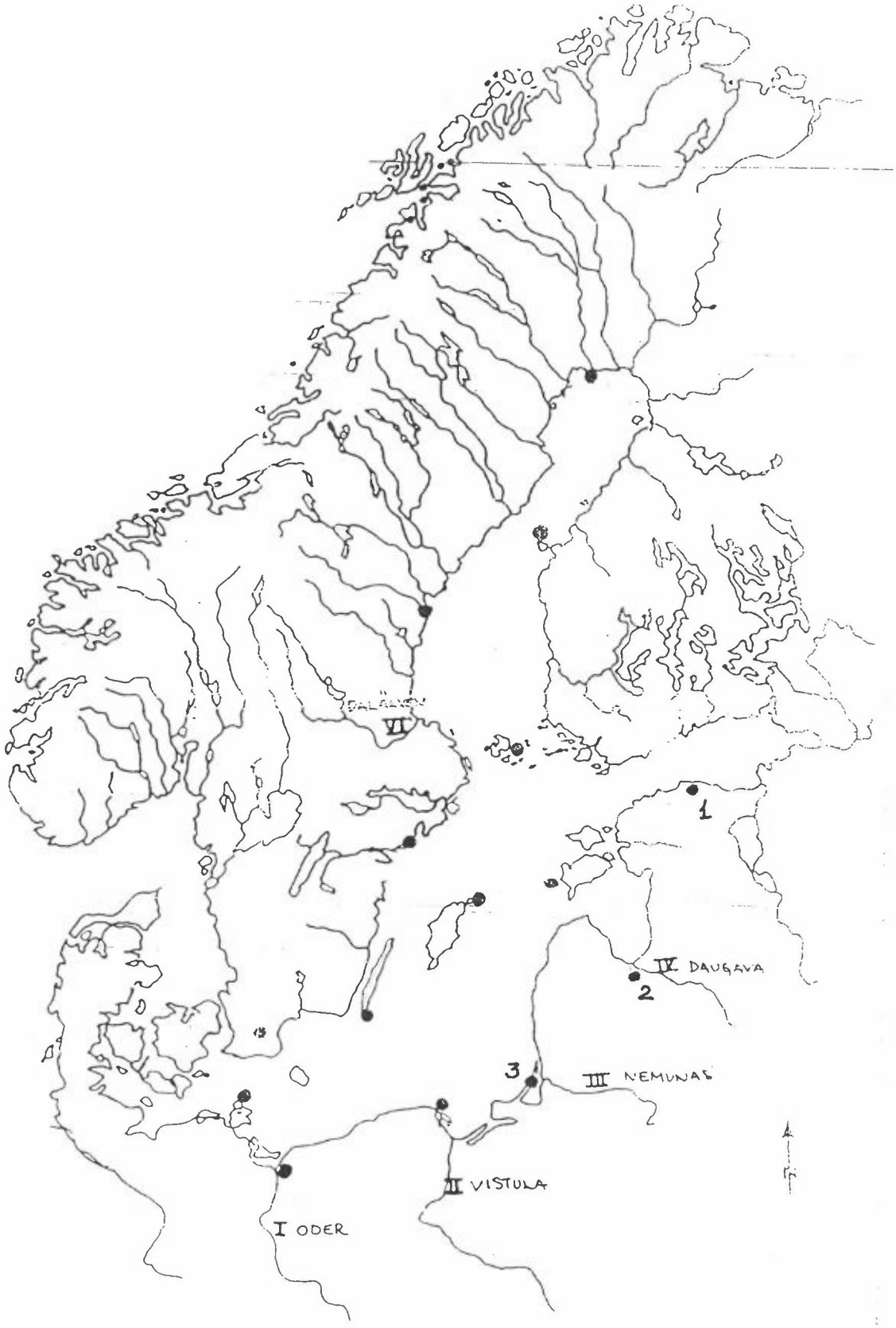

Fig.3. Sampling sites.

AIR POLLUTION IN ESTONIA

Leo Saare

Ministry of the Environment of Estonia

North-East Estonia is one of the most polluted areas in the Baltic Sea surrounding countries. In 1990 the stationary sources of the Estonian enterprises emitted 610,9 thousand tons of air pollutants including 302,1 thousand tons of solids(dust,ash) and 308,9 thousand tons of gases(1). North-East Estonia form 7,1% of the territory of Estonia but provide 71% of the total sulphur emission originating from the country. The most important source of energy in Estonia is oil-shale. It is used for heating the two big power plants- the Estonian and Baltic Thermal Power Plants, as well as some smaller power plants and three plants of oil-shale processing and chemistry. Besides this oil-shale is also used as fuel in "Estonian Cement". Estonian oil-shale has a complicated chemical composition. Over one half of the material is its mineral part which remains in the kilns as ash. Sulphur makes approximately 1,65%, nitrogen-0,1%, chlorine-0,2% of the organic and inorganic part of oil-shale. In 1990 the three main fuels included oil-shale(59,5%), heavy oil(16,1) and natural gas(14,5%), making 90,1% of the total of fuels used(2).

According to the recommendations of Working Group of the Economic Commission for Europe and the Nordic Council, a sulphur deposition level of 1,000 mgS/m^2 year is considered as critical load protecting sensitive ecosystems(3). By the data E.Klimova(3) and figure demonstrates that about 150 km^2 of sea and land territory of Estonia are covered with sulphur deposition exceeded this critical load. The most polluted area is situated near Narva(1,3). In 1992 due

to the changed economic pricimples,disintegration of large enter - prises as well as the lack of raw materials and fuel(and their prices),the volumes of pollutants from stationary sources have decreased almost 30%(4)

I.Kallaste T.,Roots O.,Saar J.,Saare L.I992.Air Pollution in Estonia I985-I990.Environmental Report 3,Environmental Data Centre, Helsinki,6I p.

2.Eensaar A.,Tarand A.I99I.The change of climate and Estonian energetics.Problems of Contemporary Ecology,Tartu,pp.I4-I7.

3.Klimova E.I993.Modelling of transfer and impact on ecosystems of emissions from oil-shale power plants in Estonia.-Oil Shale, v.IO,No.I,pp.67-78.

4.Estonian Environment I992.I993.Environmental Report 6,Environmental Data Centre,Helsinki,92 p.

Fig.Spatial distribution of sulphur depositions,/mg/m^{2}year/,in the investigated region(without considering of filtering effect) (3).

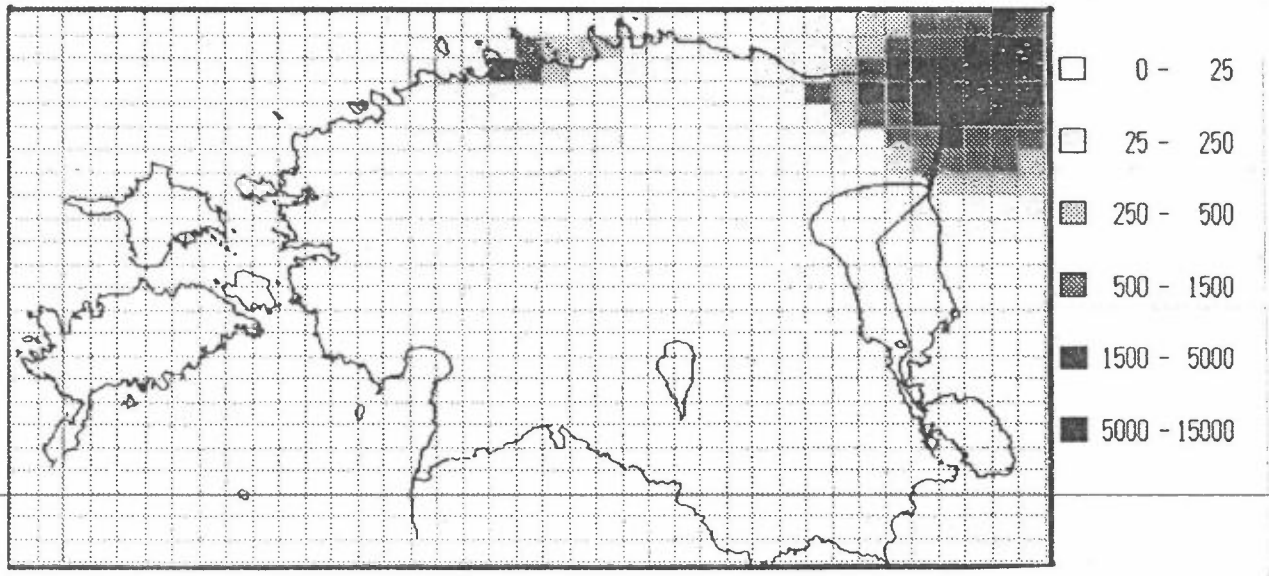

Trends in observed ozone and precursors 1988-1993 Birkenes, South Norway

Sverre Solberg, Frode Stordal, Norbert Schmidbauer,
Ulf Pedersen and Kjetil Tørseth
Norwegian Institute for Air Research

Summary

Time trends of nine non-methane hydrocarbons (NMHC), of NO_2 and of ozone measured at Birkenes in South Norway were estimated for the period 1988-1993. No trends in NO_2 or the sum of NMHC were found, while a significant trend in the NMHC composition was revealed. A marked decrease in the concentration of ethene and propene was found, whereas the acetylene concentration showed a significant upward trend. For ozone, an increase of about 1 ppb/year was estimated.

Measurements

All the measurements were taken at the rural NILU station Birkenes on the South coast of Norway (58°N, 8°E, 119 m a.s.l.), as part of the EMEP and TOR station networks. Continous measurements of ozone have been taken by an automatic UV-absorption monitor at Birkenes since 1987, and NO_2 has been measured by daily filter samples in the same time period. Manual grab samples of NMHC have been collected in electropolished steel bottles and sent to NILUs laboratory for analysis regularly since autumn 1987, normally 2-3 times a week. From 1987 to 1991 the grab samples were analysed for nine light NMHC (C_2 - C_5). Since 1992 the analyses were extended up to C_7, and some aromatics were included. The lab analyses were made by gas cromatography equipped with a flame ionization detector on an automated Chrompack VOC-AIR instrument. A detailed description of the sampling technique and analytical method is given in Schmidbauer and Oehme (1986), and a documentation of the NMHC measurements made at Birkenes is given in Solberg et al. (1993).

Trend analysis method

Due to the scatter in the daily data and the large seasonal cycle, a straight forward regression of daily measured concentrations against time is known to be uncertain and produce errors for atmospheric trace constituents (Gilbert, 1987). Several approaches have been attempted for sorting out the often minor time trends from the daily and seasonal scatter in such data sets. In this work we used a non parametric method, named seasonal Kendall slope estimation, which is suited for short time series with seasonally dependent data.

The basic idea in this method is to count the postive and the negative forward time differences between different years for each month separately, and then average over the months. If the resulting averages then give a very high number of either negative or positive differences, then it is probable that there is a significant trend in the data. This

trend may then be estimated. The seasonal Kendall slope estimator estimates it to be the median of all the forward time differences described (all months).

A standard normally distributed variable, Z, is defined to be a function of the quantity

$$S_i = \sum_{k=1}^{n_i-1} \sum_{l=k+1}^{n_i} sign\,(x_{il} - x_{ik})$$

where x_{jl} and x_{ik} are the values at season i, year l and k respectively.

S_i counts the signs of the changes in observed trace gases. The significance level for rejecting a null hypothesis of no trend is found in a look up table.

If the null hypothesis is rejected, the estimated slope is the median of all the forward time differences

$$Q_i = \frac{x_{il} - x_{ik}}{l - k}$$

Also the confidence limits for the slope estimation may be calculated. A detailed description of the seasonal Kendall slope estimation method is given in Gilbert, 1987.

Since the method described above, assumes monthly data, the monthly median concentrations of measured ozone, NO_2 and NMHC were used in our analysis. This will also rule out outliers in the data (most important for NMHC). The monthly median concentrations of the continous ozone data were calculated from hourly values.

Results

Table 1 shows the calculated Z-statistic for all the components, and the estimated slope with 80% confidence limits for the components for which the null hypothesis of no trend was rejected. The 5 % significance level of Z, used for rejecting the null hypothesis, was ± 1.645. Also the most important sources of the components is noted in the table.

There were no significant trends in the sum of NMHC or NO_2. It should be mentioned, however, that many daily concentrations of NO_2 were below the detection limit of approx. 0.1-0.4 µg(N)/m^3, and that the analysis is uncertain for this component. Ozone, on the other hand, showed a significant upward trend of about 1 ppbv/year, which may be an indication of a steady increase in the background tropospheric concentration of ozone.

Although the change in the sum of NMHC was not significant, there was a significant decline in the alkene concentration of 8-9 %/year, while an upward trend of 5 %/year was found for acetylene. The monthly median concentrations, and the estimated slopes for acetylene, ethene, propene and ozone are shown in Figure 1. The different trends in acetylene and the alkenes are surprising, and there is no obvious explanation for the result, especially since the anthropogenic sources of these components are mostly the same (Table 1).

One reason may be that the alkenes are highly reactive compounds, while acetylene has a rather long lifetime (2-3 weeks). A small change in the atmospheric oxidation would therefore cause a much larger change in the alkene concentrations measured at Birkenes than for acetylene. A change in the atmospheric oxidation could be due to either a change in the meteorological transport pattern, or a rise in the tropospheric background concentration of OH or ozone (which was actually found in this work). Whereas the alkenes are oxidized by both OH and O_3, acetylene only reacts with OH.

Another possible explanation for the opposite trends in acetylene and the alkenes could be a reduction in the biogenic emissions of the alkenes.In any event, an interpretation is quite uncertain, since the time series are relatively short, and the data scattered, and therefore influenced by episodes.

Acknowledgement

The ozone and NO_2 measurements are part of a national monitoring program funded by the State Pollution Control Authority. The VOC measurements were partly financed by the Norwegian Research Council.

References

Gilbert R.O., (1987) Statistical methods for enviromental pollution monitoring, Van Nostrand Reinhold Company, New York.

Schmidbauer, N. and Oehme, M. (1986) Improvement of a cryogenic preconcentration unit for C2-C5 hydrocarbons in ambient air at ppt levels. J High Res. Chromatogr. & Chromatogr. Commun., 9, 502 - 505.

Solberg, S., Stordal, F., Schmidbauer, N. and Hov, Ø. (1993) Non-methane hydrocarbons (NMHC) measured at Birkenes in South Norway, 1988-1993, NILU OR 47/93.

Table 1: Calculated Z-statistic, slope and significance levels for NMHC, NO_2 and ozone.

	Z*	Slope**	80 % limits**		Sources***
Ethane	-2.669	-31 ppt/y (-2%/y)	-18	-53	1
Ethene	-3.047	-37 ppt/y (-8%/y)	-19	-55	2,4
Acetylene	+3.248	+28 ppt/y (+5%/y)	+19	+35	2
Propane	-0.454				1
Propene	-3.278	-10 ppt/y (-9%/y)	-7	-15	2,4
N-butane	+0.065				3
I-butane	+0.972				3
N-pentane	-3.234	-15 ppt/y (-8%/y)	-9	-20	(3)
i-pentane	-0.323				3
SUM (VOC)	-0.522				
NO_2	-1.587				2
Ozone	+1.738	+1 ppb/y (3.5%/y)	+0.4	+1.4	

* Sign.level: 1.645

** Only given for components with a significant trend.

*** 1: Natural gas, 2: Engine exhaust, 3: Fuel vapour, 4: Biogenic.

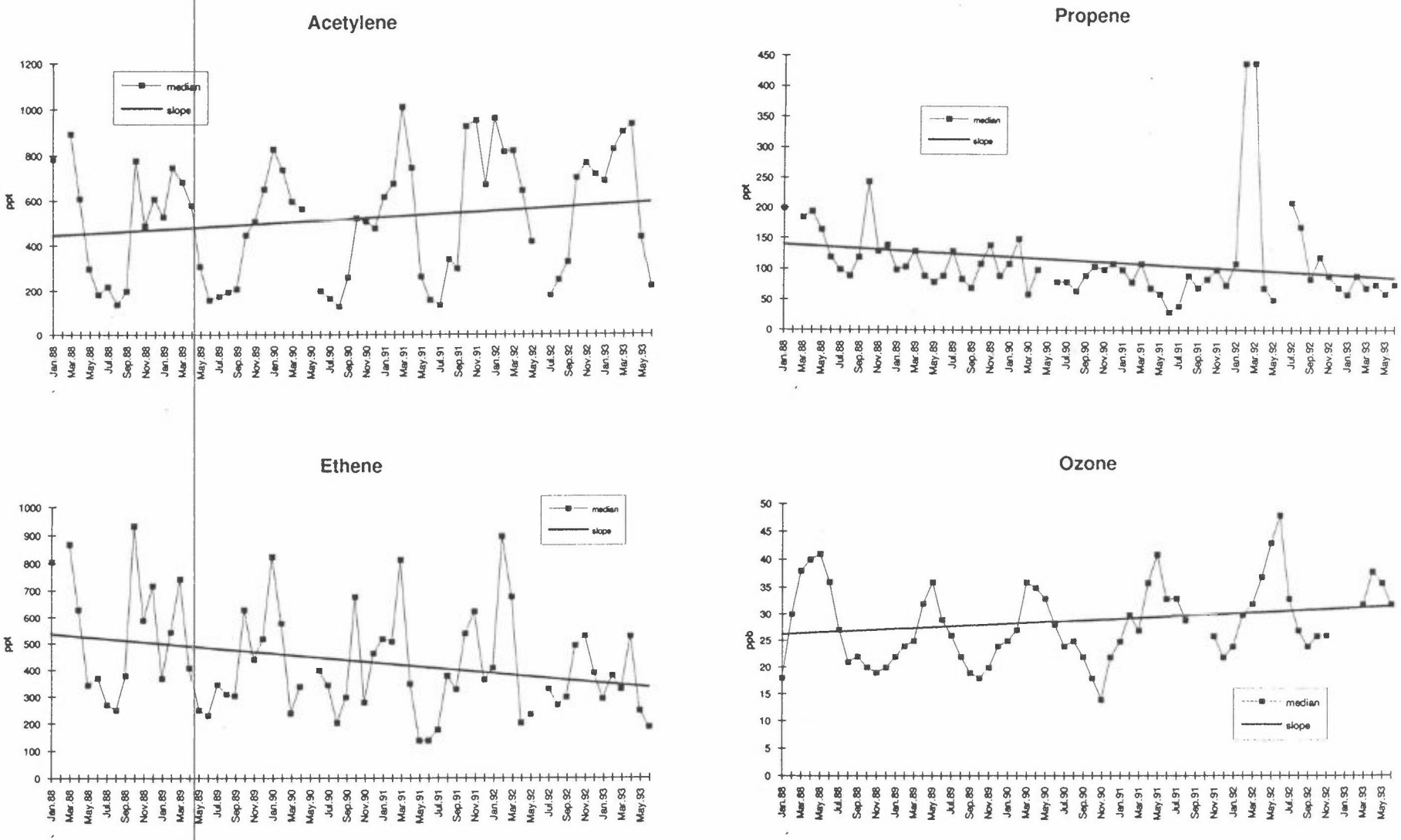

Figure 1: Monthly median concentrations and the Kendall slopes.

LITHUANIAN CONTRIBUTION TO THE AIRBORNE NITROGEN DEPOSITION FLUX TO THE BALTIC SEA

D. Sopauskiene
Institute of Physics, A.Gostauto 12, 2600 Vilnius, Lithuania

SUMMARY

Measurements of wet deposited NH_4^+ and NO_3^-, as well as airborne concentrations of these species and gaseous HNO_3, NH_3 and NO_2 have been made in Preila, Lithuania, a rural site in the south-eastern part of the Baltic Sea. Using these data together with calculations of air mass back trajectories for every 12 h at the 850 mb level allowed us to assess the most important emission sources of pollutants. It is found that nitrogen from Lithuanian sources of pollution can not contribute more than 30% to the total deposition of airborne nitrogen to the Baltic Sea.

In recent years considerable concern has been expressed over the input of airborne nitrogen to the sensitive ecosystems [1-5]. The Baltic Sea is rather vulnerable to the antropogenic pollution because of its special characteristics. The purpose of this work is the assessment of the airborne nitrogen flux to the Baltic Sea, using precipitation chemistry and air concentration data, as well as the contribution of Lithuanian sources of pollution to it. Simultaneous measurements of gaseous, aerosol and rain water species were started in 1980 in Preila [6]. It is a rural site on the Baltic Sea coast and it can be considered as representative for the southern Baltic Sea area. Monthly averages of the precipitation weighted concentrations of nitrate and ammonium show a rather similar annual cycle, with a maximum during spring months. The NO_3^- lowest precipitation weighted concentration value is 0.34 mgN/l in July, and this for NH_4^+ is 0.84 mgN/l in June-August. The maximum values are around 0.97 mgN/l for NO_3^- and 1.34 mgN/l for NH_4^+. Wet deposition fluxes of various nitrogen compounds have been calculated directly from their concentrations in precipitation samples averaged for one month. Fig.1 shows that annual wet deposition fluxes of Tot-N as well as oxidized and reduced nitrogen are variable in time. Estimates for 12 years period show that the annual wet deposition fluxes of total N vary from 600 mgN/m^2 to 1675 mgN/m^2. The average ratio between oxidized and reduced nitrogen in wet deposition flux is estimated being 41 and 59%, respectively.

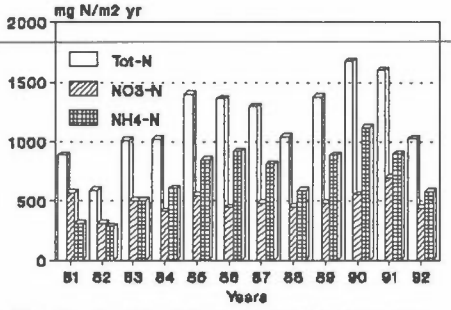

Fig.1. Experimental wet deposition fluxes of nitrogen at Preila, Lithuania, 1981-1992.

Table 1. Average concentration (c) and average annual wet deposition (AAWD) of nitrogen components in Preila for the period 1981-1992

Component	C mg N l^{-1}	AAWD mg N $m^{-2}yr^{-1}$
NO_3^-	0.73	493
NH_4^+	1.02	700
Total-N	1.75	1193

Table 1 presents the average concentration and annual average wet deposition fluxes of nitrogen components in Preila for the period 1981-1992. These data are consistent with those reported by other authors [7-8].

The data presented in Fig. 2 show the evid[illegible] leposition fluxes of nitrogen during four seasons. Generally, wet de[illegible] gen was maximum during the autumn and minimum during the wi[illegible] ition fluxes of two nitrogen components in autumn, particulary in N[illegible] ributed to the high amount of precipitation (the average value for 12[illegible] n).

Dry deposition fluxes of nitrogen compounds were estimated on the basis of averaged concentrations of gaseous and aerosol nitrogen species measured in Preila over 12 years [9]. Using the dry deposition velocities given in the EMEP model [10], we have got annual dry deposition fluxes for nitrogen compounds which are presented in Table 2. As it can be seen, there is evidence now that dry deposition is dominated by the gaseous compounds.

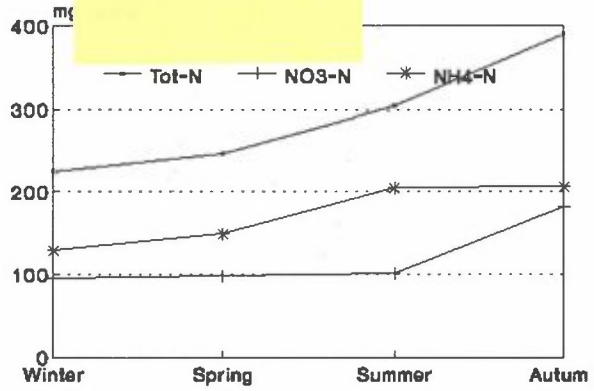

Fig.2. Average seasonal variations of wet fluxes of Nitrogen in Preila (Lithuania) for 1981-1992 (mg N/m2).

Table 2. Average concentration (c), dry deposition velocity (Vd) and average annual dry deposition (AADD) of nitrogen components in Preila for the period 1981-1992.

Component	C $\mu g\ N\ m^{-3}$	Vd cm s^{-1}	AADD mg N $m^{-2}yr^{-1}$
NO_2 gas	2.50	0.1	67
HNO_3 gas	0.11	4.0	118
NH_3 gas	0.75	0.8	160
NO_3^- particle	0.35	0.1	10
NH_4^+ particle	1.36	0.1	36

This estimation of dry deposition of total nitrogen, on the whole, coincide with those reported by Finish Meteorological Institute [11]. However, the discrepancies in the estimates of deposition of gaseous NO_2, HNO_3 and aerosol NO_3^- are obviously due to the dry deposition velocities parametrization of these components.

Table 3. Annual average wet (AAW) and dry (AAD) of nitrogen components in Preila for the period 1981-1992.

	Oxidized N components	Reduced N components	Total
AAWD mgN $m^{-2}yr^{-1}$	493 (32%)	700 (43%)	1193 (75%)
AADD mg N $m^{-2}yr^{-1}$	195 (12%)	196 (13%)	391 (25%)
Total	688 (44%)	896 (56%)	1584 (100%

Total nitrogen deposition, calculated as the sum of average values for wet and dry depositions is presented in Table 3. As it can be seen, wet deposition flux contributes 75% to the total nitrogen deposition to the Baltic Sea.

Fig. 3 shows the relative contribution of each deposition processes of all nitrogen forms.

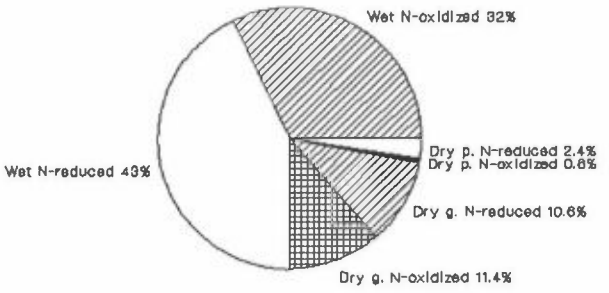

Fig.3 Contributions of nitrogen components to the annual total deposition of Tot-N in Preila, 1981-1992

The analysis of the obtained data has shown that concentrations of the chemical pollutants in the atmosphere are variable from day to day and often are quite high [12]. This variation of pollutants concentrations may be a consequence both of varying emissions and meteorological factors. Therefore, the alteration of daily concentrations of chemical compounds was discussed in conjunction with meteorological conditions. Every day samples were classified by the area of origin of air mass. The back trajectories of air mass were classified according to the way travelled by them into four sectors as shown in Fig.4. Sector 0 is either a small cyclone standing over Lithuania or a center of anticyclone which allows local emission sources to reveal themselves. Based on rather numerous statistical data both annual and seasonal variations of air masses have been calculated in the sectors mentioned above. The greatest annual recurrence (39.7%) has been observed in the case of air masses coming via sector 1. Sector 2 takes the second place (37.8%) among the recurring sectors. The lowest number (2.7%) of recurrence is in Sector 0. It should be mentioned that the highest recurrence (9.3%) of air masses via Sector 3 has been observed in winter months.

Surface winds also influence the expansion of pollutants and their transport in a certain direction from emission sources. The highest concentrations of sulphur and those of nitrogen have been measured in the air masses which have come to Lithuania over Europe and the Ukraine, i.e. via Sector 2 and Sector 3, and it is obviously indicative of considerable sources of pollution being located in the above areas. The lowest concentrations of SO_4^{2-} and NO_3^- have been observed in the air masses coming via the Baltic Sea, i.e. Sector 1.

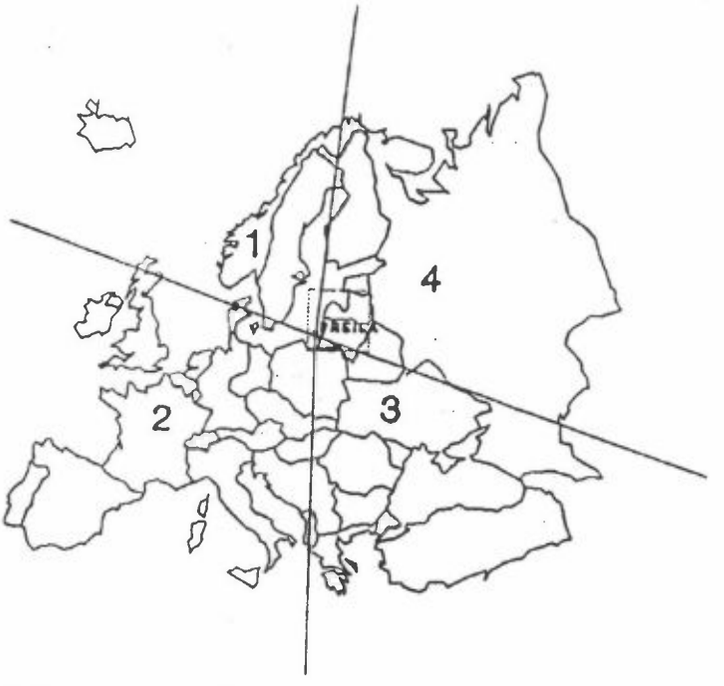

Fig. 4. Sectors definition for classification of back trajectories for background station Preila.

We have calculated the percentage loading of pollutants from each sector using the component mean concentrations in corresponding sector and the annual percentage recurrence of each sector.

Table 4. Percentage loading* from each sector

	Sector				
Ion	1	2	3	4	0
SO_4^{2-}	27.6	45.9	14.2	9.7	2.6
NO_3^-	36.2	43.0	10.2	8.8	1.9
Cl^-	58.2	27.9	4.2	7.5	1.9
NH_4^+	23.6	44.0	18.2	11.9	2.2

* - loading defined as:

$$\text{loading} = \frac{\text{sector mean concentration} \cdot \text{n of days}}{\text{total mean concentration} \cdot \text{total n of days}} * 100\%$$

As can be seen from Table 4, the main load of oxidized nitrogen (about 53%) and reduced nitrogen (about 62%) is from industrial areas in West and South Europe.

CONCLUSIONS

12 years of continuous measurements of precipitation and air chemistry as well as meteorology have led us to such conclusions: 1) Significant variability of meteorological factors in Lithuania controls the concentration of nitrogen compounds in the atmosphere and their deposition fluxes; 2) Wet deposition of total N exceed considerably the dry deposition; 3) Taking into account long-range transport of pollutants and regional background concentrations of pollutants we find out that transport of pollutants to Lithuania is predominantly from West and North-West. Local sources contribute relatively small amount of airborne nitrogen to total Nitrogen load to the Baltic Sea.

REFERENCES

[1] Grennfelt, P. and Hultberg, H. „Effects of nitrogen deposition on the acidification of terrestrial and aquatic ecosystems". Wat. Air Soil Pollut., 1986, 30, 945-963.

[2] Nixon, S. „Marine Eutrophication. A Growing International Problem". Ambio, 1990, vol 19, No 3, 101.

[3] Rosenberg, R. et al. „Marine eutrophication case studies in Sweden". Ambio, 1990, vol 19, No 3, 102-108.

[4] Nehring, D., Wilde, A. „Untersuchungen uber den atmospherichen Nahrstoffliihtrag in der Ostsee". Acta Hydrochim. Hydrobid., 1982, vol 10, No 1, 89-100.

[5] Rodhe, H., Soderlund, R. and Eksted J. „Deposition of airborne pollutants on the Baltic". Ambio, 1980, vol 9, No 3-4, 168-173.

[6] Protection of Atmosphere against pollution No 6. „Atmosphere background pollution determination in the southern Prebaltic". 1982, Vilnius, Institute of Physics.

[7] HELCOM, 1991. „Airborne polluted load to the Baltic Sea 1986-1990." Balt. Sea Environ. Proc. No 39, 31-35.

[8] Heidam, N.Z. „Nitrogen depositions to the Baltic sea: experimental and model estimates". Atmospheric Environment, 1993, vol 27A, No 6, 815-822.

[9] Giedraitis, B. et al. „The SO2 and NO2 measurements in Lithuania using passive sorbent method", Annual Report, 1992, 56, Institute of Physics, Vilnius.

[10] EMEP/MSC-W, 1991, Iversen, T. et al. „Calculated budgets for airborne acidifying components in Europe, 1985, 1987, 1988, 1989 and 1990." Report 1/91, 23.

[11] Lindors, V., Joffre, S.M., and Damski, J. „Determination of the wet and dry deposition of sulphur and nitrogen compounds over the Baltic Sea using actual meteorological data", Finnish Meteorological Institute Contributions, 1991, No 4, 53-73.

[12] Sopauskiene, D. and Budvytyte, D. „Chemical charac-teristics of atmospheric aerosol in rural site of Lithuania", Atmospheric Environment, 1994, in press.

Theoretical Studies

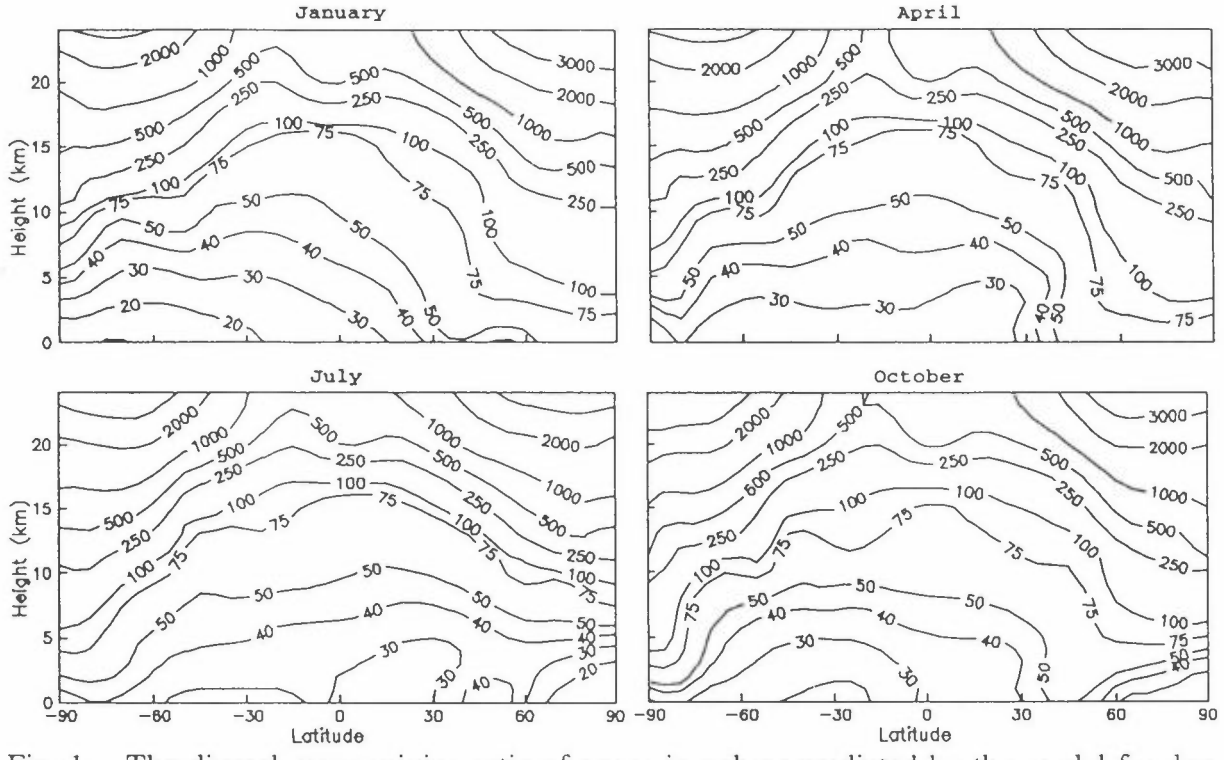

Fig. 1. The diurnal mean mixing ratio of ozone in ppb as predicted by the model for day 15 of the month.

Ozone loss in the Northern Hemisphere, spring 1993: Trajectory model simulations

Inga Fløisand and Frode Stordal
Norwegian Institute for Air Research
Lillestrøm Norway

Introduction

A trajectory model with coupled modules representing gas phase photochemistry, microphysics (particle growth) and heterogeneous chemical reactions has been used for simulations of the chemistry of the stratosphere. The model has been developed through a collaboration between NILU, the University of Oslo and the Danish Meteorological Institute. The two-dimensional trajectories for the isentropic level corresponding to a potential temperature of 475 K and potential vorticity fields have been obtained from the European Centre for Medium-Range Weather Forecasts.

The model

The trajectory model has been developed to study stratospheric ozone. The model takes a Lagrangian coupled photochemical-microphysical approach (like Jones et. al,1989). The gasphase chemistry is the same as that in the Oslo 2-D model (Stordal et al., 1985; Isaksen et al., 1990). It calculates the concentration of 63 chemical species with more than 150 rate constants determining the photochemistry and the reactions between compounds. The model is initialized with chemistry data from the Oslo 2-D model. The microphysics model (Larsen, 1991) describes the formation of PSC type I and II particles, but in the present calculations only PSCs type I were formed. The formation of PSCs depends upon H_2O and HNO_3 gas phase mixing ratios and temperature. The model also includes Pinatubo aerosols with a sulphur aerosol area of 20×10^{-8} cm^2/cm^3. Heterogeneous reactions occur on both PSCs and aerosols. Reactions and sticking coefficients are given in Table 1.

Table 1: Heterogeneous reactions, sticking coefficients, and reaction rate dependence on temperature on sulphur aerosols

Heterogeneous reaction	Sticking coef. on sulphur particles (γ)	Temperature dependent on sulphate aerosols	Sticking coef. on PSC particles (γ)
$N_2O_5 + HCl = ClNO_2 + HNO_3$	0.006	No	0.003
$N_2O_5 + H_2O = 2HNO_3$	0.06	No	0.0006
$ClONO_2 + HCl = Cl_2 + HNO_3$	0.004	<205 K	0.3
$ClONO_2 + H_2O = HOCl + HNO_3$	0.004	<205 K	0.006
$HOCl + HCl \doteq Cl_2 + H_2O$			0.3

Experiments and results

For February and March 1993, calculations have been made along 10 day trajectories ending at different sites in northern Europe. Ozone loss per 10 days has been calculated and is used as a qualitative measure for the different experiments. Different case studies have been made.

In the first experiment calculations along trajectories ending at mid-latitude stations (approximatly 50°) Lindenberg, Hohenpeissenberg and Aberystwyth were performed. Ozone depletion at the three stations are of the same magnitude and vary in a similar pattern. There are two days where all three curves dip simultaniously, namely Julian day 52 and 66. On these days the polar vortex covers all three sites. The opposite is the case for day 60 where all three stations are outside the vortex and the change in ozone is considerably smaller. This example suggests that ozone depletion varies with the position and extent of the polar vortex.

Figure 1: Ozone change at 475 K over mid-latitude stations Lindenberg, Hohenpeissenberg and Aberystwyth.

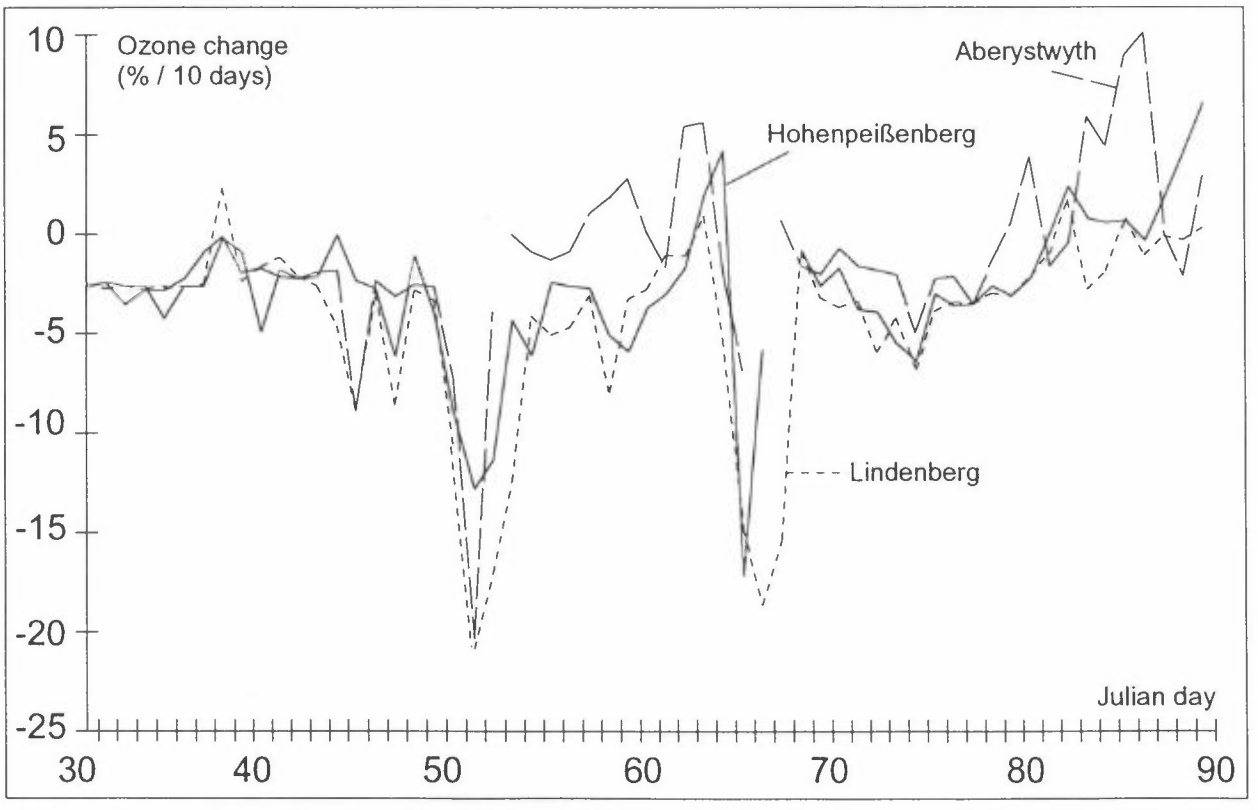

The model has also been run with different levels of chlorine. This example shows trajectories ending at Bear Island. Trajectories have been run under the same conditions for different chlorine levels: One with the current level of chlorine and one with a pre-industrial chlorine level which is set to 20 % of the current level. The results here show a substantial difference in ozone loss for the two cases. The mean relative ozone change over the two months is -11 % for the case with current chlorine level and -1,5 % for the case with pre-industrial chlorine level.

Figure 2: Ozone change at 475 K over Bear Island with different chlorine levels.

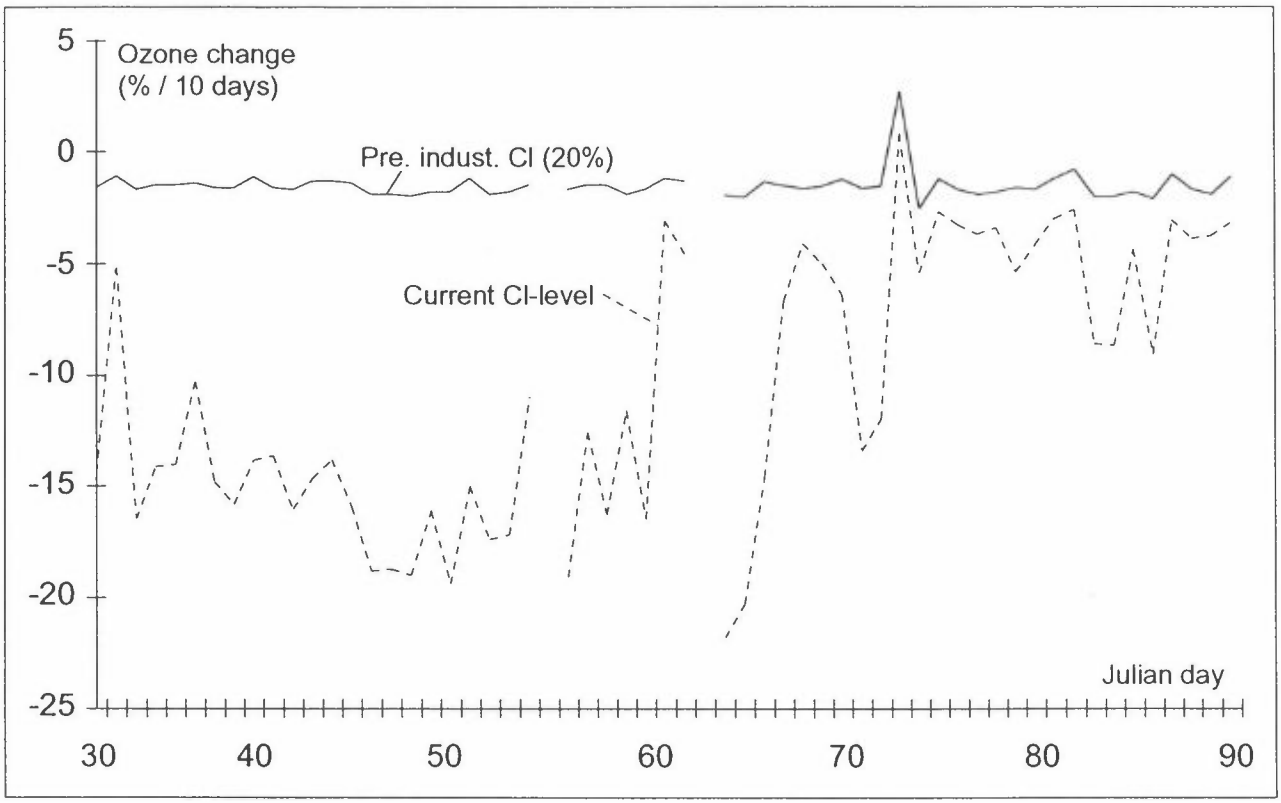

References

Isaksen, I.S.A., B. Rognerud, F. Stordal, M.T. Coffey, W.G. Mankin,(1990), Studies of Arctic Stratospheric Ozone in a 2-D Model Including Some Effects of Zonal Asymmetries, *Geophys.Res. Lett., 17,* 557-560.

Jones, R.L., J. Austin, D.S. McKenna, J.G. Anderson, D.W. Fahey, C.B Farmer, L.E. Heidt, K.K. Kelly, D.M. Murphy, M.H. Proffitt, A.F. Tuck and J.F. Vedder, (1989) Lagrangian Photochemical Modeling Studies of the 1987 Antarctic Spring Vortex, 1. Comparison With AAOE Observations, *J. Geophys. Res., 94,* 11529-11558.

Larsen, N., (1991) Polar Stratospheric Clouds: A Microphysical Simulation Model., Copenhagen, Danish Meteorological Institute, (DMI Sc. report 91-2)

Stordal, F., I.S.A. Isaksen, K. Horntvedt, (1985), A Diabatic Circulation Two-Dimensional Model With Photochemistry: Simulations of Ozone and Long-Lived Tracers With Surface Sources, *J. Geophys. Res., 90,* 5757-5776.

HILATAR and FINOX, 3-dimensional grid models for regional air pollutant dispersion studies

Marke Hongisto. Finnish Meteorological Institute (FMI), Air Quality Department.
Sahaajankatu 22 E, 00810 Helsinki. tel. 358-0-75811, fax 358-0-7581396

Abstract

The variation of air pollutant concentrations, their exposure times and deposition are simulated at the FMI using Eulerian type air quality models. The models are built mainly for acid deposition studies, covering nitrogen and sulphur compounds. Results of calculations made by a grid model for oxidized nitrogen compounds over Finland (FINOX) as well as experience with shorter time sulphur pollution studies with HILATAR model are discussed.

THE STRUCTURE OF THE MODEL

The transport and deposition of air pollutants emitted into the lower troposphere is studied at the Finnish Meteorological Institute using regional air quality models of Eulerian type. The dispersion is described by a set of differential equations, where the advection of the compounds by wind, their diffusion by atmospheric turbulence, chemical conversion to other species and deposition to the ground, are solved numerically in a grid of 10-56 km horizontal distance with 7-10 vertical layers below 3 km. The method of fractional steps is used, the transport equation is decomposed into one-dimensional subproblems, which are solved successively, each subpart by a suitable algorithm.

In the first applications, the dispersion of oxidized nitrogen compounds has been studied with NO, NO_2, HNO_3 and nitrate as model variables. In 1993 the chemical submodel has been extended to include also reduced nitrogen and sulphur compounds. A one dimensional cloud oxidation module of the conversion of sulphur to sulphate in water droplets with pH dependent reaction rates has also been constructed. The cloudiness is estimated from the specific humidity profile, although the liquid water content is a slightly rough approximation depending on the assumed cloud type, and convective rain between time steps can depress the average humidity of the period.

Because the iteration of the pH of the droplets and the cloud module as whole are computationally heavy, the concentrations of the alcalic particles or oxidizing species as well as their consumption rates in the liquid phase are inaccurate, this module has at least so far not been connected to the transport part. However the results of it are used in estimating a weighting factor for the oxidation speed of SO_2 in the cloudy and non-cloudy parts along the transport path. If the chemical transformation of NO_x, SO_2 and NH_3 compounds in an isolated box filled partly with clouds is followed with 50 $\mu g\ m^{-3}$ O_3 and 1 ppb H_2O_2 initial concentrations, almost all SO_2 in the cloudy part is oxidized in less than 12 hours in wintertime (T=263 ^oK), in less than 2 days in summertime (T=283 ^oK), while oxidation is very slow in clear air. The rates depend on the emission strengths of ammonium and acidic compounds. The residence time of SO_2 calculated with the EMEP model with $SO_2(t) = SO_2(t_o)\ e^{-kt}$, $k = 3.10^{-6} + 2.10^{-6}\sin\{2\pi(day-80)/365\}\ s^{-1}$, if chemistry is assumed to be the only sink considered, is about 1 day, 15 h (min. $T_{1/2}$) during mid-summer, about 8 days in December (max. half life), and 10 % of SO_2 stays in air 5,33 (summer) - 26,6 days (winter). In November (time of the case simulations described later), $T_{10\%}$ = 15 d 17 h (1.11) and $T_{10\%}$= 23 d, 22 h (30.11), thus the conversion rate in the droplets of the cloud module, with 12 hour depletion time, $k = 5.33\ 10^{-5}\ s^{-1}$, is about 38 times faster than the average EMEP oxidation rate in November. The EMEP rate is a combination of the slow OH- and other clear air reactions and the wet phase transformation, still during the simulations of real sources, at least 10 times higher oxidation rates in the cloudy parts of the transport, might be reasonable.

MODEL INPUT DATA AND PARAMETERIZATION

The advected long-range transported (LRT) compounds along all grid borders are added to the air flowing through the simulation area boundaries. LRT estimate, the daily average concentration of each compound, evenly distributed below the mixing height, has been calculated at the EMEP MSC-W centre using 150*150 km resolution.

The time variation of the emissions is calculated, whenever possible, using seasonal, monthly, weekly or diurnal time indices or with temperature dependency. The effective source height is estimated with plume rise formulas for each hour. Instant dilution inside the grid box (width σ_z at dx/2) is assumed. Usually the spatial resolution of the emission inventories available is not sufficient for calculations with dx=10 km grid over wide geographical areas. For national studies stack parameters of the biggest sources are known, still the inventory has not been completed. Co-operation with some Russian and Estonian institutes have been started in order to collect specific emission data from the sources, which might have an effect on the air quality of Finland; for other foreign areas EMEP MSC-W emissions with the CORINAIR (the CORINe - COoRdination d'information Environnementale- AIR emission inventory) are planned to be used.

The meteorological data consist of synoptic measurements and soundings or of output of the Nordic-Dutch weather prediction model HIRLAM (High Resolution Limited Area Model). In the former case the 3-dimensional vertical variation of the wind speed, temperature etc. is estimated using stability dependent profile functions in the surface layer. At the higher model layers, surface values are extrapolated or sounding values are used. The HIRLAM data has 0.5^{o} horizontal and 6 h time resolution, synoptic data 3-12 h resolution, and both are interpolated into 1 hour values.

The dry deposition on different surfaces is calculated using actual meteorology and resistance analogy. The surface resistance over forests depends on the exposure time of sulphur contaminants, thus the saturation of gaseous pollutant intake during long time pollution stress is simulated. For national studies the surface type can be determined quite accurately from satellite data. The scavenging by rain depends of the rain type and height. Comparison with the EMEP model parameterization e.g. for HNO_3 gives 20-30 % less deposition with 1 mm/h precipitation during the first hours, about the same values with 0.5 mm/h rain and more efficient scavenging by low rain.

The output of the models consists of concentration and deposition distributions, time series at selected locations and exposure times for selected concentration levels. The FINOX model has been applied with 30 km grid over several year periods, HILATAR models with about 56 km and 11 km horizontal grid distances with shorter simulation periods.

APPLICATIONS

FINOX model results for oxidized nitrogen compounds over South and Central Finland are presented in HONGISTO (1992). The interannual variation was high, depending on the meteorological conditions, although also the model code has been improved continuously during the work. The residence times of the compounds in air were shorter than the previous estimates calculated by the EMEP MSC-W trajectory model (year 1988: see IVERSEN et al.,1990), in any case the modelled wet deposition was underestimated when compared with the measurements. In 1988 the domestically originated deposition over land areas was, according to the EMEP calculations, about 67 % of the corresponding FINOX model value. The differences are due to the model structure, (slower advection near the surface, where traffic emissions are emitted), resolution

(higher concentration levels close to the sources in a fine grid model), as well as meteorological and other parameterization.

The first version of the 0.5 degree resolution model HILATAR, with HIRLAM data, linear sulphur chemistry and approximate surface types has been used for Northern Lapland, where the wet phase conversion of sulphur compounds in clouds is not important. The dispersion of sulphur emissions of a few extremely large sources located in the Kola peninsula has been studied. The emissions were mixed downwind to the closest grid element. The vertical distribution and time variation of the emissions were simply assumed because detailed information on the sources was not available. The model was able to predict almost all of the measured concentration variation in the grid boxes near the sources (Jäniskoski and Kirakkajärvi) although the complicated terrain should affect the circulation of the pollutants. However, at measurement points several grid distances from the source, the model underestimates the measurements. The reason may partly be the scarce grid, the numerical diffusion of the advection algorithm, partly the meteorological parameterization and northern conditions.

SIMULATION OF THE ESTONIAN OIL SHALE POWER PLANTS

The Estonian oil shale burning power plants have often named to be the major pollutant sources of south-eastern Finland; they are located close to the coast of the Gulf of Finland near Narva, at about 130 km distance from the Virolahti EMEP background station on the northern coast of the gulf. The annual emissions of SO_2 of the two power plants have decreased from 165 000 in 1991 (Kivivasara, 1994) to 141 700 t in 1992 and 97 200 t in 1993 according to the preliminary results of a measurement based inventory (Aunela et al., 1994), earlier estimates being over 250 000 t SO_2 (Plancenter LTD,1991). The dust emissions were 225 000 t, 186 300 t and 135 500 t in respective years, of which SO_4 particles 7250 t (S) in 1991 and 4410 t (S) in 1993. The main reason for the emission abatement has been the decline of the production of energy.

November 1993 was on average a cold month, the wind direction distribution presented in Fig. 1 deviated from the ordinary situation by frequent south-eastern flow of air. Thus the big pollution sources located in Russia and Estonia could affect the air quality at the Finnish side of the border. At the EMEP background stations elevated sulphur dioxide concentrations were measured, and the aim of the study was to evaluate, how much of the pollution detected during this month could be originated from the two Estonian power stations described above. For the purpose the 11 km resolution, 10 layers HILATAR model with sulphur chemistry has been used. Because a detailed emission inventory of the total simulation region was not ready, only the Estonian and the Baltic power plant sulphur emissions were included.

Parameters, which describe average dispersion conditions in November 1993, are presented in Table 1. Meteorological data of the HIRLAM model has been used; synoptic data outside the borders was not available at the moment, comparison with measured surface temperature and precipitation input data will be made later. On the average, the lowest atmosphere was neutrally or slightly unstable stratified over the warm sea, being more stable over land. This is reflected in all the dispersion parameters calculated. Precipitation was generally twice as high over the Gulf of Finland and Lake Ladoga as over land areas, over the rest Baltic sea rain was heavier. The meteorological input has been interpolated smoothly from the original 0.5^{o} resolution data without bearing in mind the exact sea-land distribution, thus the zones near the coastal areas do not present exactly the abrupt change of the meteorological conditions at the shore.

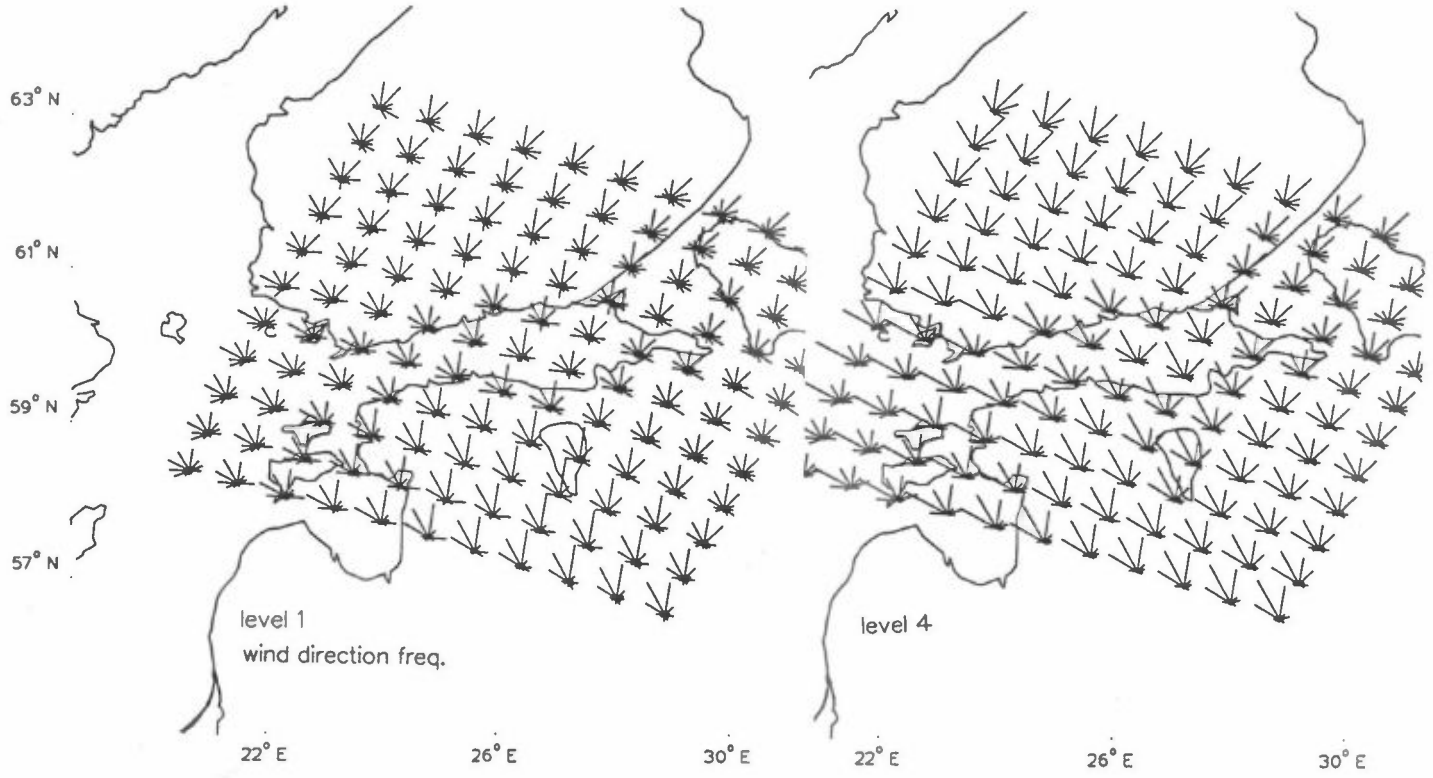

Fig. 1. Wind direction frequency distribution, November 1993. Non-meteorological presentation: number of wind directions counted downwind to the wind rose centre. Average heights: Level 1: 30 m, Level 4: 920 m.

Table 1. Meteorological parameters describing November 1993 average dispersion conditions.

	Over Sea	Over land (over the simulation area)				Lake
		Finland	Karelian Isthmus	Estonia	Russia	Ladoga
Friction velocity,cm s^{-1}	40-50	16..22	20..24	15..30	12..20	30..40
Mixing height,m	360	300	270	270	290	300
L^{-1}, $1/m*10^3$	0..-4	10..24	0..7	1..20	10..30	0..-5
Kz,m^2/s	30-38	4-7	9-18	5-15	3-7	14-30
wind velocity,m s^{-1}	5.5-6.3	3.3-4.	3.3-4.3	3.7-4.2	2.5-3.5	4.2-5.4
vd of SO_2, cm s^{-1}	.2-.4	.06-.1	.09-.11	.1-.14	.08-.11	.1-.17

L = the Monin-Obukhov length, vd = dry deposition velocity. Sea area = Gulf of Finland, Kz and wind velocity calculated at the lowest model layer (about 30 m). The coastal zones or extreme values are not included, the averages represent typical values of the regions.

The monthly average concentration distribution at 4 model layers is presented in the Fig. 2. One can conclude, that most of the polluted air is transported on higher layers over Finland. The monthly average concentration over Virolahti was 0.5 - 1 μgm^{-3} in model layers 3-5 (330-1000 m) being less than 0.5 μgm^{-3} in the lowest layers; even the mixing over the sea was not efficient enough to transport the power plant emissions down so that their maximum effect could be detected at the coastal measurement stations. However some part of the elevated surface air sulphur pollution detected at Helsinki, Virolahti and Utö on 19-26th during November is emitted by the Estonian plants. The modelled SO_2 concentration at Virolahti at 6 lowest model layers is presented in Fig. 3. According to the results the highest concentrations detected (40 - 90 μgm^{-3} hourly

average peaks during 28-23th November) were not originated from the Estonian power plant, even though the wind blew for some hours directly to Virolahti. Most of the pollution might be transported from Russia, St. Petersburg and the industrial region nearby.

Sulphur particles were devided into three size classes, the smallest being borne from SO_2. Dry deposition of the emitted particles was calculated using additional settling velocity sink terms in the chemistry subprogram instead of using vertical diffusion algorithm; if they are treated as other compounds, their contribution is insignificant because of high stack heights and low emissions. Dry deposition velocity was more efficient above sea due to meteorological conditions. The deposition of the period consists mainly on wet deposition. However, because scavenging efficiency of SO_2 close to the sources should be modified by a factor, which depends on the residence time, sulphur dioxide should be transported slightly longer distance than presented in Fig. 4.

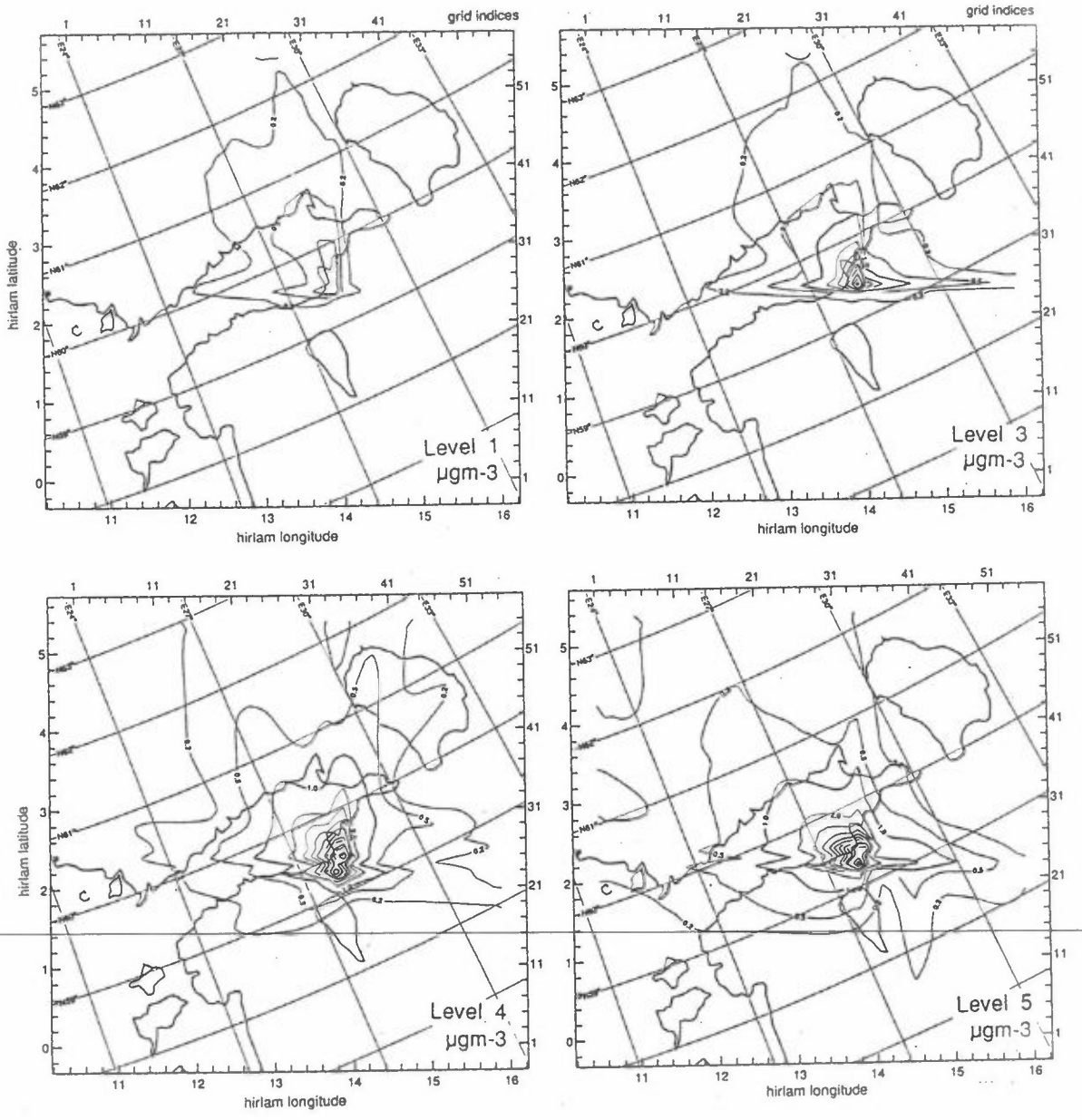

Fig. 2. Monthly average concentration distributions at model layers with average heights of 30, 320, 620 and 920 m.

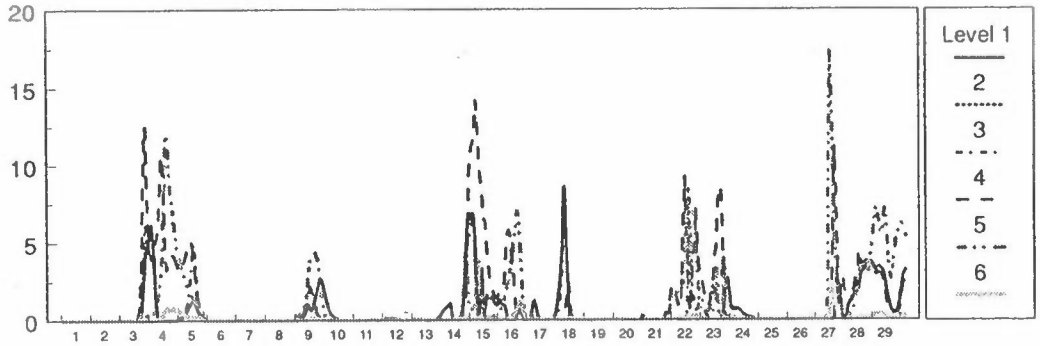

Fig. 3. Simulated SO_2 concentrations at the Virolahti EMEP station at different model layers, μg m^{-3}. Contribution from the Estonian and Baltic Power Plants. November 1993.

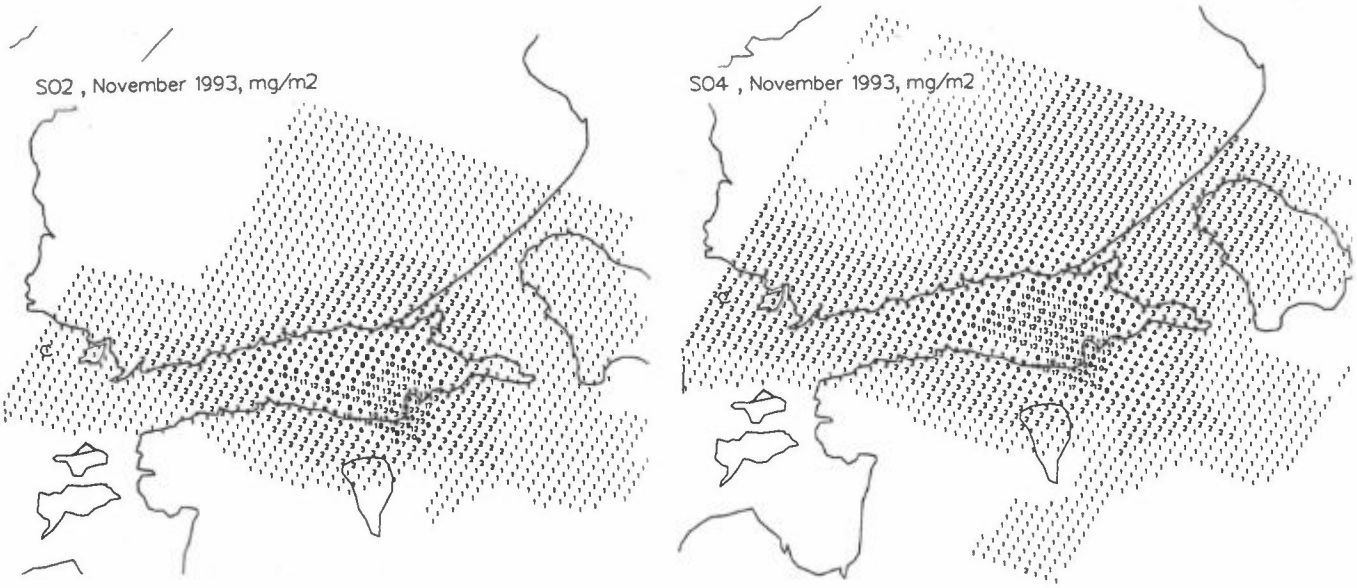

Fig 4. Total deposition, mg m^{-2} (S), November 1993. Contribution from the Estonian and Baltic Power Plants

CONCLUSION

Measurements at the background stations show that the concentrations of air pollutants appear episodically, thus if the goal is to estimate the damage to natural ecosystems, the exposure times of air pollutants should be simulated with at least one hour resolution. Therefore, grid models are an essential tool to explain the 3-dimensional transport of pollutants from industrial areas .

Acknowledgements: I would like to thank for financial support of the Ministry of the Environment and NMR and the colleagues of the FMI Air Quality Department, specially Ilkka Vallinoja for Uniras program for Fig. 2.

REFERENCES

Aunela L. et al., 1993 and 1994. Emissions of Estonian and Baltic oil-shale power plants. VTT/LVI tech. lab., will be published in 1994., Status report of the project, VTT, September 1993, 38 p. (in Finnish)

Hongisto M., 1992. A simulation model for the transport, transformation and deposition of oxidized nitrogen compounds in Finland. Part A) 1985 and 1988 simulation results. FMI Contributions No. 9, 1992, 114 p., Part B) Technical description of the model. FMI Publications on Air Quality 14/1993, 51 p.

Iversen T., Halvorsen N.,E., Saltbones J. and Sandnes H., (1990). Calculated budgets for airborne sulphur and nitrogen in Europe. EMEP/MSC-W Report 2/1990, 61 p.+A.

Kivivasara J. Summary of air pollutant emissions in Estonia. FMI, Air Quality Department, 1994, 3 p. (in Finnish)

Plancenter LTD, 1991. Environmental priority action programme for Leningrad, Leningrad region, Karelia and Estonia. Synthesis report. Ministry of the Environment of Finland, 193 p.

BROMINE CHEMISTRY IN THE STRATOSPHERE AND ITS IMPACT ON OZONE: MODEL CALCULATIONS.

By Ivar S.A. Isaksen and Bjørg Rognerud
Institute of Geophysics
University of Oslo.

Abstract

Two-dimensional model calculations of the impact of bromine reactions on the stratospheric ozone is calculated. The model includes gas phase as well as heterogeneous reactions on polar stratospheric clouds (PSCs) and on background aerosol particles. The calculations of the impact of the different chemical cycles are time dependent and are performed for a 5 year period. They represent stratospheric conditions in the time interval 1990 to 1995. Results are presented for middle and high northern latitudes during winter (February) and spring (May). Heterogeneous reactions, involving HCl, $ClONO_2$, HOCl, N_2O_5, and H_2O are included in the model calculations, and they are found to significantly enhance the concentrations of ClO, and partly BrO in the lower stratosphere, and thereby the role of chlorine and bromine as ozone depleting substances. BrO is found to be the dominant inorganic bromine compound at all heights. At most heights $BrONO_2$ is the second most abundant compound. In contrast to the chlorine family, where HCl is the dominant compound, HBr is the minor bromine compound at all heights. The bromine reactions, together with chlorine reactions, are found to contribute significantly to the chemical loss of ozone in the lower stratosphere at 60 degree N and at 50 N degree. Indeed, at 60 degree N during winter when polar stratospheric clouds are present, the calculated loss of ozone at stratospheric heights below about approximately 25 km is completely dominated by the chlorine and bromine reactions. As we proceed towards summer the significance of the chlorine chemistry rapidly becomes less significant. With current levels of chlorine and bromine in the stratosphere, both the reaction ClO + BrO and the reaction HO_2 + BrO contribute significantly to ozone depletion at mid - and high - latitudes (0.5 to 1.0 % of total ozone loss each at present). If this is compared to total man induced ozone loss it is concluded that the bromine chemistry accounts for approximately 20 % of the ozone loss on a global scale, with a somewhat larger contribution at mid latitudes. However, the large uncertainty in the rate constant for the reaction HO_2 + BrO introduces uncertainties in the calculated effect of bromine reactions on ozone. Time dependant calculations of the ODP for CH_3Br reveal that the value is significant larger than one if we operate on a time scale up to approximately 30 years.

1. Introduction

The precence of bromine containing species in the stratosphere is believed to be responsible for a significant fraction of the estimated loss by chemical reactions in the lower stratosphere (WMO/UNEP, 1991). The most abundant source for free bromine in the stratosphere is methyl bromide (CH_3Br). Mixing ratios are in the range of 10 to 15 ppt in the troposphere, where it is controlled by the reaction with OH. The second larges source are the halons: H-1211 and H-1301. The concentrations of the two halons are in the range 2-4 pptv (1990), and most important, their concentrations have been increasing substantially (15 to 20 %) towards 1990 due to man made emissions. This increase is expected to slow down in accordance with Montreal agreement on ozone depleting substances. Due to the dominant role CH_3Br plays as source gas for stratospheric bromine, its sources and atmospheric distribution and change is important for the ozone depletion problem.

Measurements of the key bromine compound (BrO) in the ozone destructing cycles have been measured from high flying airplane, and indicate that this compound is a dominant inorganic compound in the lower stratosphere (Toohey et al, 1990). However, there are still large uncertainties connected to the partitioning between the different bromine compounds, and also to the efficiency of the catalytic bromine cycles destructing ozone. The two issues are therefore the focus of this model study.

2. Catalytical loss reactions

The main catalytical bromine reaction cycles responsible for the ozone destruction is believed to be:

$$
\begin{array}{lccccccccc}
 & BrO & + & ClO & \rightarrow & Br & + & Cl & + & O_2 \\
 & Cl & + & O_3 & \rightarrow & ClO & + & O_2 & & \\
 & Br & + & O_3 & \rightarrow & BrO & + & O_2 & & \\
\hline
\text{Net} & O_3 & + & O_3 & \rightarrow & O_2 & + & O_2 & + & O_2
\end{array}
$$

or

$$
\begin{array}{lccccccccc}
 & BrO & + & HO_2 & \rightarrow & HOBr & + & O_2 & & \\
 & HOBr & + & h\nu & \rightarrow & Br & + & OH & & \\
 & Br & + & O_3 & \rightarrow & BrO & + & O_2 & & \\
 & OH & + & O_3 & \rightarrow & HO_2 & + & O_2 & & \\
\hline
\text{Net} & O_3 & + & O_3 & \rightarrow & O_2 & + & O_2 & + & O_2
\end{array}
$$

These cycles are particularely efficient in the lower stratosphere, where they mainly compete with the chlorine destructing cycle:

	ClO	+	ClO	+	M	→	Cl_2O_2			
	Cl_2O_2	+	hν			→	Cl	+	ClO_2	
	ClO_2					→	Cl	+	O_2	
	2(Cl	+	O_3)			→	2(ClO	+	O_2)	
Net	O_3	+	O_3			→	O_2	+	O_2	+ O_2

Model calculations for mid northern latitudes of the distribution of bromine compounds, and of the impact of the different chemical cycles on stratospheric ozone is presented and discussed. The calculations should give an indication the potential role of bromine in the depletion of stratospheric ozone.

3. Model assumptions

The 2-D chemistry/transport model at the Institute of Geophysics, University of Oslo (Stordal et al, 1985, Rognerud et al, 1991) is used for time dependent model studies of the chemical distribution and the man made impact on the ozone layer. The calculations are representative for the chemically perturbed atmosphere between 1990 and 1995 (5 years time integration). The focus is on the impact on ozone from bromine compounds (the reactions: BrO+ClO and BrO+HO_2) at mid- and high- northern latitudes in the lower stratosphere. Calculations are performed with the following heterogeneous chemistry included:

$ClONO_2$	+	HCl	→	Cl_2	+	HNO_3
$ClONO_2$	+	H_2O	→	HOCl	+	HNO_3
N_2O_5	+	HCl	→	$ClNO_2$	+	HNO_3
N_2O_5	+	H_2O	→	HNO_3	+	HNO_3
HOCl	+	HCl	→	Cl_2	+	H_2O

These reactions are assumed to occur on PSCs and on background aerosol particles.

A scenario, based on recent estimates of the development of the emissios of CFCs and halons after 1990 is included in calculations.

4. Calculated distribution of bromine and chlorine compounds.

We are present the calculated distribution of the main inorganic bromine compounds at mid - latitudes (50 deg N lat) during winter and spring in the atmosphere in Figure 1. BrO is the dominant inorganic compound in both situations at all heights in the stratosphere, exceeding 10 ppt in the middle stratosphere. $BrONO_2$ is the second most abundant compound in the lower stratosphere. Other bromine compounds are found to be precent only in small quanteties in the lower stratosphere. BrO is also found to be the dominant compound at 60 deg N latitude.

In order to illustrate the effect heterogeneous chemistry has on the two key compounds ClO and BrO, the mixing ratios of the two compounds are given for 21 km for February and May at 50 and 60 deg N in Table 1. ClO is significantly enhanced both at mid latitudes and at high latitudes

which are directly affected by polar stratospheric clouds. BrO is also enhanced in most cases, although less significant than ClO (mixing ratios increase with approximately 50 %).

5. Ozone loss reactions.

Chemical loss of ozone in the stratosphere by the different cycles is given in Figures 2 for 1993 levels of chlorine and bromine. Loss by chlorine and bromine reactions is given by the indvidual reactions. The loss is given as the fraction of the total loss at each height. Total ozone loss (in molecule/(cm^3*s)) at each height is also given in the figures. Bromine contributes significantly to the ozone loss in the lower stratospere (in the height region around 20 km) particularely during winter. Both reaction BrO + ClO and the HOBr loss reaction contribute to this loss. The main source of HOBr is the reaction BrO + HO_2.

6. The effect of bromine reactions on total ozone.

The effect of the bromine reactions on ozone column densities is obtained by running the model for a 5 years period (from 1990 to 1995) sucessively cutting off from 1990 (a): The reaction BrO + ClO and (b): HOBr loss reactions (which is equal to assuming that the reaction BrO + HO_2 proceeds slowly). The results are shown in Figure 3 for (a) and in Figure 4 for (b). Both reactions lead to an approximate 1 % or less reduction at high latitude, and a reduction of 0.4 to 0.6 at low latitudes. The rate constants which has been used in the calculation are based on the JPL (1992) compilation.

7. Conclusions.

Although the contribution to ozone loss from the bromine reactions are less than the contribution from chlorine reactions, their contributionn to total ozone loss is significant and of the order of 20 %. However, in the lower stratosphere at mid latitudes during winter the bromine reactions are responcible for a larger fraction of the loss.

The uncertainties connected to rate constants in the bromine cycles (particularely releated to the reaction HO_2 + BrO), and in the pathway of some of the reactions add some uncertainties to the modelled results of the bromine chemistry.

It is clear that introduction of heterogeneous chemistry in stratospheric model calculations have increased the significance of the bromine reactions (as well as chlorine reactions) in the lower stratosphere as ozone loss reactions. One interesting feature that is apparent from the calculations is that while chlorine induced ozone loss in the lower stratosphere is more or less restricted to high latitudes, bromine induced ozone loss is clearly significant at mid latitude also.

8. Referances

Rognerud B., F. Stordal, I. S. A. Isaksen, Heterogeneous eeduction in the Arctic stratosphere. A model study of long term changes. Air Pollution Research Report 34, 235-238, 1991

Stordal F., I. S. A. Isaksen, K. Horntveth, A diabatic circulation two-dimentional model with photo-chemistry: Simulations of ozone and long-lived tracers with surface sources, J. Geophys. Res., 90, 5757 - 5776, 1985.

Toohey D. W., J. G. Anderson, W. H. Brume, K. R. Chan, In situ measurements of BrO in the Arctic stratosphere, Geophys. Res. Lett., 17, 513 - 516, 1990.

WMO. Scientific Assesment of Ozone Depletion: 1991. World Meteorological Organization Global Ozone Research and Monitoring Project, Report No. 25.

1993

21 Km (ppt)

	50° N		60° N		
	gas.	het.	gas.	het.	
BrO	4.7	7.6	9.4	9.3	Feb.
	4.0	5.6	3.4	5.4	May.
ClO	16.6	99.9	115.0	689.0	Feb.
	14.1	37.2	11.3	36.4	May.

Table 1

Figure 1. Modelled calculated height distribution of bromine compounds in the stratosphere in the 1990 atmosphere for February and May at 50 deg latitude N.

Figure 2. Modelled calculated ozone loss by different chemical cycles, and total ozone loss at 50 deg. latitude N during February.

Figure 3. Modelled calculated total ozone loss by the reaction BrO + ClO for the 1990 atmosphere.

Figure 4. Modelled calculated total ozone loss by the reaction BrO + HO_2 for the 1990 atmosphere.

Table 1. Calculated mixing ratios of BrO and ClO in the lower stratosphere with and without | heterogeneous included in the calculations.

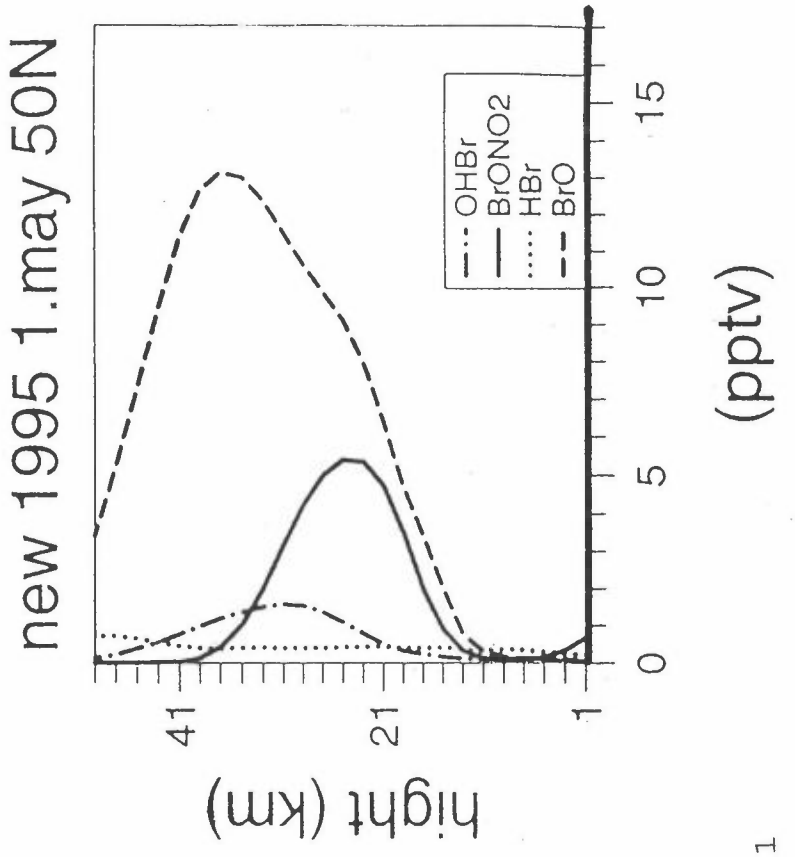
new 1995 1.may 50N
OHBr
BrONO2
HBr
BrO
41
21
1
0
5
10
15
(pptv)
hight (km)

Figure 1

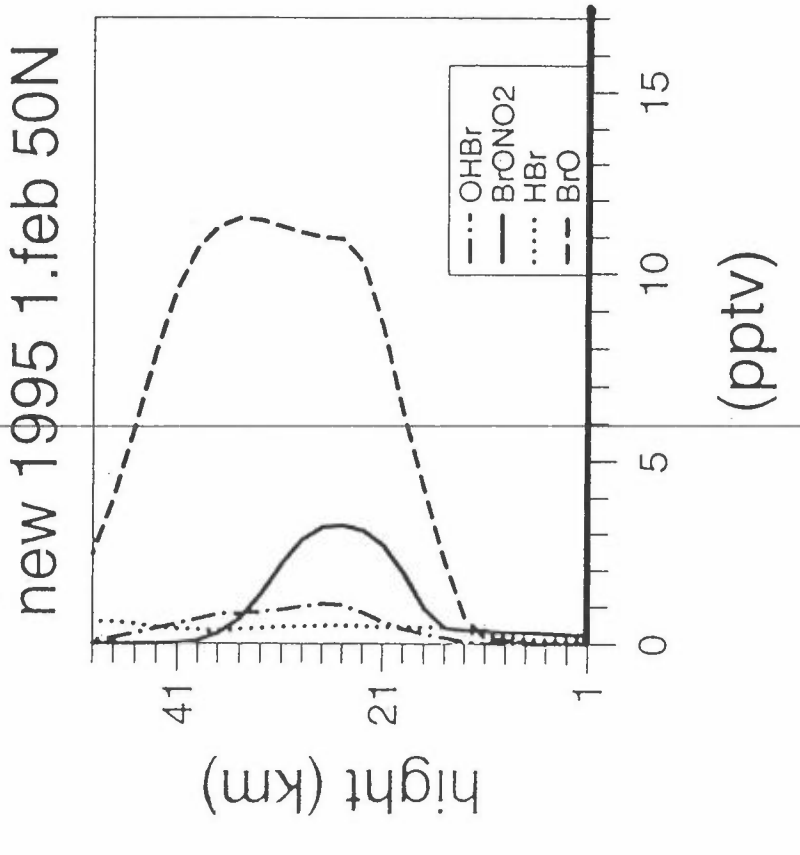
new 1995 1.feb 50N
OHBr
BrONO2
HBr
BrO
41
21
1
0
5
10
15
(pptv)
hight (km)

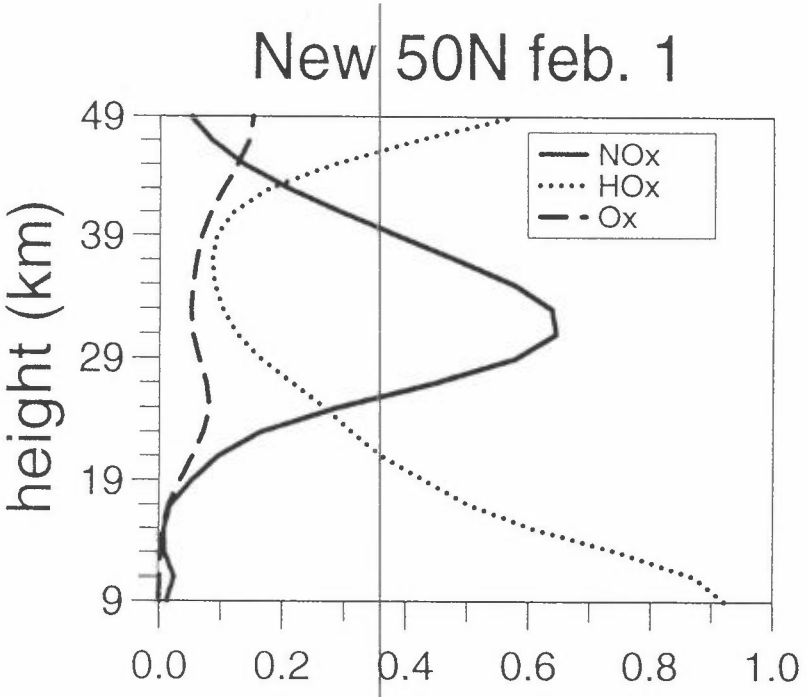
New 50N feb. 1
height (km)
49
39
29
19
9
0.0
0.2
0.4
0.6
0.8
1.0
NOx
HOx
Ox

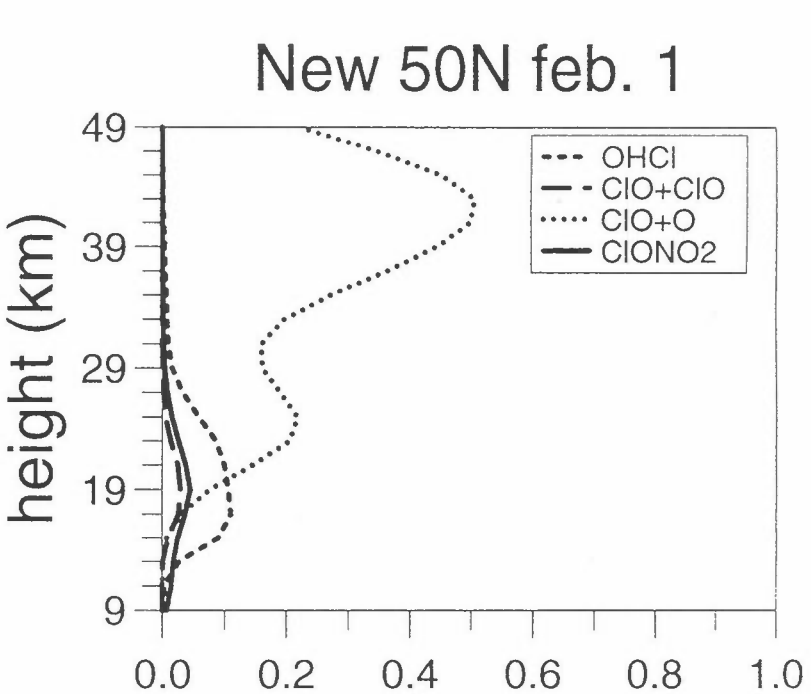
New 50N feb. 1
height (km)
49
39
29
19
9
0.0
0.2
0.4
0.6
0.8
1.0
OHCl
ClO+ClO
ClO+O
ClONO2

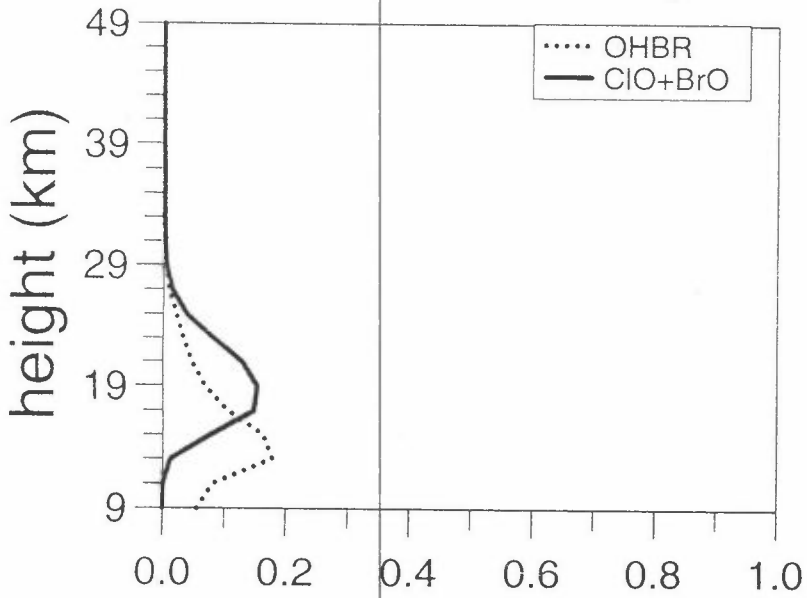
height (km)
49
39
29
19
9
0.0
0.2
0.4
0.6
0.8
1.0
OHBR
ClO+BrO

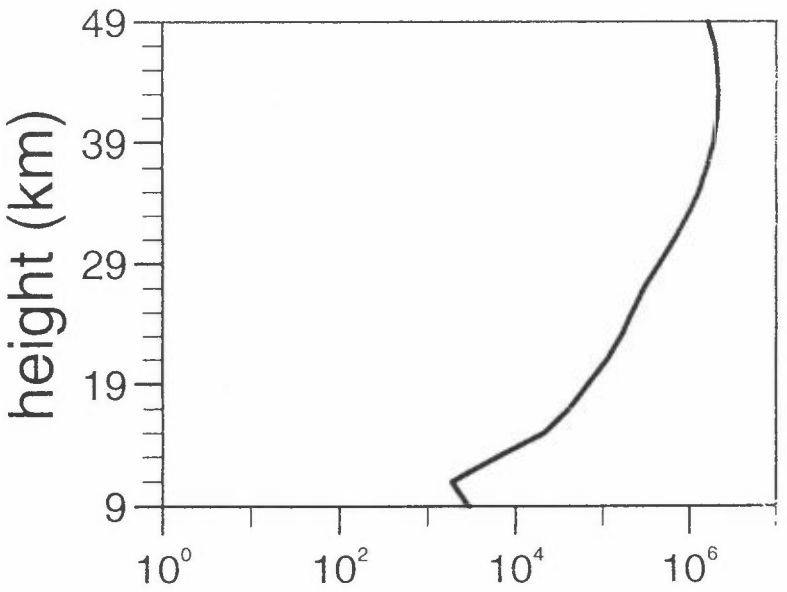
height (km)
49
39
29
19
9
10^0
10^2
10^4
10^6

Figure 2

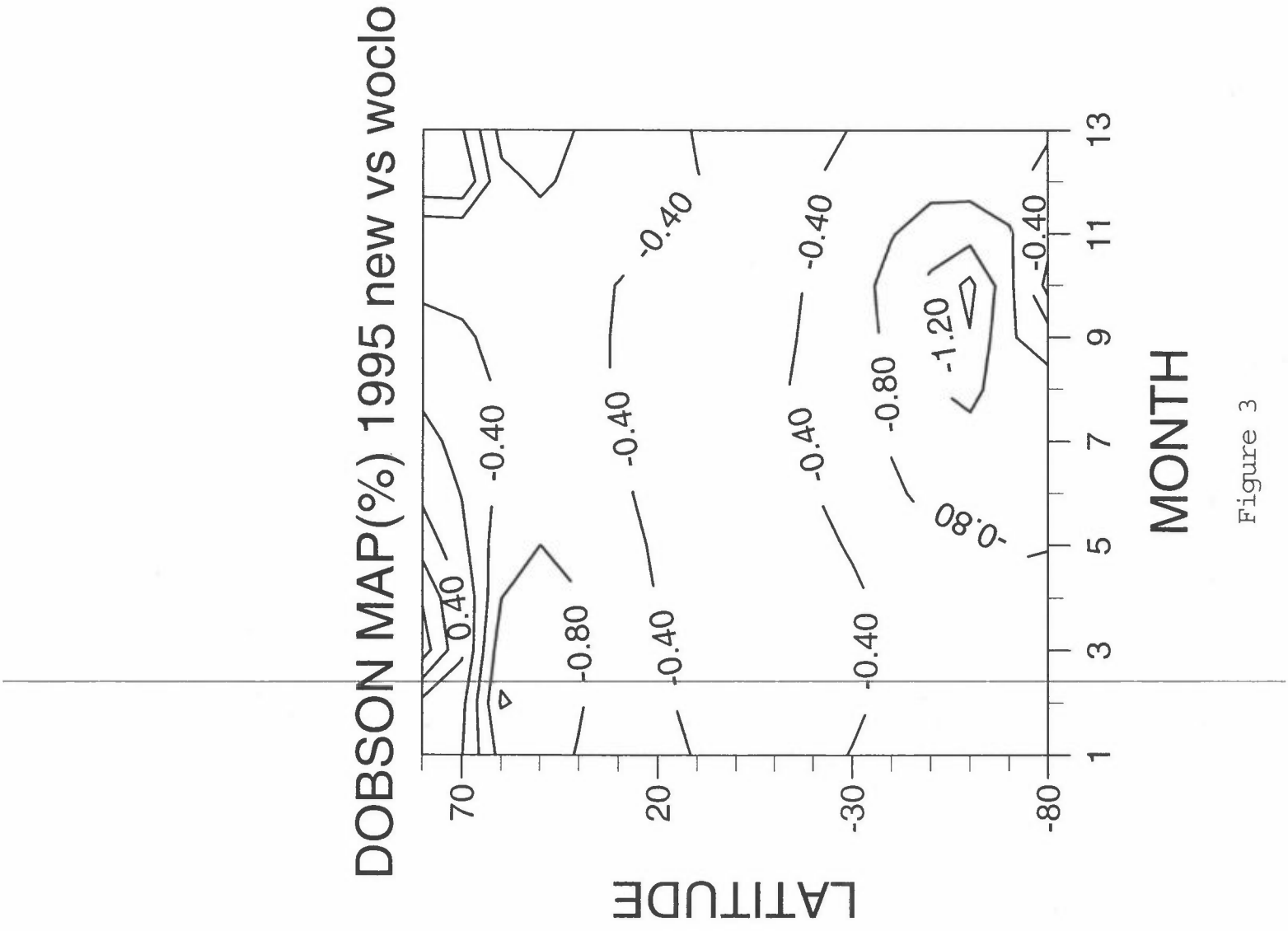
DOBSON MAP(%) 1995 new vs woclo
LATITUDE
70
20
-30
-80
MONTH
1
3
5
7
9
11
13
0.40
-0.40
-0.80
-1.20

Figure 3

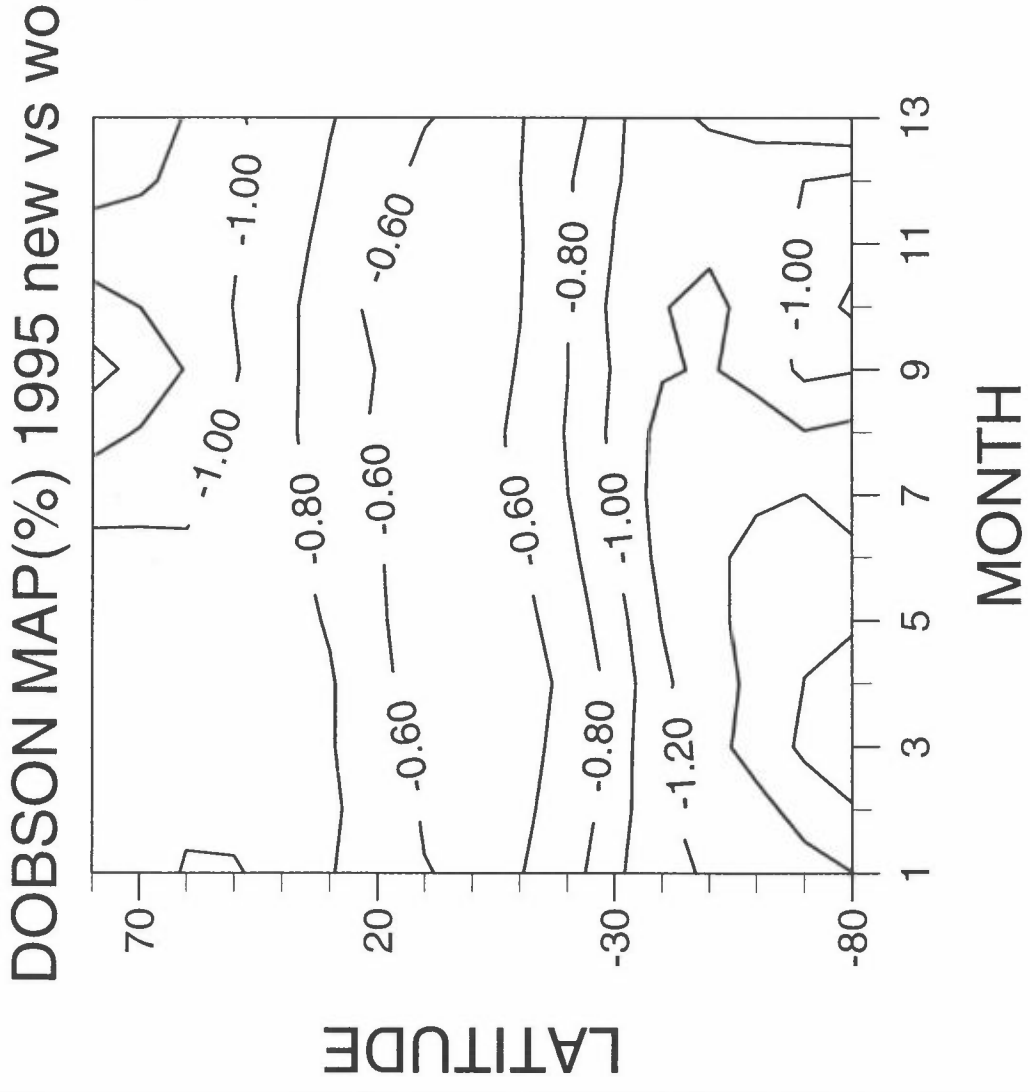
DOBSON MAP(%) 1995 new vs wo
LATITUDE
MONTH
70
20
-30
-80
1
3
5
7
9
11
13
-1.00
-0.80
-0.60
-1.20

Figure 4

Alternative degreasing solvents and their impact on ozone formation

Sara Janhäll and Yvonne Andersson-Sköld

Swedish Environmental Research Institute, IVL, Göteborg, Sweden

SUMMARY

A photochemical trajectory model has been used to simulate the influence on tropospheric ozone formation by replacing traditional degreasing solvents with the alternative degreasing solvents; methyl lactate, ethyl lactate and isopropyl lactate. The change will not, according to this study, affect the concentrations of ozone in Sweden significantly.

Introduction

Due to health effects and environmental risks of the degreasing solvents currently in use alternatives are required. At present chlorinated organic compounds and aromatic compounds are frequently being used as degreasing solvents by the Swedish industry. The aromatic compounds may cause health problems and the main environmental issue is their contribution to ozone and other oxidants in the lower troposphere. Also the chloro-organic compounds may cause health effects, of perhaps more importance is that some are stable enough to reach the stratosphere where they will contribute to the ozone layer depletion.

Consequently there is an urgent need to find alternatives less harmful to the environment. Lactates and paraffines have been suggested. In order to avoid other environmental problems, IVL is investigating the environmental and health effects of these alternative degreasing solvents. The alternatives included in this study are lactates, i.e. methyl lactate, ethyl lactate and isopropyl lactate. This work phocuses on the influence on the tropospheric ozone formation due to these compounds.

To study the influence on ozone formation, the IVL photochemical trajectory model has been used (1).

Model description

The IVL-model was initially developed at Harwell in England to study the London plume (2, 3, 4). At IVL the model has been updated and chemically expanded (5, 6, 7).

The model describes the chemical transformation of pollutants in the boundary layer air. At present, the model describes the chemical transformation of 80 organic compounds. It includes approximately 500 species and about 1000 reactions.

In most studies the air parcel of boundary layer air is split into two layers to provide a realistic description of the diurnal variations in the boundary layer depth and the exchange of pollutants at the underlying surface. In this study, however, the model is simplified to

include only one parcel of air with a constant mixing depth and constant emission rates. All simulations have been conducted to describe a high photochemical activity, i.e. a high pressure situation with clear sky around midsummer.

Case studies

This work includes some initial studies on the influence of the lactates on ozone formation. Simulations have been conducted to calculate the Photochemcial Ozone Creation Potentials (POCPs) which describe the change in the amount of ozone formed due to a certain change in the emission of a particular compound.
There are some different approaches in calculating the POCP, for example:

* The contribution to the ozone formation at peak ozone concentration
* The maximum contribution to the ozone formation
* The average contribution to the ozone concentration over a number of days.

In Sweden the environmental effects of ozone are mainly due to long time exposure at relatively high concentrations, and not the episodic ozone concentrations. In this study, therefore, the average contribution of ozone over four days, including the amount of ozone deposited along the trajectory, has been calculated.

The POCPs of the lactates have been calculated for different types of emission scenarios of Sweden, and two different types of hydrocarbon profiles have been used. One hydrocarbon profile has been estimated for Sweden by SNV (8), the Swedish Environmental Protection Board, with further details from IVL (6). The other hydrocarbon profile has been estimated for the UK by Derwent and Jenkin (9). The simulations have been conducted with and without diurnal variation in emissions due to traffic. The various scenarios are given below:

Scenario*	Total emissions (ton year^{-1} km^{-2})			Hydrocarbon profile	Diurnal variation of emissions
	VOC	NOx	CO		
1. (South of Sweden in average)[a]	3.382	2.82	12.4	SNV&IVL	yes
2. (Sweden in average)[b]	1.091	0.91	4.00	SNV&IVL	yes
3. (Sweden in average)[b]	1.091	0.91	4.00	SNV&IVL	no
4. (Sweden in average)[b]	1.091	0.91	4.00	Derwent&Jenkin	no
5. (Sweden in average)[b]	1.091	0.91	4.00	Derwent&Jenkin	yes

* The total emissions in Sweden are equally divided by the population of Sweden and the emissions are assumed proportional to the population density. (a: 62 pers./km^2 , b: 20 pers./km^2)

To estimate the influence on the ozone concentration as a consequence of replacement from the more traditional solvents to the lactates, the following preliminary simulations have been studied where:
a) all solvents were changed to lactates,
b) all solvents except methanol, ethanol and acetone were changed to lactates,
c) all chlorinated solvents were changed to lactates.

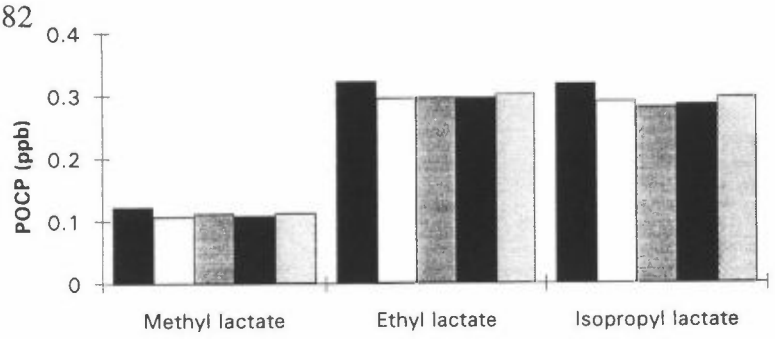

Figure 1. The POCPs calculated in the different environments.

In addition some sensitivity studies have been carried out in which the initial ozone concentration has been varied. In these simulations both the influence on the ozone concentration and the POCPs were calculated.

Results and discussion

As shown in figure 1 methyl lactate has about three times smaller POCP than the other lactates independent of the emission scenario studied. For all of the three lactates the highest POCPs are obtained in scenario 1 (average for the south of Sweden). For all lactates the calculated POCPs obtained in the scenarios 2-4 all are within the same range, i.e. only small differences are found between the different scenarios describing the total emissions for Sweden on average. The lowest POCPs are obtained in the simulations which include diurnal variation in the emission pattern and where the hydrocarbon profile as estimated by SNV and IVL has been used. Also in the runs without diurnal variation in the emission pattern, the use of the hydrocarbon profile as estimated by SNV and IVL resulted in lower POCPs than when the UK profile was used.

As can be seen in figure 2, the replacements of traditional solvents to ethyl lactate do not significantly alter the calculated ozone concentration. The maximum difference is found when all solvents are changed to the lactates, which gave a decrease in ozone concentration by less than 0.5 ppb, or about 1%. Simulations also were conducted when methyl lactate and isopropyl lactate were used as alternative solvents. The choice of lactate did, however, not affect the results significantly.

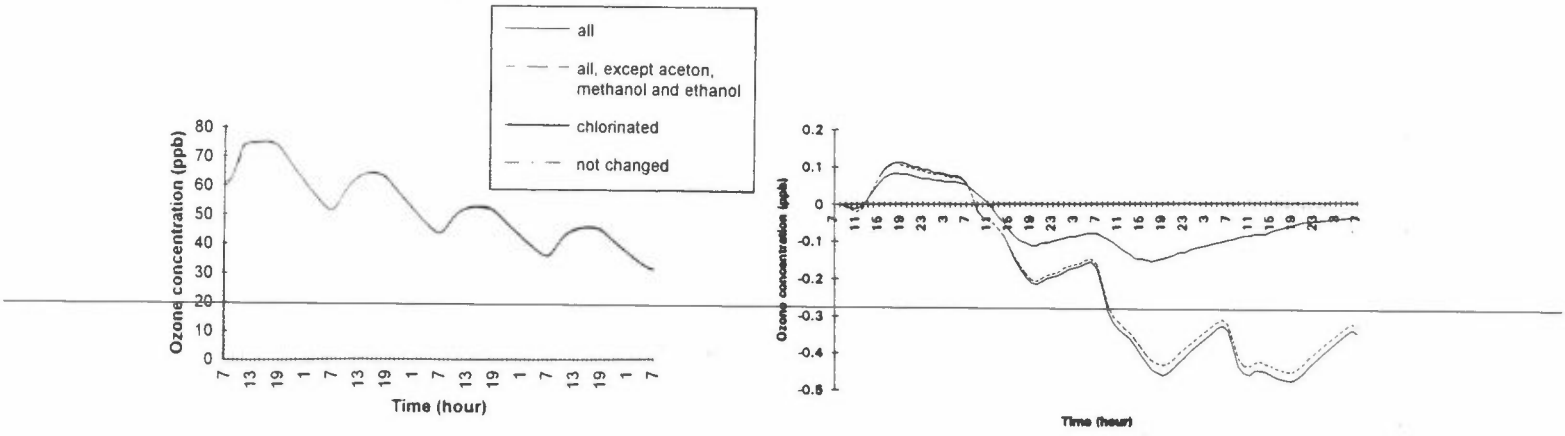

Figure 2. The calculated ozone concentrations and the difference in ozone concentrations due to replacement of traditional solvents by ethyl lactate in scenario 4.

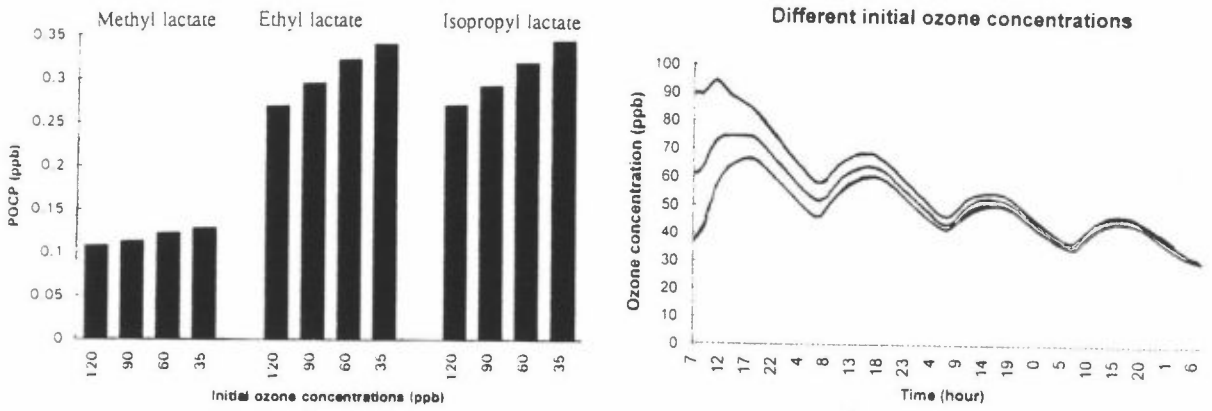

Figure 3.The POCPs for the lactates and the ozone concentration when the initial ozone concentration is altered.

In accordance with figure 3, the calculated ozone concentration is highly dependent on the initial concentration used. The effect becomes less pronounced already during the second day of the simulation. As would be expected, the POCPs increase as the initial ozone concentration decreases.

According to the results obtained from the simulations conducted so far, methyl lactate, ethyl lactate and isopropyl lactate do not affect the ozone concentrations in Sweden.

Acknowledgement

The sponsorship from Arbetsmiljöfonden, SNV and IVL is gratefully acknowledged.

REFERENCES

(1) Andersson-Sköld, Y. Hur oxidantbildning studeras i modeller. Kemisk tidskrift, 11/93, 34-40.

(2) Derwent, R.G. and Hov, Ö. Computer modelling studies of photochemical air pollution formation in North West Europe. AERE R 9434, Harwell Laboratory, Oxfordshire, England, 1979.

(3) Isaksen, I. S. A.,Hessvedt, E. and Hov, Ö. A Chemical Model for Urban Plumes. Atmospheric Environment", 1978, 12, 599-604.

(4) Hough, A. M. and Derwent, R. G. Computer Modelling studies of the distribution of photochemical ozone production between different hydrocarbons. Atmos. Environ., 1987, 21, pp. 2015-2033.

(5) Andersson-Sköld, Y., Pleijel, K., Grennfelt, P. and Rohndahl, L. Miljöeffekter av lösningsmedel - underlag till åtgärdsstrategi. IVL B-1041. 1991, Swedish Environmental Research Institute, Göteborg, Sweden.

(6) Andersson-Sköld, Y., Grennfelt, P. and Pleijel, K. Photochemical ozone creation potentials: a study of different concepts. J. Air Waste Manage. Assoc. 1992, 42:9, pp. 1152-1158.

(7) Andersson-Sköld, Y. and Moldanová, J. Atmosfärskemisk modellstudie av termiskt och marint initierad bildning av oxidanter under svenska förhållanden. IVL B-1064, 1992, Swedish Environmental Research Institute, Göteborg, Sweden.

(8) "Strategi för flyktiga organiska ämnen (VOC). Naturvårdsverket rapport 3763, 1990.

(9) Derwent, R. G., Jenkin, M. E. Hydrocarbon involvement in photochemical ozone formation in Europe. 1990, Harwell Laboratory, Oxfordshire, England.

OZONE IN THE MARINE BACKGROUND BOUNDARY LAYER IN THE SOUTHERN HEMISPHERE

by Sigrun Karlsdottir and Ivar Isaksen

INTRODUCTION

In remote, unpolluted regions, photochemical theory predicts net destruction of ozone

$$HO_2 + O_3 \rightarrow OH + 2O_2 \qquad \text{R1}$$

To study the ozone budget in remote areas, Penket et al.(1992) made observations of ozone and hydrogen peroxide in the period Febuary 1991 to March 1992, at Cape Grim, Tasmania (41°S). Their results showed a clear link between ozone loss and hydrogen peroxide production. A category model is used to study the mixing ratio of ozone in the boundary layer at background areas in the Southern Hemisphere (40°S). The results are compaired with the observations from Cape Grim.

THE MODEL

The category model is a 2 dimensional (2-D) zonally averaged, global model. It has a resolution of 10 degrees latitude and a vertical resolution of 500 m from the surface up to 3.25 km. At this height interval each latitude is devided into 4 categories, defined depending on the emission rate of pollutant gases (see table 1). Above 3.25 km the vertical resolution is 1 km, and the concentration are zonally averaged up to 16.25 km.

EMISSION			
category 1	category 2	category 3	category 4
0.00	0.005	2.0	20.0

Table 1: *Emission rate for categories 1-4 (numbers for each category should be multipied by the latitudiunal average values).*

RESULTS

The results presented here are taken from category 1 in the model, with no emission of pollutant gases. In Figure 1 we compare our model results of mixing ratios for ozone with observartion at two height levels. The model results are from the lowest grid box, centered at 0.25 km altitude. The observations are from the boundary layer, at Cape Grim, and from 2 km altitude (800 hPa) at Aspendale in Australia, 300 km North of Cape Grim (measurements taken in the period 1965-1973). In the boundary layer the model results are in good agreement with the observations. The mixing ratio varies from 15 to

30 ppbv, with a summer minimum and winter maximum. At 2 km altitude (800 hPa) the mixing ratio is higher, than in the boundary layer, due to transport from the upper troposphere.

Figure 2 shows the modeled seasonal concentration of hydrogen peroxide in the boundary layer. Its mixing ratio varies between ca. 110 to 750 pptv, with winter minimum and summer maximum. This agrees well with observations.

Figure 3 which shows the measured mixing ratio of ozone and hydrogen peroxide in the boundary layer at Cape Grim in the period February 1991 to March 1992, demonstrate the relationship between ozone minimum and hydrogen peroxide maximum in the marine boundary layer in the Southern Hemisphere.

Figure 4 shows the average net production of ozone at two height intervals in the model; at all heights below 2 km and for heights between 0.5 and 2 km. The net production of ozone is clearly negative, when the boundary layer with surface deposition is included. However, when the boundary layer with surface deposition is excluded, we calculate a small net positive production from March to October (of the order $0.5 \times 10^6 molecules/cm^3 sec$). During summer a more pronounced ozone loss is found in this height interval (up to $3 \times 10^5 molecules/cm^3 sec$).

Figure 5 shows the average mixing ratio of NO in the interval between 0.5 and 2 km. Its mixing ratio varies between approximately 5.5 to 21 pptv, with a winter maximum and summer minimum.

DISCUSSION

Both the calculated and measured results are in good agreement with the photochemical theory. The seasonal variation of the mixing ratio of ozone is higher in the boundary layer than at 2 km altitude (see Figure 1). This indicates that the deep summer minimum in the ozone mixing ratio, in this region, is caused by photochemistry. Thus our results support the conclutions drawn by Penkett et al.(1992) that in situ photochemistry, rater than transport, is the major cause for the seasonal variation of ozone in the boundary layer in this region.

The net production of ozone is very low. It is caused by low NO mixing ratio (see Figure 4 and 5). In the period March to October the net production of ozone is positive and the mixing ratio of NO are above 10 pptv. This indicates that the threshold level for NO is approximately 10 pptv in the category model.

Figure 1

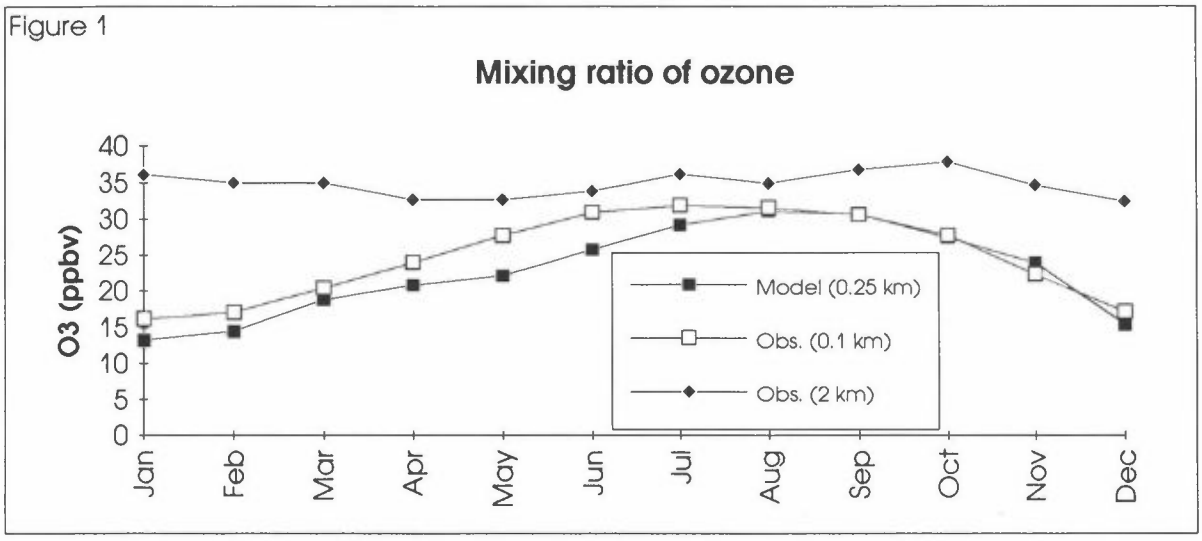

Figure 2

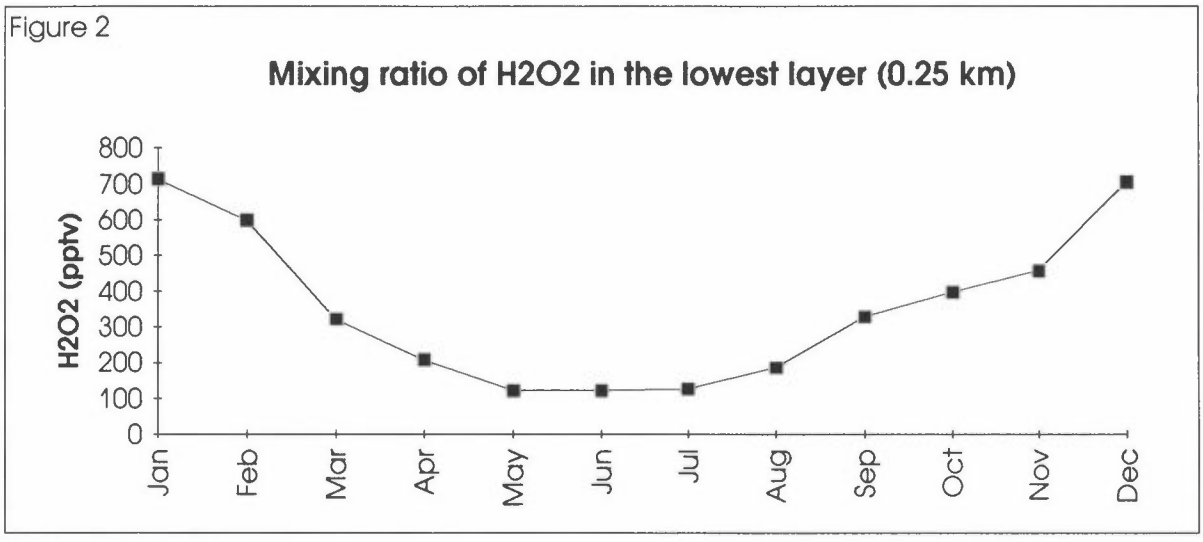

Figure 3

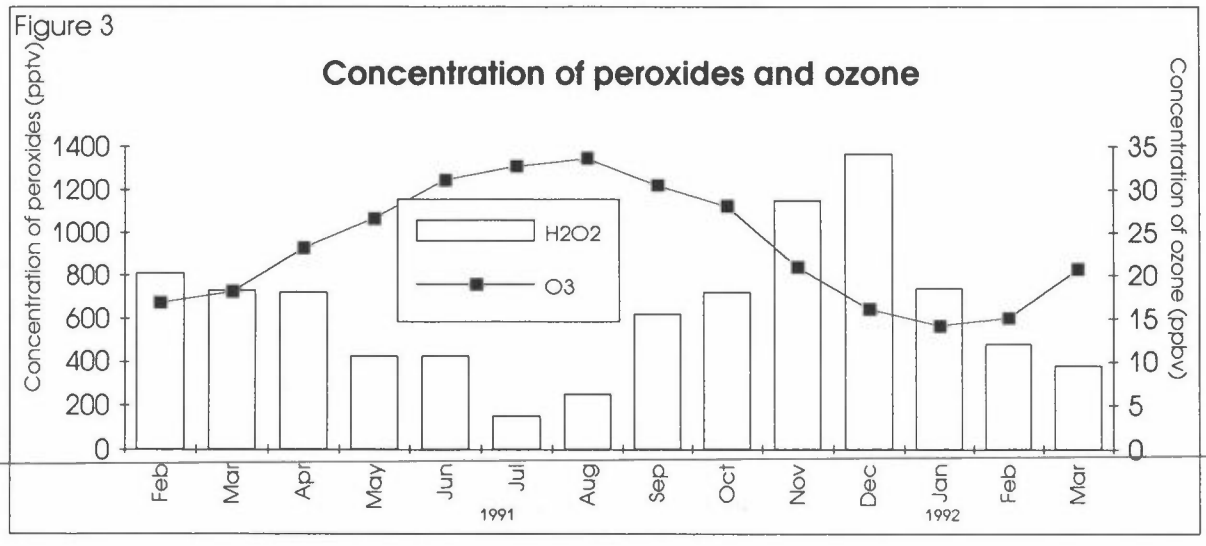

Figure 4

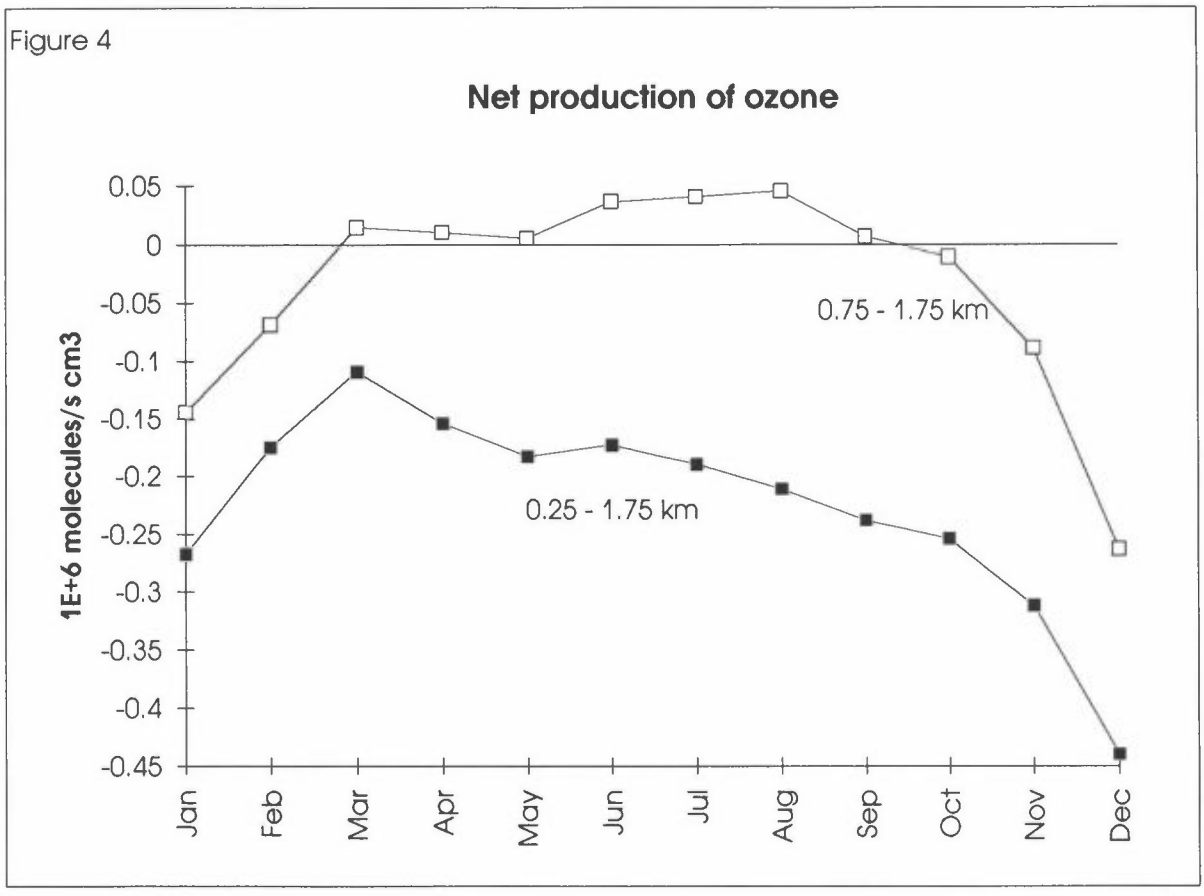

Figure 5

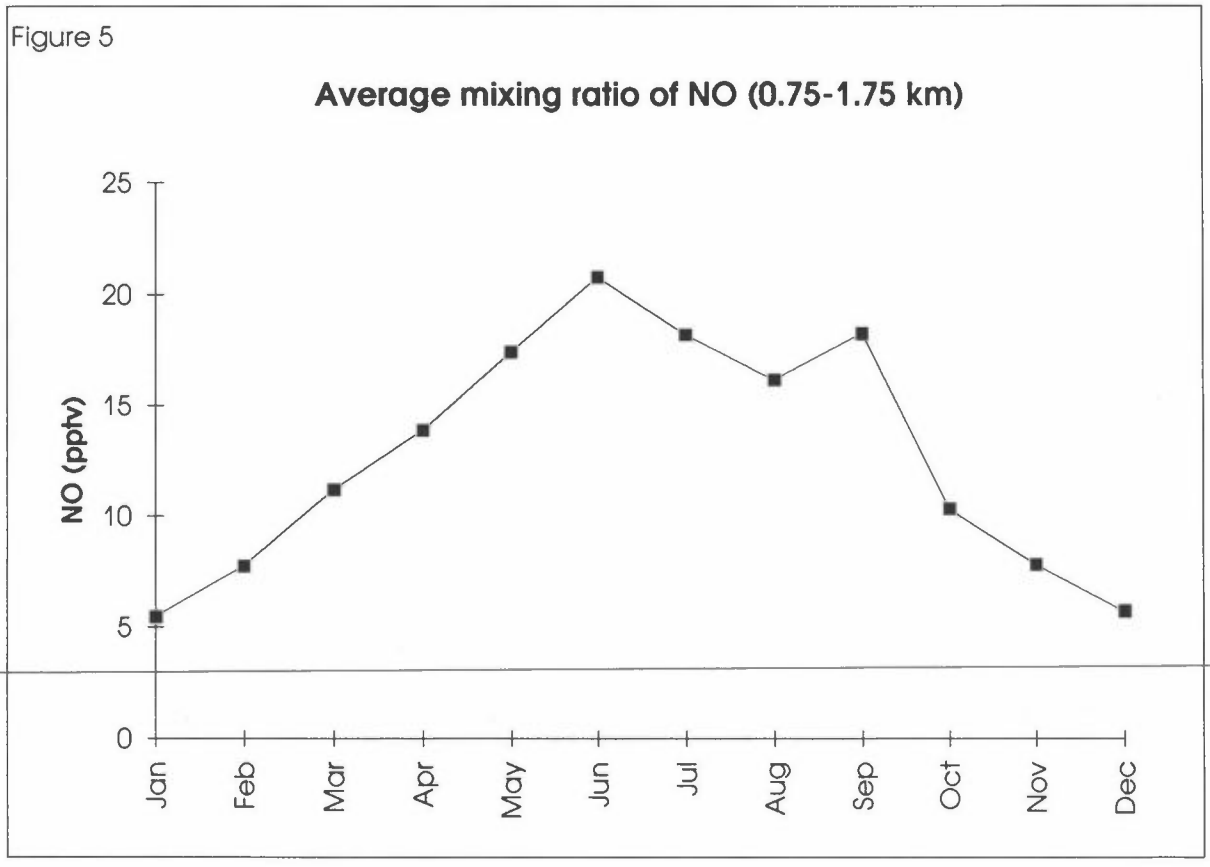

IMPACT OF NO_x-EMISSIONS FROM AIRCRAFT ON OZONE CHEMISTRY

Anne Gunn Kraabøl and Frode Stordal
Norwegian Institute for Air Research (NILU)

Introduction

The NO_x- emissions ($NO+NO_2$) from aircraft cause a larger change in ozone compared to man-made NO_x-emissions at the surface. An ozone change near the tropopause also has a stronger impact on the radiative forcing, and thereby the climate. We have used a trajectory model to study the effects of aircraft NO_x-emissions on the ozone chemistry at cruise altitude.

The distribution of NO_x in the troposphere, and particulary the distribution and seasonal variations in the upper troposphere, are not well known (Ehhalt et al., 1992). Due to a short atmospheric lifetime coupled with inadequate monitoring networks, the determination of long-term trends and spatial and temporal distribution is difficult (IPCC, 1992). We were therefore particulary interested in how the the impact of NO_x-emissions changed with different initial values of nitrogen in the airparcel.

Model

The present trajectory model contains ECMWF isentropic trajectories and chemistry from the Oslo 2-D stratospheric model (Stordal et al., 1985). The initial values of the trajectories are also from that model. We use a 3-D global distribution of aircraft NO_x-emissions from Warren Spring Laboratory (Mc Innes et al., 1992). The model assumes that there is no exchange between the airparcel and the surrounding air.

Results

We present results from a trajectory at isentropic level 350 K, ending above Athens in April 1992 (Figure 1). Figure 2 shows the NO_x-aircraft emissions that the airparcel is exposed to when the trajectory is at cruise level for subsonic air-traffic, which is approximately 8-12 km.

Figure 3 shows the mixing ratio of NO_x and HO_2 along the trajectory in a case without aircraft emissions. During the first days NO_x and HO_2 change rapidly until an equilibrium level is reached. The initial values of some main components are given in Table 1.

To quantify the impact of NO_x-emissions the change in relative net ozone production ($PO_{3,net}$) is calculated along the trajectory. $PO_{3,net}$ is defined as:

$$PO_{3,net} = PO_3\text{-}QO_3 \text{ (molecules cm}^{-3}\text{s}^{-1}\text{)}$$

where PO_3 and QO_3 are the chemical production and loss respectively (molecules $cm^{-3}s^{-1}$).

To study the change in $PO_{3,net}$ due to aircraft NOx-emission with different NOy-initial values, four model runs were made (Table 2). Figure 4 shows the change in $PO_{3,net}$ between a run with and without NOx-emissions when the NOy-initial value is reduced and increased by 20 % . The most pronounced effect is during the first day in both cases because the HO_2 level is at its highest and the NO_x level is at its lowest (Figure 2).

The main reactions governing the ozone production are:

$$(1)\ NO_2+h\nu \rightarrow NO+O(^3P)$$
$$(2)\ O(^3P)+O_2+M \rightarrow O_3+M$$
$$(3)\ NO+HO_2 \rightarrow NO_2+OH$$
$$(4)\ NO+RO_2 \rightarrow NO_2+RO.$$

Reactions (3) and (4) are the net ozone production reactions in the reaction chain. When NO_x is increased in the background atmosphere (without aircraft emissions) the net ozone production increases (Table 2) as the rates of reaction (3) and (4) are propotional to the NO concentration. However, the increase in ozone production is weaker than the increase in NO_y ,since the concentrations of HO_2 and RO_2 are suppressed, also through reactions (3) and (4). The suppression of HO_2 and RO_2 concentrations also influence the effect of aircraft NO_x-emissions, so that the net ozone production decreases with increased background concentration of NO_y.

Conclusions

The effects of aircraft NO_x-emissions are highly dependent on the background concentration of NO_y in the model results presented here. The effect of aircraft emissions on ozone is therefore somewhat uncertain, since the spatial and temporal distribution of NO_y in the middle and upper troposphere is not sufficiently known.

HNO_3(ppbv)	NO_y(ppbv)	O_3(ppmv)	OH(pptv)	HO_2(pptv)	CH_3O_2(pptv)
0.37	0.24	0.11	0.11	5.22	0.73

Table 1: Initial values in the airparcel at the trajectory start.
*(NO_y=NO+NO_2+NO_3+2*N_2O_5+HNO_2+HO_2NO_2+$ClONO_2$+$BrONO_2$)*

	Background NO_x	Including aircraft NO_x
-20% NOy	$3.30 \cdot 10^{10}$	$3.85 \cdot 10^{10}$
+20 % NOy	$4.01 \cdot 10^{10}$	$4.23 \cdot 10^{10}$

Table 2: $PO_{3,net}$ (molecules cm^{-3}) integrated over ten days for four different model runs.

References

Ehhalt D.H, Rohrer F.and Wahner A., (1992), Sources and distributions of NO_x in the upper troposphere and northern mid-latitudes. *J. Geophys. res.*, 97, 3725-3738.

Intergovernmental panel on climate change (IPCC) , (1992), The suplementary report to the IPCC scientific assesment, *Cambridge. University Press,Cambridge, U.K.*

Stordal F., Isaksen I.S.A and Horntveth K. , (1985), A diabatic circulation two dimensional model with photochemistry: simulations of ozone and long lived tracers with surface sources. *J. Geophys. res.*, 90, 5757-5776.

McInnes G and Walker C.T, (1992) The global distribution of aircraft air pollutant emissions. *Warren Spring Laboratory. Gunnels Wood Road. Stevenage Hertfordshire SG1 2BX.*

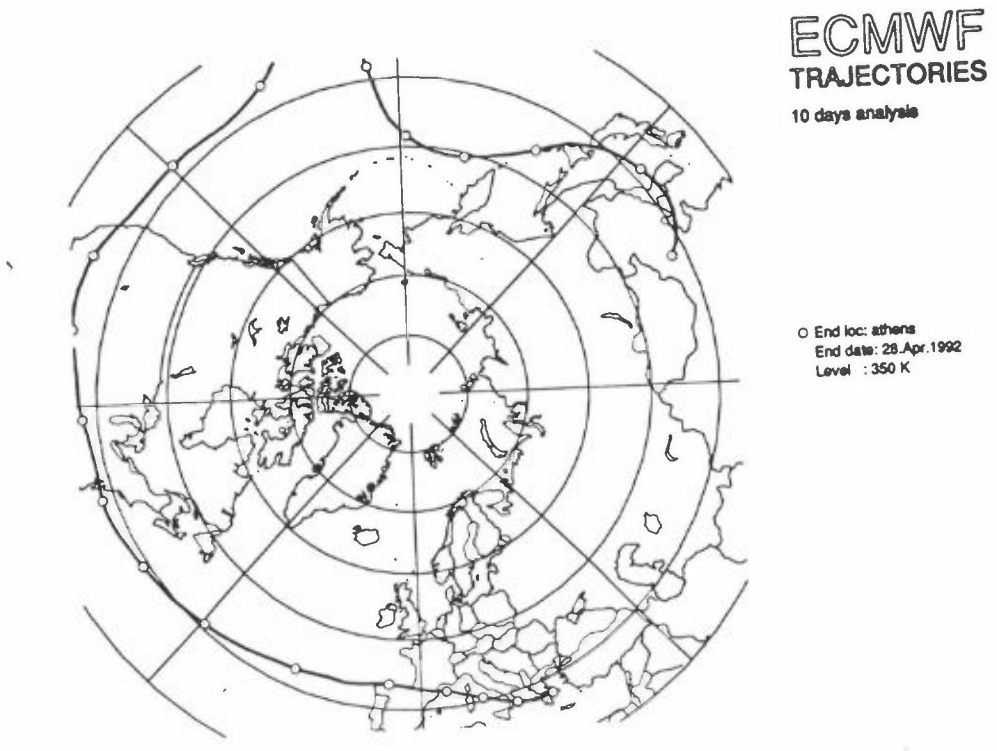

Figure 1: *The trajectory at isentropic level 350 K, ending above Athens 28.4.92*

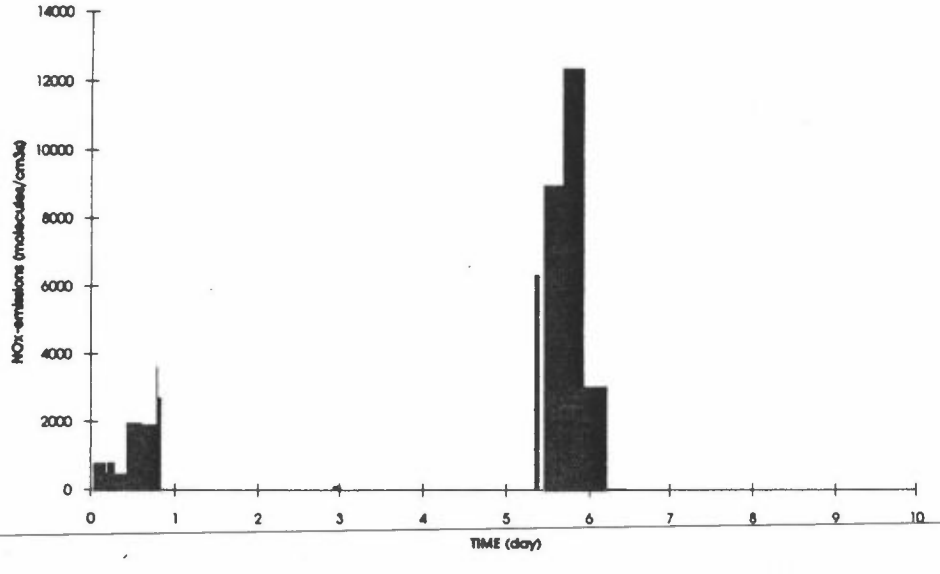

Figure 2 : *Aircraft NO_x-emissions which the airparcel is exposed to when the trajectory is at cruise level for subsonic air-traffic (8-12 km.)*

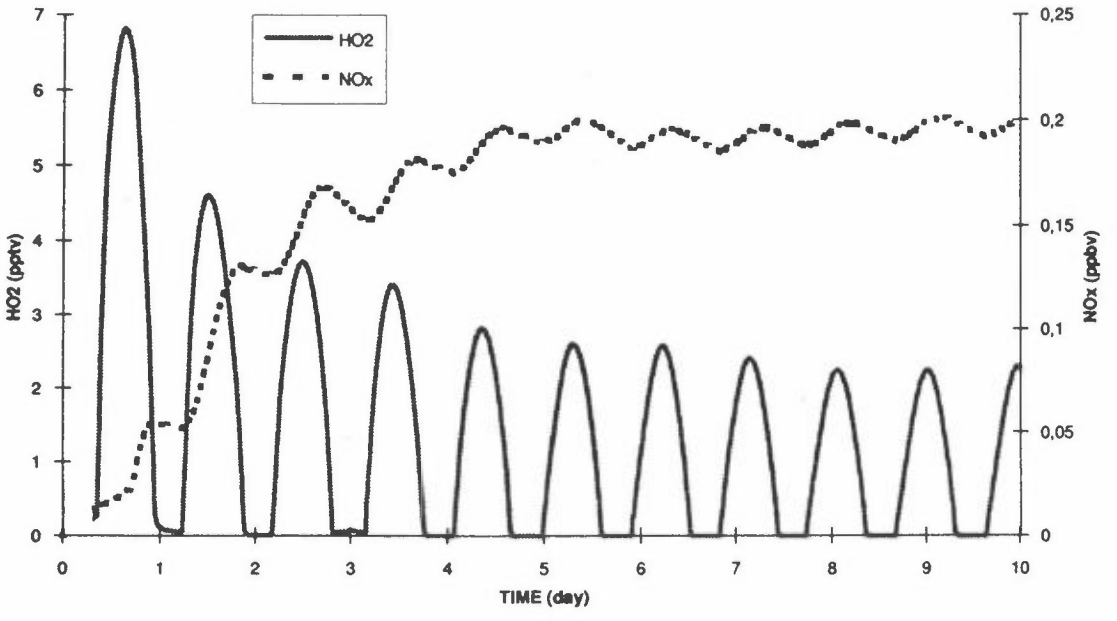

Figure 3 : *Mixing ratios of HO_2 and NO_x ($NO+NO_2$) along the trajectory without aircraft emissions.*

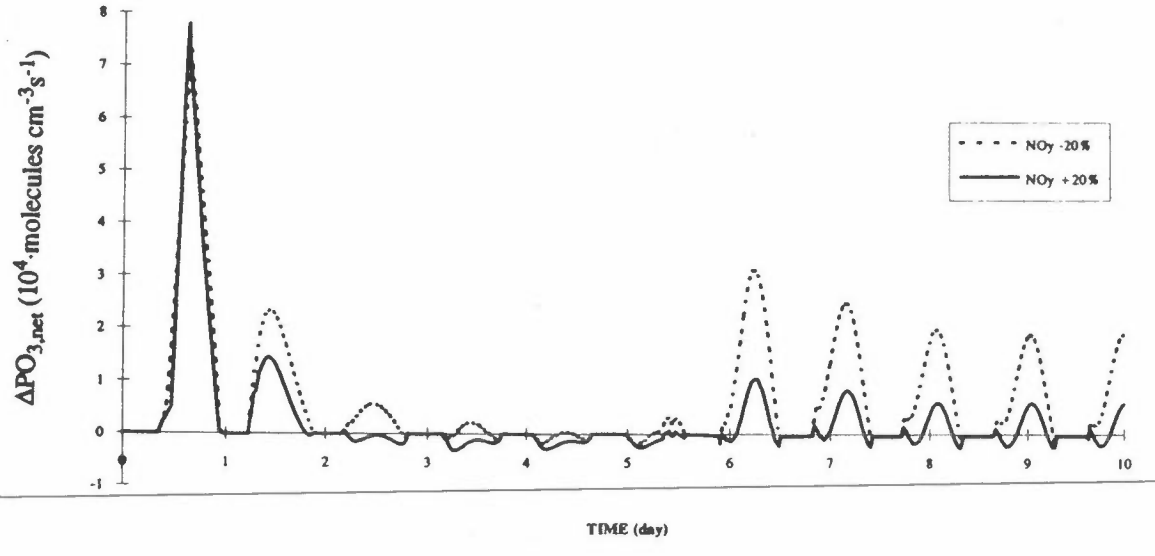

Figure 4 : *The change in net ozone production ($\Delta PO_{3,net}$) due to aircraft NO_x-emissions with different initial NO_y- values.*

Chemistry and Physics of Aerosol Dynamics in the Atmosphere

Markku Kulmala
Department of Physics
P.O. Box 9
FIN-00014 University of Helsinki, Finland

Abstract

Aerosol dynamics, particularly formation and growth of aerosol particles and cloud droplets are strongly dependent on atmospheric chemistry. The chemical reactions in the gas phase and in the liguid phase as well as surface reactions influence on mass fluxes. On the other hand the size, concentration and composition of aerosol particles determines the surface and volume available for surface and liquid phase chemical reactions. Wide spectrum of chemistry and physics is needed to understand air pollution. In this presentation I will outline the connection between atmospheric chemistry and aerosol science.

Aerosols and atmospheric chemistry

Aerosols have a central role in the atmosphere. Their importance for cloud formation has been recognized for years. Furthermore, the aerosols participate in numerous chemical processes, and they also influence the visibility and the electrical properties of the atmosphere. In addition, they may affect the climate on earth by influencing the radiation budget.

The formation and growth of particles in the presence of condensable vapours represent processes of major importance in aerosol dynamics. The formation of new aerosol particles will change the composition distribution of aerosol particles. The composition is closely related to the growth rate, which influences on the actual size of particles. Aerosol deposition is determined by particle size, and deposition transfers chemical compounds from the atmosphere.

Aerosol particles are typically characterized by size distributions (see e.g. Hinds, 1982; Seinfeld, 1986). The most general size distributions are number distribution, surface distribution, mass distribution and several composition distributions. Different aerosol properties are presented by different size distributions. Chemical and physical properties of aerosol particles are changing significantly as a function of size. E.g. acid aerosol consists typically of submicron (aerodynamic diameter smaller than 1 μm) particles and dust particles are bigger. Aerosol distributions are very dynamical (see e.g. Fig. 1.): they change rapidly as a function of time and position. This causes some problems to estimate global aerosol effects. For more details of aerosol dynamics I refer to textbooks by Friedlander (1977), Fuchs (1964), Hinds (1982), Seinfeld (1986) and Williams and Loyalka (1991).

The main phenomena in aerosol dynamics are homogeneous nucleation (formation of new particles), condensational growth of particles, coagulation of particles to form bigger particles and deposition. In certain cases the heterogeneous nucleation initialize condensation (see e.g. Lazaridis et al., 1991).

Aerosol science and atmospheric chemistry are very closely related to each other. Chemical reactions determines aerosol composition and also significantly the aerosol dynamics. The number, size and composition of aerosol particles determine conditions for chemical reactions. There is also

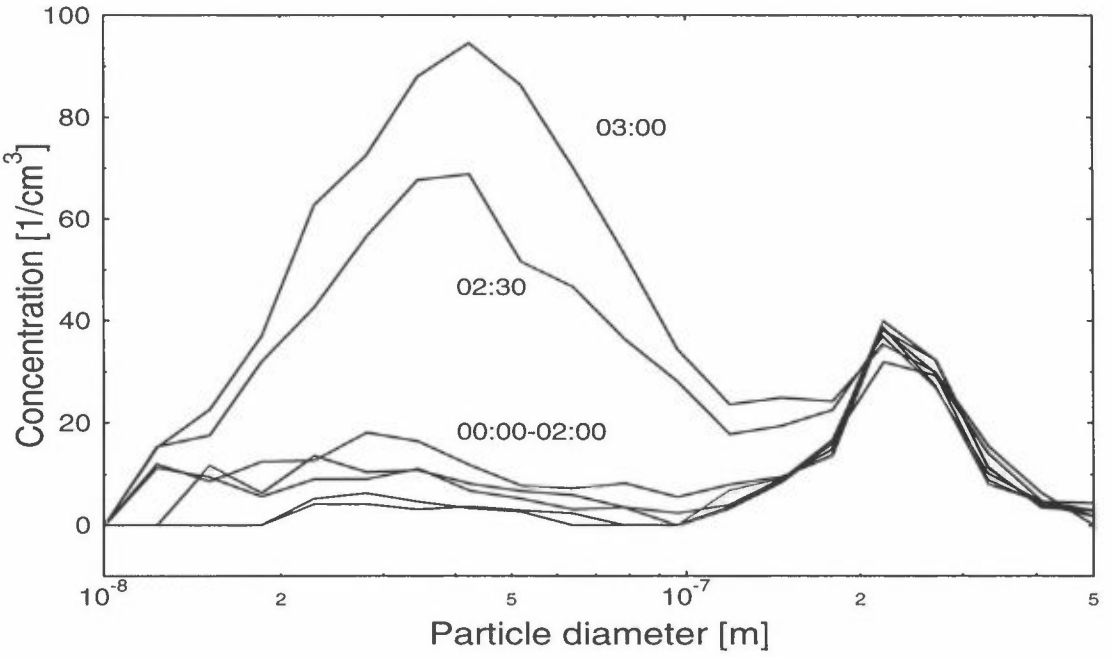

Figure 1: Number distribution of arctic aerosols. Measured at Värriö Measurement Station in Lappland on 31.3.1992 by Differential Mobility Analyzer and Condensation Nucleus Counter (Aalto, 1993).

another connection between aerosol science and chemistry: modelling the aerosol dynamics and cloud microphysics physico-chemical input data is needed. Vapour pressures, activity coefficients, surface tensions, densities, diffusion coefficients, thermal conductivities, viscosities etc. should be known as a function of composition and temperature (see e.g. Vesala, 1991).

Gas-to-particle conversion

The formation of aerosol particles (e.g. acid aerosols: particles containing acids, sulphates or nitrates) by gas-to-particle conversion can take place through several different mechanisms including: 1) reaction of gases to form low vapour pressure products (e.g. the oxidation of sulphur dioxide to sulphuric acid), 2) homomolecular or heteromolecular (in the atmosphere generally with water vapour) nucleation of those low pressure vapours, 3) vapour condensation onto surfaces of pre-existing particles 4) reaction of gases with the surfaces of existing particles and 5) chemical reactions within particles.

The formation of new particles is a significant process, since it will change the dynamics (e.g. deposition) of aerosols. In cases where no new particles are formed, the dynamical behaviour of particles does not change very much. Thus we have recently studied binary nucleation (Kulmala and Laaksonen, 1990). For generating the nucleating species, the gas phase reactions (step 1) are important. Nucleation (step 2) will follow gas phase reactions, if there exists enough gas molecules for formation of new particles. The condensation term (step 3) will decrease the concentration of the nucleating species. We have recently presented an analytical expressions for binary condensation (Kulmala et al., 1993a). The other parts of gas-to-particle conversion (steps 4 and 5) will not affect so much on the formation of new particles. However they are important for particle composition and determine partly the mass fluxes to or from the droplet.

For formation of new acid particles the most important system is H_2SO_4 - H_2O mixture (see

e.g. Kulmala, 1990). Sulphuric acid molecules, together with water molecules, can form new particles in some practical situations in the atmosphere. These particles will grow to visible size through condensation and coagulation. In the growth process the hygroscopic behaviour of acid particles is important. E.g. nitric acid molecules in the troposphere can only absorb into or condense onto existing particles, and liquid phase chemistry will complete the gas-to-particle conversion of nitric acid molecules.

Activation of cloud droplets

Traditionally, the activation of aerosol particles into cloud droplets has been described with the Köhler theory (see e.g. Pruppacher and Klett, 1978): as the saturation ratio S of water increases, hygroscopic salt particles take up water so that they stay in equilibrium with the environment. When S exceeds 100 % (usually by a fraction of 1 per cent, the exact number depending on the particle size and on its composition), the particles start to grow spontaneously. A Köhler curve plots the particle radius versus the saturation ratio: a maximum of S is seen at the activation radius of the particle in question.

If there is another condensable vapor involved in the process, we get a Köhler surface rather than a Köhler curve, the axes being particle radius and the saturation ratios of the two vapors. To determine the surface properly one needs thermodynamical data such as equilibrium vapor pressures as functions of mole fractions and temperature for the (dilute) three-component system. (Actually, the system has more than three components, as far as the thermodynamical data are concerned, because the salt and the nitric acid are decomposed into various ionic species in the liquid phase.) Recently we have studied the effect of nitric acid on activation of cloud droplet (Kulmala et al., 1993b). In our study we have used vapour pressures given by Clegg and Pitzer (1992). One of the results is shown in Fig. 2.

We have also studied activation and growth of cloud droplets using an air parcel model describing the formation of a convective cloud (Korhonen et al., 1993). In the model the simultaneous condensation of water and nitric acid vapours is investigated. Result of the study was that the risen nitric acid concentration enhanced the droplet activation. Cloud droplet concentration was increased and average size decreased. These variations in the cloud droplet distributions altered also the shortwave optical properties (e.g. albedo and absorptivity) of the forming cloud.

Stratospheric clouds

Heterogeneous chemical reactions on the surface of polar stratospheric cloud (PSC) particles are believed to initiate the catalytic destruction of ozone in the polar lower stratosphere. The PSC formation is one of the best examples, where aerosols affect on atmospheric chemistry. We have recently studied homogeneous and heterogeneous nucleation, freezing and condensation in stratospheric sulphuric acid – nitric acid – water system (Laaksonen et al., 1993; MacKenzie et al., 1993) and find out the possible formation mechanisms of stratospheric cloud particles.

Acknowledgements

The author would like to thank several helpful comments from Pasi Aalto, Kaarle Hämeri, Pekka Korhonen and Timo Vesala. Finally, the financial support of the Academy of Finland is acknowledged.

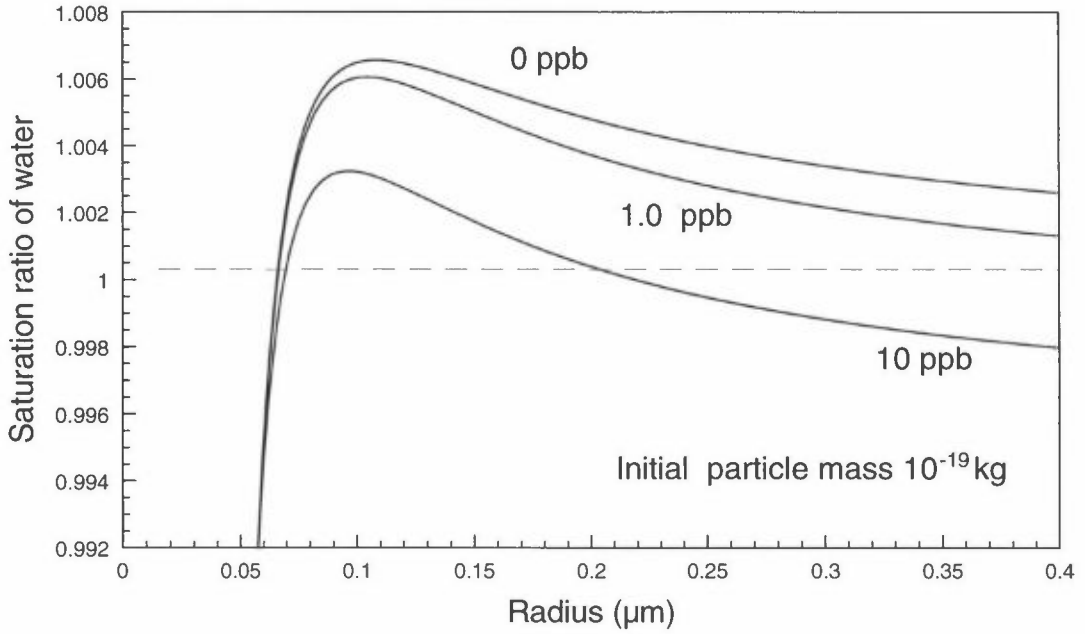

Figure 2: The binary Köhler curves of $NaNO_3$ particle with dry mass of 10^{-19} kg (0.02 μm. The uppermost curve is with zero acid concentration, the lowest curve with 10 ppbv nitric acid concentration and the curve between with 1 ppbv. Temperature is + 20 °C and the ambient pressure is 1000 mbar (Kulmala et al., 1993b).

References

Aalto, P., Personal communication, University of Helsinki, 1993.

Clegg, S.L. and K.S. Pitzer, Thermodynamics of multicomponent, misciple ionic solutions: Generalized equations for symmetrical electrolytes, J. Phys. Chem., 96: 3513-3520, 1992.

Friedlander, S.K. *Smoke, Dust and Haze*, John Wiley & Sons, 1977.

Fuchs, N.A. *The Mechanics of Aerosols*, Pergamon Press, 1964.

Hinds, W.C. *Aerosol Technology*, John Wiley & Sons, 1982.

Korhonen, P., H. Savijärvi, M. Kulmala, A. Laaksonen, T. Vesala, Effects of nitric acid vapour on the radiative properties of convective clouds. Report Series in Aerosol Science Vol. 23, pp. 132 - 137, 1993.

Kulmala, M., Simulating the Formation of Acid Aerosols. In Acidification in Finland. Ed. by Pekka Kauppi, Pia Anttila, Kaarle Kenttämies, Springer Verlag, Berlin, 1990, pp. 95 – 110.

Kulmala, M., and A. Laaksonen, Binary nucleation of water–sulfuric acid system: Comparison of classical theories with different H_2SO_4 saturation vapor pressures. J. Chem. Phys. 93:696-701, 1990.

Kulmala, M., T. Vesala, and P.E. Wagner, An analytical expression for the rate of binary condensational growth. Proc. R. Soc. Lond. A, Vol. 441, pp. 589-605, 1993a

Kulmala, M., A. Laaksonen, P. Korhonen, T. Vesala, T. Ahonen, J.C. Barrett, The effect of atmospheric nitric acid vapour on CCN activation. J. Geophys Res., 1993b (in press)

Lazaridis, M., M. Kulmala, and A. Laaksonen, Binary heterogeneous nucleation of water–sulphuric acid system: the effect of hydrate interaction. J. Aerosol Sci. Vol. 22, pp. 823-830, 1991

Laaksonen, A., A. R. MacKenzie, M. Kulmala, Polar Stratospheric Cloud formation: Nucleation and freezing mechanisms of nitric acid and sulphuric acid aerosols. Report Series in Aerosol Science Vol. 23, pp. 138 - 143, 1993.

MacKenzie, A.R., M. Kulmala, A. Laaksonen, and T. Vesala, On the formation of type 1 polar stratospheric cloud particles, submitted to J. Geophys. Res., 1993.

Pruppacher, H.R. and J.D. Klett, *Microphysics of Clouds and Precipitation*, D. Reidel, 1978.

Seinfeld, J.H. *Atmospheric Chemistry and Physics of Air Pollution*, John Wiley & Sons, 1986.

Vesala, T., Binary droplet evaporation and condensation as phenomenological processes, Ph.D. thesis, Commentationes Physico – Mathematicae et Chemico – Medicae, 127, The Finnish Society of Sciences and Letters, Helsinki, 1991.

Williams, M.M.R., and S.K. Loyalka, *Aerosol Science Theory and Practise*, Pergamon Press, 1991.

ON THE IMPORTANCE OF NITRATE RADICAL REACTIONS IN SCANDINAVIA

E. Ljungström

Department of inorganic chemistry
University of Göteborg and Chalmers university of technology
S-412 96 Göteborg
Sweden

SUMMARY

The only important source of NO_3 in the troposphere is the reaction between NO_2 and O_3. The ambient NO_3 formation rate may be calculated from NO_2 and O_3 measurements. The monthly NO_3 dose, calculated from such measurements, is surprisingly constant between years, seasons and different locations.

INTRODUCTION

Much work has been performed over the last decade to investigate nitrate radical reactions with various organic and inorganic compounds.[1,2] Today, a good body of kinetic data is available and it is also possible to have a fair idea about the products to expect from a certain reaction. Nitrate radical reactions are considered to be important for atmospheric chemistry only during the dark hours since this species is readily photolysed by visible light.[1]

In order to judge the actual flow through a reaction channel, it is necessary to know not only the rate coefficient for the reaction but also the concentrations of the reacting species. The concentration information is seldom at hand. In particular, measurements of nitrate radical concentrations in the ambient are still rather exotic and, for Scandinavia, non-existent. The nitrate radical concentration at a given instant is the result of a balance between formation and destruction. While destruction is distributed over several direct and indirect channels, the only tropospheric source of NO_3 is reaction (I). Knowledge about the distribution of formation rates is a first step towards understanding the actual importance of nitrate radical reactions.

$$NO_2 + O_3 \text{ ---> } NO_3 + O_2 \qquad \text{(I)}$$

CALCULATIONS

To obtain a reasonable statistical foundation, the original intention was to use one-hour mean values of NO_2 and O_3 concentrations measured at representative locations in Scandinavia for the months of January, May, July and October for 1990, 1991 and 1992. Data of this kind is scarce however, and as a first attempt, this investigation employs two sources. Urban data were taken from the "Femman" station while rural data came from the "Aspvreten" station. The "Femman" station is operated by the Environmental and Health Protection Agency, City of

Göteborg and is situated in the centre of Göteborg. The "Aspvreten" station is operated by ITM, Luftlaboratoriet, University of Stockholm and is located about 70 km south-west of Stockholm. Mean hourly NO_3 formation rates were calculated from one-hour mean values of the NO_2 and O_3 concentrations. The rate constant used was $k_I=1.4x10^{-13}$ exp(-2500/T) [3]. Only the dark hours, including dawn and dusk hours were considered. The absolute frequencies of production rates were then calculated. The intervals were arbitrarily chosen to be $5x10^5$ molecules cm^{-3} s^{-1} wide.

RESULTS

Figures 1 a-c show an example of the variability of the distributions for the month of May between different years.

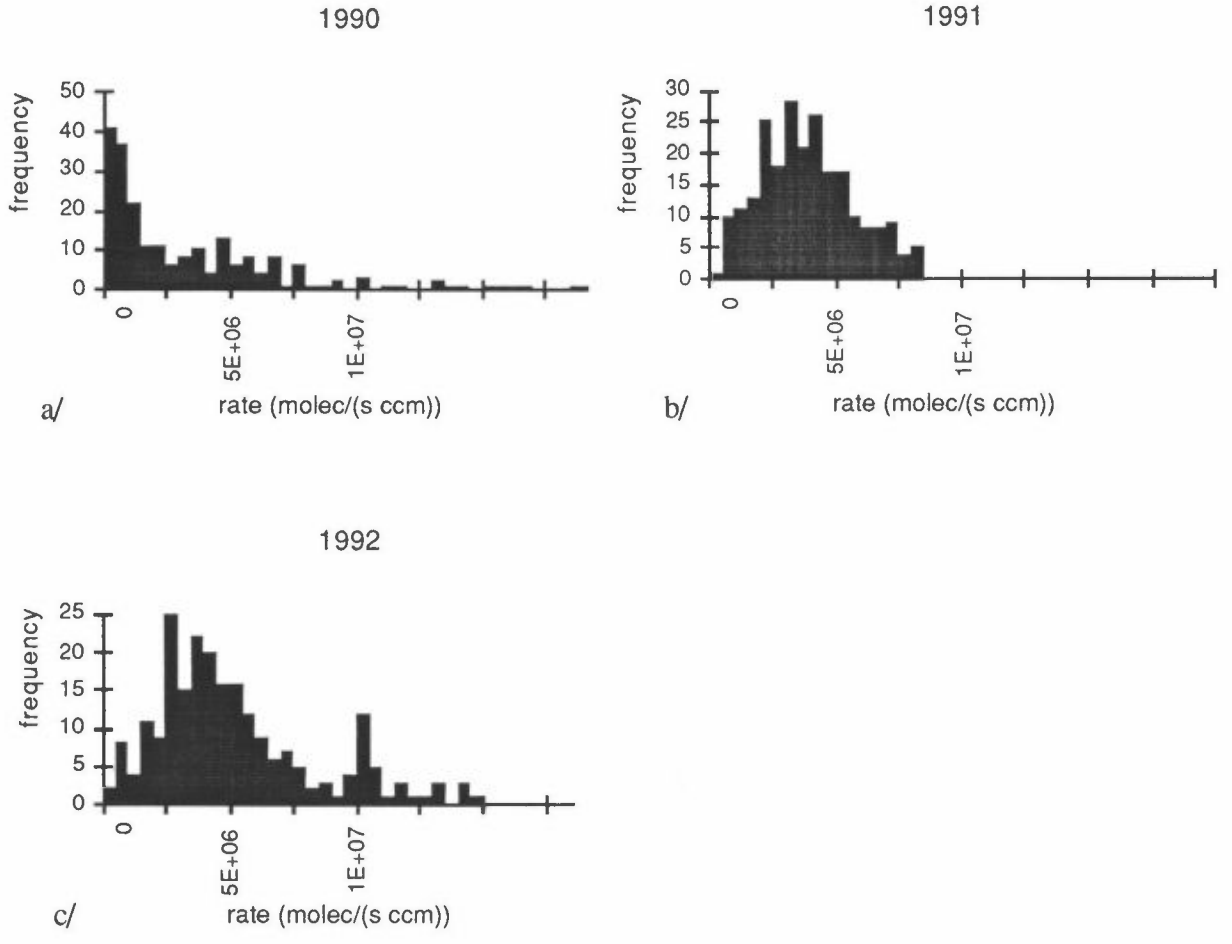

Figure 1a-c. Distribution of NO_3 formation rates for the month of May at "Femman". a/ 1990 b/1991 c/1992. Note that the y-axis scale differ between figures.

It is obvious that the appearance differs and a conclusion close at hand is that the importance of nitrate radical reactions should vary considerably between years. To take out the year-to-year

variation, the comparison between the different months in Figures 2 a-d are presented as combined distributions over three years. Thus, these distributions contain all usable data for the tree-year period. It can be seen that the summer month-distributions have a somewhat higher mean value than the winter distributions. The number of dark hours during winter is however much greater than during summer and counter-balance the somewhat lower ozone

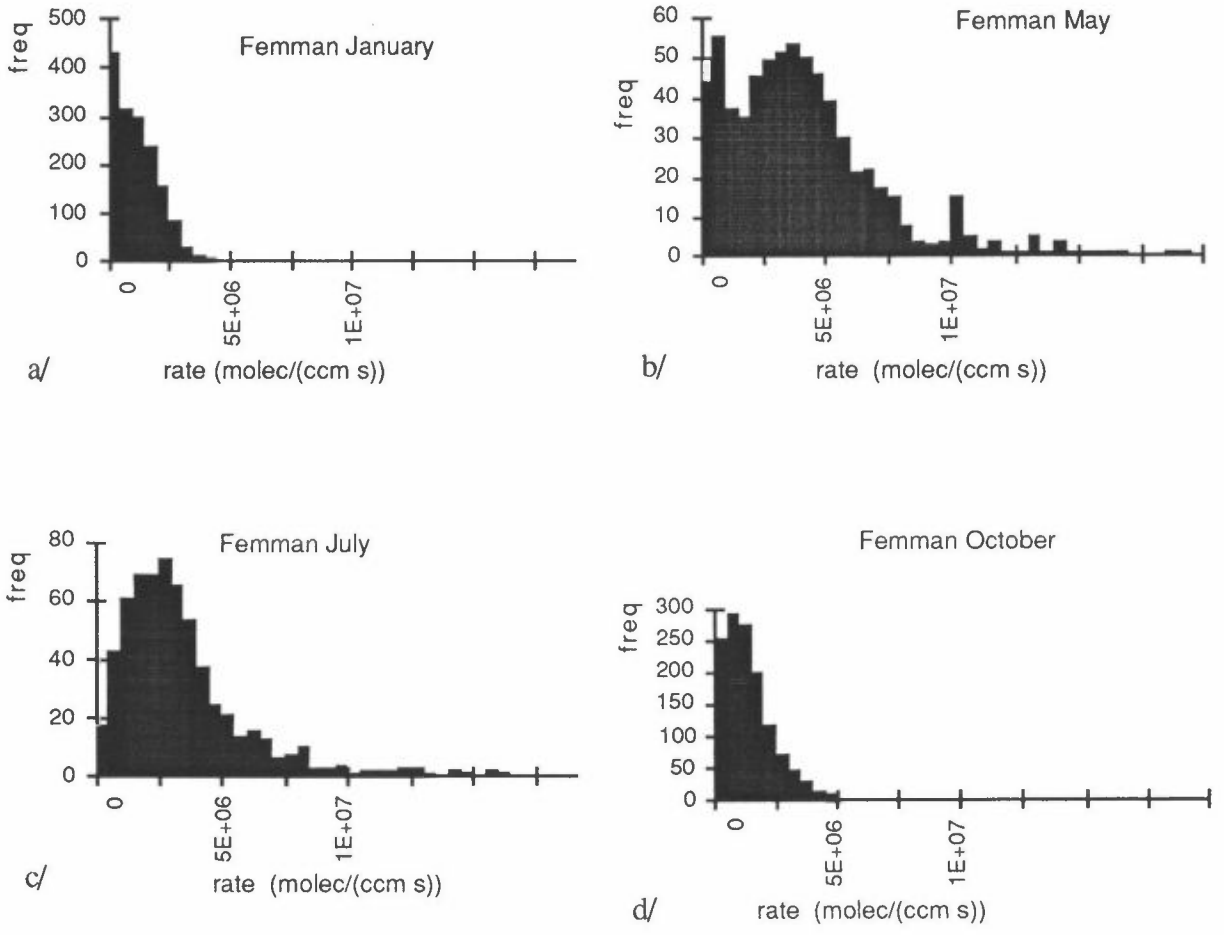

Figure 2 a-d. Additive formation rate distributions over 1990, 1991 and 1992 for January, May, July and October for station "Femman". Note that the y-axis scale differ between figures.

concentrations during winter. The monthly NO_3 dose is a good measure to illustrate the compensation effect between concentrations and dark hours. This quantity is the total number of NO_3 radicals formed per cubic centimetre during a particular month. Since most simple atmospheric reaction rates are linearly dependent on concentration, the dose gives an indication of the total effect expected from a reactant. These numbers are given in Table 1. When the coverage is less than 100%, the dose has been scaled to correspond to 100%. When doses are considered, it is striking how little difference there is between the same month for various years

and between the averages for the various months. The difference between the urban and rural sites is also unexpectedly small.

Table 1. Monthly coverage C (%) and NO_3 dose D ($x10^{12}$ molec. cm^{-3}). The coverage is the percentage of hours actually measured referenced to the theoretical number of available dark hours. (Loss of data may be caused by instrument failure, calibration etc.) The monthly dose is calculated as Σ(formation rate)*(frequency)*3600

FEMMAN

Year	January		May		July		October	
	C	D	C	D	C	D	C	D
90	99.6	2.25	96	2.57	92	2.15	100	2.32
91	100	2.34	100	3.23	100	3.42	100	2.02
92	100	2.24	100	4.27	100	2.52	100	2.14
Average		2.28		3.37		2.72		2.16

ASPVRETEN

Year	January		May		July		October	
	C	D	C	D	C	D	C	D
91	31	0.49	30	0.40	36	0.30	66	0.90
92	76	1.33	85	1.00	46	1.40	85	1.65
Average		1.08		0.81		0.89		1.33

ACKNOWLEDGEMENT

The access to measured data from the Environmental and Health Protection Agency, City of Göteborg and ITM, Luftlaboratoriet, University of Stockholm is gratefully acknowledged.

REFERENCES

[1] R.P. Wayne, I. Barnes, P. Biggs, J.P. Burrows, C.E. Canosa-Mas, J. Hjorth, G. Le Bras, G.K. Moortgat, D. Perner, G. Poulet, G. Restelli and H. Sidebottom, Atmos. Environ. 1991, **25A**, 1.

[2] R. Atkinson, J. Phys. Chem. Ref. Data, 1991, **20**, 459.

[3] W.B. DeMore, S.P. Sander, D.M. Golden, M.J. Molina, R.F. Hampson, M.J. Kurylo, C.J. Howard and A.R. Ravishankara, 1987 Chemical kinetics and photochemical data for use in stratospheric modelling, JPL publication 87-41

Global Warming Potentials for CF_4, C_2F_6 and SF_6

Gunnar Myhre and Frode Stordal
Norwegian Institute of Air Research
Lillestrøm, Norway

Introduction

Global Warming Potentials (GWP) for CF_4, C_2F_6 and SF_6 are calculated. These gases have probably mostly antropogenic sources. CF_4 and C_2F_6 are produced in the aluminium industry and SF_6 is used in magnesium industry and as insulating gas in electrical switch gear. These fully fluorinated gases are stable species and they are not destroyed below the mesosphere. This implies that they have very long lifetimes.

CF_4 and C_2F_6 have probably lifetimes longer than 10 000 years and SF_6 has a lifetime of about 3 200 years. The mixing ratios of the gases are small; CF_4 70-80 ppt, C_2F_6 2-4 ppt and SF_6 2.5 ppt. There are indications of an increase of approximately 2 % per year for CF_4 and 7 % per year for SF_6.

Models

A wide band model (Stordal, 1988; Myhre 1993, NILU-model) and a 2D narrow band model (Shine, 1991) for infrared radiation transfer are used in the calculations. Both models include the major infrared absorbing gases. Overlap between gases are included when more than one gas absorb in a region.

In the NILU-model the water vapor absorption is based on the work of Ramanathan and Downey (1986). Kiehl and Ramanathan (1983), Ramanathan and Dickinson (1979) form the basis for the formulation used for carbon dioxide and ozone respectively. For most of the other trace gases the formulation in Ramanathan et al. (1985) is used. The narrow band model has a higher spectral resolution than the NILU-model. In the narrow band model all absorption bands due to water vapor, carbon dioxide, methane, nitrous oxide, CFC-11 and CFC-12 are incorporated from spectral line data in the Hitran 1986 data base (Rothman et al., 1987). The spectroscopic data for the calculations in both models are taken from MPI Mainz (Isaksen et al., 1992), Varanasi and Chudamani (1988), Ko et al. (1993) respectively for CF_4, C_2F_6 and SF_6.

GWP

The GWP has been developed as a tool to rank the effectiveness of climate gases in terms of the relative contribution of their emissions to the greenhouse effect. The GWP is defined to give the global annually-averaged radiative forcing, as a cumulative measure over a specified time horizon, taking into account the decay of the atmospheric concentration following the emission of the compound. All the GWP-values are relative to a reference gas.

The definition is

$$GWP = \int_o^n a_i \cdot c_i \cdot dt \Big/ \int_o^n a_r c_r dt$$

where a_i is the radiative forcing due to a unit increase in the concentration of trace gas i, c_i is the concentration after the time t and n is the time horizon, the number of years of integration. The denominator contains the corresponding values for the reference gas.

We can see that the lifetime of the trace gas is important for GWP-value as the concentration after the time t is a part of the integral. The radiative forcing, lifetime and time horizon determines the GWP-value.

Radiative forcing

In Figure 1 the radiative forcing from the three species calculated with the NILU-model is shown from 80 degrees south to 80 degrees north for all 12 months. The radiative forcing calculated with the narrow band model is shown in Figure 2. In Figure 2 the radiative forcing is presented for CF_4 and SF_6 for January and July in the northern hemisphere.

The radiative forcing varies for the three fully fluorinated gases. There is also a strong latitudinal variation. The radiative forcing is stronger at lower latitudes than at higher latitudes. For CF_4 the latitudinal variation of the radiative forcing is smaller than for the two other components. This is because CF_4 absorbs in the same long wave region as water vapor, yielding an overlap which maximizes at low latitudes. Clouds are included in the calculations. Clouds reduce the radiative forcing because the cloud tops have lower temperature than the surface. The radiative forcing is reduced differently for the three gases; between 15 % and 40 %.

Results

GWP-values from the NILU-model are calculated to be:

CF_4 : 4 100
C_2F_6 : 8 400
SF_6 : 17 400

with 100 years time horizon and CO_2 as reference gas. The lifetimes of the fully fluorinated gases are extremely long, so the GWP-values increase with increasing time horizon. CO_2, CH_4, N_2O and CFC (direct effect only) are main contributors to the total increased greenhouse effect. The present contribution to the increased greenhouse effect on a global scale for the three fully fluorinated species are about:

CF_4 : 0.6 %
C_2F_6 : 0.07 %
SF_6 : 0.1 %

In e.g. aluminium and magnesium producing countries (as Norway) these gases can have a much larger contribution to the national greenhouse budgets.

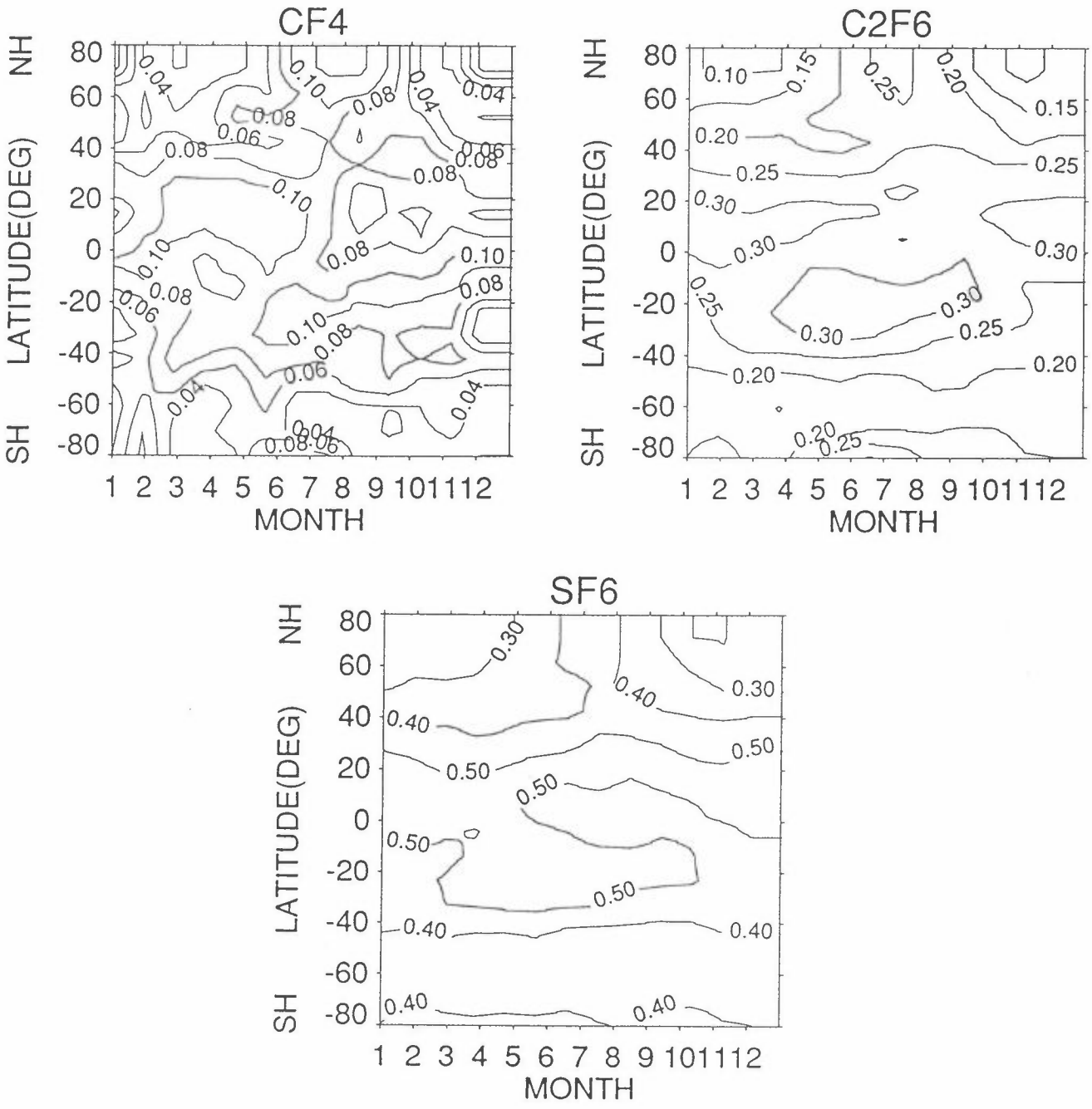

Figure 1: Radiative forcing (W/m²) calculated with the NILU-model from 80 degrees south to 80 degrees north and 12 months, due to 1 ppb of a) CF_4, b) C_2F_6, c) SF_6.

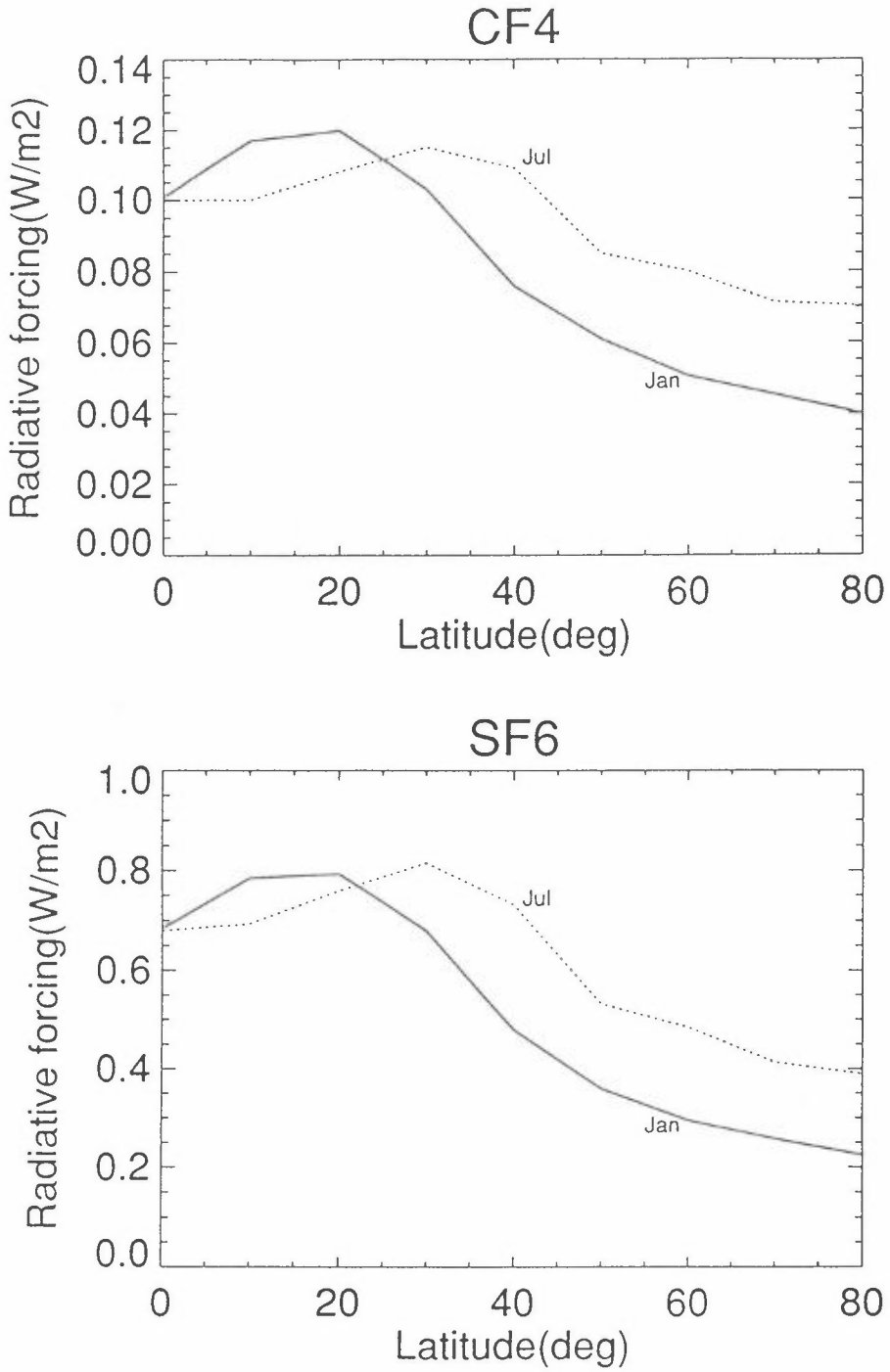

Figure 2: Radiative forcing (W/m²) calculated with the narrow band model for 0-80 degrees north for January and July month, due to 1 ppb of a) CF_4, b) SF_6.

References

Isaksen, I.S.A., C. Brühl, M. Molina, H. Schiff, K. Shine, F. Stordal (1992) An assessment of the role of CF4 and C2F6 as greenhouse gases, Policy Note 1992:6, Center for International Climate and Energy Research - Oslo (CICERO).

Kiehl, J.T., V. Ramanathan (1983) CO_2 radiative parameterization used in climate models: Comparison with narrow band models and with laboratory data, J. Geophys. Res., 88, 5191-5202.

Ko, M.K.W., N.D. Sze, W.-C. Wang, G. Shia, A. Goldman, F.J. Murcray, D.G. Murcray, C.P. Rinsland (1993) Atmospheric sulfur hexafluoride: Sources, sinks and greenhouse warming, J. Geophys. Res., 98, 10499-10507.

Myhre, G. (1993) Overføring av langbølga stråling i atmosfæren: Modellering av skyer, Hovedfagsoppgave.

Ramanathan, V., R.E. Dickinson (1979) The role of stratospheric ozone in the zonal and seasonal radiative energy balance of the earth-troposphere system, J. Atmos. Sci., 36, 1084-1104.

Ramanathan, V., R.J. Cicerone, H.B. Singh, J.T. Kiehl (1985) Trace gas trends and their potential role in climate change, J. Geophys. Res., 90, 5547-5566.

Ramanathan, V., P. Downey (1986) A non-isothermal emissivity and absoptivity formulation for water vapor, J. Geophys. Res., 91, 8649-8666.

Rothman, L.S., R.R. Gamache, A. Goldman, L.R. Brown, R.A. Toth, H.M. Pickett, R.L. Poynter, J.-M. Flaud, C. Camy-Peyret, A. Barbe, N. Husson, C.P. Rinsland, M.A.H. Smith (1987) The Hitran data base: 1986 edition, Appl. Opt., 26, 4058-4097.

Shine, K.P. (1991) On the cause of the relative greenhouse strenght of gases such as the halocarbons, J. Atmos. Sci., 48, 1513-1518.

Stordal, F. (1988) A wide band model for transfer of infrared radiation: Altitude, latitudinal and yearly variation of cooling rates in the troposphere and the stratosphere, Rep. no. 68, Institute for Geophysics, University of Oslo.

Varanasi, P., S. Chudamani (1988) Infrared intensities of some chlorofluorocarbons capable of perturbing the global climate, J. Geophys. Res., 1666-1668.

Atmospheric mercury modelling at IVL

KARIN PLEIJEL AND JOHN MUNTHE
Swedish Environmental Research Institute (IVL)
Box 47086, 402 58 Göteborg, SWEDEN

SUMMARY

A model has been developed, describing the mass transport and chemical turnover of different forms of mercury in the atmosphere. An air parcel including a fog, is simulated during 48 hours, and the influence on dissolved oxidised mercury (Hg(II)) of varying physical and chemical parameters has been studied. Calculations are carried out, using different aqueous phase chemistry schemes for different pH levels. The results show a reduction in the dissolved Hg(II) by 11 to 65% if the SO_2 concentration and emissions are doubled and an increase in dissolved Hg(II) by 20 to 130% when increasing the O_3 concentration by 40% and doubling the NOx and VOC emissions. The total Hg(II) concentration increases by 0 to 57% when doubling the soot concentration. By adding the reaction $Hg^0(aq) + OH(aq) \rightarrow\rightarrow Hg^{2+}(aq)$ the dissolved Hg(II) increased by 5 to 244% depending on which chemical scheme and which pH was used.

MODEL DESCRIPTION

In the model presented here, the only significant redox reactions of mercury are assumed to take place in the aqueous phase. Twelve chemical reactions describing the development of mercury species have been included ([1], [2]), and are identical in all simulations carried out here.

The gas phase chemistry in total is described by 33 species in 79 reactions, mainly following the CBM-IV mechanism ([3], [4]). The aqueous phase chemistry in the reference case, called IVL(Hg) here, is described by 62 species in 98 reactions, of which 18 are chemical equilibria, taken from [5], [6], [7], [8], [9], [10]. The mass transport from the gas phase into the cloud droplet, and vice versa, is assumed to be controlled by gas phase diffusion. The rate of adsorption of oxidised mercury onto particulates within the droplet is assumed to be limited by aqueous diffusion.

This work is focusing on the chemical behaviour of mercury taking place in a fog during 48 hours. The number of physical and meteorological parameters influencing a cloud is minimised in order to focus on a thorough treatment of the chemical process. Other parameters accounted for in the model are emissions, dry deposition, wind speed, temperature and relative humidity.

The three different schemes for aqueous chemistry that have been compared to the IVL(Hg) chemistry are described in detail in [6], called "Jacob" here, [8] and [5], which we have chosen to call "Adewuyi" and "M&M", respectively, in this text.

The Jacob aqueous chemistry scheme includes 98 chemical reactions of which 12 are chemical equilibria. The Adewuyi aqueous chemistry scheme includes 34 chemical reactions of which 15 are chemical equilibria. The M&M aqueous chemistry scheme includes 58 chemical reactions of which 13 are chemical equilibria.

SET OF CASES STUDIED

- The "**+SO_2**" case is described by an increase of initial SO_2 concentration from 1.2 ppb in the standard case to 3.0 ppb in the "+SO_2" case. A doubling of the SO_2 emissions along the trajectory has also been added.
- The "**+O_3**" case is described by an increased initial O_3 concentration from 35 to 50 ppb, plus a doubling of the emissions of NO_x and VOC along the trajectory.
- The "**-HCl**" case indicates that the initial HCl concentration has been changed from 1 to 0.1 ppb.
- The "**+20% sol**" and "**-20% sol**" are two cases where the solar radiation has been increased/decreased by 20%. The standard case simulates clear sky conditions.
- The "**+mixing height**" and "**-mixing height**" cases are carried out by changing the mixing height from the standard value of 600 meters up to 800 and down to 400 meters respectively.
- The "**+soot**" case is described by an increase of the soot concentration from 5 to 10 $\mu g/m^3$.

RESULTS

The percentual change in dissolved Hg(II) for the eight cases, with the four different aqueous chemical schemes used, are shown in figure 1. Where no pH level is indicated, the pH is not set to a constant value, the "no-set-pH" cases. Tests have also been carried out for pH set to a fixed value of 3, 4.5 and 5.2 respectively.

An addition of SO_2 induces a reduction of dissolved Hg(II) independently of aqueous chemical scheme and of pH. The M&M scheme yields some extreme changes as pH is changed, from a 90% decrease of Hg(II) in the no-set-pH and pH=3 cases, to nearly no response in the pH=5.2 case. For the other schemes the decrease range from 11 to 65%. The decrease is caused by an increase in concentration of the complex $HgSO_3$, which spontaneously will decompose forming volatile Hg^0 as an end product. The Hg^0 will be transported out of the droplet due to its low water solubility.

An addition of O_3 both by setting an higher initial value and indirectly by increased emissions of NO_x and VOC, adds to the Hg(II) in all cases studied. The percentual

change varies from 20 to 130%. The explanation is that a higher amount of O_3 available, gives a faster oxidation rate of $Hg^0(aq)$ through a reaction with $O_3(aq)$ which is the initial oxidation step to form Hg(II).

A decrease in HCl results in a decrease of Hg(II) for all schemes and pH:s except the M&M scheme. When the M&M scheme is used a small increase of 1 to 4% in Hg(II) can be seen for all pH values chosen. The other schemes gives a reduction of 6 to 48%.

An increased solar radiation will increase the amount of Hg(II) by 2 to 27%, except when the level of pH is set to 3 for the IVL(Hg) and Jacob schemes. In these two cases a small decrease of 1% in Hg(II) is seen. When the solar radiation is decreased the opposite reasoning is true, and a decreased Hg(II) level of 1 to 72% is found, except in the IVL(Hg) and Jacob at the pH 3 level, where a small increase of 0.4% is observed.

An increased mixing height will, for all cases studied, give an increased level of dissolved Hg(II) in the range 5 to 94%, where the highest values are seen from the pH 4.5 case for IVL(Hg) and Jacob. A decreased mixing height gives the opposite result; a reduction of 9 to 95% is seen. The lowest values are now reached for the M&M scheme with no-set-pH and pH = 3.0. The changes in Hg(II) from a change in mixing height is caused by changes in the dry deposition fluxes of the reactant gases (mainly O_3), which are extremely dependent on the height of the mixing layer. An air parcel in a low mixing layer situation can be almost "emptied" due to dry deposition, while the influence on a high mixing layer is more moderate.

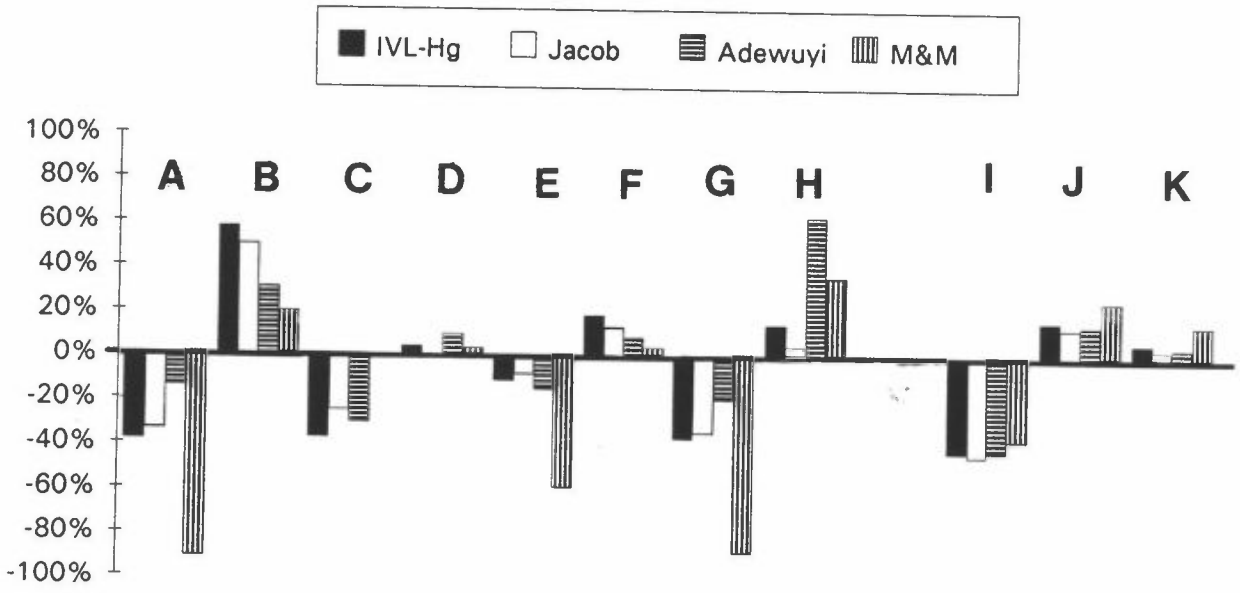

Figure 1. The result of the sensitivity test, as modelled by the four different aqueous phase chemistry schemes described in the text, for the "no-set-pH" case. **A** + SO_2, **B** + O_3, **C** - HCl, **D** + 20% SOL, **E** -20% SOL, **F** + mixing height, **G** - mixing height, **H** +(Hg^0 + OH) **I** -Soot (Hg (ads), **J** + Soot (total Hg)

A soot addition will increase the total amount of Hg(II), which includes dissolved Hg(II) and Hg(II) bound to particles within the droplet, adsorbed Hg(II). This increase is very small for the pH 3 level, and also for the case of M&M, pH = 5.2. The increase varies from 0.3 to 57%. Of the amount of the total Hg(II), the part that is dissolved in the droplet is reduced by 14 to 46%, and the amount adsorbed onto particulates is increased by 9 to 71%. The total increase is caused by an increase in adsorbed Hg(II), while the dissolved Hg(II) is decreased.

When the reaction $Hg^0(aq) + OH(aq) \rightarrow\rightarrow Hg^{2+}(aq)$ is added to the mercury chemistry in the aqueous phase, an increase of Hg(II) is seen in all cases, varying from 5 to 244%. The highest values are reached in the Adewuyi scheme at pH = 4.5 and 5.2.

REFERENCES

[1] Munthe, J. (1992) The aqueous oxidation of elemental mercury by ozone. *Atmospheric Environment* **26A**, 1461 - 1468.

[2] Munthe, J., Xiao, Z. F. and Lindqvist, O. (1991) The aqueous reduction of divalent mercury by sulfite. *Water, Air, and Soil Pollution* **56**, 621 - 630, .

[3] Gery, M. W., Whitten, G. Z., Killus, J. P. and Dodge, M. C. (1989). A photochemical kinetics mechanism for urban and regional scale computer modelling. *J. of Geophysical Res.* **94**, 12,925-12,956.

[4] Dodge, M. C. (1990). Formaldehyde production in photochemical smog as predicted by three state-of-the-science chemical oxidant mechanisms. *J. of Geophys. Res.* **95**, 3635-3648.

[5] Möller, D. and Mauersberger, G. (1992) Cloud chemistry effects on tropospheric photooxidants in polluted atmosphere - model results. *J. of Atmospheric Chemistry* **14**, 153-165.

[6] Jacob, J. D. (1986) Chemistry of OH in remote clouds and its role in the production of formic acid and peroxymonosulfate. *J. of Geophysical Research* **91**, 9807-9826.

[7] Chameides, W. L. and Davis, D. D. (1982) The free radical chemistry of cloud droplets and its impact upon the composition of rain. *J. Geophys. Res.* **87**, 4863-4878.

[8] Adewuyi, Y. G., Cho, S., Tsay, R. and Carmichael, G. R. (1984) Importance of formaldehyde in cloud chemistry. *Atmospheric Environment* **18**, 2413-2420.

[9] Graedel, T. E. and Goldberg, K. I. (1983) Kinetic studies of raindrop chemistry, 1, Inorganic and organic processes. *J. Geophys. Res.* **88**, 10,865-10,882.

[10] Neta, P., Huie, R. E., Ross, A. B. (1988) Rate constants for reactions of inorganic radicals in aqueous solution. *J. of Phys. and Chem. Ref. Data.* **17**, 1027-1284.

Stratospheric Chemistry in a 3-D Global CTM

Markku Rummukainen,
FMI/Sodankylä Observatory, Ilmala, FIN-99600 SODANKYLÄ, FINLAND

Ivar S. A. Isaksen, Frode Stordal
Inst. of Geophysics, Univ. of Oslo, P.O.Box 1022, Blindern, N-0315 OSLO, NORWAY

Abstract

Together with the modelling team at the University of Oslo, FMI has started to work on running a consistent stratospheric chemistry formulation in a global three-dimensional Chemical Transport Model (CTM). So far, the model has been used for studying tropospheric chemistry, especially at high northern latitudes.

The stratospheric chemistry scheme has now been successfully incorporated into the CTM. This presentation will focus on the coupled troposphere-stratosphere formulation of the CTM, and an update on this project will be given, together with some preliminary results.

1. Introduction

Atmospheric modelling is done to learn more about the complex interactions between physics, chemistry and radiation in the atmosphere as a consistent system. Observational approaches in atmospheric studies are more often than not hampered by the inevitable inhomogeneity in observations and their limited spatial and temporal resolution. In modelling, homogeneity in the studied domain is achieved by defining the calculational domain as desired, and in theory, any degree of resolution is available. In practice, however, one has to compromise between the model domain, resolution and computational resources. With a model, it is possible to isolate specific processes and to look at the significance of them, as well as how changes to them might alter atmospheric phenomena. The latter point means that we can extend our scope of view to the future. Predictive capabilities have become more and more important during the last few years, due to the expected global and regional changes in climate.

Atmospheric modelling is done in a number of different formulations, depending on the processes to be studied. As the real atmosphere is a 3-dimensional medium, the 3-dimensional approach is by far the most realistic. This fact is emphasized by the land-sea -contrasts, orography, uneven energy input in the horizontal and the vertical as well as the inhomogeneity in sources for many of the chemically important trace species, which provide the atmosphere zonally asymmetric features and its typical vertical structure. As atmospheric processes span a large scale of temporal and spatial scales, any model can only be an approximation of the real atmospheric system. Clearly, a global 3-D model is computationally more demanding than models operating in fewer dimensions or on a sub domain of the entire globe. The cost of calculations may be kept down in such models by separating dynamics and radiative processes from the chemistry. This is the case in the global 3-D Chemical Transport Model (CTM) in use at the University of Oslo. The model has already proven itself to be a valuable tool in studies of tropospheric chemistry and now it is being extended to incorporate stratospheric chemistry as well.

2. Model description

The CTM has a horizontal grid resolution of 8° by 10°, latitude by longitude, and nine layers in the vertical up to 10 hPa. The latitudinal spacing is made denser at the polar regions, where the longitudinal resolution is conversely reduced in the transport calculations by combining several adjoining grid squares into the so-called extended polar zones. This is done to preserve the stability in the model. In the vertical, sigma coordinates are used, so that the actual amount of mass in a grid box at in a given layer varies from one horizontal location to the next, as well as with time in a given horizontal position, due to the varying surface pressure. Surface pressures are the actual values, so that at e.g. Antarctica, a typical value would be around 600-700 hPa, with the free tropospheric and stratospheric pressures defined by the σ-levels. As the vertical structure of the model is crucial for the differentiating between the troposphere and stratosphere, it is depicted in Figure 1.

	0.000000	10 hPa	10 hPa	10 hPa
9	0.061602	46 hPa	65 hPa	74 hPa
8	0.143737	95 hPa	138 hPa	159 hPa
7	0.251540	158 hPa	234 hPa	271 hPa
6	0.390144	240 hPa	357 hPa	416 hPa
5	0.554415	337 hPa	503 hPa	587 hPa
4	0.728953	440 hPa	659 hPa	768 hPa
3	0.866530	521 hPa	781 hPa	911 hPa
2	0.948665	570 hPa	854 hPa	997 hPa
1	1.000000	600 hPa	900 hPa	1050 hPa
Layer	Sigma		Surface	

Fig. 1. The vertical structure of the CTM. There are nine layers and only the top of the model is fixed at 10 hPa. Actual pressure at any layer is calculated by $\sigma_i(p_{sfc}-p_{top})+p_{top}$. The three right-hand side columns give examples of the pressures in the various layers for surface pressures of 600, 900 and 1050 hPa, respectively.

The CTM has been originally formulated by Prather et al. [1987]. They have also provided the dynamical driver for our work with the necessary meteorological parameters from a two-year run of the NASA GISS Global Circulation Model (GCM) [Hansen et al., 1983]. The GCM has thus provided the global wind fields, wet and dry convection data,

distributions and temporal development of surface pressure, temperature, water vapor and optical thicknesses, all given in the model grid. Horizontal diffusion has also been included in the CTM. The actual transport in the CTM is formulated with a second-order moments method [Prather, 1986], which more than doubles the grid resolution, without leading to excessive increases in computational demands. This amelioration does not extend to chemistry, which is done with grid-box averages. The timestep for advection is one hour with a subdivision into shorter successive steps to simplify calculating the advection.

At present, the model is being used in tropospheric chemistry studies [e.g. Berntsen and Isaksen, 1992]. This formulation includes 46 chemical species or groupings of individual species known as chemical families, 16 photochemical reactions, about 85 other chemical reactions and 10 species with explicit source descriptions. This chemistry package is run embedded in the integration of transport in the CTM with a time step of thirty minutes.

The chemistry of the troposphere and the stratosphere is quite different. Many of the species being released at ground level from natural or anthropogenic sources are not transported to the stratosphere. These include the non-methane hydrocarbons, water-soluble species and species which are sensitive to solar radiation in the near-UV and the visible wavelengths. The stratosphere is characterised by the ozone layer, which interacts with the incoming solar radiation and induces a marked vertical variation in the spectral distribution and photon flux of available radiation. This means that photochemistry has to be accounted for in a different way in the stratosphere than in the troposphere. Species which behave as inert tracers in the troposphere are broken down higher up into reactive fragments so that a whole new set of chemical processes has to be included. Some species are abundant in both the troposphere and the stratosphere, but what is special for the stratosphere is the number of halogenated species, combined with the extreme dryness of the layer.

3. Stratospheric chemistry

The basic formulation of the stratospheric chemistry being added to the CTM is already incorporated in the 2-dimensional global model at the University of Oslo, as well as in 0-dimensional trajectory modelling at NILU [Stordal et al., 1985, Floisand et al., 1993]. The scheme incorporates heterogeneous chemistry on both PSCs and sulfate aerosols [Isaksen and Stordal, 1986, Isaksen et al., 1990]. During its expansion to 3-D, a few reactions have been added to the scheme. At present, the tropospheric chemistry described earlier is still run in the lower layers. The partitioning between the troposphere and the stratosphere at each horizontal grid position is based on the lapse rate and the definition of the tropopause by WMO. On the average, the stratosphere encompasses the topmost 1-3 layers (c.f. Fig. 1).

Coupling between the two chemistries through the tropopause is maintained by the various transport processes. Even though some of the species and reactions are the same in the two chemical schemes, the total number of chemical entities (species or families) has increased to 92 and the number of photochemical reactions to 47. In stratospheric chemistry alone, the number of other chemical reactions is 119. For long-lived gases that reach the stratosphere, constant volume mixing ratios in the lowest layer in the model are applied as lower boundary condition. The various chemical components in the coupled chemistry schemes are listed in Table 1. Photodissociation coefficients have been calculated off-line [Isaksen et al., 1977] for a set of optical thicknesses, which span typical atmospheric conditions.

Table 1. Chemical Species in the Oslo CTM. Tropospheric chemistry applies to the species # 1-46, stratospheric chemistry treats the species #47-92, as well as # 1, 4, 6, 13, 15, 16, 17, 21, 22, 38, 39, 40, 41, 42, 43, 44, 46

1=O_3	2=NO_X	3=NO_Z	4=HNO_3	5=PANX	6=CO
7=C_2H_4	8=C_2H_6	9=C_3H_6	10=C_4H_{10}	11=C_6H_{14}	12=C_6HXR
13=CH_2O	14=CH_3CHO	15=H_2O_2	16=CH_3O_2H	17=HO_2NO_2,	18=CH_3COY
19=CH_3COX	20=ISOPRENE	21=HO_2	22=CH_3O_2	23=C_2H_5O2	24=$C_4H_9O_2$
25=$C_6H_{13}O_2$	26=CH_2O_2OH	27=CH_3COB	28=CH_3X	29=AR1	30=AR2
31=AR3	32=ISOR1	33=ISOK	34=ISOR2	35=HCOHCO	36=RCOHCO
37=CH_3X	38=$O(^3P)$	39=$O(^1D)$	40=OH	41=NO_3	42=N_2O_5
43=NO	44=NO_2	45=O3NO	46=CH4	47=H	48=HNO_2
49=Cl	50=ClO	51=OHCl	52=$ClONO_2$	53=Cl_2	54=OClO
55=Br	56=BrO	57=HBr	58=$BrONO_2$	59=OHBr	60=Br_2
61=ClOO	62=Cl_2O_2	63=BrCl	64=MCF	65=CF_2HCl	66=$CFCl_3$
67=CF_2Cl_2	68=CCl_4	69=CH_3Cl	70=N_2O	71=HCl	72=H_2
73=H_2O	74=MBR	75=H-1211	76=H-1301	77=H-2402	78=F-113
79=F-114	80=F-115	81=HNO_3s	82=H_2Ohet	83=HCls	84=HCFC-123
85=HCFC-141	86=HCFC-142	87=Cl_{xx}	88=NO_xstr	89=SO	90=Cl_y
91=SH	92=Br_y	93=tracer			

Stratospheric chemistry is run with a fifteen minute timestep, embedded in the integration of the transport. With the larger calculational domain, the increased number of species and reactions, as well as modifications of the boundary conditions the model is considerably more expensive to run. Currently, the simulation of one hour in the model takes about a minute of CPU-time with an IBM RS6000/580. The model can be made more efficient by either parallellising or vectorising the code, or some of the processes could be parameterized further. Possibly, the various timesteps could be made longer, so that fewer calculations would be required for a given length of a simulation.

There are also a number of other obstacles, which have to be dealt with, especially with the boundary conditions. A top at 10 hPa is quite artificial, and it does not correspond to a real barrier to transport, so fluxes of many trace gases through it must be parameterised. Fortunately the Oslo 2-D model can provide us with the means to do this with a fair degree of resolution and accuracy. A realistic agreement between the two chemistry schemes in the CTM, especially at their interface at the tropopause, is not self-evident and it must be evaluated very carefully. The parameterization of heterogeneous chemistry in the stratosphere has to be looked into as well. It is sensitive to the distributions of temperature and water vapor. It is quite unlikely that the 3-D CTM would automatically produce the same kind of settings for the heterogeneous processes than the 2-D or the trajectory box model for which this parameterization has been optimized.

4. Selected results

The stratospheric chemistry scheme has now been modified to 3-D and it is now running as a part of CTM in test simulations in Oslo. The early results are promising, even though it is evident that there is yet a lot to be done. In Figure 2, global fields of total ozone from a recent run with the modified CTM are presented. The model was initiated with conditions corresponding to May 1 and the model was run for four months. Tropospheric chemistry was started from 3-D fields, which had been saved from an earlier run with tropospheric chemistry only. For the stratospheric initial fields, latitude-altitude species distributions for the same season were extracted from the Oslo 2-D model and these were then spread zonally

in the stratosphere of the CTM. The zonal inhomogenities apparent in Fig. 2a, the initiated state of the CTM before the integration began, are due to the three-dimensionality of the tropospheric fields, as well as the nature of the sigma coordinates in the vertical. As can be seen from Fig. 2, the distribution of total ozone is in qualitative accordance with observations. However, the model is underestimating the global average, as well as the amount of ozone in the tropics. Possible reasons for this are the crude estimation of the residual column above the model top and the parametrization of the vertical flux through the model top. For this run, fluxes at the middle of the topmost gridboxes were used to keep the calculations more simple. Spesifying the fluxes at 10 hPa may improve the results.

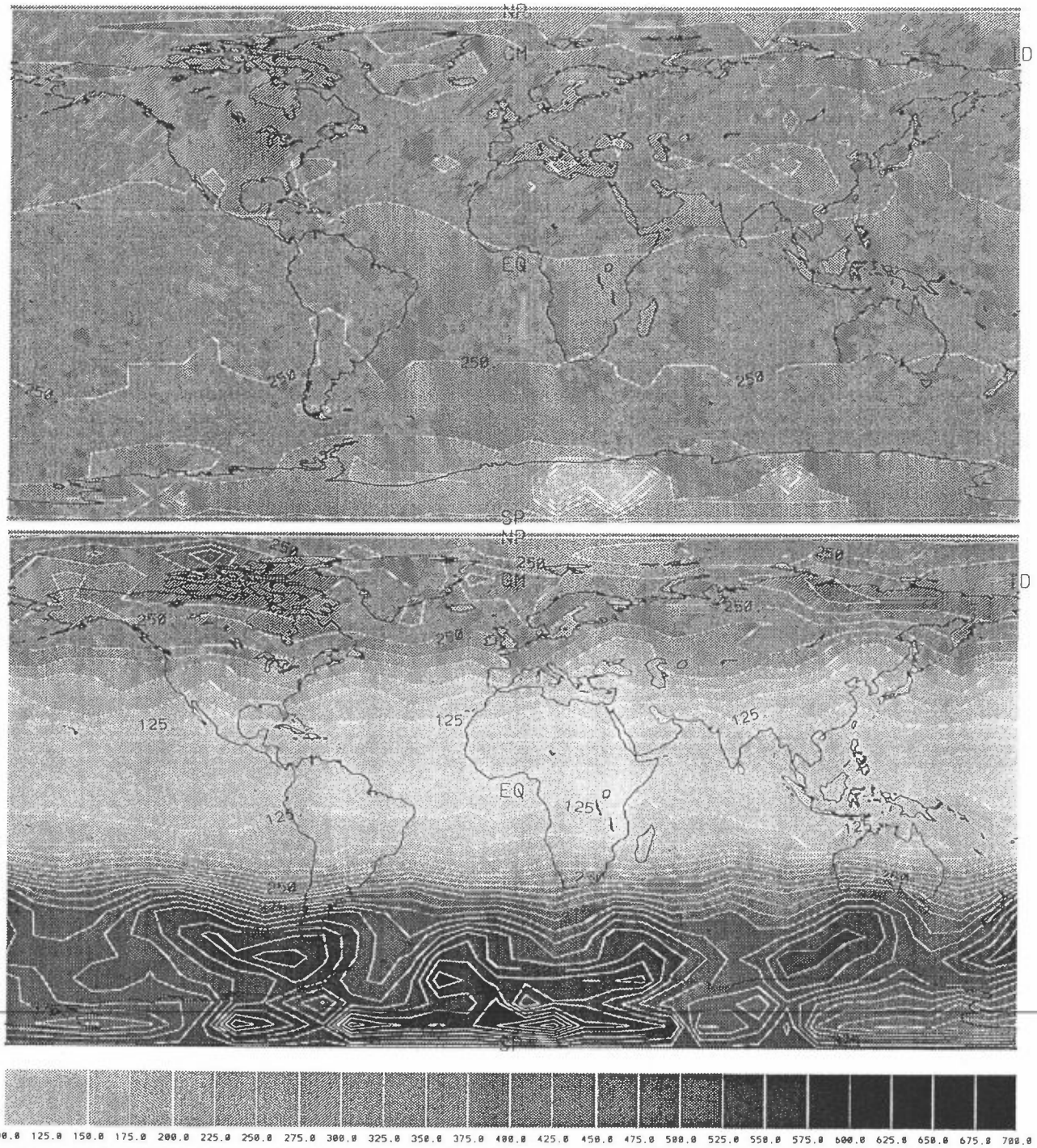

Figure 2. Total Ozone [DU], integrated column up to 10 hPa and estimated residual, a) Model initialisation on May 1, b) After four months of simulation, August 29.

5. Future developments

At present the framework provided by the GISS/GCM and the Oslo CTM is crude for stratospheric studies, especially when it comes to the vertical resolution. Having only a fixed, although temporally varying, set of the dynamics is also a limitation. A separate model version that uses products from ECMWF as a dynamical driver is currently being developed. This will also permit upgrading both the horizontal and the vertical resolution in the CTM, which will produce a model having 19 layers in the vertical, 5-7 of which will be in the stratosphere. The top will still be at 10 hPa. The actual choice for the horizontal spacing will depend on how effectively the code can be optimized, but it will most likely be in the range of 2.9-1.9° (T42 or T63). The possibility to use data from ECMWF will also mean that the simulations will correspond to actual, as opposed to climatic, atmospheric conditions.

Acknowledgements. We would like to acknowledge the rest of the team at the Institute for Geophysics for their help with the CTM. Financial support to this work has been received from the Academy of Finland, the Nordic Council of Ministers and NorFA.

References

Berntsen, T., and I. S. A. Isaksen, 1992, Ozone Formation During an Episode over Europe: A 3-D Chemical/Transport Model Simulation, *Proc. Quadr. Ozone Symp. 1992,* Charlottesville, Virginia, USA.

Floisand, I., F. Stordal, and G. O. Braathen, 1993, Chemical ozone depletion at Bear Island during the winter and spring of 1992 and 1993. *Poster presented at the NATO ASI on Low Temperature Chemistry of the Atmosphere,* Maratea, Italy, 30 August - 11 September, 1993.

Hansen, J., G. Russell, D. Rind, P. Stone, A. Lacis, S. Lebedeff, R. Ruedy, and L. Travis, 1983, Efficient three-dimensional global models for climate studies: Models I and II, *Mon. Weather Rev., 111,* 609-662.

Isaksen, I. S. A., K. H. Midtboe, J. Sunde, and P. J. Crutzen, 1977, A simplified method to include molecular scattering and reflection in calculations of photon fluxes abd photodissociation rates, *Geophysica Norvegica, 31,* 11-26.

Isaksen, I. S. A., and F. Stordal, 1986, Antarctic Ozone Depletion: 2-D Model Studies, *Geophys. Res. Lett., 13,* 1327-1330.

Isaksen, I. S. A., B. Rognerud, F. Stordal, M. T. Coffey, and W. G. Mankin, 1990, Studies of Arctic Stratospheric Ozone in a 2-D Model Including Some Effects of Zonal Asymmetries, *Geophys. Res. Lett., 17,* 557-560.

Prather, M. J., 1986, Numerical Advection by Conservation of Second-Order Moments, *J. Geophys. Res., 91,* 6671-6681.

Prather, M., M. McElroy, S. Wofsy, G. Russell, and D. Rind, 1987, Chemistry of the Global Troposphere: Fluorocarbons as Tracers of Air Motion, *J. Geophys. Res., 92,* 6579-6613.

Stordal, F., I. S. A. Isaksen, and K. Horntveth, 1985, A Diabatic Circulation Two-Dimensional Model With Photochemistry: Simulations of Ozone and Long-Lived Tracers With Surface Sources, *J. Geophys. Res., 90,* 5757-5776.

BIOGENIC VOC EMISSIONS IN EUROPE : MODELLING THE IMPLICATIONS FOR OZONE CONTROL POLICIES.

David Simpson

EMEP MSC-W
The Norwegian Meteorological Institute
P.B. 43 Blindern, N-0313 OSLO, Norway

SUMMARY

Meteorological data from the EMEP MSC-W ozone model have been used together with several biogenic VOC algorithms to generate estimates of the emissions of isoprene from European forests and agricultural crops over several summer periods. All of these estimates are subject to considerable uncertainty; factors of 5-10 uncertainty are not unlikely for episodic ozone calculations.

The implications of these uncertainties for the results of control strategy evaluations in Europe have been assessed with the EMEP MSC-W ozone model. The model results suggest that uncertainties in isoprene emissions are not very important for the evaluation of long-term ozone scenarios in Europe, but must be considered for episodic ozone events.

1. Introduction

This paper summarises the most important findings of a study to evaluate the likely magnitude of isoprene emissions in Europe, and to explore the importance which uncertainties in these emissions have for model predictions concerning the effects of man-made emission control. The study consists of 2 parts. Firstly, we have estimated isoprene emissions with a number of isoprene-temperature-emissions algorithms available from the literature, in order to get an idea of the magnitude of these emissions and their uncertainties. Secondly, we have conducted modelling studies which allow for the possibility of isoprene emissions a factor of 5 higher than our "best-estimate" gives. Details of this study can be found in Simpson (8).

2. Natural VOC Emission Estimates for Europe

Biogenic isoprene emissions have been calculated over the summer period April-Sept. 1989 using meteorological data (temperature, radiation) from the EMEP MSC-W ozone model, forest-coverage and biomass data mainly derived from Veldt (11,12) and Lubkert & Schöpp (4), and the emissions-temperature-sunlight relationships illustrated in Fig. 1. In this Figure, G91 refers to the formulii of Guenther et al. (2), BEIS refers to the emissions formulii from the Biogenic Emission Inventory System (5), and old-PHOXA/EMEP refers to the emission curves used in the early PHOXA project (1), and previous EMEP modelling work (6,7). For the G91 and BEIS formulii, we have calculated emissions both with and without the use of a the BEIS forest canopy model which calculates leaf temperature and radiation throughout a canopy (3,5). Where a forest canopy model is not used, we assume that leaf temperature and sunlight are equal to ambient values.

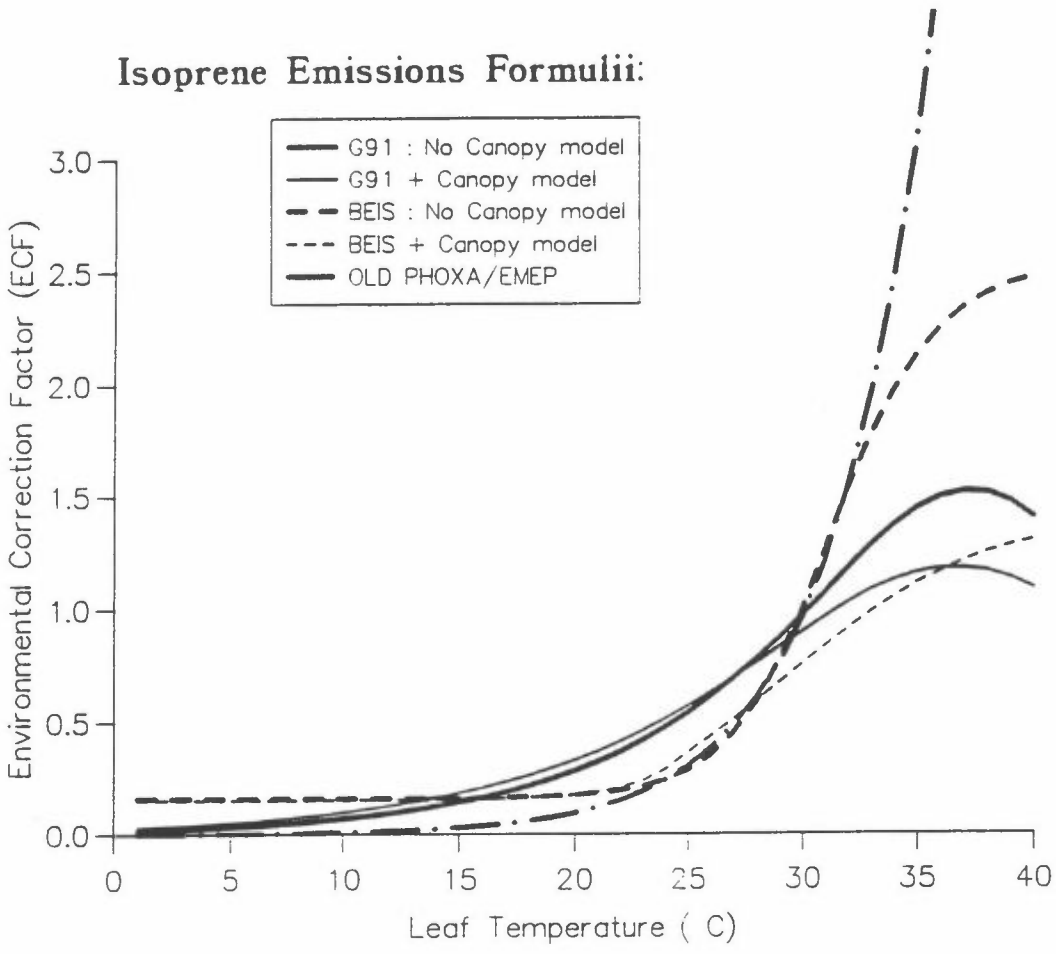

Fig. 1. The variation of isoprene emissions with temperature for 5 different formulii.

Table 1 illustrates the total isoprene emissions for 1989, as calculated by these different methods, including the isoprene emissions estimated with the previous EMEP methodology (6,7). Man-made VOC emissions for 1989 are also shown for comparison. On a yearly basis we see that the man-made emissions substantially exceed biogenic VOC in all countries except Turkey. However, as shown in previous EMEP work, on a monthly basis this is not always true, so that isoprene emissions in countries like Spain exceed man-made VOC emissions during the summer months (6,7).

Comparing either the BEIS or G91 methodologies with the old-PHOXA/old-EMEP methodologies, we see that in most cases the different estimates are within a factor of 2. The biggest difference occurs for the U.K, and this can be simply ascribed to the inclusion of some Spruce trees as isoprene emitters (8).

However, Table 1 illustrates only uncertainties relating to choice of formulii. In addition, we should also allow for problems related to transferring North American data to Europe, difficulties in specifying correct leaf-temperatures and radiation values, and not least the lack of good data on forest coverage for different species. It seems that a factor of 500% is not unlikely for these annual average European estimates. In episodic conditions, accuracy can be expected to be substantially poorer, and possibly of a factor of 10.

3. Modelling the implications of biogenic VOC for control strategies

The EMEP MSC-W ozone model has been designed for the assessment of possible emissions control strategies in Europe (6,7,9). In view of the uncertainties in our knowledge of biogenic emissions discussed above, we have conducted a number of experiments to evaluate the importance of biogenic emissions for such emissions control strategy evaluations. We have re-run the latest version of the EMEP model (10) over the period April-Sept. 1989, with the following 4 "base-cases", where a base-case refers to a run without any control of the man-made NO_x or VOC precursors :

Normal Isoprene: Isoprene emissions are estimated using the Guenther et al. (1991) formula (G91). We use the non-canopy version in the model runs.

High Isoprene : Isoprene emissions as generated for the "normal isoprene" case above are multiplied by a factor of 5, in order to investigate the possibility that isoprene emissions are significantly greater than those calculated in the normal case.

No Isoprene : We assume zero isoprene emissions, in order to investigate the possibility that isoprene emissions are significantly lower than assumed in our normal case.

No soil Nitrogen : We assume zero emissions of nitrogen from soils. Isoprene emissions are as calculated in the normal case.

For each of these base-cases we have calculated the effects which 50% reductions in NO_x or man-made VOC emissions have on ozone levels over the summer period. In order to simplify the analysis we consider below changes in ozone concentration along a cross-section of the EMEP grid (with EMEP x-coordinate=19), from S.W. Spain to N.W. Russia, and passing through areas of high and low NO_x and biogenic VOC concentrations.

Mean Ozone

In Fig. 2(a) we have plotted the percentage reductions in 6-monthly mean ozone predicted to arise from a 50% reduction in man-made VOC emissions, for each of the biogenic emissions scenarios discussed above. The corresponding results for 50% man-made NO_x control are illustrated in Fig. 2(b).

It is clearly seen that although the choice of biogenic emission level has some consequence for the predicted response of ozone to the man-made control measure, the differences are rather small in nearly all areas. In fact, the only significant difference appears for NO_x control in southern Spain, in which case the assumption of high isoprene emissions would lead to a 50% greater reduction in ozone than in the normal isoprene case.

The explanation for these results is probably rather simple. In those countries where natural VOC emissions are substantial compared to the man-made VOC, the concentrations of NO_x are rather low (<1 ppb). The ozone formation is thus usually NO_x limited, and rather insensitive to the ambient VOC concentrations. On the other hand, in those countries where ozone formation is strongly dependent on VOC emissions, eg. Belgium/the Netherlands, the natural VOC emissions are much lower than the man-made VOC emissions, whichever algorithm we use.

Maximum Ozone values

The effects of 50% NO_x and 50% man-made VOC reduction on the maximum ozone values along our cross-section are shown in Figures 3(a),(b). It is clearly seen that the choice of isoprene emissions levels has a substantial effect on our predictions concerning maximum ozone concentration.

Analysis of these changes has proven to be rather complicated because of the possibility of ozone maxima occurring on different days in the different base-cases and also in the control strategy runs. For example, for the grid square labelled BE (Belgium), the maximum ozone value predicted in the NO_x control scenario occurred on a completely different day to that of both the base-case and the high-isoprene case. The important conclusion is that the effectiveness or not of emissions control cannot then be predicted by a consideration of the chemistry occurring at the time of the base case maxima, but rather only by long-period modelling over the summer period.

Acknowledgements

Thanks are due to Dr. Thomas Pierce (US-EPA) for sending the code for the BEIS forest canopy model, and for useful discussions. Thanks also to Dr. Nick Hewitt (Lancaster University, UK) and Chris Veldt (TNO, NL) for helpful discussions. The chemical mechanism used for these studies has been substantially revised, with valuable help from Dr. Y. Anderssen-Sköld (IVL, Sweden) and Dr. M. E. Jenkin (AERE, UK).

References

(1) Builtjes, P.J.H, Stern, R.M., and Reynolds, S.D. (1988). The use of a photochemical dispersion model for several episodes in North-Western Europe. In *Air pollution modelling and its application VI*, Ed. H. van Dop, Plenum Press, New York, 1988, pp 431-450.

(2) Guenther, A.B., Monson, R.K., and Fall, R. (1991) Isoprene and monoterpene rate variability: observations with Eucalyptus and emission rate algorithm development. *J.Geophys. Res.*, **96**, No. D6, 10 799-10 808.

(3) Lamb, B., Gay, D., Westberg, H. and Pierce, T.E. (1993) A biogenic hydrocarbon emission inventory for the U.S.A. using a simple forest canopy model. *Atmos. Environ.*, **27**, No. 11, 1673-1690.

(4) Lubkert, B. and Schöpp, W. (1989) A model to calculate natural VOC emissions from forests in Europe. International Institute for Applied Systems Analysis . Working paper WP-89-082

(5) Pierce, T.E. and Waldruff, P.S. (1991). PC-BEIS: a personal computer version of the biogenic emissions inventory system. *J. Air & Waste Management Assoc.*, **41**, No. 7, 937-941.

(6) Simpson, D. (1993) Photochemical model calculations over Europe for two extended summer periods: 1985 and 1989. Model results and comparisons with observations. *Atmos. Environ.* **27A**, No. 6, 921-943.

(7) Simpson, D. (1992) Long period modelling of photochemical oxidants in Europe. Calculations for July 1985. *Atmos. Environ.* **26A**, No. 9, 1609-1634.

(8) Simpson, D. (1993) Biogenic VOC emissions in Europe: implications for ozone control strategies. Presented in "Regional Photochemical Measurements & Modeling Studies", A&WMA Conference, November 8-12, 1993, San Diego, California. To be submitted, J.Geophys. Res.

(9) Simpson, D. and Styve, H. (1992) The effects of the VOC Protocol on ozone concentrations in Europe. EMEP MSC-W Note 4/92.

(10) Simpson, D., Andersson-Sköld, Y., and Jenkin, M. (1993) Updating the chemical scheme for the EMEP MSC-W model: current status. EMEP MSC-W Note 2/93.

(11) Veldt, C. (1989) Leaf biomass data for the estimation of biogenic VOC emissions. Apeldoorn, The Netherlands, MT-TNO Report 89-306.

(12) Veldt, C. (1991) The use of biogenic VOC measurements in emission inventories. Apeldoorn, The Netherlands, MT-TNO Report 91-323.

Table 1. Comparison of Isoprene emission estimates, 1989

Emissions have been calculated using either the Guenther et al. (1991), BEIS or old-PHOXA/old-EMEP emission curves. Estimates made using a forest canopy model are labelled CPY. Estimates without the canopy are labelled N-CPY. Units ktonnes a^{-1}

Country[1]	Guenther et al.		BEIS		Old	man-made
	CPY	N-CPY	CPY	N-CPY	PHOXA/EMEP[3]	VOC
Albania	14.7	14.9	10.3	11.0	16.6	33
Austria	10.8	15.3	8.4	13.1	11.2	408
Belgium	10.3	12.6	7.4	10.1	6.6	335
Bulgaria	51.4	54.4	36.2	40.5	49.0	167
Czechoslovakia	23.8	30.9	17.0	23.6	25.0	294
Denmark	1.1	1.5	1.2	1.7	0.9	176
Finland	17.0	31.8	15.2	30.1	30.7	208
France	231.0	265.6	164.4	209.0	127.0	1972
German Dem. Rep	7.5	9.7	5.5	7.8	13.4	1050
Germany, F.R.	31.2	40.3	23.2	32.0	41.5	2536
Greece	55.2	58.3	36.1	38.1	46.0	185
Hungary	28.8	32.9	20.0	25.2	33.0	205
Iceland	0.0	0.0	0.0	0.0	0.0	8
Ireland	0.8	1.1	0.8	1.1	0.3	90
Italy	95.2	104.7	68.2	82.5	96.3	1642
Luxembourg	0.6	0.7	0.4	0.6	0.9	13
Netherlands	2.3	2.8	1.7	2.2	3.2	442
Norway	7.4	12.9	9.1	17.6	7.3	216
Poland	15.7	19.3	11.3	14.9	34.6	982
Portugal	74.3	86.9	52.0	73.9	57.1	149
Romania	56.1	63.7	40.0	48.6	67.0	386
Spain	277.9	322.3	199.9	282.1	371.0	897
Sweden	27.4	47.0	28.2	53.2	24.7	460
Switzerland	1.7	2.3	1.4	2.1	4.3	305
Turkey	371.3	400.4	238.7	260.3	204.8	263
USSR[2]	581.5	860.4	415.9	671.9	1461.4	8156
United Kingdom	7.4	10.6	6.9	11.1	1.9	1986
Yugoslavia	62.8	67.0	45.4	52.3	152.3	290

Notes :
(1) Political units are defined after those existing at the time of the modelling run, ie. 1989.
(2) European part of the U.S.S.R.
(3) Old-EMEP emissions, as calculated in Simpson, (7).

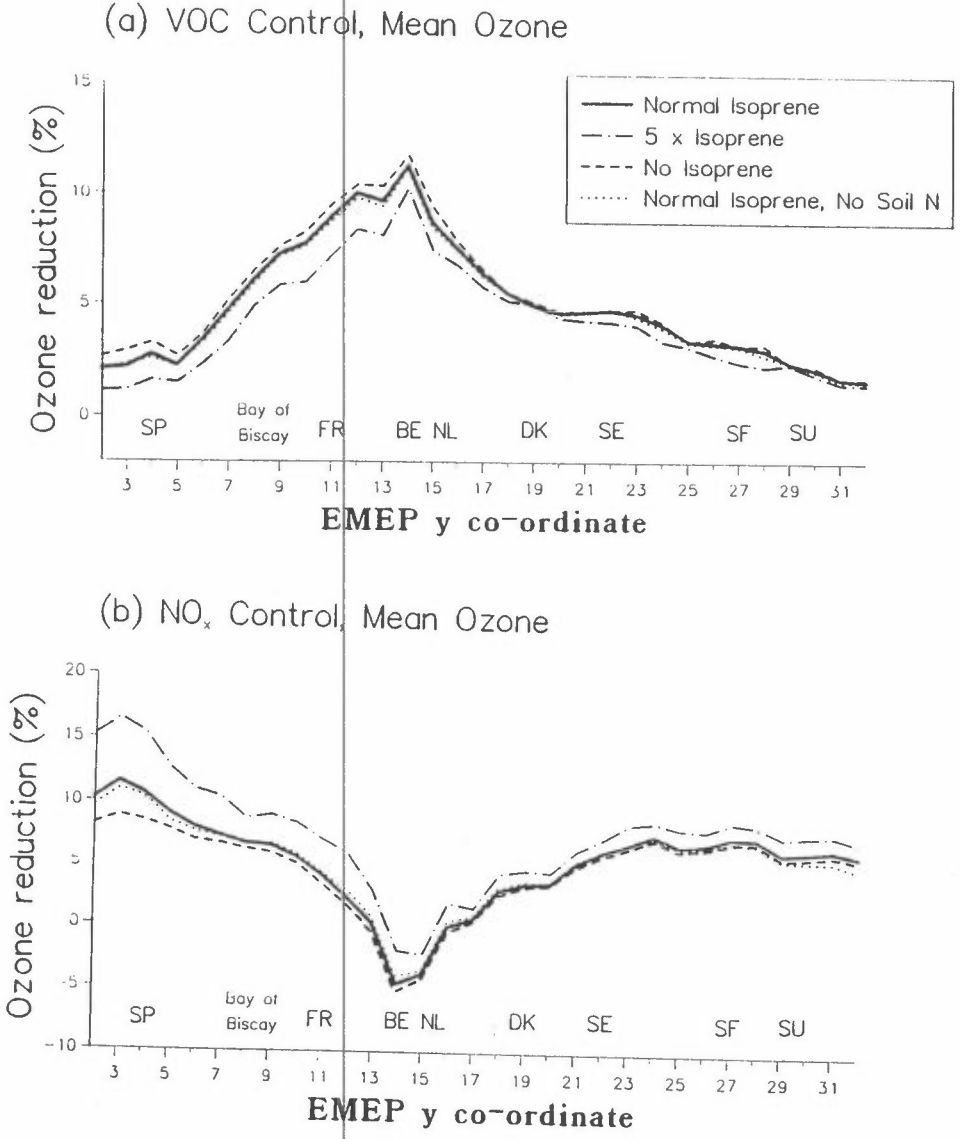

Fig. 2. Effect of (a) 50% VOC and (b) 50% NO_x emissions control on the mean of daily maximum ozone concentrations for April-September 1989, calculated along a cross-section of the EMEP grid from S.W. Spain to N.W. Russia. Calculations are performed with 4 different assumptions concerning biogenic emissions of VOC and NO_x. In each case, only man-made emissions have been controlled in the emission scenario.

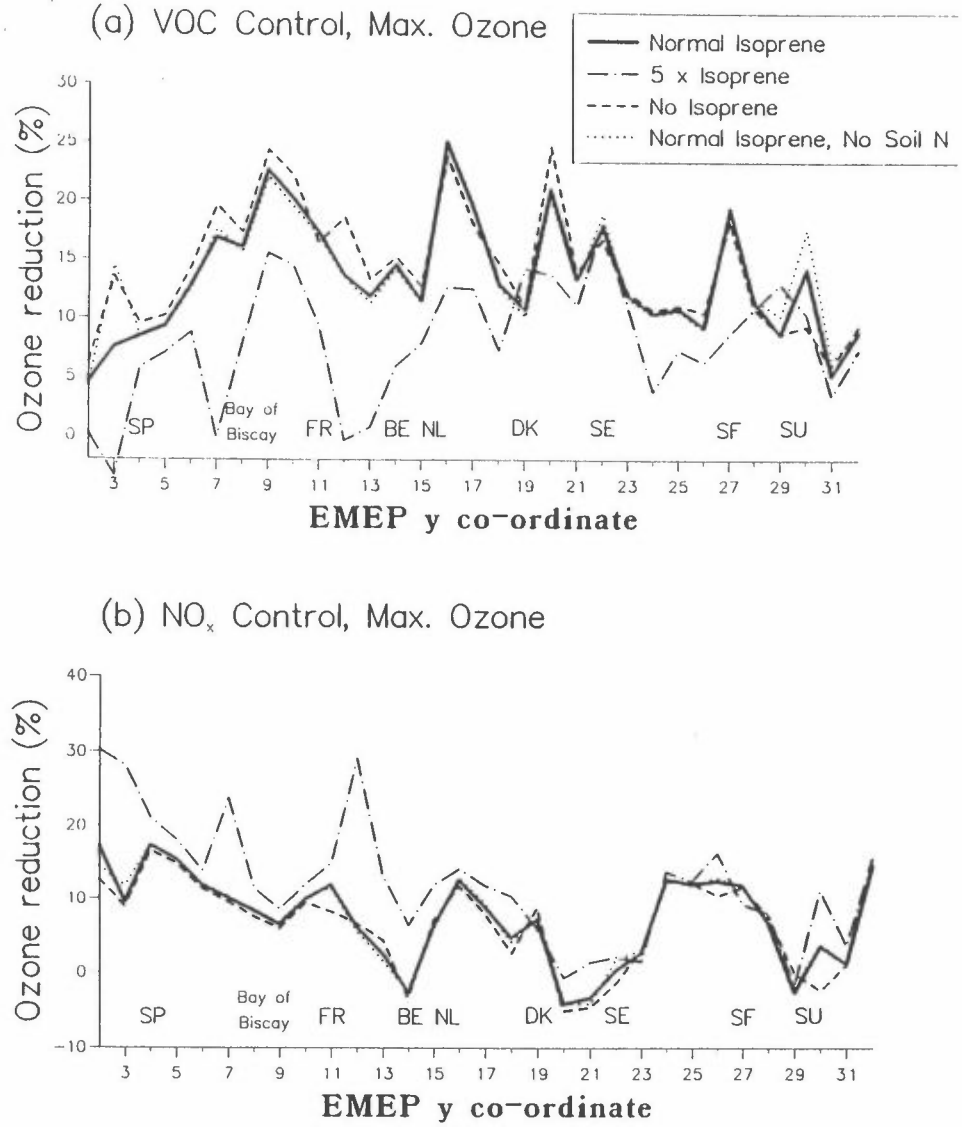

Fig. 3. Effect of (a) 50% VOC and (b) 50% NO_x emissions control on the maximum ozone concentrations during April-September 1989, calculated along a cross-section of the EMEP grid from S.W. Spain to N.W. Russia. Calculations are performed with 4 different assumptions concerning biogenic emissions of VOC and NO_x. In each case, only man-made emissions have been controlled in the emission scenario.

A TWO-DIMENSIONAL GLOBAL STUDY OF THE TROPOSPHERIC OZONE PRODUCTION

ASBJØRN STRAND AND ØYSTEIN HOV

Geofysisk Institutt, Universitetet i Bergen, Allégt. 70, N-5007 Bergen, Norway

SUMMARY

The ozone production in the troposphere has been studied by means of a zonally averaged model which consists of a two-dimensional transport model, a description of the emissions, wet and dry deposition and chemical processes of importance for the ozone production in the troposphere. The transport model describes a closed circulation in the meridional plane below 10 hPa, and has a resolution and a numerical solution which compares favourable with earlier 2-D studies. The transport model also takes into account the fast vertical mixing in convective clouds and in frontal circulation. The production of nitrogen oxides by lightning has been coupled to the convection parameterization by assuming that the nitrogen oxides are transported vertically in the thunder clouds and released at the altitudes where boundary layer air entrained in the convective cells is released. Comparisons with observations indicate that the model is able to reproduce the seasonal variation of ozone in the meridional plane quite realistically. The calculated distributions of the chemical species which determine tropospheric ozone also compare well with measurements. A few simple experiments demonstrate the potential of the model as a tool to investigate the effect of emission reduction strategies. A 2-D model can never simulate the real atmosphere as realistic as 3-D models, but the complexity of the chemical reaction scheme combined with the possibility of cheap integrations over periods of several years, make the results from such models interesting for environmental policies.

1. MODEL DESCRIPTION

The conservation of mass in the meridional plane of p chemical species can be expressed on the general form

$$\frac{\partial c_i}{\partial t} = L\,c_i + f_i(c_1,\ldots,c_p) + E_i - D_i - W_i \qquad (1)$$

where c_i, i=1,...,p is the number density of the components, L is the zonally averaged differential operator determining the transport in the meridional plane, f_i is the chemical formation and depletion rate of species i, E_i is the rate of change in concentration due to emissions of species i, and D_i and W_i rate of change in concentration due to dry and wet deposition respectively, of species i. In the present model study the contribution from each

of these terms is calculated separately by operator splitting. The transport of the chemical compounds in the atmosphere is described by the two-dimensional zonally averaged transport model of [1]. This model uses a horizontal resolution of 75 equally spaced latitude points from pole to pole and a vertical resolution of 33 equally spaced pressure levels from 1000 to 10 hPa, which is a resolution comparing favourably with earlier 2-D studies of tropospheric chemistry.

The change of concentrations due to chemical reactions is calculated separately in each grid-box using a chemical scheme involving 44 chemical species and 126 chemical reactions. The chemical mechanism is similar to that used by [2] for long-period modelling of photochemical oxidants in Europe, but the chemistry of the organic peroxy radicals and nitrogen oxide is somewhat extended. Wet and dry deposition are taken into account for the same species as in [3], using the same dry deposition velocities at 1 m, and the same water solubilities. The model in [3] calculates diurnal averages, while the present model uses chemical reaction rates and dry deposition rates depending on time of day as described by the actual zenith angle. The dry deposition rate is limited by the vertical diffusion coefficient in the planetary boundary layer, and this is assumed to be proportional to cosine of the zenith angle in this model. The wet deposition fluxes are estimated using the observed latitudinal precipitation rates from [4]. Vertical and latitudinal liquid water content in the troposphere for four seasons are available from the zonally averaged cloud data from [5], and the vertical profiles of precipitation formation are estimated from these data assuming proportionality between the precipitation formation rate and the liquid water content in the clouds.

The emission inventory used here is taken from [3], but with a different grouping of the hydrocarbons. Moreover, the production of NO_x by lightning is described by a new strategy in the present study. As described in [1], two data sets dependent on latitude and season determine the fast vertical mixing by convective and frontal activity. The first is the flux of air out of the planetary boundary layer due to this activity, and the second, the detrainment profiles, determine the destination altitudes of this air. The NO_x produced from lightning is transported vertically and released at the altitudes of the outflow layers of the thunder clouds [6]. The altitudes of this outflow are described by the detrainment profiles. Therefore, in the present study the NO_x produced from lightning is released in the vertical model layers as described by the detrainment profiles for the convective

parameterization. Whether the NO_x is produced at these altitudes or not, the fast vertical transport and the low photochemical activity inside the dark convective clouds indicate that little NO_x is oxidised before it is detrained. Releasing the NO_x directly at the altitudes of outflow should therefore be reasonable.

The ozone transport from the stratosphere is estimated to be of the same order of magnitude as the tropospheric production of ozone [7] and is therefore important for the ozone distribution in the troposphere. For this flux to be reasonable in the model, the distribution of ozone in the stratosphere must be realistic. The ozone production from the reaction between molecular oxygen and ground state oxygen atoms formed by photolysis of molecular oxygen is not described in the model, but is parameterized by fixing the mixing ratio to the observed level in the highest model layer. The mixing ratios at ~25 km are available from satellite observations, and at steady state the model will be adjusted to these prescribed values.

2. MODEL RESULTS

The calculated meridional distribution of the concentration of ozone is given in Figure 1. It can be seen how the ozone produced in the stratosphere is transported downward. The transport of ozone from the stratosphere to the troposphere is stronger per unit area in high latitudes than in the tropics due to the dominant upward transport of air in low latitudes and the corresponding descending of air at high latitudes. Particular over the winter pole significant amounts of ozone are transported down in the troposphere. Ozone is also produced photochemically in the troposphere by processes different from those in the stratosphere. In sunlight NO_2 is dissociated to form NO and $O(^1P)$ (Reaction J_3). As in the stratosphere, the ground state oxygen atom immediately reacts with O_2 to form ozone. The rate of the ozone production therefore depends on the ratio NO_2/NO, which again depends on the access of organic peroxy radicals. The average characteristic time for removal of ozone by dry deposition in the boundary layer is less than one week, while the transport time from high to low latitudes is more than a month. But in the figure the high latitude mixing ratio is never more than about a factor 2 higher than the low latitude mixing ratio, indicating a significant production of ozone in the lower troposphere.

The ozone budgets for the troposphere as predicted by the model are given in Table 1. The annually averaged ozone production on the northern hemisphere is $16.6 \cdot 10^{10}$ molecules/cm^2 s, on the southern hemisphere $5.1 \cdot 10^{10}$ molecules/cm^2 s, and the annually and globally averaged stratospheric injection is $4.1 \cdot 10^{10}$ molecules/cm^2 s, which corresponds well with other estimates [8].

The importance of the anthropogenic emissions for the tropospheric ozone production can be quantified by some simple model experiments. Two different emission reductions have been tested in the model, a 50% reduction in the man-made emissions of NO_x and a 50% reduction in the man-made emissions of organic compounds. In the southern hemisphere there is only a small reduction in the ozone production in the lower troposphere resulting from the lower NO_x. In the northern hemisphere the 50% reduction of man-made NO_x emissions reduces the ozone production in the lower troposphere by 23%. In the upper troposphere the production in fact increases by 3% because the access of peroxy radicals increases. The effect of the reduction in the emissions of organics is less complicated. There is no difference in the southern hemisphere. In the northern hemisphere the ozone production in the lower troposphere is reduced by 13% and in the upper troposphere by less than 2%. This indicates that a reduction in the NO_x emissions is more efficient than a reduction in the emissions of organic compounds when the aim is to reduce the tropospheric ozone production. Moreover, the reduction which results from lower NO_x emissions is concentrated in the most polluted latitude belts.

REFERENCES

[1] Strand, A., and Ø. Hov, A two-dimensional zonally averaged transport model including convective motions and a new strategy for the numerical solution, *J. Geophys. Res., 98*, 9023-9037, 1993.

[2] Simpson, D., Long-period modelling of photochemical oxidants in Europe. Model calculations for July 1985, *Atmos. Environ., 26*, 1609-1634, 1985.

[3] Hough, A. M., The development of a two-dimensional tropospheric model: The model transport, *J. Geophys. Res., 96*, 7325-7362, 1991.

[4] Jaeger, L., Monatskarten des Niederschlages fur die ganze Erde, *Ber. Dtsch Wetterdiengtes, 18*(139), 1976.

[5] Lelieveld J., P. J. Crutzen, and H. Rodhe, Zonal average cloud characteristics for global atmospheric chemistry modelling, *Rep. CM-76,* Dep. of Meteorol., Stockholm, Sweden, 1989.

[6] Ehhalt, D. H., and J. W. Drummond, NO_x sources and the tropospheric distribution of NO_x, during STRATOZ III, in *Tropospheric Ozone, Regional and Global Scale Interactions, NATO ASI Ser. C, vol. 227,* edited by I. S. A. Isaksen, pp. 217-237, D. Reidel, Hingham, Mass., 1988.

[7] Seinfeld, J. H., *Atmospheric Chemistry and Physics of Air Pollution,* John Wiley, New York, 1986.

[8] Crutzen, P. J., Tropospheric ozone: An overview, in *Tropospheric Ozone, Regional and Global Scale Interactions, NATO ASI Ser. C, vol. 227,* edited by I. S. A. Isaksen, pp. 217-237, D. Reidel, Hingham, Mass., 1988. e.g. *Crutzen*, 1988]

FIGURES AND TABLES

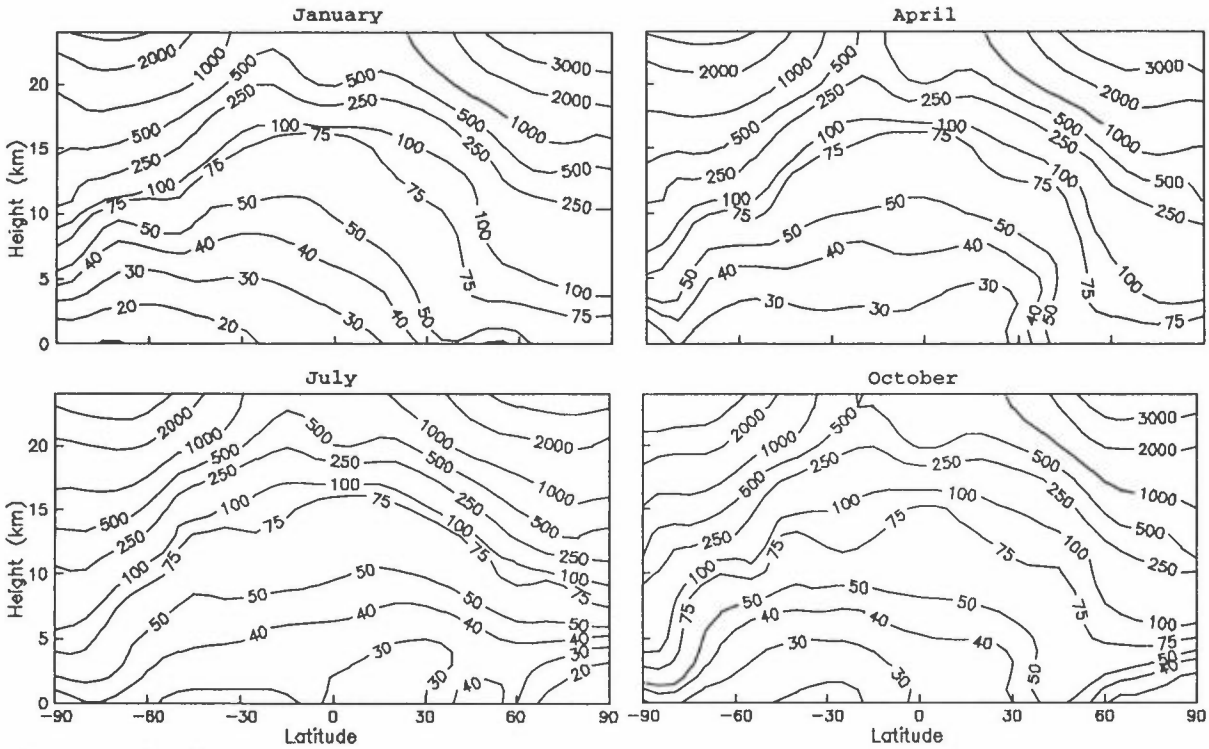

Fig. 1. The diurnal mean mixing ratio of ozone in ppb as predicted by the model for day 15 of the month.

Table 1. The Tropospheric Ozone Budget

	PLS	PUS	PLN	PUN	DS	DN	IN	IS
Full model:								
Dec.-Feb.	-0.2	5.3	7.6	6.1	7.4	19.4	5.7	2.3
Mar.-May	2.3	5.4	8.5	4.8	8.9	22.0	8.7	1.2
Jun.-Aug.	1.3	4.8	12.7	6.4	10.4	20.5	1.4	4.3
Sep.-Nov.	-3.3	4.8	12.2	7.9	9.2	21.2	1.1	7.7
50% NO_x reduction:								
Jun.-Aug.	1.0	4.8	9.8	6.6	10.2	18.1	1.7	6.8
50% CO & HC reduction:								
Jun.-Aug.	1.3	4.8	11.1	6.3	10.4	19.3	1.9	4.3

All numbers are in 10^{10} molecules/cm^2 s. The abbreviations used in the table are based on the following: P=Production, D=Dry deposition, L=Lower troposphere, U=Upper troposphere, S=Southern hemisphere, N=Northern hemisphere, I=Injection from stratosphere.

Air Quality Management System in Riga

ANDRIS LEITASS
RIGA CITY COUNCIL

Riga - the capital of newly independent state of Latvia - is a city of more than one million inhabitants and with highly concentrated industries of different type. Air pollution in Riga is a serious problem affecting health and damaging valuable buildings of historical importance as acid rain and smog take their toll. Therefore, the practical aspects and applications of atmospheric chemistry science come into particular prominence.

In Latvia the environmental programs received significant support from the Swedish Government and an environmental project for Riga was validated by BITS and has now been successfully implemented. Central to the project is an INDIC AIRVIRO system which simulates and evaluates air pollution levels at various locations and processes the data in order to predict air quality based on a number of predetermined parameters and criteria.

Further, the project was designed to ultimately lead to a more wide spread environmental awareness in Latvia which was hoped would spread throughout the Baltic region.

Observations of ozone and precursors at Norwegian stations

FRODE STORDAL, SVERRE SOLBERG, NORBERT SCHMIDBAUER
NORWEGIAN INSTITUTE FOR AIR RESEARCH

AND

ØYSTEIN HOV
DEPARTMENT OF GEOPHYSICS, UNIVERSITY OF BERGEN

Ozone and precursors have been measured at Birkenes in South Norway and at the Zeppelin Mountain at Spitzbergen since 1987 and 1989 respectively. A comparison of ozone concentrations measured at the two stations indicate that continental Europe acts as an ozone source during the summer and a sink during the winter.

Concentrations of several NMHC (non methane hydrocarbons) show a marked seasonal cycle, with minimum values in the summer, when photochemical reactions reduce their concentrations during the transport from the source regions. The summer values are smaller at Spitzbergen than at Birkenes, due to the longer travel distance from the sources. Sector analyses of the NMHC yield that the highest concentrations for most species are found when the transport is from continental Europe or the UK.

List of participants

BEINE, Harald
Department of Geophysics
University of Oslo
P.O. Box 1022, Blindern
N-0315 Oslo, Norway

Tel.: +47-22 85 57 56
Fax.: +47-22 85 52 69
E-mail: HARRYB@SMAUG.UIO.NO

E-mail: FTHB@ACAD3.ALASKA.EDU

BUDVYTYTE, Dalia
Institute of Physics
A. Gostauto str. 12
2600 Vilnius, Lithuania

Tel.: +370-2-64 12 27
Fax.: +370-2-61 70 70
E-mail: DAVIDAVICIUS@FI.LT

CEBURNIS, Darius
Ecological spectrosc. laboratory
Institute of Physics
A. Gostauto str. 12
2600 Vilnius, Lithuania

Tel.: +370-2-64 15 02
Fax.: +370-2-61 70 70
E-mail:

CHRISTENSEN, Carsten Stenholt
National Envionmental Research Institute
Div. of Emission and Air Pollution
Frederikborgsvej 399
P.O. Box 358
DK-4000 Roskilde, Denmark

Tel.: +45-46 30 12 00
Fax.: +45-46 30 11 14
E-mail:

EERME, Kalju
Department of Pysics
University of Oslo
P.O.box 1048, Blindern
0316 Oslo, Norway

Tel.: +47-22-85-56-71
Fax.: +47-22-85-56-71
E-mail:

ELLERMANN, Thomas
National Envionmental Research Institute
Frederikborgsvej 399
P.O Box 358
DK-4000 Roskilde, Denmark

Tel.: +45-46 30 11 62
Fax.: +45-46 30 12 14
E-mail: LUTEL@WPGATE.DMU.MIN.DK

ENGDAHL, Anders
Thermochemistry
Chemical Center
P.O. Box 124
S-22100 Lund, Sweden

Tel.: +46-46 10 81 84
Fax.: +46-46 10 45 33
E-mail: ANDERS.ENGDAHL@TERMK.LU.SE

FLØYSAND, Inga
NILU
P.O. Box 64
N-2001 Lillestrøm, Norway

Tel.: +47-63 81 41 70
Fax.: +47-63 81 92 47
E-mail: INGA@NILU.NO

GIRGZDIENE, Rasa
Institute of Physics
A. Gostauto str. 12
2600 Vilnius, Lithuania

Tel.: +370-2-64 18 27
Fax.: +370-2-61 70 70
E-mail: DAVIDAVICIUS@FI.LT

GRANBY, Kit
National Envionmental Research Institute
Frederikborgsvej 399
P.O. Box 358
DK-4000 Roskilde, Denmark

Tel.: +45-46 30 11 33
Fax.: +45-46 30 11 14
E-mail:

HALLQUIST, Mattias
Dept. of Inorg. Chemistry
Univ. of Göteborg
S-41296 Göteborg, Sweden

Tel.: +46-31-77 22 860
Fax.: +46-31-16 71 94
E-mail: MATTIAS@CTKEM.PHC.CHALMERS.SE

HERMANSEN, Ove
NILU
P.O. Box 64
N-2001 Lillestrøm, Norway

Tel.: +47-63 81 41 70
Fax.: +47-63 81 92 47
E-mail:

HONGISTO, Marke
Finnish Meteorological Institute
Air Quality Department
Saahaajankatu 22 E
00810 Helsinki 81, Finland

Tel.: +358-0-75 81 342
Fax.: +358-0-75 81 396
E-mail:
HONGISTO_M%HILMA.DNET@POUTA.FMI.FI

HORN, Anne
Department of Chemistry
University of Oslo
P.O.Box 1033, Blindern
N-0315 Oslo, Norway

Tel.: +47-22 85 43 51
Fax.: +47-22 85 54 41
E-mail: AHORN@KJEMI.UIO.NO

IGNATAVICIUS, Mecislovas
Institute of Physics, Vilnius University
A. Gostauto str. 12
2600 Vilnius, Lithuania

Tel.: +370-2-63 07 49
Fax.: +370-2-61 70 70
E-mail: ANDRIUS.MESKAUSKAS@FF.VU.LT

ISAKSEN, Ivar
Department of Geophysics
University of Oslo
P.O. Box 1022, Blindern
N-0315 Oslo, Norway

Tel.: +47-22 85 58 22
Fax.: +47-22 85 52 69
E-mail: IISAKSEN@EXTERN.UIO.NO

JAFFE, Dan
Department of Geophysics
University of Oslo
P.O. Box 1022, Blindern
N-0315 Oslo, Norway

Tel.: +47-22 85 58 31
Fax.: +46-22 85 52 69
E-mail:

JALKANEN, Liisa
Finnish Meteorological Institute
Air Quality Department
Sahaajankatu 22E
SF-00810 Helsinki, Finland

Tel.: +358-0-75 81 305
Fax.: +358-0-75 81 396
E-mail: LIISA.JALKANEN@FMI.FI

JANHÄLL, Sara
IVL
P.O. Box 47086
S-402 58 Göteborg, Sweden

Tel.: +46-31-46 00 80
Fax.: +46-31-48 21 80
E-mail:

JANSON, Robert
Dept. of Meteorology
Stockholm University
S-106 91 Stockholm, Sweden

Tel.: +46-8-16 24 14
Fax.: +46-8-15 92 95
E-mail: ROBERT@MISU.SU.SE

JOHNSSON, Klas
IFM / Chemical Physics
University of Linköping
S-58183 Linköping, Sweden

Tel.: +46-13-28 26 64
Fax.: +46-13-14 23 37
E-mail:

JOSEFSSON, Bjørn
Department of Analytical Cemistry
University of Stockholm
S-108 91 Stockholm, Sweden

Tel.: +46-8-16 24 38
Fax.: +46-8-15 63 91
E-mail:

KARLSDOTTIR, Sigrun
Department of Geophysics
University of Oslo
P.O. Box 1022, Blindern
N-0315 Oslo, Norway

Tel.: +47-22 85 58 23
Fax.: +47-22 85 52 69
E-mail: SIGRUN@SMAUG.UIO.NO

KLÆBOE, Peter
Department of Chemistry
University of Oslo
P.O.Box 1033, Blindern
N-0315 Oslo, Norway

Tel.: +47-22 85 56-78
Fax.: +47-22 85 54-41
E-mail: PETER.KLABOE@KJEMI.UIO.NO

KRAABØL, Anne Gunn
NILU
P.O. Box 64
N-2001 Lillestrøm, Norway

Tel.: +47-63 81 41 70
Fax.: +47-63 81 92 47
E-mail: ANNEGUNN@NILU.NO

KULMALA, Markku
Aerosol physics laboratory
Department of Physics
PL 9 (Siltavuorenpenger 20 D)
SF-00014 Univ. of Helsinki , Finland

Tel.: +358-0-19 18 308
Fax.: +358-0-19 18 318
E-mail: KULMALA@PHCU.HELSINKI.FI

KVIETKUS, Kestutis
Ecological spectroscopy lab.
Institute of Physics
A. Gostauto str. 12
2600 Vilnius, Lithuania

Tel.: +370-2-64 16 81
Fax.: +370-2-61 70 70
E-mail:

LANGER, Sarka
Department of Inorg.Chemistry
GU / CTH
S-41296 Göteborg, Sweden

Tel.: +46-31-77 22 865
Fax.: +46-31-16 71 94
E-mail: SARKA@CTKEM.PHC.CHALMERS.SE

Larsen, Niels Wessel
Chemical Laboratory 5
The H.C. Ørsted Institute
Universitetsparken 5
DK-2100 København Ø, Denmark

Tel.: +45-35-320324
Fax.: +45-31-350609
E-mail: NWL@KL5VAX.KI.KU.DK

Lasson,Emilie
Department of Chemistry
University of Oslo
P.O. Box 1033, Blindern
N-0315 Oslo, Norway

Tel.: +47-22 85 56 77
Fax.: +47-22 85 54 41
E-mail: ELASSON@KJEMI.UIO.NO

LEITASS, Andris
3, K.Valdemara str.,
Riga PDP, LV-1539, Latvia

Tel.: +371-2-32 07 41
Fax.: +371-2-22 07 85
E-mail:

LJUNGSTRÖM, Evert
Department of Inorg. Chemistry
GU / CTH
S-41296 Göteborg, Sweden

Tel.: +46-31-77 22 880
Fax.: +46-31-16 71 94
E-mail:

LUND, Anders
University of Linköping
IFM
S-58183 Linköping, Sweden

Tel.: +46-13-28 26 65
Fax.: +46-13-14 23 37
E-mail:

LUND, Cathrine
Department of Chemistry
University of Oslo
P.O. Box 1033, Blindern
N-0315 Oslo, Norway

Tel.: +47-22 85 54 73
Fax.: +47-22 85 54 41
E-mail:

MIRME, Aadu
Department of Environmental Physics
Tartu University
Ulikooli str.18
EE2400 Tartu, Estonia

Tel.: +372-34-33 450
Fax.: +
E-mail: AADU@AEL.UT.EE

MOLDANOVA , Jana
Department of Inorg. Chemistry
CTH / GU
S-41296 Göteborg, Sweden

Tel.: +46-31-77 22 880
Fax.: +46-31-16 71 94
E-mail:

MUNTHE, John
Swedish Environmental
Research Institute (IVL)
P.O. Box 47086
S-40258 Göteborg, Sweden

Tel.: +46-31-46 00 80
Fax.: +46-31-48 21 80
E-mail:

MYHRE, Gunnar
NILU
P.O. BOX 64
N-2001 Lillestrøm, Norway

Tel.: +47-63 81 41 70
Fax.: +47-63 81 92 47
E-mail:

NELANDER, Bengt
Thermochemistry
Chemical Center
P.O. Box 124
S-22100 Lund, Sweden

Tel.: +46-46-10 81 83
Fax.: +46-46-10 45 33
E-mail: BENGT.NELANDER@TERMK.LU.SE

NIELSEN, Claus Jørgen
Department of Chemistry
University of Oslo
P.O. Box 1033, Blindern
N-0315 Oslo, Norway

Tel.: +47-22 85 56 80
Fax.: +47-22 85 54 41
E-mail: CLAUS.NIELSEN@KJEMI.UIO.NO

NIELSEN, Ole John
Research Center Risø
KER - Environment
DK-4000 Roskilde, Denmark

Tel.: +45-46 77 42 01
Fax.: +45-42 37 04 01
E-mail: OJN@RISOE.DK

NOREMSAUNE, Ingse
Department of Chemistry
University of Oslo
P.O. Box 1033, Blindern
N-0315 Oslo, Norway

Tel.: +47-22 85 56 75
Fax.: +47-22 85 54 41
E-mail: INGSEN@KJEMI.UIO.NO

PETTERSEN, Marit Viktoria
Department of Chemistry
University of Oslo
P.O. Box 1033, Blindern
N-0315 Oslo, Norway

Tel.: +47-22 85 54 20
Fax.: +47-22 85 54 41
E-mail: MARITVP@KJEMI.UIO.NO

PLEIJEL, Karin
IVL
Box 47086
S-40258 Göteborg, Sweden

Tel.: +46-31-46 00 80
Fax.: +46-31-48 21 80
E-mail:

ROOTS, Ott
Estonian Ministry of Environmental Protection
Kotka Str. 2
Tallin, Estonia

Tel.: +372-2-
Fax.: +372- 2 45 18 64
E-mail:

RUMMUKAINEN, Markku
University of Oslo
Department of Geophysics
P.O. Boks 1022, Blindern
N-0315 Oslo, Norway

Tel.: +47-22 85 57 56
Fax.: +47-22 85 52 69
E-mail:
MARKKU.RUMMUKAINEN@GEOFYSIKK.UIO.NO

SAARE, Leo
Estonian Ministry of Environmental Protection
Kotka str. 2
Tallin, Estonia

Tel.: +372-2-
Fax.: +372- 2 45 18 64
E-mail:

SAASTAD, Ole Widar
Department of Chemistry
University of Oslo
P.O. Box 1033, Blindern
N-0315 Oslo, Norway

Tel.: +47-22 85 56 60
Fax.: +47-22 85 54 41
E-mail: O.W.SAASTAD@KJEMI.UIO.NO

SCHREINER, Camilla
Department of Geophysics
University of Oslo
P.O. Boks 1022, Blindern
N-0315 Oslo, Norway

Tel.: +47-22 85 44 30
Fax.: +47-22 85 52 69
E-mail: CAMILLAS@SMAUG.UIO.NO

SEHESTED, Jens
Research Center Risø
KER -Environment
DK-4000 Roskilde, Denmark

Tel.: +45-46 77 42 00
Fax.: +45-42 37 04 03
E-mail:

SELAND, John Georg
Department of Chemistry
University of Oslo
P.O. Box 1033, Blindern
N-0315 Oslo, Norway

Tel.: +47-22 85 54 20
Fax.: +47-22 85 54 41
E-mail:

SIIGUR, Katrin
Inst. of Chem. Phys. and Biophys.
Estonian Academy of Sciences
Rävala Puiestee 10
EE0100 Tallinn, Estonia

Tel.: +372-2-52 95 75
Fax.: +372-2-52 95 79
E-mail:

SIMPSON, David
Department of Meteorology
P.O. Box 43, Blindern
N-0313 Oslo, Norway

Tel.: +47-22 96 32 13
Fax.: +47-22 96 30 50
E-mail: MIFADS@CRAY.SINTEF.NO

SOLBERG, Sverre
NILU
P.O. Box 64
N-2001 Lillestrøm, Norway

Tel.: +47-63 81 41 70
Fax.: +47-63 81 92 47
E-mail: SVERRE@NILU.NO

SOPAUSKIENE, Dalia
Institute of Physics
A. Gostauto str. 12
2600 Vilnius, Lithuania

Tel.: +370-2-64 12 27
Fax.: +370-2-61 70 70
E-mail: DAVIDAVICIUS@FI.LT

STORDAL, Frode
NILU
P.O. Box 64
N-2001 Lillestrøm, Norway

Tel.: +47-63 81 41 70
Fax.: +47-63 81 92 47
E-mail: FRODE@NILU.NO

STRAND, Asbjørn
Department of Geophysics
University of Bergen
N-5007 Bergen, Norway

Tel.: +47-55-21 28 98
Fax.: +47-55-96 05 66
E-mail: STRAND@GFI.UIB.NO

TANNER, Heikki
Institute of Chemical Physics and Biophysics
Estonian Academy of Sciences
Rävala Puiestee 10
EE0100 Tallinn, Estonia

Tel.: +372-2-52 95 75
Fax.: +372-2-52 95 79
E-mail: JACK@ANUBIS.KBFI.EE

TIMONEN, Raimo
Department of Physcal Chemistry
University of Helsinki
Meritullinkatu 1C
SF-00170 Helsinki, Finland

Tel.: +358-0-19 13 565
Fax.: +358-0-19 13 528
E-mail: RTIMONEN@CC.HELSINKI.FI

ÜBELIS, Arnolds
Department of Spectroscopy
University of Latvia
Raina Bulv. 19
Riga LV 1586, Latvia

Tel.: +371-2-22 97 27
Fax.: +371-2-22 59 92
E-mail:

WÄNGBERG, Ingvar
Department of Inorg. Chemistry
CTH
University of Göteborg
S-412 96 Göteborg, Sweden

Tel.: +46-31-77 22 865
Fax.: +46-31-16 71 94
E-mail:

WÜRGLER, Roland
Nordiska Balzers AB
P. O. Box 10412
S-43424 Kungsbacka, Sweden

Tel.: +46-300-710 80
Fax.: +46-300-172 85
E-mail:

Index of authors

Norsk institutt for luftforskning (NILU)
Norwegian Institute for Air Research
Postboks 64, N-2001 Lillestrøm

RAPPORTTYPE Oppdragsrapport	RAPPORT NR. OR 20/94	ISBN-82-425-0562-4	
DATO Mars 1994	ANSV. SIGN.	ANT. SIDER 238	PRIS NOK 270,-
TITTEL Third Nordic Symposium on Atmospheric Chemistry. Proceedings of NORSAC '93.		PROSJEKTLEDER C.J. Nielsen	
		NILU PROSJEKT NR. E-93086	
FORFATTER(E) Redigert av C.J. Nielsen		TILGJENGELIGHET * A	
		OPPDRAGSGIVERS REF.	

OPPDRAGSGIVER
Department of Chemistry,, University of Oslo
P.O. Box 1033 Blindern
N-0315 OSLO

and

Norsk institutt for luftforskning
Postboks 64
N-2001 LILLESTRØM

STIKKORD		
Chemistry	Atmosphere	Air pollution

REFERAT
Rapporten inneholder deltakernes innlegg ved det tredje nordiske symposium om atmosfærens kjemi som ble avholdt på Geilo i desember 1993.

TITLE

ABSTRACT
The report contains the extended abstracts from the Third Nordic Symposium on Atmospheric Chemistry which took place in Geilo in December 1993.

* *Kategorier:*
- *A* *Åpen - kan bestilles fra NILU*
- *B* *Begrenset distribusjon*
- *C* *Kan ikke utleveres*